HIGH PRESSURE SCIENCE AND TECHNOLOGY

PROCEEDINGS

XI AIRAPT International Conference

NAUKOVA DUMKA

33

HIGH PRESSURE SCIENCE AND TECHNOLOGY

XI INTERNATIONAL AIRAPT KIEV-87 CONFERENCE

PROCEEDINGS

XI AIRAPT International Conference

KIEV 1989

INTERNATIONAL ASSOCIATION FOR THE ADVANCEMENT OF
HIGH PRESSURE SCIENCE AND TECHNOLOGY

HIGH PRESSURE SCIENCE AND TECHNOLOGY

PROCEEDINGS

XIth AIRAPT International Conference

In 4 volumes

Volume 3

Kiev Naukova Dumka 1989

)C 62-987:539.89

High Pressure Science and Technology: Proc.XIth AIRAPT
it. Conf.: In 4 vol /International Association for the Advan-
ement of High Pressure Science and Technology. -Kiev: Nauko-
a Dumka, 1989. -Vol.3.- 380 p.
SBN 5-12-001177-2 (т.3)
SBN 5-12-001176-4

The Proceedings composed of four volumes contain papers resented at the XIth AIRAPT International Conference "High ressure Science and Technology" (Kiev, USSR, 12-17 July 1987).

Volume 3 of the Proceedings includes the papers on the ollowing topics: superconductivity, electrical and magnetic roperties; equations of state of condensed matter, extreme conitions, plasma; industrial applications of high pressure.

The book is a direct reproduction of the camera-ready manusripts submitted by the authors. No corrections have been made in he texts.

В сборник, состоящий из четырех томов, включены труды, представленные на XI Международную конференцию МАРИВД "Высокие давления в науке и технике" (Киев, СССР, I2-I7 июля I987 г.).

В третий том вошли работы по следующим разделам: сверхпроводимость, электрические и магнитные свойства; уравнения состояния сжатых веществ, экстремальные состояния, плазма; промышленное применение высоких давлений.

Сборник отпечатан методом прямого репродуцирования с рукописей, представленных авторами. Авторские тексты не редактировались.

N.V.Novikov, Editor-in-chief.
Ye.M.Chistyakov, Scientific secretary

Н 1604090000-214
M221(04)-89
ISBN 5-12-001177-2 (т.3)
ISBN 5-12-001176-4

C O N T E N T S

SUPERCONDUCTIVITY, ELECTRICAL AND MAGNETIC PROPERTIES

INDUSTRIAL APPLICATIONS OF HIGH PRESSURE

INSULATOR-METAL TRANSITIONS AND SUPERCONDUCTIVITY OF AMORPHOUS SEMICONDUCTORS AT PRESSURES UP TO 250 kbar

I.V. Berman, N.B. Brandt
M.V.Lomonosov State University, Moscow, USSR

The problem of the insulator-metal (I-M) transition in amorphous substances has recently become the subject of a great interest. Of particular interest is the behaviour of such systems near the I-M transition. We shall consider the Anderson I-M transition which takes place when the Fermi level E_F crosses the mobility threshold E_c as some outer parameter is changed.

To classify disordered substances from the point of view of their proximity to the Anderson transition, the so called Anderson parameter $\delta = \frac{I}{W}$ is used, where I is the value which is proportional to the occupied states band wide (for doped semiconductors it is the impurity band, for d-electrons - d-band, etc), W - the energy scatter, characterising the disorder. The Anderson transition occurs at $\delta \approx 1$. It is obvious that it is very difficult to reach Anderson transition in metallic systems with large Fermi energy.

New interesting possibilities to study I-M transition come from experiments in substances in which E_F is small. Such situation can probably be in glassy chalcogenide semiconductors (GCS) over some pressure intervals.

For many GCS the electroresistivity ρ and the activation energies E_a, determined from ρ on T dependences, decrease smoothly with increasing pressure /1-3/. The optical gap E_g in a-As_2Se_3 and a-As_2S_3 show the same behaviour /4/. The equality of twice the E_a to the E_g in a-As_2Se_3 indicates that the Fermi level lies at the centre of an energy gap at high pressure as it does in most GCS at P=0. E_a vanishes at P_c depending on the substance. At $P > P_c$ these substances behave like metals. It is natural to suggest that the decrease in E_a and the transition to the metallic state in GCS can be due to the variation of the relative position of E_F and E_c. Just the same situation can take place in other groups of amorphous semiconductors.

The investigations of the superconducting (SC) properties of

amorphous substances near I-M transition make it possible to put up and to decide the number of principle questions : about the forming the SC state and its peculiarities near I-M transitions ; about the nature of pressure influence on the SC transition temperature T_c ; about the peculiarities of the SC state in the system of weakly localized electrons ; about the possibility of the superconductivity in the localized state ; about the behaviour of T_c in crystallizing amorphous system in the vicinity of the crystallization threshold. The behaviour of T_c, critical magnetic fields H_{c2} (T) and critical currents J_c in disordered materials is now especially important in connection with the discovery the SC high temperature ceramics with the considerable degree of the disorder. In examining the superconductivity in these materials it is necessary to differ their properties, connected with the disorder or with the nature of the superconductivity.

X-ray data

X-ray studies of an a-As_2Te_3 /5/ after the compression up to 100 kbar showed that the sample crystallized into the phase c-As_2Te_3, stable under normal conditions. More detailed X-ray studies of an a-As_2Te_3 over the pressure range (0-100 kbar) and after releasing pressure to zero showed that the real picture of the crystallization of the sample was more complicated. The sample has been amorphous for 2-3 months at high pressures. At releasing pressure it was still amorphous for 1-2 days. After its extraction from the high pressure chamber and standing for longer time the crystallization of the sample occured.

X-ray studies of an a-$Si_{15}Ag_{15}Te_{70}$ showed that this sample remained amorphous for not less that 1/2 year at applying and releasing pressure over the pressure interval up to 100 kbar.

The electrical properties of GCS at high pressures

In a-Ge_2S_3 at P > 180 kbar followed by the parts of ρ(T) curves on which the exponential change in ρ is observed (300-150 K), the parts of a very slow increase in ρ are registrated in the interval (150-114 K). There is no superconductivity in a-Ge_2S_3.

There are conformities to natural laws for the behaviour of the electrical and superconducting properties in a-As_2Se_3, a-As_2Te_3, a-Ge_2Se_3, a-GeTe, a-$Ge_{33}As_{12}Se_{55}$, a-$Si_{15}Ag_{15}Te_{70}$ at high pressures. At $P > P_c$ parts of the ρ(T) curves on which an exponential change in ρ is observed can be clearly detected (in temperature

range (300-150 K), $\rho \sim e^{\frac{-(E_F-E_c)}{kT}}$, $E_F - E_c = E_a$). As T decreases the increase in ρ becomes less visible. It is impossible to discribe the ρ (T) curves by any known expression for hopping conductivity over the interval (150-1.4 K). E_a vanishes at P=60, 70, 90, 160, 180, 200 kbar for a-$Si_{15}Ag_{15}Te_{70}$, a-As_2Te_3, a-GeTe, a-$Ge_{33}As_{12}Se_{55}$, a-Ge_2Se_3, a-As_2Se_5, accordingly. It is necessary to take into account the uncertainty in P_c determination caused, first of all, by the change in the preexponential coefficient under pressure.

Pressure dependence of T_c

At $P > P_c$ over some pressure interval (20-30 kbar) the ρ (T) curves retain their poorly defined semiconducting nature. However, followed by the increase in ρ with decreasing T one can see the sharp drop in ρ at low temperatures. The supperconductivity sets in at $P \approx P_c$. The $2E_a$ and T_c on P dependences are shown in Fig.1.

The superconductivity appears at very low temperatures ($\sim$0.06 K) /6/. Fig.2. shows the T_c on P dependences for all enumerated above GCS. The results for a-As_2Se_5 are not shown because the beginning of the SC transition in this material is registrated at $P \approx 200$ kbar. It also moves to higher temperatures with increasing pressure. The most interesting and unusual (for the crystalline state of a nontransition materials) aspect of the onset of the superconductivity is the strong increase in T_c with the applied pressure near I-M transition and the saturation (or decrease) in T_c at higher pressures.

T_c for nontransition materials decrease under pressure with the typical rate $dT_c/dP \sim -10^{-2}$ K·kbar^{-1}. The main reason for T_c decrease in this case is the increase of Debye temperature θ_D and, as a result, the decrease of the value of the electron-phonon interaction.

The appearance of the superconductivity and the increase in T_c with the applied pressure in GCS near the I-M transition can not be explained by θ_D change. The investigations of the elastic properties of some GCS over the pressure interval (10-30 kbar) (a-As_2Se_3, a-Ge_2Se_3) showed their "normal" behaviour - sound velocities and θ_D increase under pressure /2/.

All the results - the persisting of the amorphous state at $P \approx P_c$, the appearance of the superconductivity in the pressure range where $E_a \to 0$, the unusually strong increase in T_c over the narrow pressure interval, the negative resistance coefficient in SC samples, the proximity of the conductivity to the Mott's minimum metallic conductivity value near P_c - indicate that the behaviour of the test systems is determined by the vicinity to the I-M transition and by the weakness of the localization effects.

The question about the localization effects on the superconductivity is so far open. There are a few models for explaining the effect of the localization on the superconductivity: the increase in the effective Coulowb repulson at the expence of the electron diffusion weakening as $E_F \to E_c$; the increase of the fluctuation effects as $E_F \to E_c$; the decrease in the density of electronic states N (E_F) near E_c. A very useful information can be received from H_{c2} (T) and J_c on P measurements.

The H_{c2} (T) mesurements have shown, that a-As_2Te_3 and a-$Si_{15}Ag_{15}Te_{70}$ are hard superconductors (Fig.3). The slope dH_{c2}/dT decreases with increasing pressure. If you estimate N (E_F) by the well-known relation

$$N(E_F) = \frac{1}{\text{sech}\rho} (dH_{c2}/dT)_{T_c},$$

the value N (E_F) for a-As_2Te_3 increases from $\sim 0.2 \cdot 10^{34}$ to $0.8 \cdot 10^{34}$ cm^{-3} erg^{-1} as P increases from 80 to 110 kbar. Such a strong increase in N (E_F) testifies about the visible modification of the N (E) on E dependence near E_c.

Now there are not reliable data which could allow to divide the enumerated mechanisms of the localization effects on T_c, however the strong increase in N (E_F) indicate to its essential role in T_c change as E_F moves away from E_c.

J_c are anomalous small at $P \approx P_c$ and increase by 2 orders of magnitude as T_c increases by 2-3 times. This indicates to the percolation nature of the superconductivity near I-M transition.

References

1. Minomura S. Pressure-induced effects and phase transitions in amorphous semiconductors. In: Amorphous semiconductors: Technology and devices, 1981, p.245-254.
2. Parthasarathy G., Gopal E.S.R. Effects of high pressure on chalcogenide glasses.-Bull. Mater.Sci.,1985,v.7,N.3-4,p.271-302.

3. I.V.Berman, N.B.Brandt. The superconductivity of amorphous substancies under high pressures.- Proceedings of VI, All-Union conference on metallic and slag melts properties, 1986, N.11, p.68-70.

4. B.A.Weinstein, K.Zallen, M.L.Slade. Optical spectra of a-As_2Se_3 under high pressure, J.Non-Cryst. Solids, 1980, v.35, N.36, p.1255-1260.

5. N.Sakai, H.Fritzche Semiconductor - metal and superconductive transitions induced by pressure in amourphous As_2Te_3. - Phys. Rev., 1977, B15, N.2, p.973-978.

6. I.V.Berman, N.B.Brandt, I.E.Kostyleva, S.K.Pavlov, V.I.Sidorov, S.M.Chudinov. Critical magnetic fields in amorphous As_2Te_3 near insulator - metal transition. - Pisma ZETF, 1986, v.43, N.1, p.48-50.

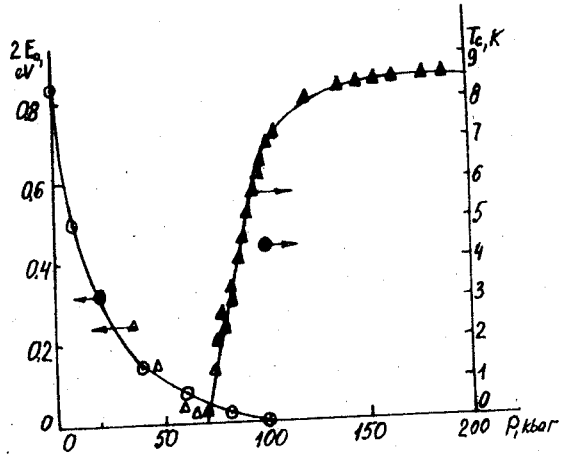

Fig.1. Pressure dependence of 2 E_a (scale at the left) and T_c (scale at the right) for a-As_2Te_3; o,● - data from /5/, △ ,▲ - data from /6/.

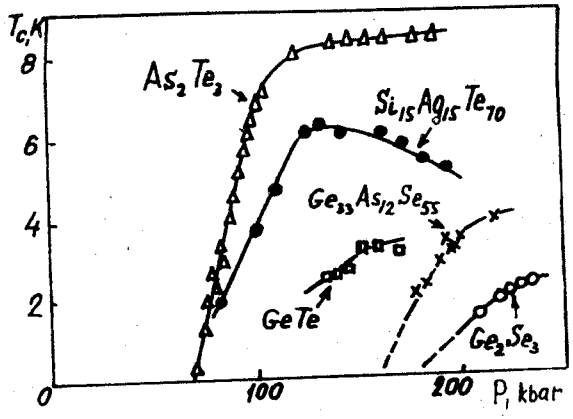

Fig.2. Pressure dependence of T_c for some chalcogenide glasses.

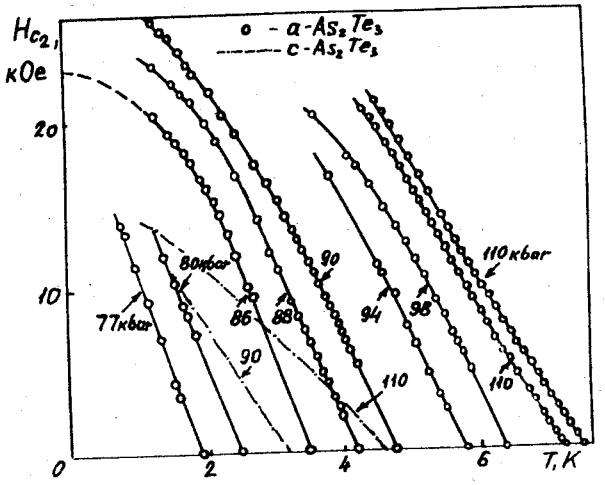

Fig.3. The critical magnetic fields of a-As_2Te_3 (solid curves) and c-As_2Te_3 (dashed curves) at various pressures.

SUPERCONDUCTIVITY UNDER PRESSURE UP TO 50 GPA: NEW EVIDENCE FOR THE S-TO-D TRANSFER IN THE ALKALINE EARTH METALS

B. Bireckoven and J. Wittig
Institut für Festkörperforschung, KFA Jülich,
D-5170 Jülich, Germany

Many elements which are normally not superconducting become superconducting at high pressure. Perhaps the most striking example so far is the element Cs[1]. Pressure-induced superconductivity has also been discovered in the alkaline earth metals Ba[2,3] and Sr[3,4]. Band structure calculations point to an appreciable s-to-d electron transfer in these metals with increasing pressure[5-7]. We believe that the occurrence of superconductivity most strikingly reflects the growing d-transition metal character of the divalent metals. Therefore, a quantitative investigation of the $T_c(p)$ dependence up to the highest possible pressure is of considerable interest. Such data could also shed light on the occurrence of structural phase transitions[8] under pressure and possible systematics of the p-T phase diagrams for the whole family of divalent metals.

Opposed anvil pressure systems employing sintered diamond anvils have been used in recent years in the investigation of the superconductivity of the alkaline earth metals[3,4]. According to our experience the useful pressure limit of such systems lies somewhere between 30 and 40 GPa. This limit depends of course on the diameter of the pressure cell and, in particular,on the desired lifetime of the anvils. In order to perform experiments at even higher pressures we have constructed a single-crystal diamond anvil cell which has routinely been used to over 50 GPa. Superconducting transitions are detected by a high sensitivity AC-SQUID system. The present paper contains a brief summary of the experimental technique[9]. In addition we present a recalibration T_c-vs-p of the "superconducting manometer" Pb with respect to the ruby scale. Finally we report our $T_c(p)$ data for Ba and Sr. Some possible implications are discussed.

Fig. 1 shows a crossection of the diamond anvil cell. A long piston (2) fits in a cylinder (1) with close tolerance. The diamonds rest on conventional rockers (3). The cylinder (1) carries an outer thread making connection to the mechanical press (4). The force generating system is essentially a variant of previous designs[10]. A worm gear (9) drives a central shaft (8). By means of gear wheels six screws (7) are simultaneously turned. They compress stacks of disk springs (6) which are located inside an intermediate piston (5). An axial bore serves as a light path. Also indicated is the position of the primary Helmholtz coil. Most parts are machined from nonmagnetic hardened CuBe2 alloy. The disk springs are of utmost importance. They guarantee that the pressure increases by less then 4% during cooling to 1He temperature due to differential thermal contraction.

Fig. 2 shows the rather delicate position of the pick-up coil in very close neighborhood to the stainless steel gasket. The inner (2) and the outer (3) coil are oppositely wound and thus form an astatic pair rigidly imbedded in the coil form (1) out of epoxy raisin. Schematically indicated in Fig. 3 is the measuring principle. The diamagnetic response of the superconducting sample (1) causes a change of the mutual inductance between the primary (3) and the pick-up coil (2). The resulting 32 Hz-signal is coupled by means of the flux transformer (4) to the SQUID sensor (5) which is immersed in a separate 1He-bath at a constant temperature of 4.2 K.

The pressure cell is a 0,2 mm hole in the pre-indented gasket. It is filled with the sample, vaseline as the protecting and pressure transmitting medium and ruby powder. The pressure is determined from the fluorescence line shift [11] ($d\lambda/d_p$ = 0.365 nm/GPa). The pressure distribution can be scanned with a focused laser beam (spot diameter roughly 6 μm).

We have made a major effort to recalibrate the superconducting Pb-manometer with respect to the ruby scale. Fig. 4 is a collection of data points for four independent series of experiments. Horizontal bars indicate the total spread of the pressure. In our conventional nomenclature vertical bars denote

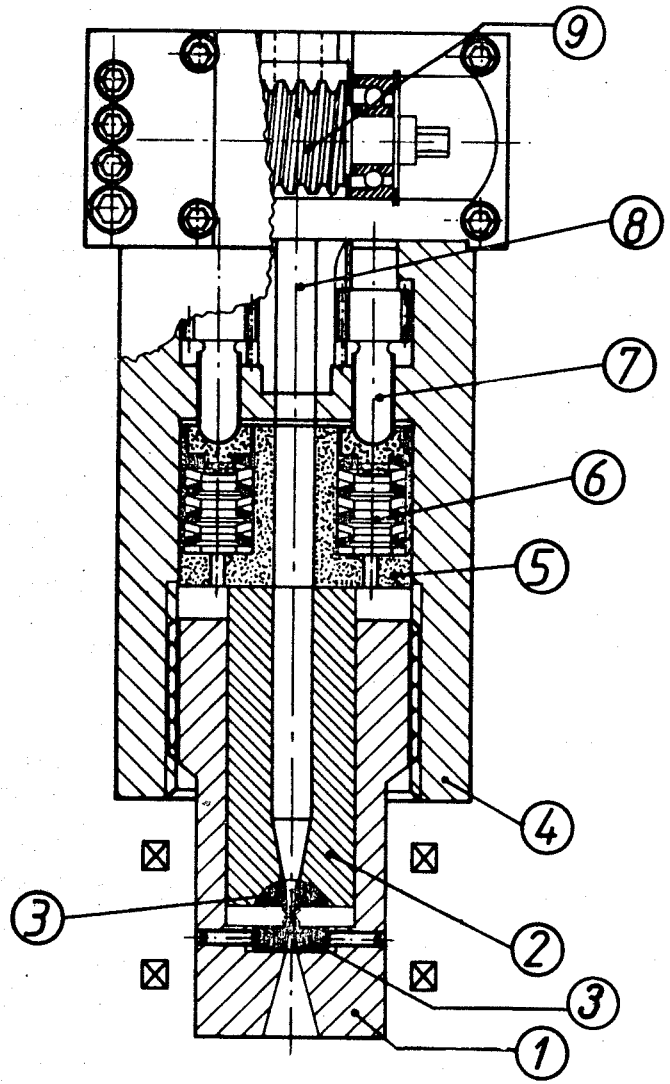

Fig. 1. Crossection of the diamond anvil cell
(1) cylinder, (2) piston, (3) rocker (4) press body
(5) intermediate piston, (6) disk springs, (7) screw driven by gear wheel, (8) centrally located shaft
(9) worm gear.

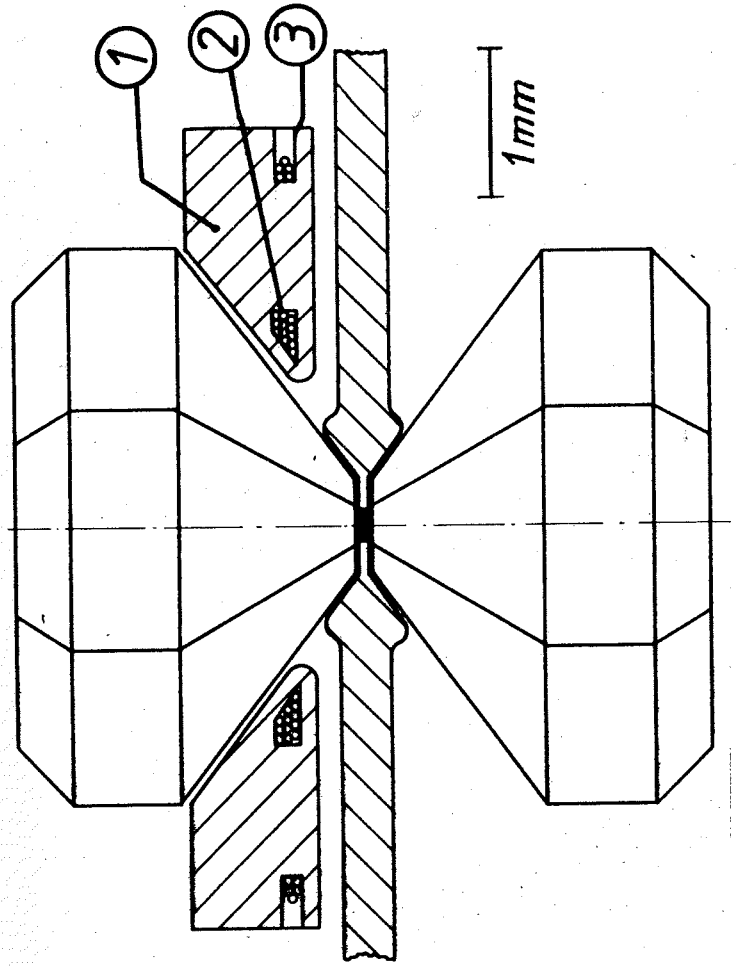

Fig. 2. Schematic representation of the high pressure cell and the pick-up coil
(1) coil former, (2) inner coil (3) outer coil.

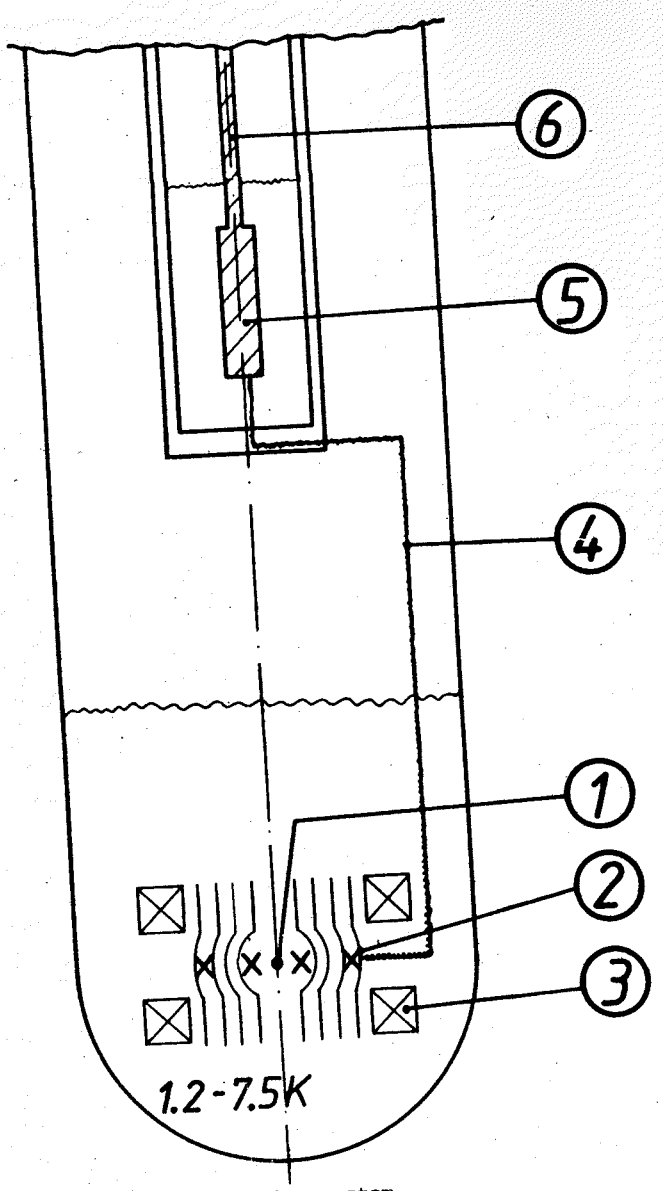

Fig. 3: SQUID detection system
(1) sample, (2) pick-up coil, (3) field coil, (4) flux transformer, (5) SQUID-probe (SHE-model MFP), (6) coaxial cable.

10%, 50% and 90% values of the superconducting transition. Open (closed) symbols have been measured on the pressure increasing (decreasing) cycle. It is evident that the T_c-p dependence of Pb is a smooth monotonously decreasing function of pressure up to 30 GPa. At this pressure the T_c is depressed to 1.3 K which is often the lowest temperature conveniently to be reached in a lHe dewar. The details of the calibration procedure are described elsewhere [9]. Here we note that, fortunately, no measurable anomaly occurs near the PbI-II phase transition at 13 GPa. For comparison the solid line in Fig. 4 shows our previous provisional pressure scale [12].

Fig. 5 shows T_c-p data for Ba to over 50 GPa for one particular pressure cell. The T_c-p dependence below 12.2 GPa [2] is represented by the solid line. The ranges of stability of the various high pressure phases[8] are marked on the bottom line. BaIV is stable between 12.2 GPa and 46 GPa. It is seen that T_c decreases rather moderately in this phase. It is also seen that the slope becomes steeper between the two highest pressure points (open triangles). The data on the releasing cycle (closed triangles) confirm our expectation that the steeper slope must be attributed to the formation of BaV. The phase BaV can metastably exist down to a pressure of about 27 GPa where its T_c exceeds 7 K. Below 35 GPa we observe two clearly separated superconducting transitions proving the coexistence of both phases. Eventually, at 13 GPa a single transition indicates complete reconversation to BaIV.

Fig. 6 shows T_c-p data for Sr between 35 and 50 GPa for two different cells together with previous data [4] below 1.2 K. Again ranges of stability of different crystallographic phases [8] are indicated on the bottom line. Like Ba, Sr becomes an excellent superconductor (by the standards of pure metals at least) T_c exceeding 7 K at 50 GPa. Two pronounced discontinuities at 35 and about 46 GPa are in good agreement with the suggested phase transitions at those pressures [8]. One may also notice that the IV-V transition is slightly hysteretic.

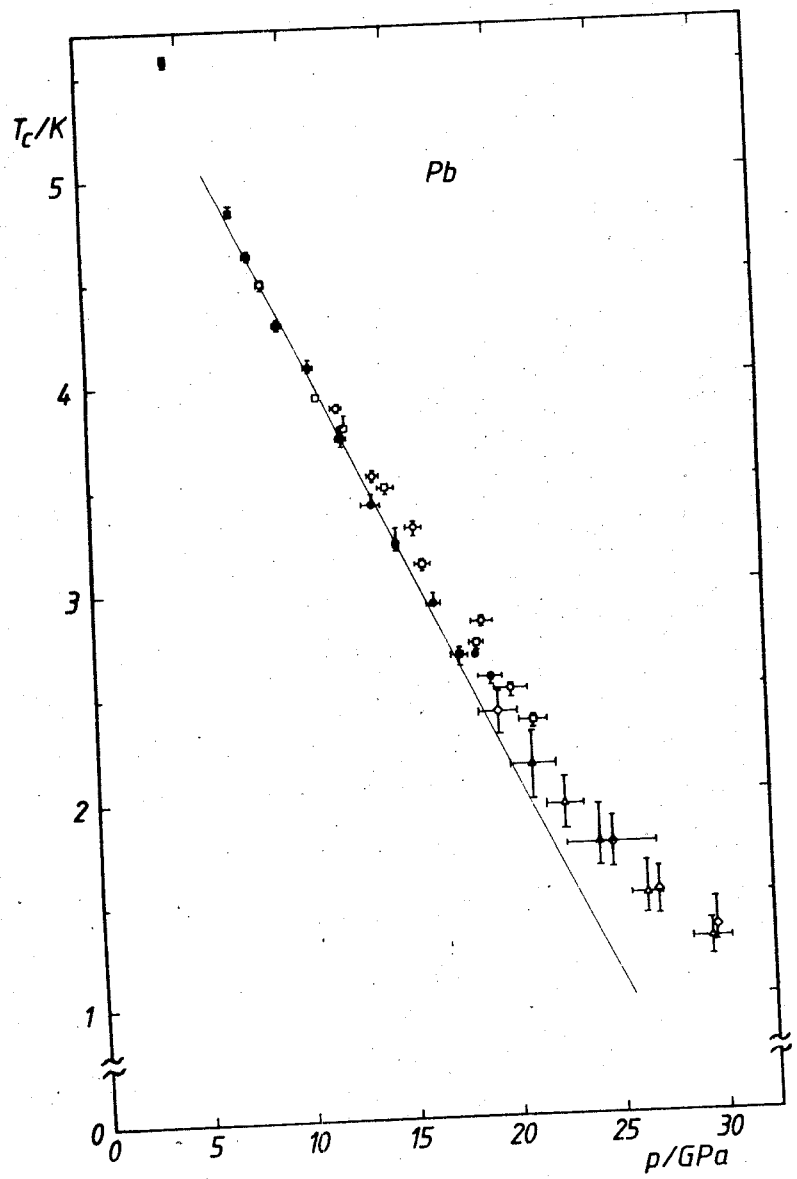

Fig. 4. Superconducting critical temperature for Pb as a function of p.

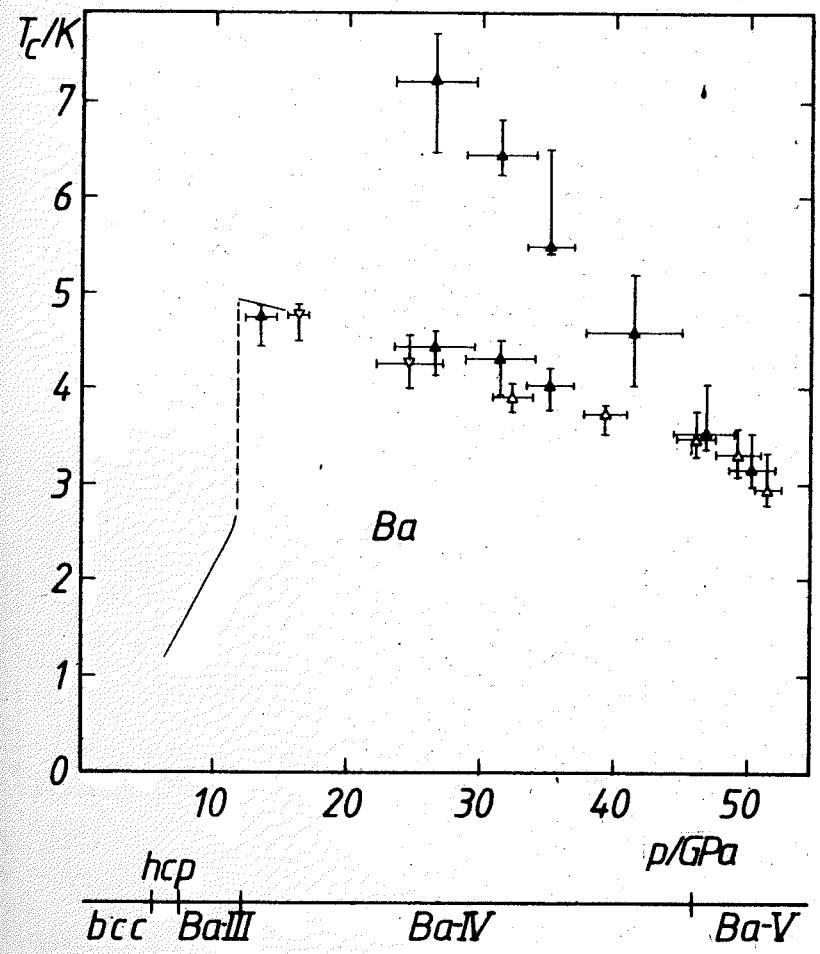

Fig. 5. Superconducting critical temperature for Ba as a function of p. Phase sequence at room-temperature from ref. 8.

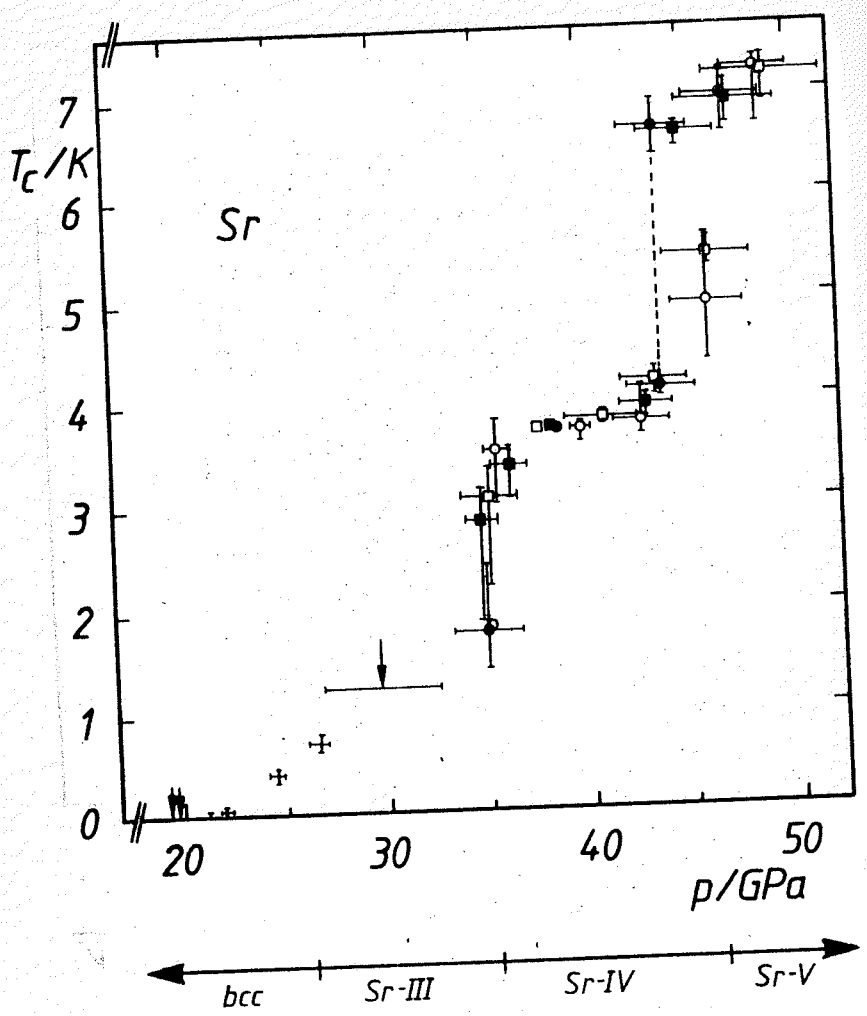

Fig. 6. T_c-p data for Sr. Phase sequence at room-temperature from ref. 8.

The possibility of a generalized phase diagram for the alkaline earth metals under pressure has often been discussed. For instance Olijnyk and Holzapfel have concluded that the high pressure phases BaIV and SrV are identical [8]. From our superconductivity data there is in fact some similarity between BaIV and SrV since T_c increases discontinuously in both metals when these high pressure phases are formed (Fig. 5 and 6). On the other hand there are two features which are pronouncedly different in these materials. Firstly, T_c rises in phase SrV with pressure whereas it decreases in BaIV. Secondly, the discontinuity at the SrIII/IV transition is entirely absent at the corresponding hcp-to-BaIII transformation (Fig. 5). We therefore think that the problem whether BaIV and SrV are identical is still unsolved. At any rate, we believe that the high T_c's wich we have discovered point to substantial d-transition metal character at high pressure [13].

We wish to thank J. Evers for the preparation of high purity Ba and Sr metal.

References

1. Wittig, J., Phys. Rev. Lett. 24, 812 (1970).

2. Moodenbaugh, A.R. and Wittig, J., J. Low Temp. Phys. 10, 203 (1973) and references therein.

3. Dunn, K.J. and Bundy F.P., Phys. Rev. B 25, 194 (1982).

4. Bireckoven, B., Wittig, J. and Evers, J., Proc. LT 17 Eckern, U. et al., eds., Elsevier Science Publishers (1984).

5. Skriver, H.L., Phys. Rev. B 31, 1909 (1985) and references therein.

6. Vasvari, B., Animalu, A.O.E. and Heine, V., Phys. Rev. 154, 535 (1967).

7. Duthie, J.C. and Pettifor, D.G., Solid State Comm. 27, 613 (1978).

8. Olijnyk, H. and Holzapfel, W.B., Phys. Lett. 100 A, 191 (1984).
J. de Phys. Colloq. C8, 157 (1984).

9. Bireckoven, B. and Wittig, J., to be published .

10. Wittig, J. and Probst, C. in: High-Pressure and Low-Temperature Physics
Chu, C.W. and Woollam, J.A., eds. (Plenum Press, New York, 1978) p. 433.

11. Piermarini, G.J., Block, S., Barnett, J.D. and Forman, R.A., J. Appl. Phys. 46, 2774 (1975).

12. Wittig, J., Z. Physik B 38, 11 (1980).

13. Bireckoven, B. and Wittig, J., to be published.

EFFECT OF PRESSURE ON SUPERCONDUCTIVE PROPERTIES OF $BaPb_{1-x}Bi_xO_3$ MONOCRYSTALS

S.L.Bud'ko[I], A.G.Gapotchenko[I], E.S.Itskevich[I], V.F.Kraidenov[I], A.V.Kuznetsov[2], A.P.Menushenkov[2], E.A.Protasov[2], V.N.Stepankin[2]

[I]Institute of High Pressure Physics, the USSR Academy of Sciences, Troitsk, USSR

[2]Moscow Physical-Engineering Institute, Moscow, USSR

Extraordinary properties of superconductive $BaPb_{1-x}Bi_xO_3$ (BPB) led to the assumption of out-of-ordinary mechanism of the superconductivity in this material. One of the models suggested is the superconductivity of localized pairs /I,2/.

So far investigations under pressure were performed only for ceramic samples and they brought out linear decrease of T_c as pressure increases with the derivative $dT_c/dp = -0.29$ K/GPa-I /3/. The behaviour of the second critical field under pressure was not investigated at all though it could be useful for determination of a mechanism of the superconductivity in BPB.

The BCS theory gives good qualitative explanation of the decrease of the critical temperature with the increase of pressure observed for the greater part of superconductors.

For present-day step of development of the theory of localized pairs it was no communication about properties of such systems under pressure. However an evaluation of the magnitude of the second critical field for the superconductor with localized pairs was presented in /2/. It gives an opportunity to determine qualitatively the pressure dependence of $H_{c2}^{lp}(p)$ in this case:

$$H_{c2}^{lp} = \frac{6\Phi_0}{\pi a^2} \quad \frac{T_c - T}{T_c}$$

where Φ_0 is the quant of magnetic flux and a is the lattice constant. Thus

$$\frac{d\ln H_{c2}^{lp}}{dp} = \frac{2}{3}\chi + \frac{dT_c}{dp}\left(\frac{1}{T_c - T}\right)\frac{T}{T_c} \qquad (*)$$

where χ is the compressibility.

Within the scope of the model of localized pairs the critical temperature is determined by the temperature of Bose-condensation /4/

$$T_c = \frac{2\pi\hbar^2}{m^* k}\left(\frac{n}{2.612}\right)^{2/3} \quad \text{so} \quad \frac{dT_c}{dp} > 0$$

So both terms in the right-hand side of equation (*) are positive and in contrast with the BCS theory this model predicts an increase of the second critical field under the pressure.

Therefore, investigation of the superconductive properties of the BPB compound under pressure, particularly, the measurement of the magnitude of H_{c2} even for the fixed temperature (for example, 4.2 K) can give arguments favouring one or another mechanism of the superconductivity in BPB because of qualitative difference in the H_{c2} behaviour for the models under consideration.

The experiments were carried out on BPB monocrystals with x=0.3 manufactured by spontaneous crystallization from the melt of BiO_3-$BaCO_3$-PbO.

The pressure up to 2.0 GPa at liquid helium temperatures exerted in a nonmagnetic cell with fixed pressure. The measurements were carried out by the inductive method. Synchroneous detecting was performed both on the first and the second harmonics of modulation frequency.

The results obtained are shown in figure where T_c as a function of pressure determined from 0.9 (I) and 0.I (2) level of the beginning and the end of superconductive transition and $H_{c2}(4.2K)$ as a function of pressure (3) are represented. As follows from the figure all this relationships are of decreasing character. The logarithmic derivative is $d\ln T_c/dp = (-6.3\pm0.5)\cdot10^{-I}GPa^{-I}$. Measured change of H_{c2} under pressure ($\Delta H=-0.22$ T for p=2.0 GPa) has a sign different from a sign corresponding to the model of localized pairs.

Thus, investigation of superconducting monocrystals of BPB compound under pressure leads to the conclusion that the change in their properties is inconsistent with the model of localized pairs. The anomalous behaviour of some superconductive characteristics must be explained by considering the specific properties of BCS mechanism of superconductivity in material investigated.

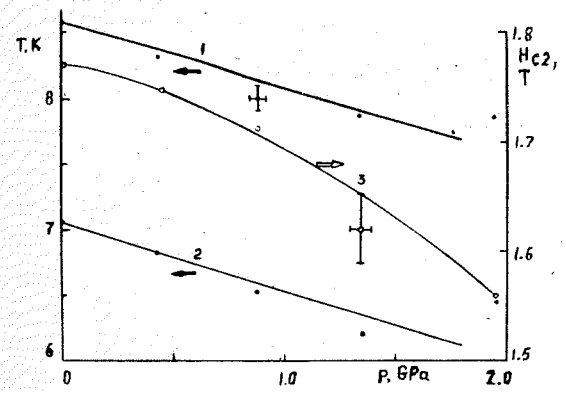

Pressure dependence of T_c and H_{c2}.

References

I. Bulaevskii L.N., Sobyanin A.A., Khomskii D.I. Superconductive properties of systems with local pairs/In: All-Union Conference Lt-23, paper abstracts, part I, p.268-269, Tallin, I984.

2. Kulic I.O. On superconducting glasses /Preprint FTINT 38, I984, 32-84, Kharkov.

3. Chu C.W., Huang S., Sleight A.W. Hydrostatic pressure effect on T_c of $Ba_{0.9}K_{0.I}Pb_{0.75}Bi_{0.25}O_3$ / Solid St.Comm.- I976.- I8, 8.- P.977-979.

4. Moyzhes B.Ya., Drabkin I.A. Superconductive materials with electron pairs, localized on lattice ions/Fiz.Tverd.Tela - I983. - 25, 7. - P.I974-I982.

THE METHOD OF DIELECTRIC-TO-METAL AND SUPERCONDUCTING TRANSITIONS INVESTIGATION USING "ROUNDED CONE - PLANE ANVIL" APPARATUS WITH PRESSURE MEASUREMENTS ON RUBY SCALE

V.B.Begoulev, Yu.A.Timofeev, B.V.Vinogradov, E.N.Yakovlev

L.F.Vereschagin Institute for High Pressure Physics of the USSR Academy of Sciences, Troitsk, USSR

The method of investigation of dielectric-to-metal phase transitions and superconductivity of high-pressure phases with simultaneous pressure measurements on ruby scale within the temperature range of 4.2÷300 K was described. The value of superconducting transition pressure of SnTe was determined (22 GPa). The superconductivity of GeTe was discovered at a pressure higher than 44 GPa.

In our experiments the "rounded cone - plane anvil" apparatus was used. The sample preparation procedure was similar to that used in /1/. The powder (the size of grain 1-5 μm) of substances (SnTe, GeTe) was deposited on a flat surface of carbonado anvil out of ethanol suspension. The thickness of the powder layer was 20-30 μm (Fig.1). The diamond-carbonado is electroconductor and fulfils the contact with the sample. The second electrocontact with the sample was fulfilled by means of metallic film 0.1 μm of silver obtained by vacuum evaporation over ruby powder (the size of grain 1-2 μm) which had been deposited out of ethanol suspension on the rounded cone anvil.

The anvils were loaded by hydraulic press and fixed by the clamp. The clamp with the anvils was placed into a helium cryostat. This construction of cryostat gives the possibility of scanning the temperature time after time within the range of 4.2-300 K. The "inverted" Dewar system /2/ was used for temperature regulation (Fig.2).

The pressure values were determined by the measurement of R_1-line shift of ruby. It was shown in /3/ that the derivative $d\lambda/dp$ of R_1-line shift is practically constant within the temperature range of 4.2-300 K. Because of this fact we used the ruby scale of /4/ at helium temperature taking into account the R_1-line shift at the decrease of temperature from 300 K to 4.2 K at atmospheric pressure.

Pressure measurements at different points of the sample were

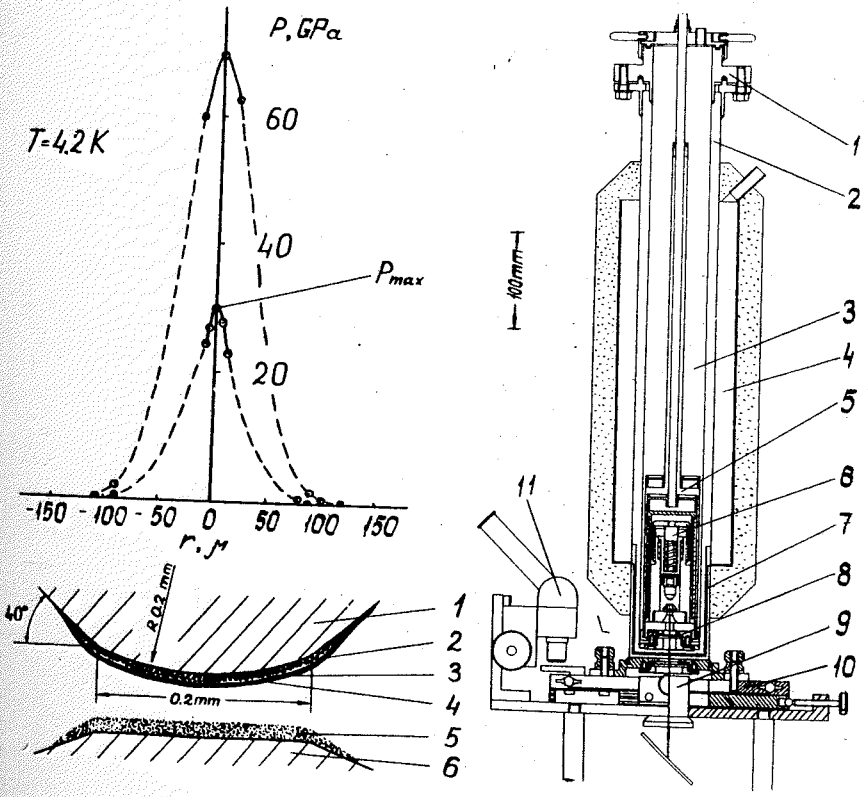

Fig.1. High pressure cell (part):
(Above) Pressure distribution in the sample at different loades.
(Below) 1 - rounded cone anvil made of "carbonado" (opaque); 2 - ruby grains; 3 - glue layer; 4 - silver film; 5 - powdered sample; 6 -flat anvil made of natural diamond (transparent).

Fig.2. Cryostat with high pressure cell:
1 - sectional flange; 2 - stainless steel tubes; 3 - liquid helium; 4 - liquid nitrogen; 5 - "inverted" Dowar; 6 - high pressure cell; 7 - heat shield; 8 - optical windows; 9 - objective; 10 -movable platform; 11 - microscope for transference measurements.

made by the cryostat with the clamp movement in the plane perpendicular to the direction of the laser beam. The cryostat was placed on a movable platform. The laser beam was directed to the objective and focused on the 10μm spot. The image of the luminous spot was projected on to the input of DFS-24 spectrometer.

Superconducting transition was determined by a resistance measurement. The temperature of the sample was taken by the "Allen Bradley" thermometer.

The compounds of the group IV-VI elements SnTe and GeTe were chosen as the objects of the research. Under ambient conditions these substances are semiconductors.

SnTe. At zero pressure SnTe has the NaCl-type structure, at 1.8 GPa SnTe undergoes the phase transition to GeS-type structure /5/. In the article /6/ it was shown that at high pressure (of unknown value) SnTe is a superconductor. The authors of /7/ observed the "GeS" → "CsCl" phase transition in SnTe at 20-25 GPa. In this connection it was of particular interest to determine the pressure of SnTe transition into superconducting state.

The resistance-temperature dependences (R(T)) at different values of maximum pressure in the anvil (P_{max}) was analysed. The analysis showed that the typical superconducting kink in the R(T) dependence of SnTe appeared at $P_{max} > 22$ GPa Fig.3. The pressure P_{max} being increased up to 50 GPa the superconductivity of SnTe remains. The comparison of the "GeS" → "CsCl" transition pressure /7/ with the pressure P_{max} of the appearance of superconductivity allowed to suppose that the superconductivity is the property of "CsCl" phase of SnTe.

GeTl. The authors of /8,9/ have studied the high pressure phases of GeTe. As well as SnTe, GeTe undergoes phase transitions at high pressure. The discovered high pressure phases of GeTe are the semiconductors. By analogy with SnTe the appearance of superconductivity of GeTe at sufficiently high pressure was expected. Fig.4. demonstrates the GeTe temperature dependences of resistance (R(T)) at different pressures P_{max}. At the pressures $P_{max} < 44$GPa the dependence R(T) has semiconducting characteristic features. At the pressures $P_{max} > 44$ GPa the dependence R(T) has the typical superconducting kink. This fact allowed us to suppose that GeTe undergoes phase transitions in the new modification with superconducting properties.

These investigations showed that the above described method makes it possible to combine the measurements of electrical pro-

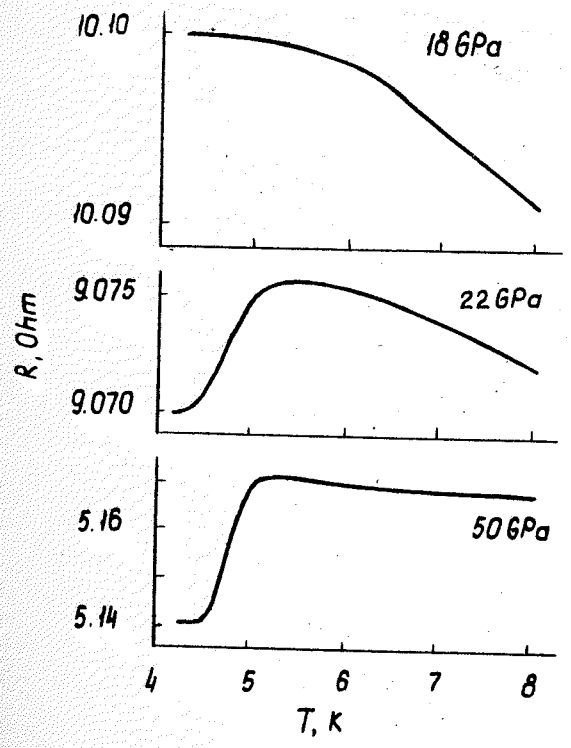

Fig.3. R(T)-dependences of sample of SnTe and anvils at different values of P_{max}.

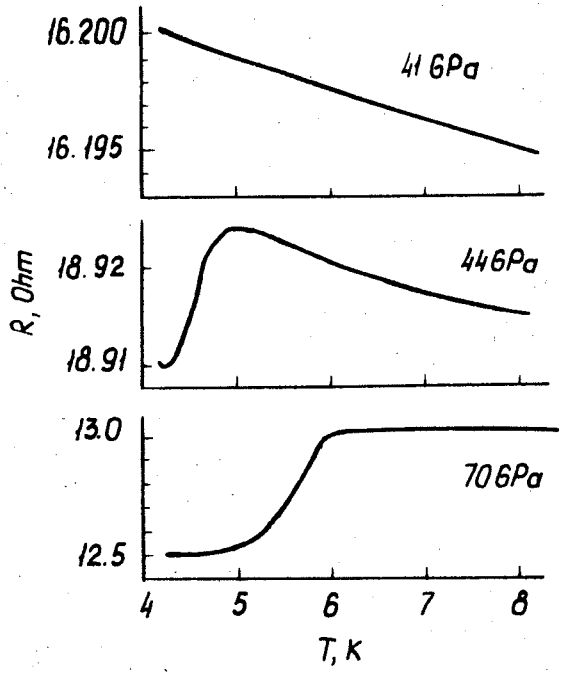

Fig.4. R(T)-dependences of sample of GeTe and anvils at different values of P_{max}.

perties of substances with pressure measurements on ruby scale and to determine the value of phase transition pressure. It would be interesting to note that at present time the information about 44 GPa phase transition in GeTe is absent. It is supposed that by analogy with SnTe the superconductivity phase of GeTe has the "CsCl" structure.

References

1. Yakovlev E.N., Vinogradov B.V., Stepanov G.N., Timofeev Yu.A. Dielectric-to-metal transitions and superconductivity of new metals. Rev.Phys.Chem. of Japan 1980, 50, 243-258.
2. Duda C.R. Liquid helium cryostat for resistance thermometer calibration. Rev. Sci. Instr.1968, 39, N10, 1484-1487.
3. Noak R.A., Holzapfel W.B. Calibration of the ruby-pressure scale at low temperatures. Proc. VIth AIRAPT Intern. High Pressure Conf., Boulder, Colorado, 1977, New York, London. Plenum press, 1979, v.1, 748-753.
4. Mao H.K., Bell P.M., Shaner J.W., Steinberg D.J. Specific volume measurements of Cu, Mo, Pd and Ag and calibration of the ruby R_1 fluorescence pressure gauge from 0.06 to 1 Mbar. J.Appl.Phys.,1978, 49, N6, 3276-3283.
5. Kabalkina S.S., Serebryanaya N.R., Vereschagin L.F. Phase transitions of IV-VI compounds at high pressures. Fizika Tverdogo Tela 1968, 10, 733-738.
6. Timofeev Yu.A., Vinogradov B.V., Yakovlev E.N., Kapitanov E.V., Kuzyan R.O. Superconductivity of SnTe at high pressure. Fizika Tverdogo Tela 1982, 24, 3143-3148.
7. Murata K., Onodera A., Fujii J., Yamaoka Y., Yagi T., Akimoto S. A new high-pressure form of SnTe. Abstracts of Intern. Symposium on Solid State Physics under Pressure. Izu-Nagaoka, Japan, 1984.
8. Kabalkina S.S., Vereschagin L.F., Serebryanaya N.R. Phase transition in GeTe at high pressure. ZhETF 1966, 51, N5 (11), 1358-1362.
9. Khvostantsev L.G., Sidorov V.A., Shelimova L.E., Abrikosov N.Kh. Phase transitions in GeTe at hydrostatic pressure up to 9.3 GPa. Phys. Stat. Sol. (a) 1982, 74, N1, 185-192.

HIGH-T_c SUPERCONDUCTING HIGH-PRESSURE PHASE IN ORGANIC METAL β-(BEDT-TTF)$_2I_3$

V.B.Ginodman[I], A.V.Gudenko[I], P.A.Kononovich[2], V.N.Laukhin[2], Yu.V.Sushko[3], I.F.Schegolev[2]

[I]Physical Institute, Academy of Sciences of the USSR, Moscow, USSR

[2]Institute of Chemical Physics, the USSR Academy of Sciences, USSR

[3]Institute of Semiconductors, Academy of Sciences of the Ukrainian SSR, Kiev, USSR

Di bis(ethylenedithio)tetrathiafulvalene thriiodide, β-(BEDT-TTF)$_2I_3$ is an organic metal drasticaly different from both BEDT-TTF salts and all organic superconductors. It's peculiarity is pressure induced phase transition from the low-T_c β-I.5 phase (T_c=I.5 K) to the high-T_c β-8 phase (T_c=7.5-8 K)/I/.

The superconducting transition shift of β-(BEDT-TTF)$_2I_3$ under pressure with a clamp cell is shown in Fig.I. The silicon-organic liquid ГКЖ-94 was used as pressure transmitting medium. Superconducting transition was detected by resistance disapearance, measured by usual 4 probe dc-method.

The pressure (P) dependence of T_c is plotted in Fig.2 (curve I). It is seen, that at moderate pressure $\sim$ I kbar the superconducting state with T_c=7.5-8 K arises. This is the highest up-to-date T_c value for organic superconductors. The attractive feature of β-(BEDT-TTF)$_2I_3$ is unusually strong pressure dependence of T_c - dT_c/dP reaches - 2 K/kbar (this value is by two orders of magnitude greater than that of conventional superconductors and at least by an order greater than that of $(TMTSF)_2X$ salts /2/). Also, the pressure dependence of room temperature conductivity β-(BEDT-TTF)$_2I_3$ is anomalous - $d[\sigma(P)/\sigma(I\ bar)]/dP$=I50%/kbar, it is from 4 to I0 times greater than that of other organic metals /2/.

The direct detection of β-I.5$\rightleftarrows\beta$-8 conversion has been carried out for the first time by the use of helium gas bomb and spring contacts /3/.

Fig. 3 shows the pressure (P) dependence of β-(BEDT-TTF)$_2I_3$ resistance (R) during pressure cycling at a number of fixed temperatures. At the beginning of each cycle the sample is in β-I.5 state. The resistance jumps correspond to the β-I.5$\rightarrow$ β-8 transition. Similar resistance jumps were observed during cooling and next warming under fixed pressure.

The transition temperature and pressure values are plotted in Fig.4 (curves I and 2). Curve I corresponds to β-8$\rightarrow\beta$-I.5 conversion during warming (off-loading). Curve 2 exhibits to formation of β-8 phase during cooling (loading). It is seen, that β-8 phase can be produced at pressures substantially lower than 0.5-I kbar reported in /I, 4/. The pressures limiting the region of β-I.5 occurence at temperatures below, say II0 K are shown by curve 3 in Fig.4.

As seen from P-T phase diagram sketch(Fig.4), the domain of β-8 phase stability is limited by lines of curves 2 and 3. The I and 2 curves are hysteresis branchs of β-I.5$\rightleftarrows\beta$-8 conversion. The hysteresis disappearence near T$\approx$I50 K, P$\approx$400 bar may indicate the change of the phase transition type. This may be due to the existence in this region of the ternary point. The one of the other lines entering this point is, for example, the superstructure phase transition (type 2) line 4 in β-I.5 state, experimentally detected by derivative dR/dT jumps at fixed pressures.

The β-8 state can exist at normal pressure also if the crystals of β-(BEDT-TTF)$_2I_3$ are obtained by thermolyses of iodine rich complex ε-(BEDT-TTF)$_2I_7$ /5/. T_c vs. P plott for two such samples (in the following β') is shown in Fig.2 - curves 2, 2' and 3, 3'. Evidently, β' crystals may also posses two superconducting state: the low and the high pressure phases.

This result can be understood if we take into account that β' crystals are mosaic with a number of misoriented twins /6/. Then one can suppose that some part of β' sample is in an ordinary β-I.5 state while another, say grain boundaries, is in β-8 state even at normal pressure /7/. This stabilization of the high-T_c β-8 state without pressurisation is obviously caused due to intrinsic stresses.

References

I. Лаухин В.Н., Костюченко Е.Э., Сушко Ю.В. и др. Влияние давления на сверхпроводимость β-(BEDT-TTF)$_2I_3$ Письма в ЖЭТФ. - 1985. - Т.41, вып.I. - С.68-70.

2. Jerome D., Schulz H.J. Organic conductors and superconductors. Adv.Phys. - I982. - V.3I, N4. - P.299-490.

3. Гинодман В.Б., Гуденко А.В., Кононович П.А. и др. Письма в ЖЭТФ. - I986.-Т.44, вып.II.- С.523-526. Прямая регистрация фазового перехода β -I,5 $\rightleftarrows$ 6-8 в триодиде ди бис(этилендитио)тетратиафульвалена - ET_2I_3.

4. Гинодман В.Б., Гуденко А.В., Засавицкий И.И., Ягубский Э.Б. Метастабильное состояние β -$(BEDT\text{-}TTF)_2I_3$ с T_c=7,5 К. Письма в ЖЭТФ.-I985.-Т.42,вып.9.-С.384-386.

5. Мержанов В.А., Костюченко Е.Э., Лаухин В.Н., и др. Повышение температуры сверхпроводящено перехода до 6-7 К при нормальном давлении в β -$(BEDT\text{-}TTF)_2I_3$. Письма в ЖЭТФ.-I985.-Т.4I, вып.4.-С.I46-I48.

6. Зварыкина А.В., Кононович П.А., Лаухин В.Н. и др. О природе высокотемпературного сверхпроводящего состояния с T_c=7+8 К и β -$(BEDT\text{-}TTF)_2I_3$. Письма в ЖЭТФ.-I986.-Т.43, вып.5.-С.257-259.

7. Кононович П.А., Лаухин В.Н., Сушко Ю.В., Щеголев И.Ф. Влияние давления на температуру сверхпроводящего перехода β -фазы иодида бис(этилендитио)тетратиафульвалена, β -$(BEDT\text{-}TTF)_2I_3$ с T_c=7,5 К. ФТТ.-I987.-Т.29, вып.3.-С.93I-934.

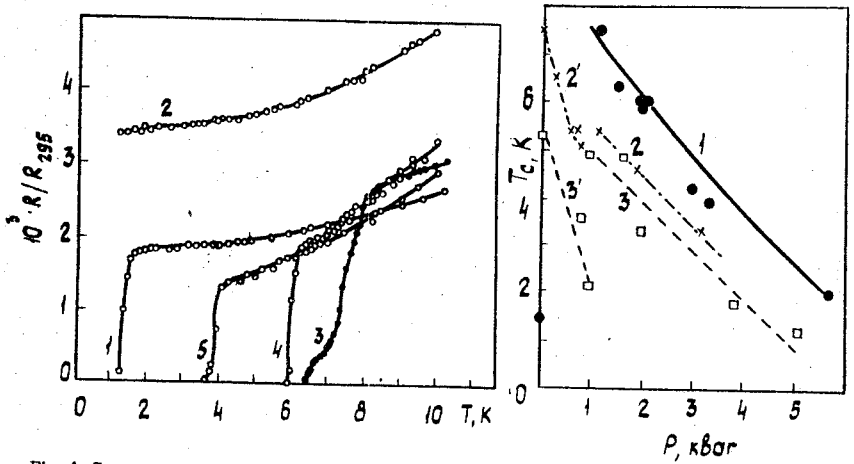

Fig.1.Superconducting transition shift in β -$(BEDT\text{-}TTF)_2I_3$ under pressure: I - P=I bar; 2 - I bar < P < I kbar; 3 - P=I.2 kbar; 4 - P=I.9 kbar; 5 - P=3.3 kbar.

Fig.2. Pressure dependence of superconducting transition temperature for β -$(BEDT\text{-}TTF)_2I_3$ samples - curve I (——) and for β'-$(BEDT\text{-}TTF)_2I_3$ samples (obtained by thermolyses of ε-$(BEDT\text{-}TTF)_2I_7$ - curves 2, 2' (-.-.-) and 3, 3' (- - -).

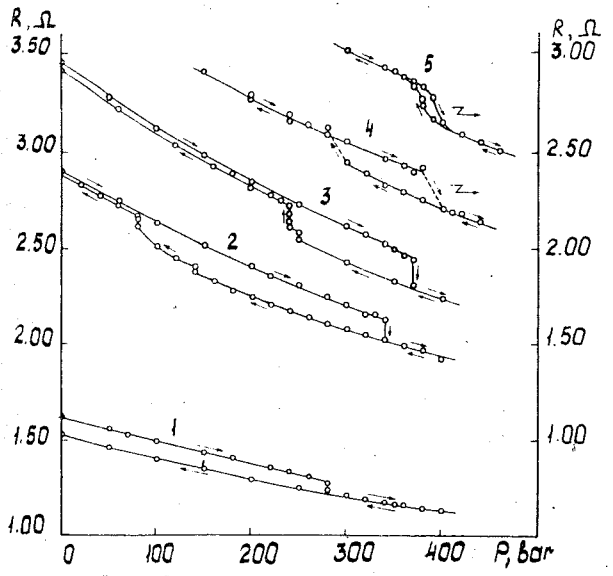

Fig.3. Pressure dependence of resistance for β -$(BEDT\text{-}TTF)_2I_3$ at a number of fixed temperatures: I - I04.5 K; 2 - I28.5 K; 3 - I36.5 K; 4 - I40 K; 5 - I5I K.

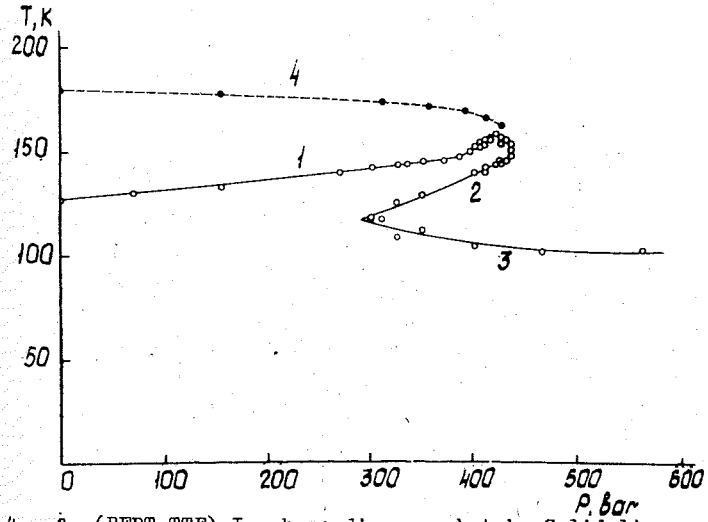

Fig.4. β -$(BEDT\text{-}TTF)_2I_3$ phase diagram sketch. Solid lines denote the boundaries of stable (curves 2, 3) and metastable (curve I) existance of high-T_c β -8 phase; dashed line 4 show line of equilibrium conversions.

EFFECT OF PRESSURE ON THE BANDSTRUCTURE AND SUPERCONDUCTIVITY

R. Asokamani, M. Rajagopalan, M.B. Suvasini, G. Subramoniam and S. Pauline

Department of Physics, College of Engineering, Anna University, Madras 600 025, India.

The aim of this paper is to explain the experimentally observed pressure induced superconductivity in some of the elemental solids based on bandstructure studies. The superconducting transition temperature (T_c) of most of the solids decreases when they are subjected to high pressures. The interesting aspect which is discussed here is with regard to the materials which become superconductors when they are subjected to high pressures. It has been experimentally observed that the trivalent as well as most of the divalent metals which are not normally superconductors become superconductors under high pressure and their T_c values increase with pressure [1]. It is more interesting to note that even non-metals such as Si and P become superconductors under high pressure. The sequence of structural phase transitions, the phenomenon of metallization of non-metals as well as the trends in T_c values as a function of pressure of the above materials have been reviewed by Jayaraman [2].

Electronic Structure and T_c Calculation

The superconducting behaviour exhibited by solids like Li, Ba, Lu and Si is explained here by performing their bandstructure calculations. Apart from the above mentioned metals, pressure induced superconductivity has been investigated in Sc and Y also. The bandstructure methods used are the Augmented Plane Wave (APW) method, its relativistic version (RAPW) and the Linear Muffin-tin Orbital (LMTO) method. To determine T_c of a solid at a

given pressure, the bandstructure results such as the Fermi energy (E_F), the density of states at the Fermi energy $N(E_F)$ as well as the phase shifts are required. The first and the foremost requirement to do the bandstructure is to know the crystal structure at the given pressure, which can be obtained from high pressure - low temperature x-ray diffraction studies. In the absence of such experimental data, the equation of state for solids have been used to determine the volume changes.

The superconducting transition temperature is determined uisng McMillan's formula,

$$T_c = \frac{\theta_D}{1.45} \exp\left[\frac{-1.04\,(1+\lambda)}{\lambda - \mu^*\,(1+0.62\lambda)}\right] \qquad (1)$$

The electron-phonon coupling constant λ is given by

$$\lambda = \frac{N(E_F)\,\langle I^2\rangle}{M\,\langle \omega^2\rangle} \qquad (2)$$

The electron-electron interaction constant μ^* can be expressed in terms of $N(E_F)$. θ_D is the Debye temperature. M is the atomic mass and $\langle\omega^2\rangle$ is the average of the square of the phonon frequency. $N(E_F)\,\langle I^2\rangle$ contained in the expression for λ is calculated using the Gaspari-Gyorffy formula [3], which is made up of the bandstructure outputs such as the Fermi energy E_F, the density of states at the Fermi energy $N(E_F)$ and the scattering phase shifts δ_0, δ_1, δ_2 and δ_3.

Effect of Pressure on the Phonon Frequency

To explain the variation of T_c with pressure the electronic structure is repeated as a function of pressure or in other words by changing the lattice constants. Neither first principle phonon bandstructure calculation nor

experimental information regarding the behaviour of phonons as a function of pressure is available. Hence in most of the calculations which attempt to explain the variation of T_c with pressure $\langle\omega^2\rangle$ is kept as a constant. But in reality it increases with pressure and its variation, even if it is very small cannot be ignored as it enters into the exponential of equation (1) through λ.

One of the salient features of the present work is that a simple procedure has been adoptd to determine the variation of $\langle\omega^2\rangle$ with pressure by studying the variation of Gruneisen parameter with pressure. The Gruneisen parameter is defined as

$$\gamma_G = - \frac{d \ln \langle\omega^2\rangle^{1/2}}{d \ln V} \qquad (3)$$

This procedure was used to study the variation of $\langle\omega^2\rangle$ as a function of pressure in the case of lanthanum [4]. The existing theoretical relations were used to study the pressure dependence of γ_G. This together with the knowledge of the volume change with pressure was used in (3) to determine the variation of $\langle\omega^2\rangle^{1/2}$ with pressure. The results obtained are given in Table 1. From the table it can be seen that the T_c values calculated by us using the above procedure are very close to the experimental values than that of Pickett et al [5] wherein $\langle\omega^2\rangle$ was kept constant. The considerable variation in the value of $\langle\omega^2\rangle$ and hence its effect of T_c from Table 1 emphasizes the importance of studying the effect of pressure on the phonon spectrum and its inclusion in the determination of T_c. The above procedure should work well as long as there is no structural transition.

Superconducting Behaviour under Pressure

Bandstructure calculations were performed for a series of pressures for the metal Lu whose electronic configuration is $5d^1\ 6s^2$. RAPW method was used to do the bandstructure calculation. The effect of pressure on the phonon

Table 1. PHONON FREQUENCIES AND T_c

Pressure (kbar)	$\langle\omega^2\rangle^{1/2}$ (K)	λ	T_c (K)		
			Pickett et al	Present work	Experiment
50	95.60	1.55	11.6	10.28	10.0
120	105.19	1.62	14.5	11.8	11.6

frequency was incorporated as was discussed in the previous section. The theoretical calculation [6] is able to explain the experimental trend viz. that T_c shows a gradual increment with pressure.

It was observed by Lin and Dunn [7] that Li shows a sudden drop in its electrical resistance at high pressure and this was attributed to the onset of superconductivity. The bandstructure calculation was performed by APW method at 247 kbar pressure since the crystal structure as well as the cell volume were known for this pressure. As Li is not a transition metal, the reduced form of the Gaspari-Gyorffy relation was used to calculate λ. The calculated value of T_c is 11.03 K [8] whereas the predicted value is 7 K.

Si when subjected to high pressures undergoes a series of structural transitions. It exhibits loss of covalency and metallisation under pressure. In the metallic state Si becomes a superconductor and has a maximum T_c of 8.2 K at 152 kbar. Recent x-ray diffraction study of Olijnyk et al showed that Si transforms to the hcp phase at 430 kbar. The bandstructure calculation was done at this pressure using the measured lattice constants. As Si has sp configuration $\langle I^2\rangle$ was calculated using the expression

$$\langle I^2\rangle = 2\, K_F^2 \left(\tfrac{2}{3} E_F\right)^2 \langle V^2\rangle \qquad (4)$$

which is based on pseudopotential formalism. The theoretically calculated value of T_c is 9.06 K whereas the experimental value is 10.0 K [9].

For Ba, pressure induced superconductivity was studied using the LMTO method. The electron-phonon matrix element can be written as

Table 2. 'd' PHASE SHIFTS AT THE FERMI ENERGY AND 'd' ELECTRON NUMBER

Pressure (kbar)	E_F (Ryd)	$\delta_2(E_F)$	Z_d
0	0.455	0.344	1.00
36	0.488	0.357	1.13
103	0.546	0.384	1.22
157	0.597	0.406	1.29
191	0.627	0.418	1.33
230	0.654	0.429	1.36

$$M_{\ell,\ell+1} = -\phi_\ell(E_F)\,\phi_{\ell+1}(E_F)\,\{(D_\ell(E_F) - \ell)\,(D_{\ell+1}(E_F) + \ell + 2) + [E_F - V(S)]\,S^2\} \quad (5)$$

The superconducting transition temperature is calculated using the McMillan's formula and the calculated value of T_c is 84 μK at 40 kbar and Ba just starts superconducting.

s → d Electron Transfer

Wittig proposed that the mechanism which is responsible for pressure induced superconductivity is the increase of d-electron population because of pressure. In the case of Lu, the Friedel sum rule was used to calculate the d electron number Z_d which is given by

$$Z_d = \frac{10}{\pi}\,\delta_2(E_F) \quad (6)$$

Table 2 gives the Fermi energy, the d phase shift and the d electron number as a function of pressure. In the case of Ba, the use of LMTO method directly gives the distribution of 5 s^2 electrons into s, p, d and f like contributions for 0 and 40 kbar pressure (Table 3) [10]. The fact that the d-electron contribution increases as a function of pressure as observed from Tables 2 and 3 confirms Wittig's prediction of s → d electron transfer to promote superconductivity.

According to Hopfield, the sign of dT_c/dp is decided from the value of γ_G. This has been tested and found to be true for small pressures. But it is not clear at this stage whether this criterion will work at high pressures. For instance, in the case of La, dT_c/dp is positive to start with and becomes negative at higher pressures.

Table 3. PARTIAL DENSITIES OF VALENCE ELECTRONS

Pressure (kbar)	E_F (Ryd)	s, p, d and f distribution			
		s	p	d	f
0	0.294	0.755	0.354	0.864	0.028
40	0.409	0.631	0.257	1.064	0.049

References

1. J.Wittig, Superconductivity in d and f band metals (Plenum, New York) 1982.
2. A.Jayaraman, Proceedings of 4th International Conference on shockwaves in condensed matter, held at Spokane, Wash, 1985.
3. G.Gaspari and B.L.Gyorffy, Phys.Rev.Lett 29, 801 (1972).
4. R.Asokamani, M.Rajagopalan, M.B.Suvasini and V.Sundararajan, Physica 138 B, 94 (1986).
5. W.E.Pickett, A.J.Freeman and D.D.Koelling, Phys.Rev.B22, 2695 (1980).
6. R.Asokamani, M.Rajagopalan, M.B.Suvasini and V.Sundararajan, Phys.Rev.B33, 7556 (1986).
7. T.H.Lin and K.J.Dunn, Phys.Rev.B33, 807 (1986).
8. M.Rajagopalan, R.Asokamani, N.Vasavi and G.Subramoniam, J.Low.Temp. Physics, 66, 169 (1987).
9. M.Rajagopalan, N.Vasavi, G.Subramoniam, V.Sundararajan and R.Asokamani, High Temperatures - High Pressures, 18, 389 (1986).
10. G.Subramoniam, V.Sundararajan, M.Rajagopalan, N.Vasavi and R.Asokamani, V International Conference on Valence Fluctuations (In Press).

INFLUENCE OF PRESSURE ON ELECTRON SPECTRA OF METALS AND SEMICONDUCTORS

E.S.Itskevich, S.L.Bud'ko, A.G.Gapotchenko, V.F.Kraidenov
Institute of High Pressure Physics, the USSR Academy of Sciences, Troitsk, USSR

I. We have already reported the results of direct observations of electron-topological phase transition (ETT) in cadmium /I/. The appearance of new dHvA-frequencies corresponding to the Fermi surface (FS) change, i.e.restoring of folding of hole "monster" and electron "needle" appearance is observed under pressure. In this report we are going to enlarge on the ETT consequences study in cadmium - on the advent of anomalous electronic features in transverse magnetoresistance and thermoelectric power.

As with the FS variations its topology changes, the $\rho_{xx}(H)$ dependence must alter its behaviour. $\rho_{xx}(H)$ measurements were conducted at I.6-4.2 K in the field up to 8 T at pressure up to 2 GPa /2/. Square dependence for $H \parallel [000I]$ and $I \parallel [II20]$ orientations at pressure below I.6 GPa and its trend towards saturation thereabove were observed. At $H \parallel [II\bar{2}0]$ and $I \parallel [000I]$ - $\sim H^2$ dependence existed within the whole range.

Thermoelectric power (E) was measured within the range of 4-300 K at a pressure up to 3 GPa by means of methodics /3/. The results are presented in Fig.I. The specimen's axis is $\parallel [000I]$. The general behaviour of the curves E(T) within the range of I0-300 K at a pressure up to 2 GPa is similar, presenting a maximum at $T \approx 30$ K, wide minimum at 70-I20 K and then a rise up to 300 K. The maximum is caused by the phonon drag and is related to the hole part of the FS in the first Brillouin zone. As pressure grows ($p > 2$ GPa) the maximum disappears due to the decrease of the said part and the revealed growth of the diffusive contribution in comparison with the phonon one. Appearence of the positive maxima at $p > 2$ GPa at T=4.7 K we related to the connection of the waists of monster as it occurs in Zn at p=0 /4/. At $T < 6$ K maximum of thermoelectric power in E(p) relationship is observed which is due to ETT and is in accordance with /2/ and theory.

2. ETT in rhenium was not observed by direct methods. There were some data on the nonlinear pressure dependence of T_c of

transition to superconducting state with $(d\Delta T_c/dp)^{max}_{nonlin.}$ at p=I.2 GPa and the anomaly of thermoelectric power was also seen at p=I.3 GPa.

dHvA-measurements at a pressure up to 2.5 GPa and the calculation of the FS by LMTO-method were conducted /5/. The measurements were carried out in the field up to 8 T at I.7-4.2 K for the field orientations along the basic crystallographic axes for closed parts of the FS in the 5^{th}, 6^{th}, 7^{th} and 8^{th} zones (h_5, h_6, h_7 - point L and h_8 - point Γ).

The obtained results are listed in Table I. All the measured frequencies (F) were observed within the whole pressure range without any deviations from the linearity F(p). No new frequencies were noted. The pressure derivatives of frequencies (PD = =d lnF/dp) are small and are in agreement with the known ones at low pressures. A large effective mass of quasi-particles on appearing part of the FS may serve as a possible reason for a fail to detect any new frequencies.

Table I. dHvA frequencies and their PD for FS of rhenium

Zone	Field direction	F, T	PD·I0^3 GPa^{-I}
h_5	I0$\bar{I}$0	78.2	II
	II$\bar{2}$0	9I.0	8.4
h_6	I0$\bar{I}$0	I650	I3
	II$\bar{2}$0	I490	34
	000I	I580	5
h_7	I0$\bar{I}$0	64I0	7
	II$\bar{2}$0	6750	2I
h_8	I0$\bar{I}$0	6630	20
	000I	4900	I4

Self-consistent calculation /5/ gave a band structure, FS and density of states at various values of lattice constants, gives true values of PD for T_c and for dHvA frequences. Spin-orbit interaction was not taken into account that did not allow to receive a detailed topological picture of the FS intersected by the AHL plane.

3. As far as indium is concerned the ETT was not observed directly either. PD for the FS in indium obtained by dHvA measurements of the electron β-arms in the 3^d zone maximal cross-section and the hole part sections of the FS in the 2^d zone at a pressure up to ~ 0.6 GPa are presented in /6/. The appearance of nonlinear component of $T_c(p)$ in In was interpreted as a consequence of ETT.

dHvA spectrum in indium is studied for four orientations of the magnetic field at a pressure up to I.5-2 GPa. dHvA frequencies connected with β-arms were observed for all orientations. The results (PD) are listed in Table 2, they are in agreement with data /6/. No anomalous behaviour of dHvA frequencies and no trace of the new ones have been seen.

Table 2. Pressure derivatives of dHvA frequencies of FS of indium in 3-d zone

Direct.of H	II0	I00	III	0II
PD, GPa^{-I}	72	74	70	68

4. There is a sound foundation to expect ETT in gadolinium. Extrapolation to zero of pressure dependence of dHvA frequency F_t=53 T measured in /7/ up to pressure of 0.4 GPa gives p_{ETT} = = 0.8 GPa. The FS possessing a number of features common with other rare earth metals and ittrium has essential differences. In a ferromagnetic state the central columns in the $3^d\uparrow$ and the $4^{th}\uparrow$ subzones and the electron many-folding ring of the ΓMK plain in the $3^d\downarrow$ subzone remain from the hole column with "webbing" appropriate to the paramagnetic state. They produce the dHvA frequencies of $(I+7)\cdot I0^3$ T. The existence of low frequencies may be explained in case we suggest that the FS saves a part of webbing in the AHL plain in subzone $3\downarrow$ near point H and the level $4\downarrow$ touches up on the Fermi level in that point.

We studied the transverse magnetoresistance in Gd on the samples with at I.7 K in the field up to 7 T with $H \parallel [000I]$ and $I \parallel [II\bar{2}0]$ and with $H \parallel [II\bar{2}0]$ and $I \parallel [I0\bar{I}0]$ orientations. The curves obtained at a pressure up to I.3 GPa are presented in Fig.2. We have revealed some qualitative changes of $\rho_{xx}(H)$ dependence at p > 0.6 GPa for both samples (the appearance of clearly seen extrema). We consider the magnetoresistance extrema to be attributed to ETT.

References

I. Itskevich E.S. The effect of the high pressure upon electron structures of metals and semiconductors / In:High Pressure in Science and Technology, Proc. 9th AIRAPT Conf., Albany, N-Y, USA, I983, part I, p.33I-340.

2. Bud'ko S.L., Gapotchenko A.G., Itskevich E.S. Magnetoresistance of cadmium in the region of electron-topological transition /Fiz.Met.Met. - I986. - 62, I. - P.76-78.

3. Bud'ko S.L., Gapotchenko A.G., Itskevich E.S., Kraidenov V.F. Measurement of the thermoelectric power of metals at low temperatures under the pressure /Prib.Tech.Exper. - I986.- 5. - P.I89-I90.

4. Rowe V.A., Schroeder P.A. Thermopower of Mg, Cd and Zn between I.2 and 300 K /J.Phys.Chem.Solids. - I970.-3I, I. -P.I-8.

5. Bud'ko S.L., Vinokurova L.I., Gapotchenko A.G., Itskevich E.S., Kulatov E.T., Pomirchi L.M. Investigation of the Fermi surface of rhenium under pressure /Preprint IOFAN SSSR, 7I, I985,Moscow.

6. O'Sullivan W.J., Schirber J.E., Anderson J.R. Fermi surface of In under hydrostatic pressure /Solid St.Comm. - I967. - 5, - P.525-527.

7. Schirber J.E., Schmidt F.A., Harmon B.N., Koelling D.D. Effect of pressure on the Fermi surface and band structure of ferromagnetic Gd /Phys.Rev. B. - I977.-I6.-P.3230-3233.

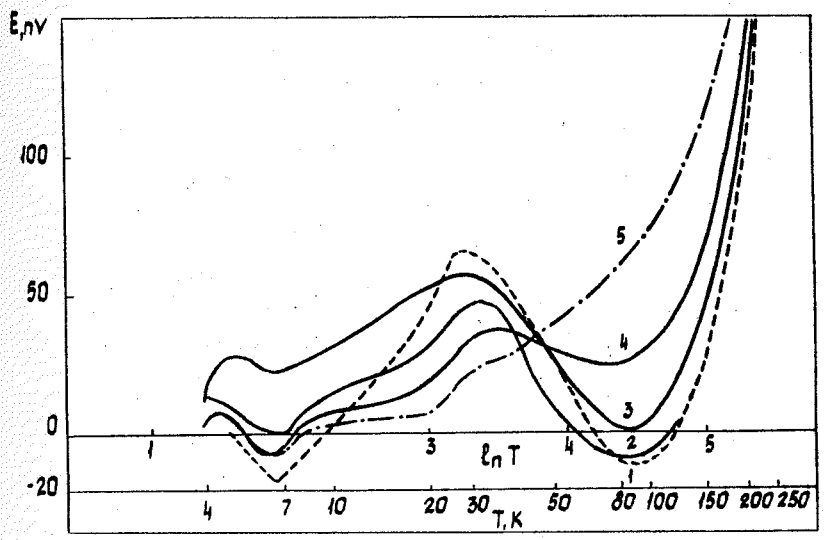

Fig.1. Temperature dependence of thermoelectric power in Cd (along [0001] direction) in pressure range 0-3.0 GPa: 1 - 1.0 GPa; 2 - 1.25 GPa; 3 - 1.6 GPa; 4 - 2.0 GPa; 5 - 3.0 GPa.

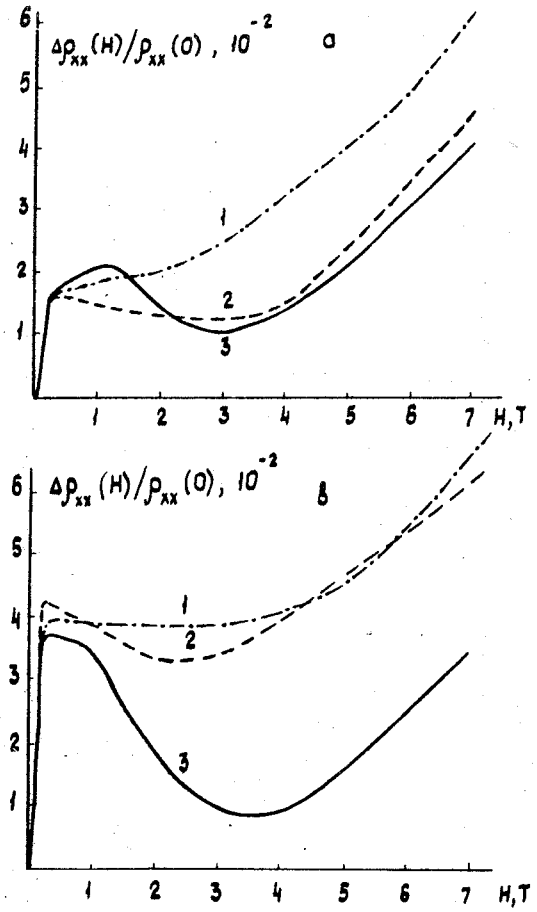

Fig.2. Field dependence of transverse magnetoresistance of Gd under pressure:
I - 0.I GPa; 2 - 0.55 GPa; 3 - I.I GPa; a) $I \parallel [II\bar{2}0]$, $H \parallel [000I]$, b) $I \parallel [I0\bar{I}0]$, $H \parallel [II\bar{2}0]$.

PRESSURE INDUCED ELECTRONIC AND STRUCTURAL TRANSFORMATION IN BULK SEMICONDUCTING AMORPHOUS Tl-Se ALLOYS

G. Parthasarathy*, S.Asokan, G.M.Naik
Instrumentation and Services Unit, Indian Institute of Science, Bangalore - 560012, India

*Present address
Fachbereich Physik, Universität-GH-Paderborn, Postfach I6 2I, D-4790 Paderborn, Federal Republic of Germany

Abstract

The electrical resistivity of bulk semiconducting amorphous Tl_xSe_{100-x} alloys with $0 \leq x \leq 25$ has been investigated up to a pressure of I4 GPa and down to liquid nitrogen temperature by use of a Bridgman anvil device. All the glasses undergo a discontinuous pressure induced semiconductor-to-metal transition.

I. Introduction

Many years ago Ferrier, Prado and Anseau (I972) have studied amorphous Tl-Te films and discovered drastic variations of the electrical conductivity and its activation energy as a function of composition. The dc conductivity measured at liquid nitrogen temperature suggested that the material changed nine times from metallic to semiconducting behaviour, with the latter occuring at compositions $T_{em}Tl_2$ for m=I, 2...7 as well as at Te_2Tl_3 and Te_5Tl_3. Paesler (I976) has studied the compositional dependence on optical edge, thermo power of amorphous Te-Tl films. Paesler (I976) observed that the width of the pseudo-gap was relatively constant over a range of compositions in which the conductivity had passed through two maxima and minima. However, it is interesting to note that the Tl-Se system do not exhibit such a drastic variations of the thermal and electrical properties as a function of composition (Cervinka and Hraby I979, Parthasarathy, Naik and Asokan I987). In this paper we report our electrical resistivity measurements on bulk amorphous Tl_xSe_{100-x} alloys as a function of pressure, temperature and composition.

2. Experimental

The preparation and characterization of the Tl_xSe_{100-x} glasses have been discussed in detail by Parthasarathy et al. (1987). High pressure electrical resistivity measurements were carried out in a Bridgman anvil system, described by Bandyopadhyay, Nalini, Gopal, Subramanyam (1980). The temperature range of investigation was limited at the low temperature region, because of the high resistance of the samples especially at low pressures.

3. Results and discussions

The variations of the electrical resistivity as a function of pressure for Tl_xSe_{100-x} glasses are summarised in Figure I. All the glasses exhibit negative pressure coefficient of the electrical resistivity, which is the general behaviour of chalcogenide semiconducting glasses (Parthasarathy and Gopal 1985). The effect of pressure on the refractive index (n) and the absorption edge (E_o) of many chalcogeride glasses has been studied by Kastner (1972) up to 0.2 GPa pressure. It is found that $\frac{1}{n}(\frac{dn}{dp})$ is positive for all the glassy chalcogenides, SiO_2 (Vedam and Davis 1967), and the other glassy materials containing chalcogens (Parthasarathy and Gopal 1985). The local field corrections appear to be responsible for a positive($\frac{dn}{dp}$). It is interesting to note that for tetrahedrally bonded Ge-class amorphous materials ($\frac{dn}{dp}$) is negative (Connell and Paul 1972, Minomura 1982). The pressure coefficient of resistivity mainly depends upon the pressure coefficient of the absorption edge (dE_o/dp). The effect of pressure on the chalcogenide glasses is only on the mushy interaction volume, to force the closed shells closer together without affecting the covalent bond lengths. The closed shell interactions result in a band broadening with a decrease in E_o with pressure (Kastner 1973). Thus the negative pressure coefficient of the electrical resistivity of chalcogenide glasses is understood qualitatively. However, a quantitative analysis of the pressure dependence on the electrical resistivity ot these glasses is complicated, because, the electrical resistivity is not only determined by the gap but also by the mobility, density of states near Fermi level and the position of the Fermi level (Mott 1987).

It is interesting to note that Tl_xSe_{100-x} glasses undergo a discontinuous pressure induced semiconductor-to-metal transition (Fig.1). The value of the electrical resistivity of the high pressure phase lies in the range of 100 to 1000 $\mu\Omega$.cm. The temperature coefficient of the samples in the metallic phase values from 0.80 $\mu\Omega.cm\ K^{-1}$ for Tl_5Se_{95} sample to 10.52 $\mu\Omega \cdot cm\ K^{-1}$ for $Tl_{25}Se_{75}$ sample. The transition pressure decreases with Tl content. The variation of dc conductivity as a function of temperatures obeys the Arrhenius relation

$$\sigma = \sigma_o \exp\ (- \Delta E/kT)$$

where σ_o ($\Omega^{-1}\ cm^{-1}$) is the pre-exponential factor; ΔE = the activation energy for electrical conduction; k = Boltzmann constant, T = temperature.

The variation of the conductivity activation energy in Tl_xSe_{100-x} glasses as a function of pressure is shown in Fig.2. All the samples exhibit a negative pressure coefficient of the conductivity activation energy. The value of the optical gap of chalcogenide glasses, decreases with pressure at a rate between -0.1 and -0.2 $ev \cdot GPa^{-1}$ (Kastner 1972). This range would be in agreement with our electrical measurements shown in Fig.2, because the conductivity activation energy ΔE and the optical gap E_o of most chalcogenide glassy semiconductors are related approximately as $-\Delta E = \frac{E_o}{2}$, which assumes that the Fermi level is near the center of the gap. This decrease of the gap is accompanied by an increase in the refractive index hence the dielectric constant, which further tends to decrease the localization of gap states and promotes metallic conduction at high pressures.

The X-ray powder pattern has been taken for the samples recovered from the high pressure cell after subjected to the transition pressure. It is found that all the glasses undergo phase separation under high pressure during the semiconductor-to-metal transition. The high pressure phase has the mixtures of Se with hexagonal structure a= 0.437 nm and c = 0.495 nm and TlSe with tetragonal structure with a = 0.80 nm and c = 0.70 nm. The X-ray diffraction studies on the samples subjected to the pressure less than the transition pressure do not show any crystallinity. So the pressure induced glass-to-crystal transition occurs simultaneous with semiconductor-to-metal transition.

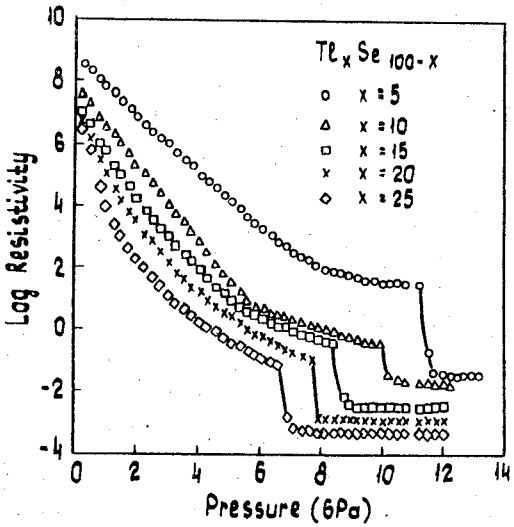

Fig.I. The variation of the electrical resistivity of Tl_xSe_{100-x} glasses as a function of pressure.

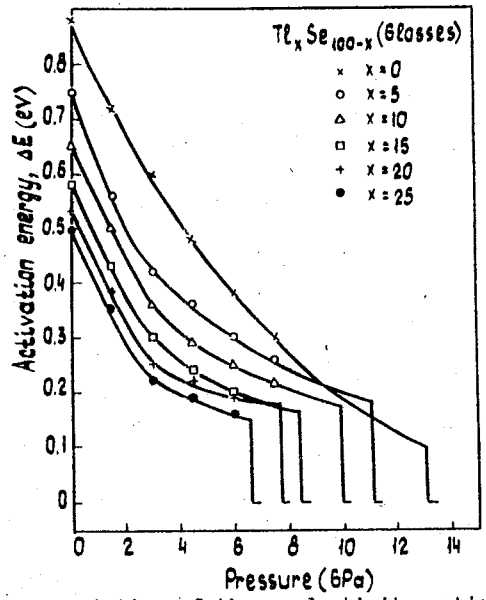

Fig.2. The variation of the conductivity activation energy of Tl_xSe_{100-x} glasses as a function of pressure.

4. Conclusion

The effect of pressure on the electrical resistivity of amorphous Tl_xSe_{100-x} alloys has been reported. It is observed that all the samples undergo the discontinuous pressure induced semiconductor-to-metal transition. The structural studies indicate that the pressure transition is also a eutectic type crystallization of the Tl_xSe_{100-x} glasses under high pressure. It is very interesting to note that the variation of electrical resistivity, activation energy for electrical conduction and the transition pressures do not exhibit any drastic behaviour as a function of Tl content, as observed in Tl_xTe_{100-x} alloys.

References

Bandyopadhyay, A.K., Nalini, A., Gopal, E.S.R., Subramani, S.V., 1980, Rev. Sci. Instrum., 51, 136.

Cervinka, L., and Hruby, A., 1979, J.Non-Cryst. Solids 34, 275.

Connell, G.A.N., and Paul, W., 1972, J. Non-Cryst. Solids., 8, 215.

Ferrier, R.P., Prado, J., and Anseau, M., 1972, J. Non-Cryst. Solids, 8 - 10, 798.

Kastner, M., 1972, Phys.Rev. B 6, 2273; 1973, Phys.Rev. B 7, 5237.

Minomura, S., 1980, in "Amorphous Semiconductors Technology and Devices", ed. Y.Hamakawa, ohm. North Holland, 1982, chapter 5, p.245.

Mott, N.F., 1987, "Conduction in Non-crystalline Materials", Clarendon, Oxford, p.71.

Paesler, M.A., 1976, Phys.Rev. B 13, 5578.

Parthasarathy, G., and Gopal, E.S.R., 1985, Bull.Mater.Sci. 1, 271, and the references there in.

Parthasarathy, G., Naik, G.M., and Asokan, S., 1987, J.Mater. Sci. Letts.6, 181.

Vedam, K., and Davis, T.A., 1967, J. Opt.Soc. Am. 57, 1140.

THERMOELECTRIC POWER OF ARSENIC, BISMUTH AND BISMUTH-ANTIMONY ALLOYS IN ELECTRONIC TOPOLOGICAL TRANSITIONS INDUCED BY CRYSTAL LATTICE DEFORMATION

M.Yu.Lavrenyuk, N.Ya.Minina, A.M.Savin
Moscow State University, Moscow, USSR

Electronic topological transitions (ETT) by I.M.Lifshitz /1/ which are accompanied by anomalies in the thermodynamic and kinetic characteristics of metals occur when the Fermi level shifts under the influence of some external factors (e.g. stress or doping), passing through singular points in energy spectrum E_{ci} where the Fermi surface (FS) changes its topology. There are two types of ETT: 1 - formation (vanishing) of a new FS cavity, 2 - disruption (formation) of the FS "neck". The anomaly in thermoelectric power (t.e.p.) α should be especially well-pronounced, because at T=0 K $\alpha \sim |Z|^{-1/2}$, ($Z = E - E_c$ being a transition parameter that characterizes the nearness of the Fermi level to the critical point) /2/. Under assumption of finite temperature and impurity scattering, it was pointed out that infinite singularity in α predicted in ref. /2/ was cut off by these two factors and had the form of somewhat smeared asymmetric peak.

The present paper is concerned with the complex investigation of the FS and t.e.p. in Bi, As and Bi-Sb alloys in the vicinity of ETT of different types with electron and hole cavities of the FS being under consideration. The measurements have been carried out at T = 4.2 K and the FS's extremal cross sections were determined with the help of the Shubnicov-de Haas (SdH) effect. The sign and the shape of t.e.p. anomalies were settled. Hydrostatic pressure and uniaxial stress were applied as the external parameters, that shifted the Fermi level through the singular points of energy spectrum.

I. ETT of "FS electron cavity formation (vanishing)" type have been observed in $Bi_{0.9}Sb_{0.1}$ +10^{-4} at.% Te single crystals. Doping the semiconducting $Bi_{0.9}Sb_{0.1}$ with Te-donors leads to filling of the electron extrema at L-point and to formation of a three-ellipsoid FS with Fermi energy $E_F \sim 10$ meV. Compression along the C_1 axis causes spillover of all the FS electrons into ellipsoid 1 (Fig.1a) and as a result ETT of type "3e⇄1e" realizes (here and further "e" and "h" indexes mean electron and hole FS ellipsoids). At the critical deformation $\varepsilon = \varepsilon_c = -0.15\%$ the observed cross sections of the increasing ellipsoid S_1 become stabilized and those of decreasing S_{23} fall to zero. At this point (T = 4.2 K) the t.e.p. as asymmetric peak of positive polarity (Fig.1b).

2. ETT with the formation of the hole FS cavity in the T point (3e⇄3e + 1h) has been realized in Bi + 10^{-3} at.% Te single crystals. The FS in such alloy consists of three electron ellipsoids in L, with E_{FL} = 44 meV, while the distance from the valence band top in T to the Fermi level is about 2 meV. The carrier redistribution among the L-valleys under compression along C_1 shifts the Fermi level downward, so that at $\varepsilon = \varepsilon_c = -0.1\%$ the Fermi level touches the term T and a hole FS appears. The critical point E_K is determined as that where experimental data deviate from the theoretical dependence S (ε) calculated in accordance with the McClure's model /3/ for the case when no overlap with T-term forms. At the transition point the t.e.p. has a peak of negative polarity.

3. The dumbbell-shaped electron FS disruption has been observed in monocrystalline $Bi_{0.73}Sb_{0.27}$ compressed along the twofold C_2 axis. According to Ref. /4/ L-terms inversion in $Bi_{1-x}Sb_x$ alloys at the antimony concentration X=0.04 gives rise to a saddle point (X=0.15) in the electron and hole spectra. With the further increase in X the curve for E (k) becomes two-hamp in shape and the FS assume a shape of dumbbell if the Fermi level disposes above the saddle point (Fig.2a). In the point of the dumbbell disruption maximum FS cross sections should decrease by a factor of two. The energy spectrum change under compression along the C_2 axis is shown in Fig.2a. In the lower part of this Figure the FC cross section S_1 slightly ($\sim 3^o$) departed from the maximum one is depicted as a function of deformation. Cross sections $S_{2,3}$ corresponds to the increasing ellipsoids and for these parts of the FS the ETT do not occur. The t.e.p. anomaly observed in the vicinity of the disruption point has a negative polarity (Fig.2b).

4. Disruption of the necks of the hole FS in arsenic was observed under uniform compression P with the help of the de Haas-van Alphen effect in ref. /5/ (P_c=0.18 GPa).

The t.e.p. measurements have been carried out in monocrystalline As along the threefold axis C_3 under high hydrostatic pressure up to P=0.6 GPa (Fig.3). Represented in Fig.3 data were obtained at T=3.5 K. The curve α/T (P) have a nonregular character. At the point P_c=0.15 GPa (that is well correlated with

the value P_c=0.18 GPa /5/) a peak of a positive polarity takes place.

Conclusion. ETT of four types, exhausted all the cases of FS topology changes, have been studied. In all cases ETT were accompanied by the t.e.p. anomaly that had a shape of a somewhat smeared asymmetric peak. A characteristic shape of the t.e.p. anomaly and its correlation with the ETT of a definite type makes it possible to use observed singularities in the t.e.p. for the band structure change investigation.

References

1. I.M.Lifshitz. Anomalies of electron characteristics in the high pressure region. - Zh.Eksp.Teor.Fiz.,1960, 38, N5, p.1569--1576.
2. V.G.Vaks,A.V.Trefilov, and S.V.Formichev. Some features of the electric resistance and thermoelectric power of metals undergoing phase transition of the 2.5 kind. - Zh.Eksp.Teor.Fiz., 1981, 80, N.4, p.1613-1621.
3. J.W.McClure. The energy band model for bismuth- Resolution of a theoretical discrepancy. - J.Low.Temp.Phys., 1970, 25, N.5 (6), p.527-540.
4. Ya.G.Ponomarev, M.V.Sudakova. The energy spectrum of $Bi_{1-x}Sb_x$ alloys.- Proc. of XII All-Union Conf. "Narrow-gap semiconductors and semimetals", Lvov, 1986, part II, p.164-166.
5. J.E.Shirber and Y.P.Van Dyke. Pressure-induced "electronic transition" in As. - Phys.Rev.Lett., 1971, 26, N.5, p.246-249.

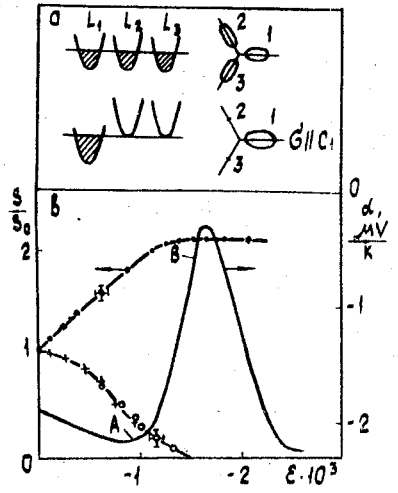

Fig.1. ETT of " 3e$_2$-1e" type in $Bi_{0.9}Sb_{0.1}$+10^{-4} at.% Te samples.

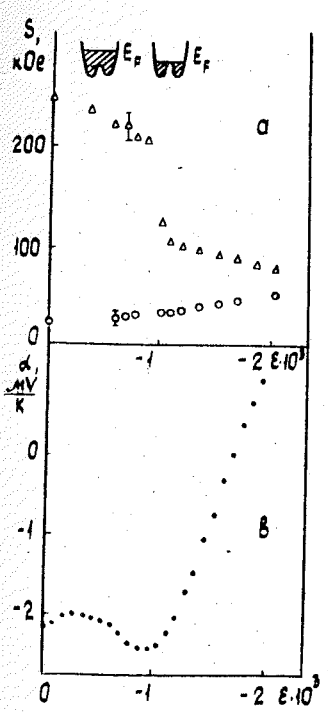

Fig.2. Dumbbell-shaped Fermi surface disruption in $Bi_{0.73}Sb_{0.27}$ samples (a) and t.e.p. singularity in the vicinity of the critical point (b).

Fig.3. T.e.p. along C_3 axis in As single crystals and relative change of the hole Fermi surface necks cross sections under hydrostatic pressure /5/.

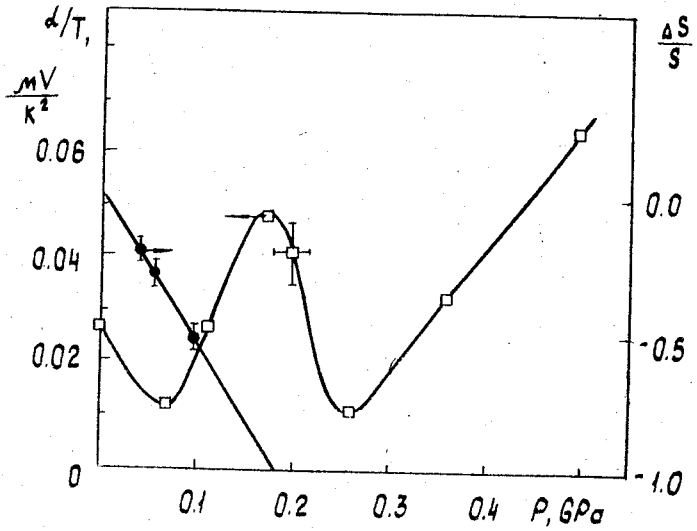

ANOMALOUS DIELECTRIC BEHAVIOR OF FERROELECTRICS CAUSED BY HYDROSTATIC PRESSURE DUE TO QUANTUM EFFECTS

E.Hegenbarth, P.Roth
Technical University Dresden, Section of Physics, German Democratic Republic

$SrTiO_3$ is a quantum paraelectric /I/. Quantum fluctuations prevent ferroelectric phase transitions (FPT). By substituting barium ions in $SrTiO_3$, that means in solid solutions of $(Ba_xSr_{I-x})TiO_3$ (BST x), there can be generated FPT /2/. The FPT-temperatures are shifted to lower temperatures by hydrostatic pressure /3/. By application of the critical pressure the FPT vanish /4/. The quantum effects dominating at low temperatures cause a nonclassic critical exponent (CE) of the electric susceptibility. We have measured the dielectric constant ε'(I.6 kHz) of polycrystalline BST 3%, 6% and 20% at different hydrostatic pressures to investigate the quantum behavior.

Figure I shows the temperature dependence of ε' of BST 3% at different hydrostatic pressures. At ambient pressure there is a FPT paraelectric-ferroelectric at the temperature $T_c(0) = 37$ K. The FPT-temperature is shifted to lower temperatures by hydrostatic pressure according to /5/

$$T_c(p) = T_c(0)\ (I - p/p_c)^{I/2}. \qquad (I)$$

At the critical pressure $p_c = 0.23$ GPa the specimen was in the quantum paraelectric state which is accompanied by a temperature independent ε' at temperatures $T \to 0$. The temperature dependence of ε' at ferroelectric above T_c is described by

$$\varepsilon' = C\ (T - T_c)^{-\gamma}. \qquad (2)$$

Usually the Curie-Weiss law is fulfilled with $\gamma = I$. Quantum statistical calculations at low temperatures yield a maximum value of $\gamma = 2$ /6/. The cross-over region between both values is marked by an increasing influence of quantum fluctuations.

The CE of our measurements was calculated by logarithmic regression of the values $\varepsilon'(T)$ with Eq.(2) within temperature intervals of about IO K. The temperature behavior of ε' with $\gamma = I$ was obtained at high temperatures $T > 100$ K and pressures $p < 0.3$ GPa.

At higher pressures $p \gtrsim 0.5$ GPa $\gamma < I$ was detected in the whole temperature range. Therefore ε' becomes more temperature independent by pressure, as it is shown in Figure I. At very high pressures the CE tends to zero.

Approaching T_c the dependence $\gamma(T)$ reaches a maximum near 50 K. At this temperature the CE was very sensitive to variations of pressure. From the dependence $\gamma(T)$ at different pressures was determined the maximum γ_M to investigate the influence of pressure on the CE. The results $\gamma_M(p)$ are plotted in Figure 2. At pressures $p \approx p_c$ we determined a strong increase of γ_M due to quantum effects. But at pressures $p > p_c$ γ_M decreases with increasing pressure. The dependence $\gamma_M(p)$ shows a sharp maximum at the critical pressure.

For the interpretation of the dependence $\gamma_M(p)$ we calculate with Eq.(2) $(\partial\varepsilon'/\partial p)_T$ under the assumption that the Curie constant C is not depending on pressure:

$$\left(\frac{\partial\gamma}{\partial p}\right)_T = \frac{I}{\ln(T-T_c)}\left[\gamma\frac{\partial T_c/\partial p}{T-T_c} - \frac{\partial \ln\varepsilon'}{\partial p}\right]_T \qquad (3)$$

The two terms in the angular brackets of Eq.(3) determine the pressure dependence of the CE. In dependence on the value of the first and the second term one gets $(\partial\gamma/\partial p)_T \gtrless 0$ at pressures $p \lessgtr p_c$ respectively. T is the temperature of the maximum of $\gamma(T)$. The sharp maximum of $\gamma_M(p)$ at the critical pressure follows from the third law of thermodynamics demanding $\lim_{T\to 0} (\partial T_c/\partial p) = -\infty$. In this case $\lim_{p\to p_c} (\partial\gamma/\partial p)_T = -\infty$ is valid. This means a change of the sign of $(\partial\gamma/\partial p)_T$ at p_c. Therefore γ_M has a maximum value at the critical pressure. A small change of pressure near the critical pressure causes a drastic change of the CE.

By plotting the reduced values of $\Delta\gamma/\gamma$ against $(p_c/p-I)^{-I}$ for $p < p_c$ one gets a relation which is not depending on the concentration x according to

$$\frac{\Delta\gamma}{\gamma} \quad \frac{\gamma_M(p) - \gamma_M(0)}{\gamma_M(0)} \approx 0.057\ (p_c/p - I)^{-I/2}, \qquad (4)$$

as it is shown in Figure 3. Inserting Eq.(I) in Eq.(4) indicates

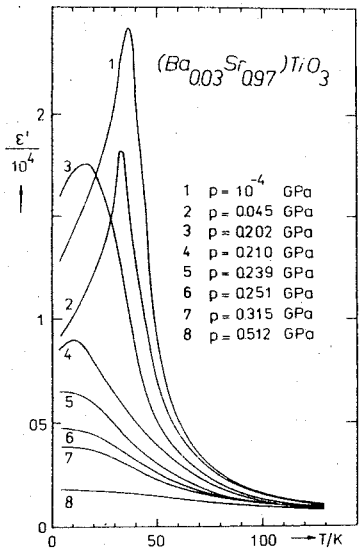

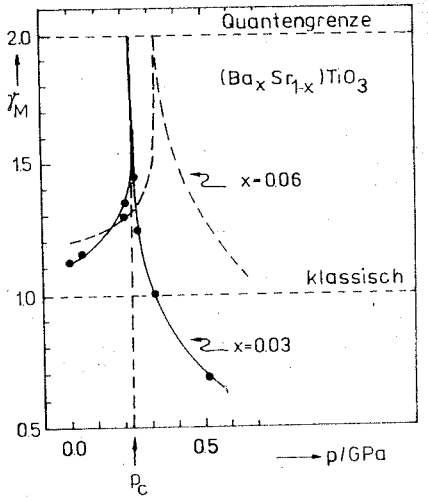

Fig.I. Temperature dependence of ε' of BST 3% at different hydrostatic pressures.

Fig.2. Pressure dependence of γ_M of BST 3% and 6%.

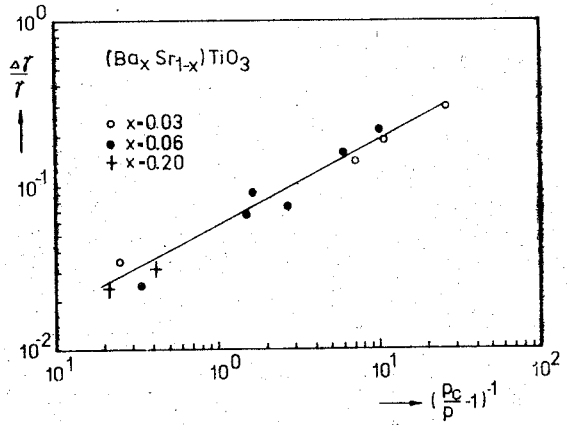

Fig.3. Reduced plot of $\Delta\gamma/\gamma$ against $(p_c/p-1)^{-1}$ for $p < p_c$.

that the pressure dependence of the CE is determined by the pressure dependence of the FPT-temperature:

$$\gamma(p < p_c) \sim \left[(T_c(0)/T_c(p))^2 - 1\right]^{1/2} . \qquad (5)$$

At pressures $p > p_c$ Eq.(I) is not fulfilled since there would arise imaginary values of T_c.

References

I. K.A.Müller and H.Burkhard, $SrTiO_3$: An intrinsic quantum paraelectric below 4 K, Phys.Rev.B (I979) Vol.I9, pp.3593-3602.

2. E.Hegenbarth, Dielektrische Untersuchungen an festen $(Ba_xSr_{1-x})TiO_3$-Lösungen im Konzentrationsbereich von x=0 bis 0.I bei tiefen Temperaturen, Phys.Stat.Sol. (I965) Vol.9, pp.I9I-200.

3. B.Pietrass and E.Hegenbarth, The influence of pressure on phase transitions at low temperatures: $SrTiO_3$ and $(Ba_xSr_{1-x})TiO_3$ Journ.of Low Temp.Phys. (I972)Vol.7, pp.20I-209.

4. G.A.Samara, Vanishing of the ferroelectricity in displacive and hydrogen-bond ferroelectrics at high pressure, Ferroelectrics (I974) Vol.7, pp.22I-224.

5. E.Hegenbarth, The influence of hydrostatic pressure on the phase transitions of some ferroelectrics, Ferroelectrics (I978) Vol.20, pp.79-86.

6. R.Morf, T.Schneider and E.Stoll, Nonuniversal critical behavior and its suppression by quantum fluctuations, Phys. Rev.B (I977) Vol.I6, pp.462-469.

ELECTRONIC SPECTRUM AND TRANSPORT PHENOMENA IN DIARSENIDE CADMIUM-TIN AT ALL-ROUND PRESSURE

M.I.Daunov, A.B.Magomedov

Institute of Physics of the Daghestan Branch of the USSR Academy of Sciences, Makhachkala, USSR

The diamond-like chalcopyrite semiconductor $CdSnAs_2$/I,2/ is representative of system II - IV - V_2 /I,2/.

A complex investigation of transport phenomena has been carried out on monocrystal $CdSnAs_2$ ($n,p \sim 10^{17}-10^{19}$ cm^{-3}) at atmospheric and hydrostatic pressure (up to I.5 GPa). The new characteristic data of the investigated concentration interval ($10^{17} \div 10^{18}$ cm^{-3}) are given in Figs.I,3 and in the Table.

For quantitative interpretation was used the triple-band Kane's model (it was being a limit case of Kildal's model and an acceptable in n-$CdSnAs_2$ /I/ as well as the known correlations for example, in /3/ and concluded in approximate of a strong electrons generation.

The magnitudes of the band parameters and baric coefficient of width exclusion band ($dE/dP = +10^{-10}$ eV/Pa) were taken from /2/.

In the investigated concentration interval at 300 and 77.6 K the unit-area resistance $\rho_0 \sim (R\sigma_0)^{-1}$ increases with growing of pressure approximately with velocity 2.5-4.5 % on 0.I GPa. The first is modified by increasing of dependence m from P with decreasing of n, the second - by lattice diffusion near the room temperature (see below). In the sample I n-$CdSnAs_2$ $(R\sigma_0)^{-1}$ increases at 77.6 and 300 K on I GPa accordingly up to 43 % and 3I % (Fig.I). The comparison of theory and experiment has shown, that the accordance takes place by the decrease ε I0 % on I GPa. It is expressed somewhat weaker than in indium antimonide /4/.

Attempts to interpretate the baric dependence of Hall mobility in the electronic impure heavily doped and heavily degenerated crystals of InSb /5/ and $CdGeAs_2$ /6/ in ε-constant approximation were unsuccesful.

Hall coefficient in the sample I n-$CdSnAs_2$ decreases with the growth of pressure (Fig.I) according to the early discovered volume-concentration effect /2/.

Theoretical analysis shows that at 77.6 K and by value of

voltage of magnetic field I5 kOe the pressure dependence of Hall factor is to be neglected and the change in Hall's potential difference V_R is defined by crystal compressibility. The value $\Delta V_R/V_R$ at 77.6 K is in agreement with early investigation /2/.

Isothermal volume compressibility χ /8/ $CdSnAs_2$ at 77.6 K is to be estimated by $\Delta V_R/V_R$. It was found that: $\chi = 3.I \cdot 10^{-11}$ Pa^{-I}.

Investigations of the classical lateral magnetic resistance $\Delta\rho/\rho_0$ at all-round pressure in n-$CdSnAs_2$ as well as n-InSb with fixation $\nu = R\sigma H$ were began in /9/.

The principal characteristics of investigated sample I n-$CdSnAs_2$ at the atmospheric pressure. Experiment and theory

T, K	-R, $cm^3 \cdot s^{-1}$	$-R\sigma_0$, $cm^2 V^{-1} s^{-1}$	α_0	$-\alpha_\infty$	$\Delta\rho/\rho_0$	$\Delta\rho/\rho_0^{\varphi}$	$\Delta\rho/\rho_0^{H}$	E_F/kT	γ_2
			$mV \cdot deg^{-1}$		$\nu = R\sigma H = 1$				
77.6	I7.24	I3600	50.4	39.6	0.0I36	0.0024	0.0II	I2.I	0.275
296	I7.28	II550	I63	I55	0.0I37	0.00I3	0.0I2	3.3	0.052

In order to analyse the experimental results on data of measurements of thermo-emf at atmospheric pressure (in vacuum) was calculated the concentration dependence of "physical" magnetoresistance $\Delta\rho/\rho_\infty^{\varphi}$ $(\nu \to \infty)$ at 77.6 and 300 K (Fig.2).

The concentration and basic dependences of $\Delta\rho/\rho_0$ are determined from parameter γ_2 at the fixed temperature and ν.

In agree with the experimental results (Fig.3) follows, that at $n > n_0$ (in point $n=n_0$ parameter $\gamma_2 = 0$) $\Delta\rho/\rho_0$ decreases ($|\gamma_2|$ decreases) with growth of pressure. At $n < n_0$ magnetoresistance increases with rising P (γ_2 as well as m are increasing). In those cases when $\Delta\rho/\rho_0 \gg \Delta\rho/\rho_0^{\varphi}$ the nonhomogeneities introduce an essential contribution into the formation of effect.

In the satisfactory approximate may be considered $\Delta\rho/\rho_0 \cong \Delta\rho/\rho_0^{\varphi} + \Delta\rho/\rho_0^{H}$.

Estimations for sample I n-$CdSnAs_2$ at 77.6 K gave $\Delta\rho/\rho_0 \cong 5\,\Delta\rho/\rho_0^{\varphi}$ at the atmospheric pressure and with pressure growth to I GPa $\Delta\rho/\rho_0$ increases by 26%, $\Delta\rho/\rho_0^{\varphi}$ - 2.3-fold and $\Delta\rho/\rho_0 = 2.8\ \Delta\rho/\rho_0^{\varphi}$.

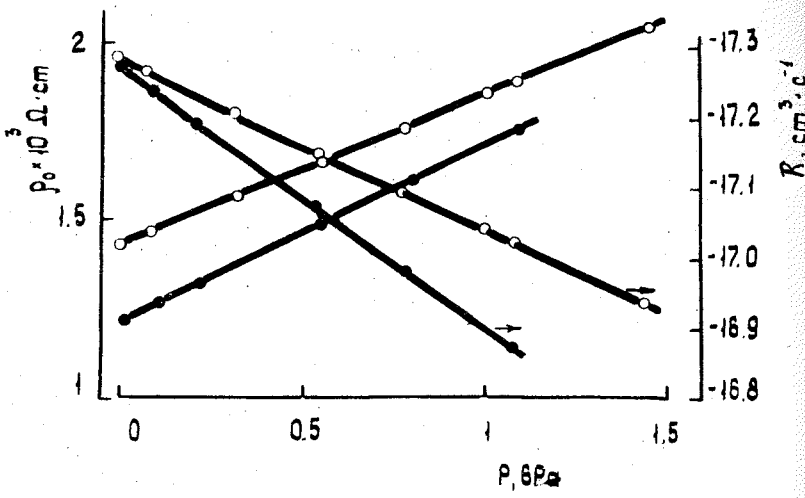

Fig.I. The baric dependences of the specific resistance ρ_o and Hall coefficient R of the sample I n-$CdSnAs_2$. The light signs - 300 K. Hall coefficient was measured at H = I5 kOe.

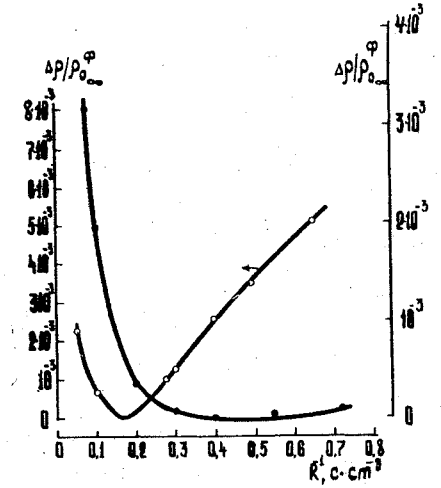

Fig.2. The concentration dependence of "physical" magnetoresistance of $\Delta\rho/\rho_{0\infty}^{\varphi}$ ($\nu \to \infty$) in n-$CdSnAs_2$. The light signs - 300 K.

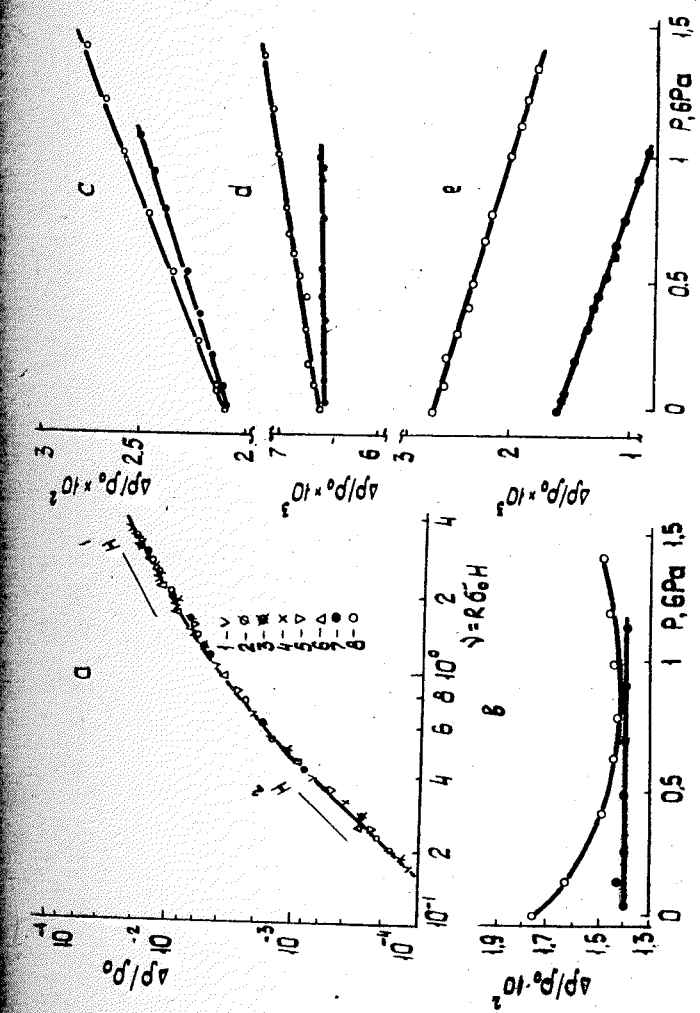

Fig.3. The baric dependences of magnetoresistance in the sample n-InSb with $n=10^{18}$ cm^{-3} (a,b) /9/ and in the samples n-$CdSnAs_2$ with $n=3.7 \cdot 10^{17}$ cm^{-3} (c), $n=1.46 \cdot 10^{18}$ cm^{-3} (d) and $n=3.43 \cdot 10^{18}$ cm^{-3} (e): a - T = 77.6 K; $P=10^{-8}$; 1 -0.33; 2 - 0.48; 3 - 1.28; 4 - 2.5; 5 - 4.7; 6 - 6.9; 7 - 8.9; 8 - 11.3; at ν: b - 2.5; c - 1.0; d - 1.0; e - 0.7. The light signs - 300 K.

References

1. Goryunova N.A., Valov U.A. Semiconductors $A^2B^4C^5_2$ - "Sovetskoe Radio", 1974 - 374 p.
2. Daunov M.I., Magomedov A.B., Ramazanova A.E. Influence of all-round pressure on energetic electrons spectrum and the kinetic properties of semiconductors II-IV-V_2. Izv.Vuzov. Physics, 1986, N 8, p.98-111.
3. Askerov B.M. Kinetic effects in semiconductors. - L.: Nauka, 1970, - 304 p.
4. Abdulvakhidov Kh.A., Volkov A.S., Galavanova V.V. Influence of all-round compression on dielectric constant of indium antimonide. //Physics and Technique of Semiconductors, 1970, p.218-182.
5. Filipchenko A.S., Nasledov D.N., Heavy doped crystals of n-type indium antimonide. Phys.stat.sol.(a), 1975, 27, N 1, p.11-26.
6. Konczewicz L., Porowski S., Polushina I.K. Influence of pressure on the resistivity and the Hall coefficient of n-type $CdGeAs_2$. High Temperature-High Pressure, 1977, 7, N 6, p.716-717.
7. Daunov M.I., Magomedov A.B., Ramazanova A.E. The volume concentration effect. Physics and Technique of Semiconductors, 1985, 19, N 5, p.936-938.
8. A.C. N 1230307 USSR, MKI 4H0 21/66. Method of determination of coefficient of the volume isothermic elastic compression of semiconductors. /M.I.Daunov, A.B.Magomedov, A.E.Ramazanova/ Discoveries inventions , 1986, -N 44, p.285.
9. Daunov M.I., Magomedov A.B., Ramazanova A.E. Investigation of static distributed nonhomogeneities in electronic InSb and $CdSnAs_2$ on the baric dependences of magnetoresistance. Thes. ref. All-Union symposium //Nonhomogeneous electronic states. Novosibirsk, 1984, p.242-243.

PRESSURE-INDUCED EFFECTS ON DEEP DONOR STATES IN GaAs AND $Al_xGa_{1-x}As$

Shigeru Minomura

Department of Physics, Hokkaido University, Sapporo, 060 Japan

EXPERIMENT

Deep donor levels in n-type GaAs and $Al_xGa_{1-x}As$ have been widely investigated by measurements of the Hall effect, DLTS and PPC. The temperature-dependent Hall effect measurements offer the information about the activation energy of donor levels. In the n-type $Al_xGa_{1-x}As$ the activation energy of donor levels remains less than 15 meV for $x<0.2$, whereas $0.2<x<0.8$ it increases rapidly up to about 160 meV. For $x>0.48$ the activation energy decreases down to about 60 meV.

The DLTS electron-emission spectra are determined by the changes in capatitance as a function of temperature after a forward-bias injection pulse for Schottky or p-n diodes under a backward-bias. The spectra provide the information about the electron population of donor levels in the depletion layer and the activation energy for the electron emission rate to the conduction band. In n-type $Al_xGa_{1-x}As$ the DLTS electron-emission spectra are observed for $0.2<x<0.8$, but for $x<0.2$ they are not observed at the atmospheric pressure. However, Mizuta et al. (1) and Tachikawa et al. (2,3) have first observed the pressure-induced DLTS electron emission spectra in n-type GaAs and $Al_xGa_{1-x}As$ ($x<0.2$).

The pressure-induced signals in GaAs:Si are shown in Fig. 3. While there is no signal below 21 kbar, at pressures of 21 kbar the growth of weak signal is observed. At 30 kbar the signal

magnitude $2\Delta C/C_o$ is interpreted as indicating that the electron population density in the deep donor levels n_{dx} is nearly equal to the donor density N_d. The variation of DLTS signal magnitude $2\Delta C/C_o$ with pressure for n-type GaAs and $Al_xGa_{1-x}As$ ($x<0.2$) is shown in Fig. 4. The insets of Fig. 4. illustrate the pressure dependences of the Γ_{1c}, L_{1c} and X_{1c} conduction band minima and the dL donor level tied to the L_{1c} minima. The Γ_{1c}-dL crossover point corresponds to the critical pressure for the growth of DLTS signals. The signal magnitude increases with increasing pressure.

The carrier density in the Γ_{1c}, L_{1c} and X_{1c} conduction band minima and the electron population in the dΓ, dL and dX donor levels are determined at thermal equilibrium by $n_i=N_d \exp(-(E_i-E_F)/kT)$, where $\Sigma n_i=N_d$ is the donor density. For n-type $Al_xGa_{1-x}As$ the variation of n_i with x is shown in Fig. 5. The electron population of the dL donor level dominates for $0.4<x<0.6$, where as for $x<0.2$ or $x>0.6$ the free carrier of the Γ_{1c} or X_{1c} minima, respectively, dominates. The compositional dependence of the fractional electron occupancy in the dL donor level n_{dx}/N_d agrees well with that of the DLTS signal magnitude n_{dx}/N_d.

The pressure-induced PPC effect is measured in n-type GaAs:Si at pressures of 17 to 30 kbar and at temperatures of 77 to 120 K (3). The variation of the pressure-induced PPC with temperature is shown in Fig. 6. The PPC effect increases with increasing pressure. At 30 kbar the PPC is quenched thermally at 120 K, which corresponds to the critical temperature for the growth of DLTS electron-emission spectra.

DISCUSSION

Experimentally, we have demonstrated the pressure-induced effects on DLTS signals and PPC in n-type GaAs and $Al_xGa_{1-x}As$

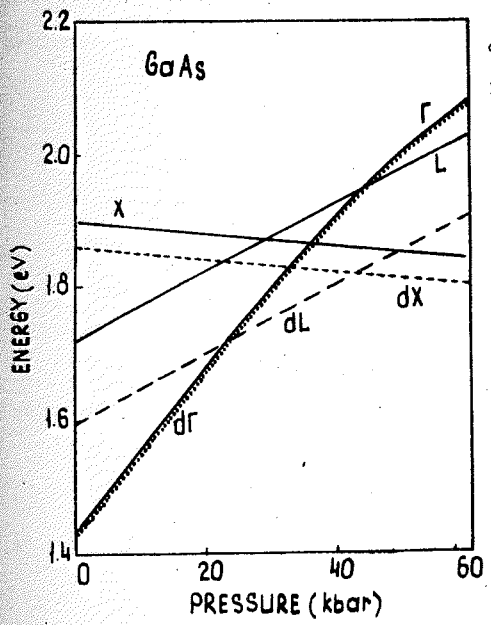

Fig. 1. Variation of conduction band minima with pressure for GaAs.

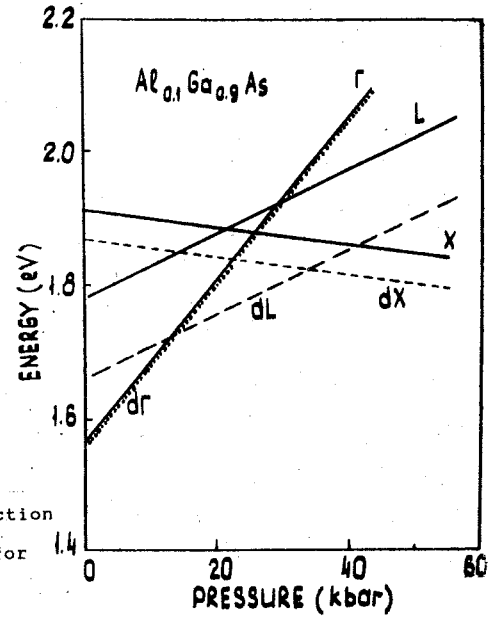

Fig. 2. Variation of conduction band minima with pressure for $Al_{0.1}Ga_{0.9}As$.

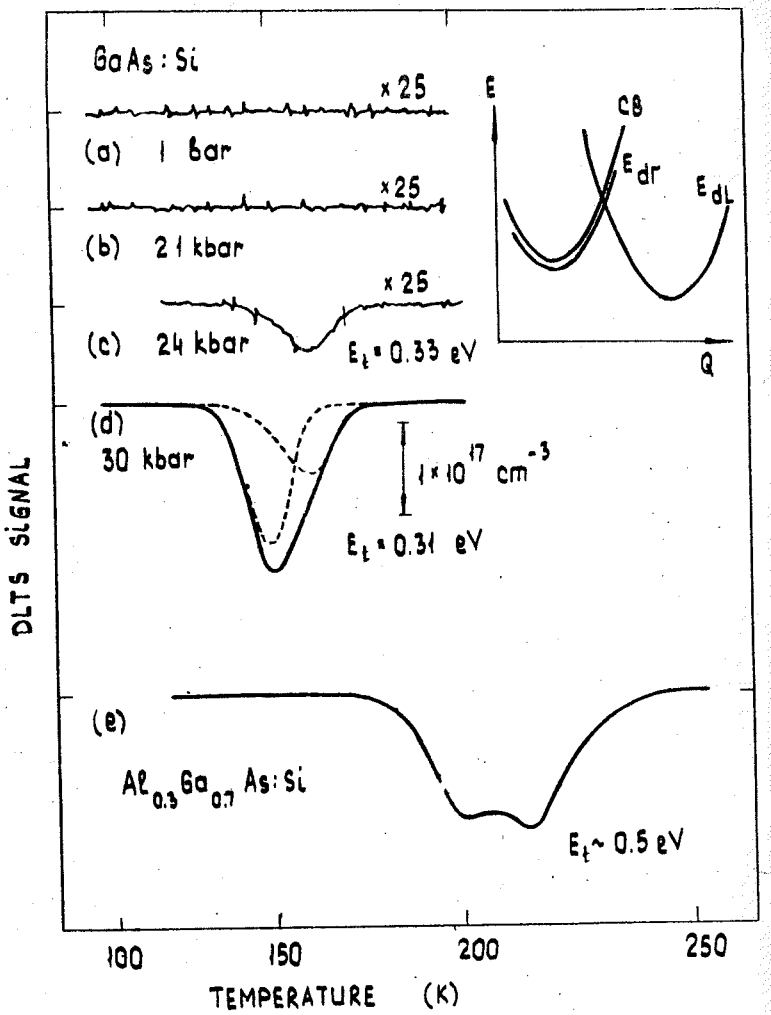

Fig. 3. Pressure-induced DLTS electron emission signals in n-type GaAs.

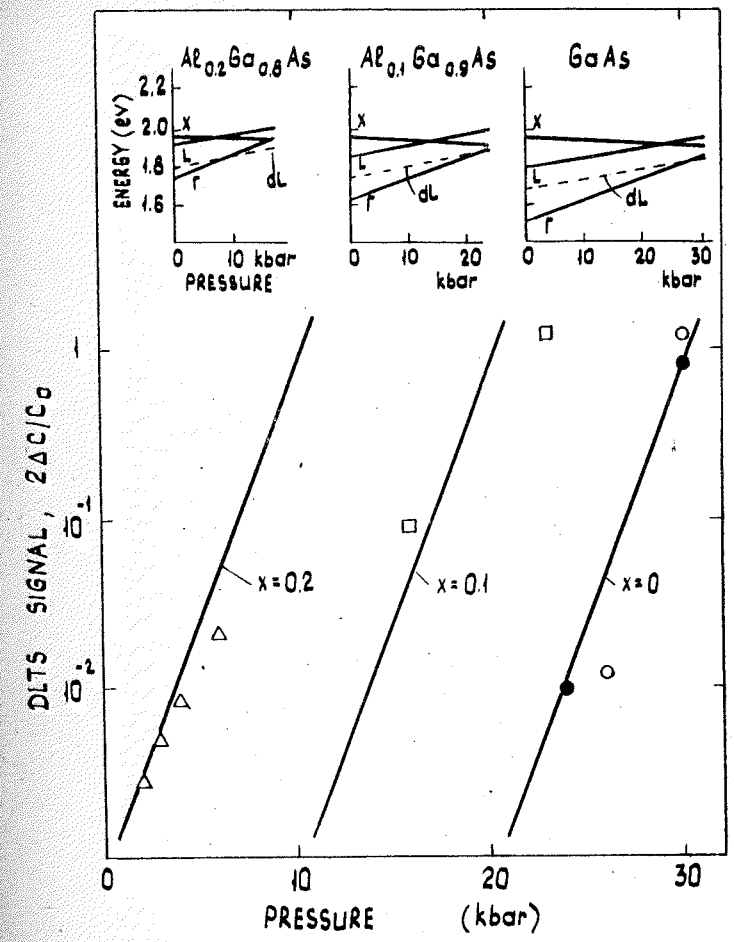

Fig. 4. Variation of DLTS signal magnitude with pressure for n-type GaAs and $Al_xGa_{1-x}As$.

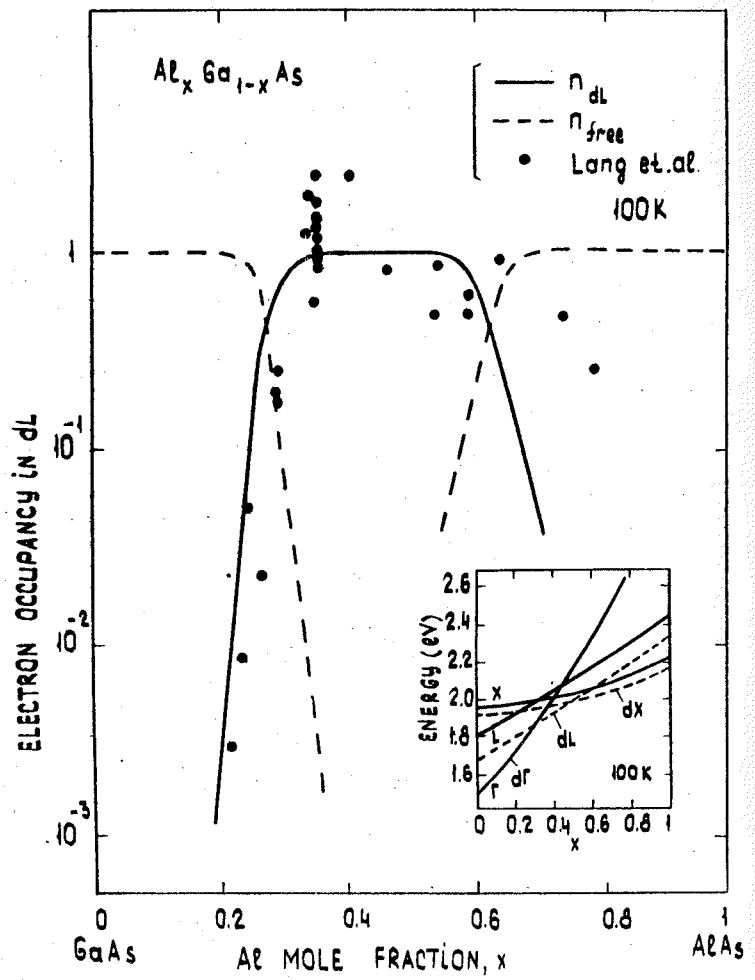

Fig. 5. Variation of fractional population of E_{dL} donor level (solid line) and free carrier concentration (dotted line) with Al mole fraction X for $Al_xGa_{1-x}As$.

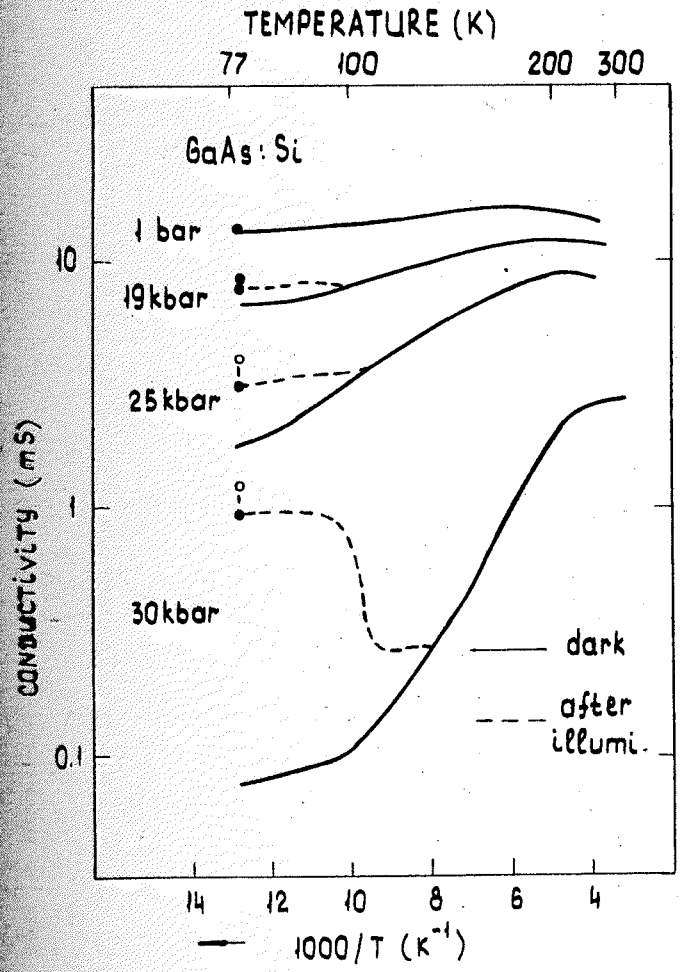

Fig. 6. Pressure-induced PPC effect in n-type GaAs.

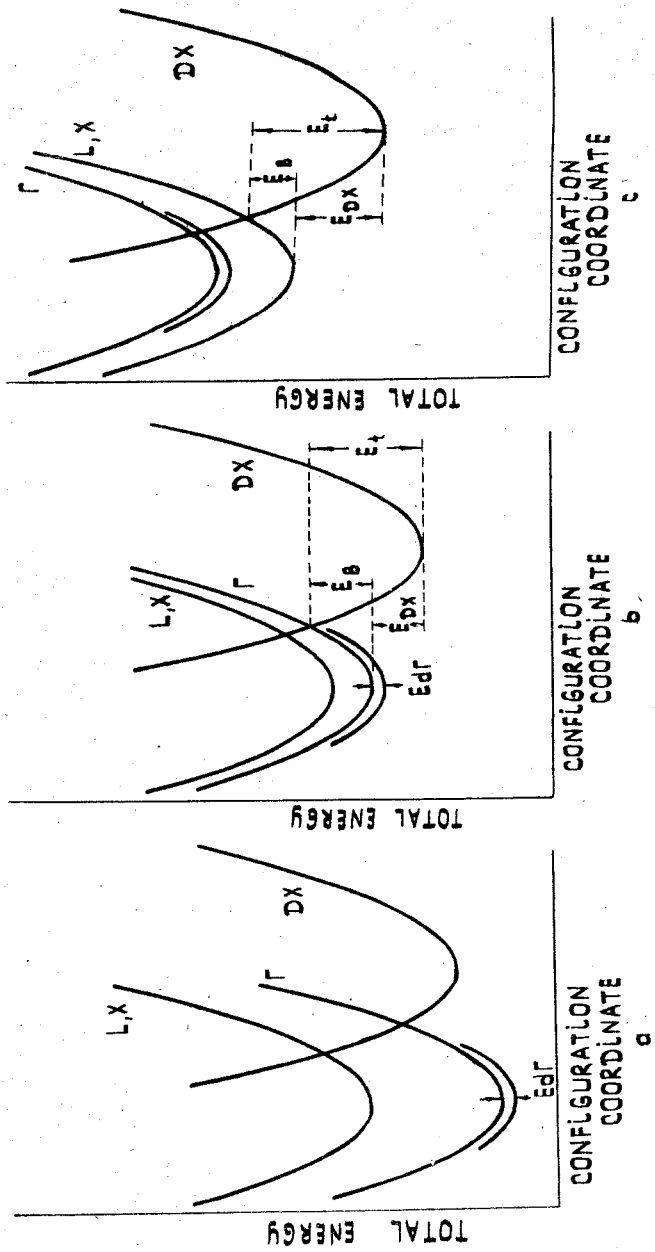

Fig. 7. Configuration coordinate diagram for the deep donor level or DX center in n-type GaAs and $Al_xGa_{1-x}As$.

(x<Ø.2). There phenomena are interpreted as indicating that the deep down level or DX center is associated with the endirect conduction band minima. The experimental results are well understood by the configuration coordinate diagram (CCD) as shown in Fig. 7. At atmospheric pressure the deep donor level tied to the L_{1c} or X_{1c} conduction band minima is metastable, but under pressure of 24kbar it becomes stable. It is assumed that the donor atom itself is displaced from its centered position without any associated vacancy or other defect. Recently Sette et al (3). provided a direct measurement for the displacement of S donor in GaAs by EXAFS, which is about Ø.12 A. Morgan proposed the displaced donor model, assuming that the donor and one of its neighbor are pushed apart by a Jahn-Teller distortion.

References

1. M. Tachikawa, M. Mizuta, H. Kukimoto and S. Minomura, Jpn. J. Appl. Phys. 24 L921 (1985).
2. M. Tachikawa, T. Fujisawa, H. Kukimoto. A. Shibata, G. Oomi and S. Minomura, Jpn. J. Appl. Phys. 24 L893 (1985).
3. F. Sette, S. J. Peartom, J. E. Rowe and J. Stohs, Phys. Rev. Lett. 56, 2637 (1986).

SUPERCONDUCTIVITIES OF HIGH-PRESSURE PHASES IN THE METAL-HYDROGEN SYSTEMS

V.E. Antonov, T.E. Antonova, I.T. Belash, V.I. Rashupkin
Institute of Solid State Physics, USSR Academy of Sciences, USSR

The superconducting properties of the d-metal hydrides rank among most interesting and less studied their characteristics. Correct and complete data have only been obtained for one superconducting hydride, the palladium hydride /1/. The long studies on phases forming in the d-metal-hydrogen systems in the well-mastered pressure range up to tens of atmospheres have not exhibited any new superconductors, and the scope of systems which could be of interest from this viewpoint has been mainly exhausted /1/.

At the same time, it became clear enough that further elucidation of superconducting properties of the metal-hydrogen systems is impossible without experimental discovery and examination of new superconducting hydrides.

The development of the technique for compressing gaseous hydrogen to high (of the order of several GPa) pressures enlarged the number of objects accessible for hydrogenation. For instance, it has become possible to produce massive homogeneous samples of Mn, Fe, Co, Ni, Mo, Tc, Rh, Re hydrides and of numerous their alloys /2, 3/.

As for the high-pressure Me-H phases on the base of pure metals, the following has been found, see /2/. The hydrides of Mn, Fe and Co possess a magnetic order and do not thus possess superconductivity. The molybdenum hydride (HCP(ε) metal lattice, H-to-metal atomic ratio n=1.23±0.03) exhibits no superconductivity at $T \geqslant 2$ K. The hydrides of Ni (FCC (γ) metal lattice, n=1.06±0.03) and Rh (γ, n=1.02±0.03) do not become superconducting at $T \geqslant 0.3$ K.

An increase in the hydrogen concentration in ε-Re (T_c=1.70 K) up to n≈0.23 and in ε-Ru (T_c=0.495 K) up to n≈0.03 leads to a decrease in their T_c-values with the slopes dT_c/dn=-5.0±0.2 K/atom H and ≈ -1 K/atom H, respectively. For the primary hydrogen solid solutions in ε-Tc ($T_c \approx 7.85$ K) with $n \lesssim 0.04$ the value $dT_c/dn \approx -10$ K/atom H; and the ε-hydrides of T_c with $0.39 \lesssim n \lesssim 0.78$ possess no superconductivity at $T \geqslant 2$ K.

Therefore, the study of pure-metal hydrides did not reveal any new superconductors, and only hydrides of the alloys remained to count on. But then the question was what rules one might follow while choosing the alloys for hydrogenation.

In the case of d-metal alloys (without hydrogen) the concentration dependences of T_c can at least be qualitatively described by the rigid band model /4/. In order to evaluate what role the changes in the degree of occupation of the host-metal conduction band by electrons may play in varying the T_c-values on hydrogenation, we examined the effect of hydrogen on T_c's of suitable for this purpose BCC(α) Nb-Ti alloys with 20, 35 and 50 at%Ti and for all the three alloys found out a sharp (~ -15 K/atom H) decrease in T_c /5/. The effect cannot be accounted for by the changes in the electron concentration of the alloys and should necessarily be attributed to the variation in their phonon spectrum. So, in the case of hydrogen solutions it is hardly possible to rely on the predictions made on the basis of the rigid band model, and for the search for new superconducting hydrides to be purposeful other guides should be taken.

And we made use of the literature data that incorporation of hydrogen into the Nb-Ru /6/, Nb-Rh /7/ and Nb-Pd /7,8/ alloys may increase the T_c-values of the samples (the Nb-Me-H samples being inhomogeneous and multi-phase, no reliable data on the hyd-

rogen content and crystal structure of superconducting phases were obtained in /6 to 8/). We have studied the phases forming under high (up to 7 to 9 GPa) hydrogen pressures and T=300 or 325 °C in the Nb-Ru-H /9/, V-Ru-H /10/ and Ta-Ru-H /11/ systems ; the basic results are listed in the table.

As one can see from the table, superconducting hydrides were found for the alloys of Ru with all the d-metals of V group (V, Nb, Ta), that is, these alloys being chemically analogous turned out to be analogous as for possessing superconducting hydrides too. Since the alloys of Nb with all the 4d-metals of VIII group (Ru, Rh, Pd) seem also to have superconducting hydrides,then proceeding from the chemical similarity of the alloys, one may expect that the alloys of all the d-metals of V group with 4d-metals of VIII group form superconducting hydrides as well. We tried to extend the scope of alloys forming superconducting hydrides by substituting Ru for its nearest analogue, Os, in the alloys with V and Ta, but no success has been achieved so far, see the table.

In general, it is worth noting that the search for new superconductors in the Me-H systems based on the alloys of d-metals turned out to be a hard experimental problem. Typical results of studying such systems are presented in Figs. 1-3. It is seen, in particular, that the pressure intervals, within which phases are formed, can be rather narrow (e.g., the γ -phase in the $V_{90}Ru_{10}$-H system, Fig. 1a), and the hydrogen content of the phase can be pressure-dependent (e.g., the ε -phase in the $V_{81.5}Ru_{18.5}$-H system, Fig. 2a). While concentration of the alloys under hydrogenation is varied, the phase equilibria sometimes change drastically and not in an obvious way (compare the data for the $V_{90}Ru_{10}$-H and $V_{81.5}Ru_{18.5}$-H systems, Figs. 1a and 2a). The T-P_{H_2} diagrams of the systems-"analogues" may differ qualitatively (for example (see Fig.3), an addition of 11.5 at%Os into Ta diminishes solubility

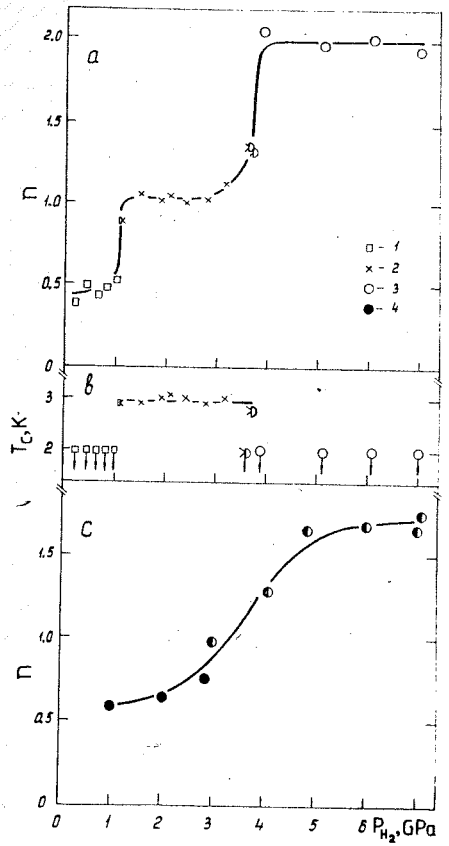

Fig.1. Hydrogen content, n, (a) and superconducting temperature, T_c, (b) for the $V_{90}Ru_{10}$-H solid solutions produced by exposure for 24 h at 300 °C and under the hydrogen pressures indicated on the abscissa ; (c) - values of n for the $V_{91}Os_9$-H solutions (24 h at 325 °C).
1 - data for the β -solutions, 2 - γ_1 , 3 - γ_2 , 4 - α. Combinations of halves of the different symbols refer to the two-phase samples. Symbols with arrows in Fig.1b show that the samples are not superconducting at $T \geqslant 2$ K.

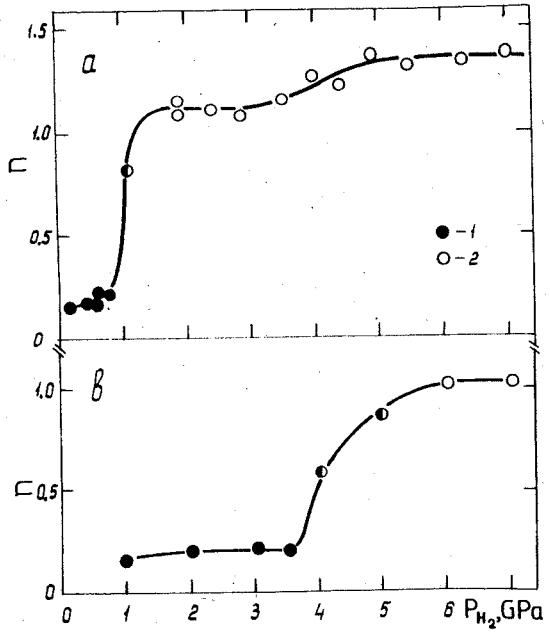

Fig.2. Hydrogen content, n, for the $V_{81.5}Ru_{18.5}$-H (a) and $V_{79.5}Os_{20.5}$-H (b) solid solutions produced by exposure for 24 h under the hydrogen pressures indicated on the abscissa and a temperatures 300 and 325 °C, respectively.

1 - data for the α -solutions, 2 - ε . Half-blackened symbols stand for the two-phase ($\alpha+\varepsilon$) samples.

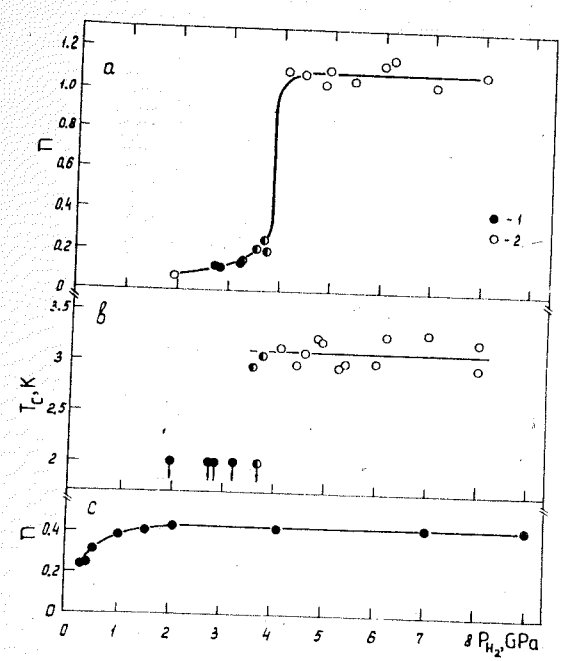

Fig.3. Values of n (a) and T_c (b) for the $Ta_{77.4}Ru_{22.6}$-H solid solutions (24 h at 300 °C) and values of n (c) for the $Ta_{88.5}Os_{11.5}$-H solutions (24 h at 325 °C) given as functions of pressure of the samples synthesis.

1 - data for the α -solutions, 2 - ε'. Half-blackened symbols refer to the two-phase samples. Symbols with arrows in Fig.3 b show that the samples are not superconducting at $T \gtrsim 2$ K.

of hydrogen down to n≈0.43 even at P_{H_2}≈9 GPa, whereas the Ta-Ru alloy with 22.6 at%Ru forms a hydride with n≈1.1 already at $P_{H_2} \gtrsim 3$ GPa).

Fortunately, at the present initial stage of investigation the sphere of quest for superconducting hydrides might be noticeably reduced. As is seen from the table, only the phases with n ≈1 based on the closest packings of metal atoms happened to be superconducting among the set of the synthesized phases. Note that the Pd hydride is also formed on the base of the closest (FCC) packing of the metal atoms, and its T_c reaches the maximum value at n ≈ 1 /1/. All the foregoing is unlikely to be of a random nature, and it would be sensible in the first place to search for superconductors in yet uninvestigated Me-H systems, namely among the phases of such type.

The data available on the composition and crystal structure of the hydrides allow one also to speculate why some phases with n ≈1 are superconducting. There are two kinds of interstitials in the close-packed lattices, the octa- and tetrahedral ones, the oscillation frequencies of hydrogens in the octapores being essentially lower /12/, and the composition n=1 corresponds to the complete filling of all the octapores with hydrogens. Superconductivity of the palladium hydride is considerably conditioned by the interaction of electrons just with the optical oscillations of hydrogens in the octapores /1/. It seems quite probable that a similar situation takes place with the Me-Ru-H superconducting hydrides as well.

Composition, superconducting temperature, pressure of synthesis, structure and parameters of the metal sublattice at atmospheric pressure and T=83 K for the Me-Ru-H and Me-Os-H solid solutions

Alloy	n	T_cK	P_{H_2}, GPa	Structure	a,Å	b, Å	c,Å
*$V_{90}Ru_{10}$	0	<2	-	α	3.011	-	-
	0.5	<2	0.8	β	2.996	-	3.302
	1.04	3.0	1.1...3.6	γ_1	3.971	-	-
	2.0	<2	>3.8	γ_2	4.265	-	-
*$V_{81.5}Ru_{18.5}$	0	<2	-	α	3.005	-	-
	1.12	<2	1.3	ε	2.787	-	4.688
	1.36	<2	7	ε	2.858	-	4.696
*$V_{66}Ru_{34}$	0	<2	-	α^{or}	2.995	-	-
	1.24	<2	2.4	ε	2.810	-	4.577
	1.34	<2	7	ε	2.822	-	4.572
$Nb_{83}Ru_{17}$	0	<2	-	α	3.242	-	-
	1.92	<2	>4	ε'	5.391	5.113	3.170
$Nb_{74.5}Ru_{25.5}$	0	<2	-	α	3.217	-	-
	1.04	5.08	1.2	γ'	4.244	-	4.180
	1.72	<2	7	ε	3.082	-	5.033
$Nb_{69}Ru_{31}$	0	<2	-	α	3.199	-	-
	1.04	4.3	2	γ'	4.23	-	4.16
	≥1.5	?	7	ε	3.05	-	4.98
$Nb_{50}Ru_{50}$	0	<2	-	γ''	4.371	4.225	3.396
	0.24	<2	1.0...1.4	γ''	4.379	4.327	3.459
	1.13...	<2	2.2...7	ε'	5.098	4.727	2.914
	1.25						
*$Ta_{77.4}Ru_{22.6}$	0	<2	-	α	3.316	-	-
	1.10	3.1	>3.2	ε'	5.188	4.951	2.966
*$Ta_{69}Ru_{31}$	0	<2	-	α^{or}	3.194	-	-
	0.95	2.8	>4.2	ε'	5.163	4.881	2.937
$V_{91}Os_9$	0	<2		α	3.012	-	-
	0.6	<2	2	α	3.110	-	-
	>1.7	<2	>3	γ_2	4.250	-	-
$V_{79.5}Os_{20.5}$	0	<2	-	α	3.004	-	-
	0.2	<2	3.5	α	3.037	-	-
	1.03	<2	>4	ε	2.848	-	4.665
$Ta_{88.5}Os_{11.5}$	0	<2	-	α	3.256	-	-
	0.43	<2	9	α	3.324	-	-

Footnote. Stars indicate the alloys hydrogenated at 300 °C, the rest alloys were hydrogenated at 325 °C. α-BCC, α^{or}- of CsCl type, β- of β-V_2H type (values of a_o and c_o for the tetragonal pseudocell are given), γ- FCC, γ'-FC tetragonal, γ''- the structure on the base of FC orthorhombic pseudocell, ε-HCP, ε'-rhombically distorted HCP.

References

1. Stritzker B., Wühl H. Superconductivity in metal-hydrogen systems. - In: Hydrogen in Metals II/Ed. G.Alefeld, J.Völkl.- Topics in Appl. Phys.Berlin, Heidelberg, N.Y.: Springer-Verlag, 1978.- vol.29, p.243-272.
2. Ponyatovsky E.G., Antonov V.E., Belash I.T. High hydrogen pressures. Synthesis and properties of new hydrides. - In: Problems in Solid-State Physics/Ed. A.M.Prokhorov, A.S.Prokhorov. Advances in Science and Technology in the USSR. Phys.Ser.Moscow: Mir Publishers, 1984, p.109-172.
3. Baranowski B. Metal-hydrogen systems at high hydrogen pressure.- In: Hydrogen in Metals II/Ed. G.Alefeld, J.Völkl. - Topics in Appl.Phys.Berlin, Heidelberg, N.Y.: Springer-Verlag, 1978, vol.29, p.157-200
4. Vonsovsky S.V., Izyumov Yu.A., Kurmaev E.Z. Superconductivity of transition metals, their alloys and compounds. - Moscow: Izd. Nauka, 1977, 383 p. (in Russian).
5. Antonov V.E., Belash I.T., Zakharov M.S., Orlov V.A., Rashupkin V.I. The effect of hydrogen on the superconducting temperature in b.c.c. niobium-titanium alloys.- Int. J.Hydrogen Energy, 1986, vol.11, No.7, p.475-478.
6. Robbins C.G., Ishikawa M., Treyvaud A., Muller J. The effect of hydrogen on the superconducting and structural properties of b.c.c. Nb-Ru alloys.- Solid State Comm., 1975, vol.17, No.7, p.903-906.
7. Oesterreicher H., Clinton J. Superconductivity in hydrides of Nb-Pd and Nb-Rh. - J.Solid State Chem., 1976, vol.17, No4, p.443-445.
8. Robbins C.G., Muller J. The effect of hydrogen on the superconducting transition temperature of some body-centered cubic niobium-palladium, niobium-palladium-molybdenum and niobium--palladium-tangsten alloys. - J.Less-Common Metals, 1975, vol. 42, No.1,p.19-27.
9. Antonov V.E., Antonova T.E., Belash I.T., Ponyatovsky E.G., Rashupkin V.I. Superconductivities and crystal structure of high pressure phases in the Nb-Ru-H system. - Fiz.tverd.Tela (Leningrad), 1987, vol.29, No.4, p.1017-1025.
10. Antonov V.E., Belash I.T., Ponyatovsky E.G., Rashupkin V.I., Romanenko I.M. Superconductivities and crystal structure of high pressure phases in the V-Ru-H system.- Fiz.tverd.Tela (Leningrad), 1987, vol.29, No.3, p.665-671.
11. Antonov V.E., Antonova T.E., Belash I.T., Malyshev V.Yu., Ponyatovsky E.G., Rashupkin V.I. Superconductivities and crystal structure of high pressure phases in the Ta-Ru-H system. - Fiz.tverd.Tela (Leningrad), 1986, vol.28, No.8, p.2352-2357.
12. Springer T. Investigation of vibrations in metal hydrides by neutron spectroscopy.- In: Hydrogen in Metals I./ Ed. G.Alefeld, J.Völkl. Topics in Appl.Phys.Berlin, Heidelberg. N.Y.: Springer-Verlag, 1978, vol.28, p.75-100.

PHOTOCONDUCTIVITY OF CdS AT HIGH PRESSURE

P. Savić
Serbian Academy of Sciences and Arts, 11000 Belgrade,Yugoslavia

V.Urošević
Institute of Physics, 11001 Belgrade, P.O.Box 57, Yugoslavia

ABSTRACT

A method for photoconductivity investigation in diamond anvil cell is described. Preliminary measurements in high-pressure (rocksalt) phase of CdS gave a decrease of photo-threshold from 1.60 eV (at 30 kbar) to 1.49 eV (at 120 kbar) in accordance with previously reported optical absorption data.

INTRODUCTION

Optical absorption and resistivity measurements of cadmium sulfide (CdS) at high pressure have been first reported by Drickamer and coworkers [1,2] which found a phase transition at 27 kbar and the stability of the new phase after reversal to lower pressure. Kabalkina and Troitskaya [3] and Owen et al [4] showed by X-ray diffraction studies that the new phase has a NaCl structure. Recent investigations of high-pressure phase of CdS have been stimulated by Brown, Homan and MacCrone [5] which observed large diamagnetism, approching 100% flux exclusion, and possible superconductivity in pressure-quenched CdS at 77K. Batlogg et al [6] found by optical absorption measurements that the energy gap is direct in low pressure (wurtzite) phase (2.4 eV at atmospheric pressure) and indirect in rocksalt phase (≤1.7 eV).

In this paper we present some preliminary results of photoconductivity measurements of pure CdS under high pressure (30-120 kbar). An experimental arrangement, different from the one used by Gonzales, Besson and Weill [7], is also described.

EXPERIMENTAL METHOD

The high pressure has been generated in a diamond anvil cell of NBS type [8] . A preindented stainless steel gasket is prepared by drilling a hole (0.5 mm in diameter) at the center of indentation and by cutting the disc in two symmetrical parts which are cemented between two mica supports with central holes greater than anvil diameters. A small CdS sample, prepared from pure powder by cold pressing and subsequent heating at 450°C for 10h,

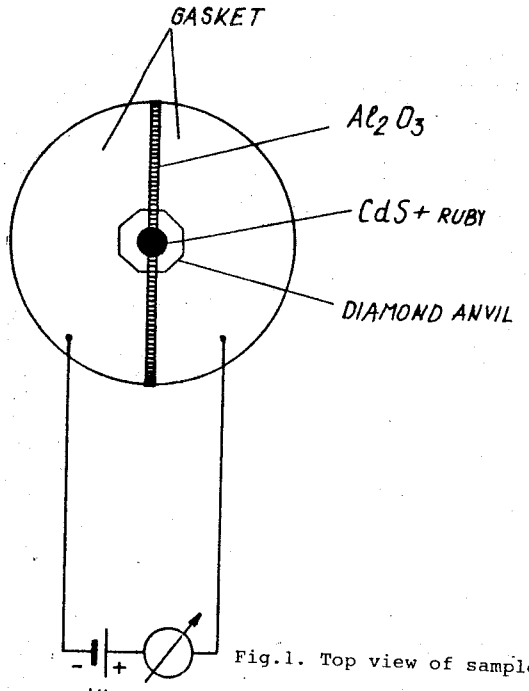

Fig.1. Top view of sample and electric scheme.

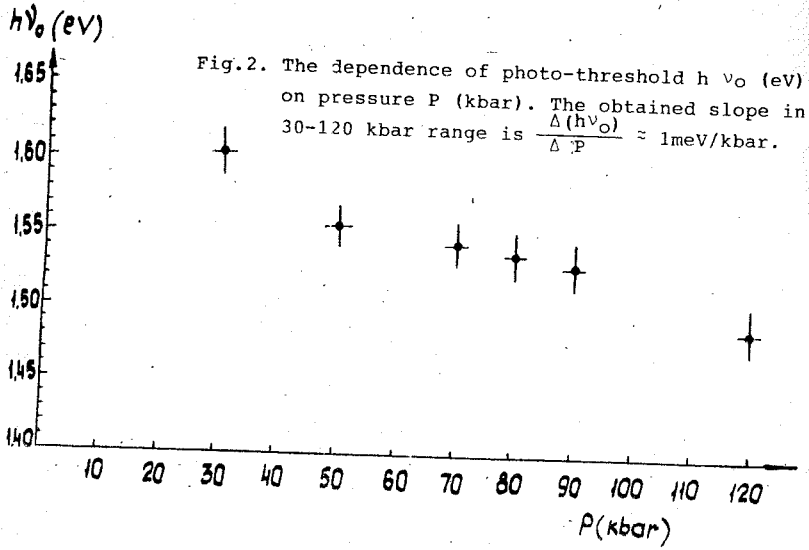

Fig.2. The dependence of photo-threshold h ν_o (eV) on pressure P (kbar). The obtained slope in 30-120 kbar range is $\frac{\Delta(h\nu_o)}{\Delta P} \simeq$ 1meV/kbar.

has been pressed into the gasket hole. The gap between two gasket segments ($\sim$ 0.3mm) was filled with fine alumina powder cemented by epoxy resin. The above configuration (Fig.1) was able to sustain up to 120-130kbar. A flat ruby chip ($\sim$ 50 μm) was inserted in the front side of CdS sample and the pressure was measured in backscattering geometry. The electrical contacts between gasket segments, which served as electrodes, and the CdS sample were obtained by applying the highest (120 kbar) pressure.

The illumination of the sample has been performed by a xenon arc lamp, a double optical monochromator and a branched light guide, for simultaneous measurement of the incident radiation flux at given warelength. The electric scheme, shown in Fig.1, consisted of a stabilized DC voltage source and a sensitive electrometer.

RESULTS AND DISCUSSION

In the experiment we measured $\frac{\Delta i}{\phi}$, where Δi is the photocurrent and ϕ is the photon flux, as a function of wavelength of incident radiation, the parameter being the applied pressure. The photocurrent threshold h ν_o (i.e. the minimal photon energy which starts the phocurrent), equal to the band gap Eg at given pressure, can be obtained by numerical determination of zero $\frac{\Delta i}{\phi}$ value. From a set of such curves we obtained the dependence of photocurrent threshold on pressure (Fig.2). In the investigated pressure range there is a decrease of h ν_o with increase of pressure from 1.60 eV (at 30kbar) to 1.49eV (at 120kbar). This confirms the finding of Batlogg et al [6] that the high-pressure phase of CdS is an indirec gap semiconductor. The slope of the curve is $\frac{\Delta(h\nu_o)}{\Delta P} \simeq$ 1meV/kbar, which agrees with $\frac{\Delta E_g}{\Delta P} \simeq$ 0.7meV/kbar [1,6] within the experimental error. A rather small difference in $\frac{\Delta E_g}{\Delta P}$ and absolute Eg values between the present and earlier works where optical absorption measurement have been used, can be explained by the absence of truly hydrostatic conditions in our work and perhaps also by the difference in two measuring methods.

The authors are grateful to Mr. B. Petrović for help in preparing the experiment.

References

1. A.L. Edwards and H.G. Drickamer, Phys. Rev. 122, 1149 (1961).

2. G.A. Samara and H.G. Drickamer, J. Phys.Chem. Solids 23, 457, (1962).

3. S.S. Kabalkina and Z.V. Troitskaya, Doklady AN SSSR 151, 1068 (1963)

4. N.B. Owen, P.L. Smith, J.E. Martin and A.J. Wright, J. Phys.Chem. Solids 24, 1519 (1963).

5. E. Brown, C.G. Homan and R.K. MacCrone, Phys. Rev.Letters 45, 478 (1980).

6. B. Batlogg, A. Jayaraman, J.E.Van Cleve and R.G. Maines, Phys.Rev. B27, 3920 (1983).

7. J. Gonzales and J.M. Besson, Rev.Sci.Instrum. 57, 106 (1986).

8. G.J. Piermarini and S. Block, Rev. Sci.Instrum. 46, 973 (1975).

EFFECT OF PRESSURE ON CURIE TEMPERATURE OF FeWB METALLIC GLASSES

J. Kamarád[1], Z. Arnold[1], E. Kisdi-Koszo[2]

[1] Institute of Physics, Czech. Acad. Sci., Na Slovance 2, 180 40 Prague 8, Czechoslovakia

[2] Central Research Institute for Physics, Hungarian Academy of Sciences, Budapest, Hungary

Introduction

The Fe-based metallic glasses exhibit pronounced magneto-volume effects and the Invar-like behaviour was observed in many of these Fe-rich alloys. To clarify the magnetic behaviour of these alloys the magnetic properties have been intensively studied under pressure during recent years /1-4/.

The relation between parameter dT_c/dp and the Curie temperature can be derived for 3d crystalline alloys within the band model of ferromagnetism. The theoretical relation:

$$\frac{dT_c}{dp} = \frac{5}{3} K T_c - \alpha T_c^{-1} \qquad (1)$$

where K is compressibility and α is positive constant, was obtained using a model of the volume dependence of the band width and the $s \rightarrow d$ transfer /5/. For the alloys with the Invar-like behaviour the second term prevails and dT_c/dp is indirectly proportional to T_c.

The high pressure behaviour of inhomogeneous alloys is quite different as was shown by Wagner and Wohlfarth /6/. Using Landau-Ginzburg model they obtained the relation:

$$\frac{dT_c}{dp} = - d_1 T_c + d_2 T_c^2 \qquad (2)$$

where d_1 and d_2 are positive constants.

The replacement of iron by a small amount of some other transition metal in the Fe-based metallic glasses lead to significant changes in their magnetic properties and also their Invar behaviour gradually disappeared /7,8/. The addition of several procent of the early transition metal (Mn, Cr) causes a steep decrease of dT_c/dp (as a function of its concentration /1/) and a minimum was observed for concentration around 5 at.% /1,2/. In this paper the results of our pressure study of T_c on the amor-

phous $Fe_{84-x}W_xB_{16}$ with ($0 \leq x \leq 8$) are presented and compared with our earlier measurements on FeCrB glasses /1/.

Experimental

The samples were prepared by the melt spinning technique. The thickness and width of the samples were 25 - 30 μm and 6 - 10 mm respectively. The composition was checked by chemical analysis.

The Curie temperature was determined from the temperature dependence of an initial susceptibility of the samples using a transformer method. T_c was defined by extrapolation of the linear part of secondary voltage as a function of temperature - see Fig.1.

The Curie temperature of the samples with $T_c > 350$ K was measured in a belt type apparatus with an internal graphite heater under the pressure up to 4.5 GPa. The sample with highest content of W was investigated in a hydrostatic CuBe cell with the fixed pressure up to 0.9 GPa. The temperature was measured by Ni-NiCr thermocouple which was in thermal contact with the sample.

Results and discussion

The values of T_c vary nearly linearly with the tungsten content at the atmospheric pressure, having an initial decrease of 35 K/at.%W. The Curie temperatures of all investigated alloys linearly decrease with the pressure in the whole pressure range. The decreases of T_c and the susceptibility under the pressure are illustrated in Fig.1, by the temperature dependence of the susceptibility.

The dependence of both T_c and dT_c/dp on the W-content in the measured samples is presented in Fig.2. The values of the parameter dT_c/dp decrease with tungsten content up to about 5 at.%W where the minimum value of $dT_c/dp = -50$ K/GPa was observed.

The results of our measurements of dT_c/dp in FeWB alloys together with earlier results on FeCrB glasses /1/ and crystalline FeNiMn /10/ alloys are plotted against T_c on Fig.3.

The metallic glasses with small content of the non-ferrous metal exhibit the pronounced Invar behaviour. The behaviour of the W-rich FeWB glasses, where the decrease of $|dT_c/dp|$ with the decrease of T_c was observed, can be connected with the existence of inhomogeneities. Their existence was deduced from the negative curvature of Arrot plots /11/. We should mention that smaller value of $\left|\frac{dT_c}{dp}\right|$ for the FeWB alloys with 7.8 at.%W in comparison

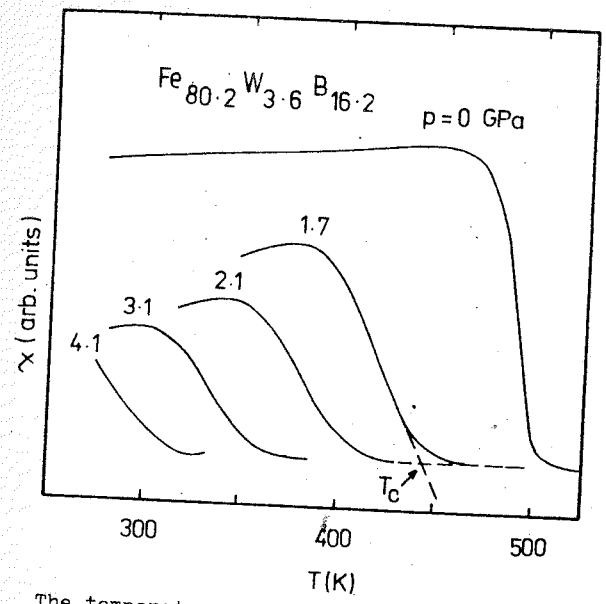

Fig. 1. The temperature dependence of the initial susceptibility χ of the $Fe_{80.2}W_{3.6}B_{16.2}$ metallic glass under the various pressures.

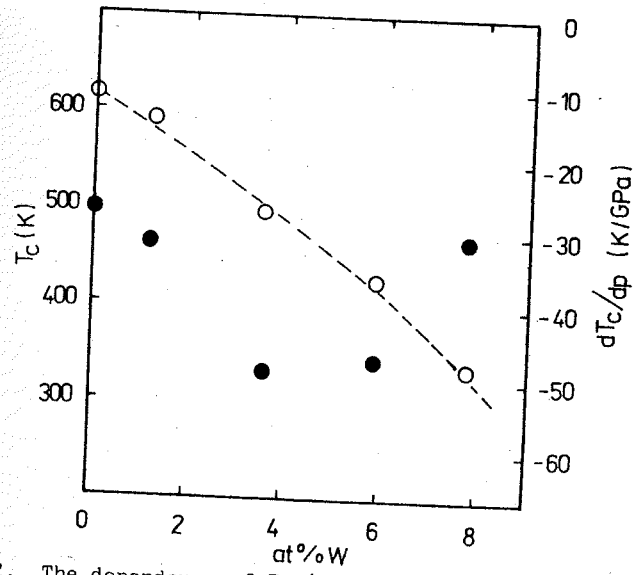

Fig. 2. The dependence of T_c (open symbols) and dT_c/dp (full symbols) on W - content for $Fe_{84-x}W_xB_{16}$ samples.

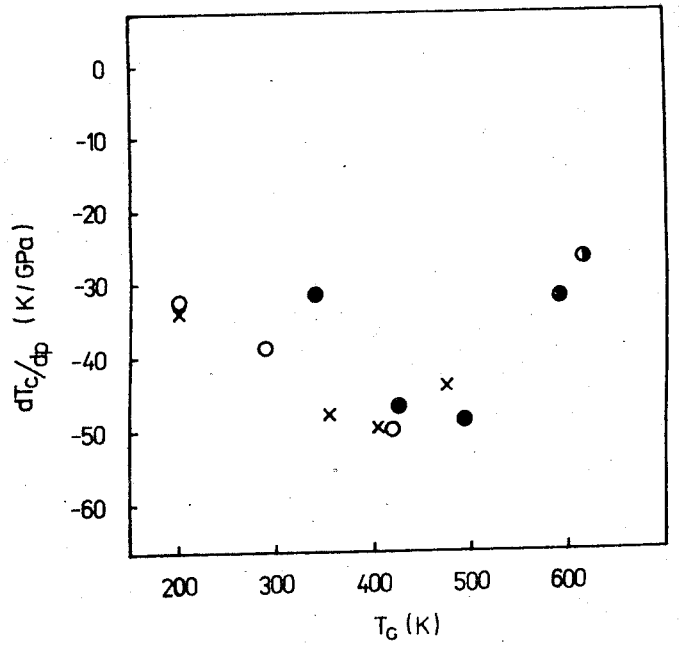

Fig. 3. dT_c/dp vs T_c for several materials; • - $Fe_{84-x}W_xB_{16}$, o - $Fe_{85-x}Cr_xB_{15}$ /2/, × - $Fe_{66}(Ni_{1-x}Mn_x)_{34}$ /11/.

with the corresponding value for the FeCrB alloys - see Fig.3 - can be connected with the larger disturbation of the short range order in the FeWB alloys caused by the large tungsten atoms. The difference in "structural imperfections" in the amorphous Cr and W alloys was deduced from the results of positron annihilation measurements /12/.

References

1. J.Kamarád, Z.Arnold and H.J.V. Nielsen, J.Magn.Mag.Mats. 23 (1981) 69.
2. H.Tange, M.Goto and S.Ishio, Physica 119 B+C (1983) 188.
3. K.Shirakawa et al., Physica 119 B+C (1983) 192.
4. J.Kamarád and Z.Arnold, Physica 139+140 B (1986) 382.
5. N.D.Lang and H.Ehrenreich, Phys.Rev. 168 (1968) 605.
6. D.Wagner and E.P.Wohlfarth, J.Phys.F 11 (1981) 2417.
7. K.Kikuchi, K.Fukamichi and T.Masumoto, Sci.Rep.RITU A 27 (1979) 210.
8. H.J.V. Nielsen, J.Magn.Mag.Mats.19 (1980) 138.
9. H.J.V. Nielsen, phys. stat. sol. 61 (1980) K 111.
10. V.E.Antonov, G.T.Dubovka and E.G.Ponyatovskij, phys. stat. sol. (a) 27 (1975) K 21.
11. S.Ramasamy et al. J. Phys. F 17 (1987) 753.
12. G.Konzos et al., J.Magn.Mag.Mats. 41 (1984) 122.

THE HYDROSTATIC PRESSURE PROPERTIES OF 2D-HOLES ON THE SURFACE OF TELLURIUM - A LOW SYMMETRICAL SEMICONDUCTOR

V.A.Berezovetz, I.I.Farbshtein, V.V.Kosarev, M.L.Shubnikov
A.F.Ioffe Physico-Technical Institut, USSR Academy of Sciences, Leningrad, USSR

The hydrostatic pressure is found to result in a considerable rise of 2D-hole concentration and mobility in an accumulation layer on tellurium monocrystal surfaces. These changes are shown to be due to a surface potential well increase.

It was established earlier (see /1/, for example), that there is an accumulation layer (AL) on Te surface and the total energy of current carriers (holes in our case) in it is represented by a series of 2D-subbands. The aim of this work is to investigate properties of 2D-holes under hydrostatic pressure.

The hole energy spectrum in tellurium has a high anisotropy:

$$E(k) = -(Ak_\perp^2 + Bk_z^2) + \sqrt{\Delta^2 + C^2k_z^2} \qquad (1)$$

(the spin-orbit interaction only between the two highest valence bands is taken into account here). But 2D-hole spectrum in (0001) crystal face has the cylindrical symmetry in this approximation:

$$E(k_\perp) = E_i + \frac{\hbar^2k^2}{2m_{\perp i}}, \text{ where } i=0, 1, 2, \ldots \qquad (2)$$

(i - is the quantum number of 2D-subbands).

For our investigation we choose tellurium monocrystals with hole concentration $p(77\ K)=10^{20}m^{-3}$; the samples with the largest (0001) face, which is perpendicular to C_3 crystal axis, were carved in a chemical way. On these faces AL was created by means of the special technology given in /1/. The fixed high-pressure chamber /2/ was used to realize the hydrostatic pressures up to 0.8 GPa. Magnetoresistance and Hall voltage and their second derivations on magnetic field (B) were measured in $B \parallel C_3$ and $B \leqq 10$ T conditions.

Shubnikov-de Haas oscillations of the measured values were observed at $T \leqq 4.2$ K and their analysis gives the amount of the subbands and also the 2D-holes mobility and concentration in each of them. Fig.1 shows a typical experimental recording of

d^2V_H/dB^2 at T=1.7 K and the change in it under pressure. At n.p. this dependence has superposition of three oscillations with periods in 1/B scale: $\Delta_0, \Delta_1, \Delta_2$, that corresponds to three 2D-subbands with total concentration of surface holes $p_{AL}=1.8\cdot10^{16}m^{-2}$. Under hydrostatic pressure the oscillation extrema move to higher fields, an amplitude of them increases, the periods decrease and the fourth period /3/ arises. This means, that hole concentration increases in each of 2D-subbands:

$$p_i = 2e/(h\cdot\Delta_i), \qquad (3)$$

where i = 0, 1, 2, 3. The dependence $p_i(P)$ in the region up to 0.7 GPa corresponds to the following empirical expression:

$$p_i(P) = p_i(0)\cdot\exp(\beta_i\cdot P), \qquad (4)$$

where β_i values are nealy to proportional dependent on the subband number i and change from 0.46 GPa^{-1} for i=0 and up to 1.6 GPa^{-1} for i=3. The total hole concentration in AL, $p_{AL}=\sum_i p_i$, can also be represented by relation (4) with $\beta_{AL}=0.6\ GPa^{-1}$.

The increase of the oscillation amplitude under pressure is caused by the 2D-hole mobility increase, that is mainly due to an effective mass m_i decrease. An experimental data on $m_\perp^c(P)$ dependence, that is to coinside with $m_i(P)$ for 2D-holes moving in (0001) plane on the subband bottom, were obtained from the cyclotron resonance investigation under pressure /4/. These data are given by the following expression:

$$m_\perp^c(P)/m_\perp^c(0) = \exp(-0.54\cdot P\ (GPa)) \qquad (5)$$

Using these empirical expressions (4,5) for all 2D-subbands and hole effective mass on the Fermi level, that was obtained in /1/, we calculated the Fermi energies $E_i^F(P)$ under pressure:

$$E_i(P) - E^F = E_i^F(P) = \pi\hbar^2 p_i(P)/m_i(P) \qquad (6)$$

Fig.2 shows the calculation results. Here it is shown, that under P=0.7 GPa the potential well depth on Te surface increases about twofold. The theoretical calculation of the energy positions for 2D-subbands in the potential well on (0001) tellurium surface is rather complicated because of k_z terms in Hamiltonian matrix for valence band, that gives $C^2k_z^2$ term in (1). By the way, as

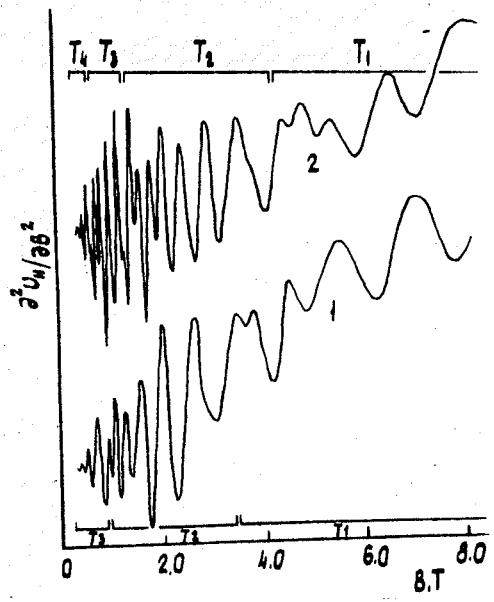

Fig.1. Shubnikov-de Haas oscillations (second derivation of the Hall voltage V_H) at T=1.7 K under n.p. (1) and P=0.72 GPa (2). The regions of oscillation periods T_0, T_1, T_2, T_3 are shown.

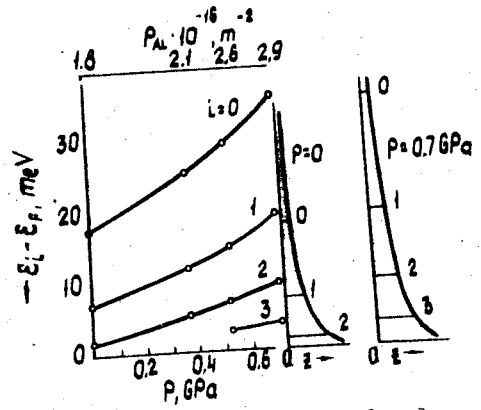

Fig.2. The P-dependence of the quantum level positions in the accumulation layer on (0001) tellurium surface. The numbers of curves are the subband quantum numbers. In the right part there is a scheme of the level positions in the potential well and their change under P=0.72 GPa.

2D-hole energy in tellurium AL increases under pressure together with the forbidden gap decrease, it is necessary to use two-band model /5/, which takes into account an interaction with the conduction band. In this model the transverse component of the effective mass is dependent on the state energy E. Therefore we have taken into account in the calculation the experimental data about band parameters of the model /5/ and P-dependences of them, 2D-hole concentrations $p_i(P)$ from (4) and effective mass $m_\perp(P)$ from (5), and also the high P-sensibility of Te dielectric coefficient (ε). Our estimation from fotoelastic coefficient data /6/ gives:

$$d\ln \varepsilon_{33}/dP = 0.42\ \mathrm{GPa}^{-1} \qquad (7)$$

that is about P-coefficient values of p_{AL} and $m_\perp$.

The authors are pleased to thank dr. R.V.Parfeniev for his encourage.

References

1. V.A.Berezovetz, I.I.Farbstein, A.L.Shelankov. The quantum kinetic phenomena in 2D accumulation layer on Te surface, FTT, 1983, v.25, n.10, p.2988-2995.
2. M.L.Shubnikov. The fixed high-pressure chamber, PTE, 1981, n.5, p.178-180.
3. V.A.Berezovetz, I.I.Farbstein, M.L.Shubnikov. The conductivity of 2D-holes on Te surface under hydrostatic pressure, FTT, 1986, v.28, n.5, p.1516-1518.
4. U.Steigenberger, M.I.Eremetz, S.G.Lapin, et al. The influence of the hydrostatic pressure on the free and bound states in tellurium, J.Phys.C: Solid State Phys. 1984, v.17, p.427-436.
5. M.Lutz, E.Bangert, T.Muzran, H.Stolze. De Haas-van Alphen-type oscillations in the interband Faraday effect of tellurium, Phys.Stat.Sol.(b), 1975, v.71, p.523-532.
6. S.Fukuda, T.Karasaki, T.Shiosaki, A.Kawabata. Fotoelasticity and acusto-optic diffraction in piezoelectric semiconductors, Phys.Rev.B., 1979, v.20, n.10, p.4109-4119.

MAGNETOPHONON SPECTROSCOPY OF A SINGLE-CRYSTAL TELLURIUM UNDER HYDROSTATIC PRESSURE

V.V.Kosarev, D.V.Mashovets, I.I.Farbstein, M.L.Shubnikov
A.F.Ioffe Physico-Technical Institute, USSR Academy of Sciences, Leningrad, USSR

Magnetophonon resonance (MPR) in Te was studied in /1-4/. We report the results on MPR in Te under hydrostatic pressure up to 1.1 GPa. A quantitative analysis is made in terms of a two-band model of energy spectrum /5/ that was not used previously for MPR analysis. Polaron corrections (PC) are included. Pressure dependences of the model /5/ parameters are determined.

Magnetoresistance (MR) was measured at T=77K on Te single crystals (hole concentration $p=2\cdot10^{20}m^{-3}$) in pulsed magnetic field $H \leq 20T$ at $\vec{H} \parallel \vec{C}_3 \parallel \vec{j}$ and $\vec{H} \perp \vec{C}_3 \parallel \vec{j}$ ($\vec{j}$ - current, $\vec{C}_3$ - crystal axis) in fixed pressure chamber.

At high pressure MPR extrema H_N shift to the low magnetic field (Fig.1). For both orientations all the $H_N(P)$ dependences are presented by an empirical relation

$$H_N(P) = H_N(0) \exp(-\beta P), \quad \beta = 0.54\ GPa^{-1}. \qquad (1)$$

At P=1.1 GPa at $\vec{H} \parallel \vec{C}_3$ a MR minimum corresponding to Peterson pseudoresonance was observed (H_{PR}(1.1 GPa) = 18 T, Fig.2). At normal pressure it was detected earlier by one of the authors /1,2/: $H_{PR}(0) = 29 \pm 1$T.

A quantitative analysis of the MPR is based on the relations:

$$\hbar\omega_o = E_N(H) - E_o(H) \text{ for one-phonon MPR,} \qquad (2a)$$

$$2\hbar\omega_o = E_1(H) - E_o(H) \text{ for the 1st pseudoresonance.} \qquad (2b)$$

Here $\hbar\omega_o$ - LO-phonon energy, $E_N(H)$ - N-th Landau level energy. In MPR field position calculations one must take into account a non-parabolicity of energy spectrum that increases at high pressure as a result of E_g decrease. In our case the non-parabolicity is included in the band model, which describes both $m^*_\parallel$ and $m^*_\perp$ energy dependences. Polaron correction causes a relative shift of single-phonon MPR transitions from the calculated value to high magnetic field. This shift is usually assumed to be equal $\sim \alpha/4$, (α - polaron coupling constant). For a two-phonon pseudoresonance process this shift should be proportional to $(\alpha/2)^2$ and was neglected further.

A comparison of experiment with Landau level calculations made with a set of parameters /5/ for normal pressure showed:

- the optical phonon energy determined by condition (2b) from pseudoresonance position /1,2/ is $\hbar\omega_o = 12.3$ meV;
- the coordination of one-phonon resonance minima positions at $\vec{H} \parallel \vec{j}$ with (2a) condition for $\hbar\omega_o = 12.3$ meV is achieved if the polaron shift is taken to be 7%, that gives $\alpha = 0.28$.

Both results ($\hbar\omega_o = 12.3$ meV and $\alpha = 0.28$) are in the limit of the existing experimental data uncertainty (see /4/). These values were used for further calculations of pressure dependences of electron spectrum. Pressure dependence of $\hbar\omega_o$ was neglected, as $\partial \ln\omega_o / \partial P \leq 0.01\ GPa^{-1}$ /6/.

The pressure shift of MPR extrema at $\vec{H} \perp \vec{C}_3$ (Fig.1) is caused mainly by P-dependence of the transverse cyclotron mass $m^c_\perp$. In model /5/ $m_\perp$ is directly connected with E_g; for band edge at $k_\perp = 0$:

$$1/2m_\perp = A + Q^2/E_g, \quad Q^2(P)/Q^2(0) = 1 + \Delta V(P)/V \qquad (3)$$

(V - crystal volume, see /7/). A calculation of MPR transitions for different pressures with the condition (1) leads to the expression for E_g as a parameter of model /5/:

$$E_g(P)/E_g(0) = 1 - 0.53P + 0.093\,P^2, \quad P - GPa \qquad (4)$$

Note that an increase of nonparabolicity at high pressure shifts the pseudoresonance stronger than one-phonon process while α does not change, according to our estimation. As a result, the relation H_{PR}/H_N grows slightly at high pressure (Fig.2). The dependence $m_\perp(P)$ derived from (4) agrees well with the cyclotron resonance high pressure data /7/.

For $\vec{H} \perp \vec{C}_3$ orientation the determination of eigenvalues for 4x4 two-band Hamiltonian is rather difficult. But in this orientation only one-phonon processes were observed, and the non-parabolicity is small; so it was taken into account by including $m_\perp(E)$ dependence into 2x2 Hamiltonian. The problem reduced to a numerical solution of an infinite system of coupled equations. A comparison with the experiment shows that the same value $\hbar\omega_o = 12.3$ meV for $\vec{H} \perp \vec{C}_3$ as for $\vec{H} \parallel \vec{C}_3$ demands the same polaron shift of 7%. The data /8/ on the pressure dependence of the spin-orbit splitting and the ratio B/S^2 were used. The best-fit value for B(P) is

$$B(P)/B(0) = 1 + 0.284\,P - 0.16\,P^2, \quad P - GPa \qquad (5)$$

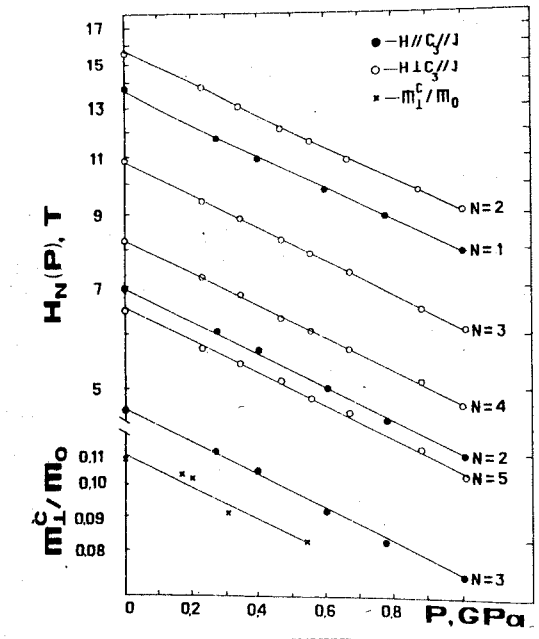

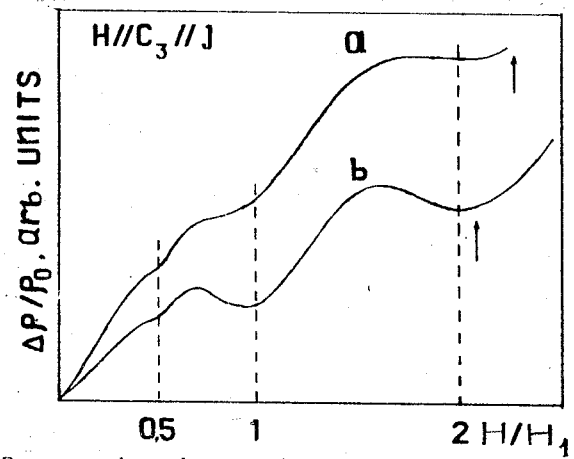

Fig.1. Pressure dependences of magnetic field values of MPR extrema $H_N(P)$ for $\vec{H} \parallel \vec{C}_3 \parallel \vec{J}$ (full circles) and $\vec{H} \perp \vec{C}_3 \parallel \vec{J}$ (open circles), this work; cyclotron resonance data on m_1^c /7/ (crosses). Numbers of lines are the numbers of MPR extrema.

Fig.2. The magnetoresistance of Te samples at $\vec{H} \parallel \vec{C}_3 \parallel \vec{J}$ vs the magnetic field (related to $H_1(P)$ position) at P=1.1 GPa (a) and at normal pressure (b).

As a result, the measured pressure dependence of MPR in Te is quantitatively explained in terms of the two-band model. The values of constants of electron and phonon spectra are determined.

The authors thank prof. R.V.Parfeniev for valuable discussions.

References

1. Д.В.Машовец, С.С.Шалыт. Осцилляции магнетосопротивления теллура, ЖЭТФ (письма),1966,т.4, в.9, стр.362-364.
2. M.S.Bresler, D.V.Mashovets. Magnetophonon resonance in tellurium, Phys. Stat. Sol., 1970, v.39, p.421-435.
3. N.Miura, R.A.Stradling, S.Askenazy et al. Anisotropic phonon coupling in the magnetophonon resonance in p-type tellurium, J.Phys.C.: Solid State, 1972, v.5, p.3332-3348.
4. Y.Maeda, N.Miura, M.Saketa, E.Ohta, Transverse magnetophonon resonance in p-Te in high pulsed magnetic fields, J.Phys.Soc. Jap., 1984, v.53, p.3120-3125.
5. M.Lutz, H.Stolze, P.Grosse. The masses of free holes and electrons in tellurium, Phys.Stat.Sol.(b), 1974, v.62, p.665-675.
6. W.Richter, J.B.Renucci, M.Cardona. Hydrostatic pressure dependence of first-order Raman frequencies in Se and Te, Phys. Stat.Sol.(b), 1973, v.56, p.223-229.
7. U.Steigenberger, M.I.Shirokov, S.G.Lapin et al. The influence of hydrostatic pressure on the free and bound states in tellurium. J.Phys.C: Solid State, 1984, v.17, p.427-436.
8. М.В.Глушков, М.И.Еремец, Ю.В.Косичкин и др. Валентная зона теллура под давлением, ФТТ, 1979, т.21, стр. 499-505.

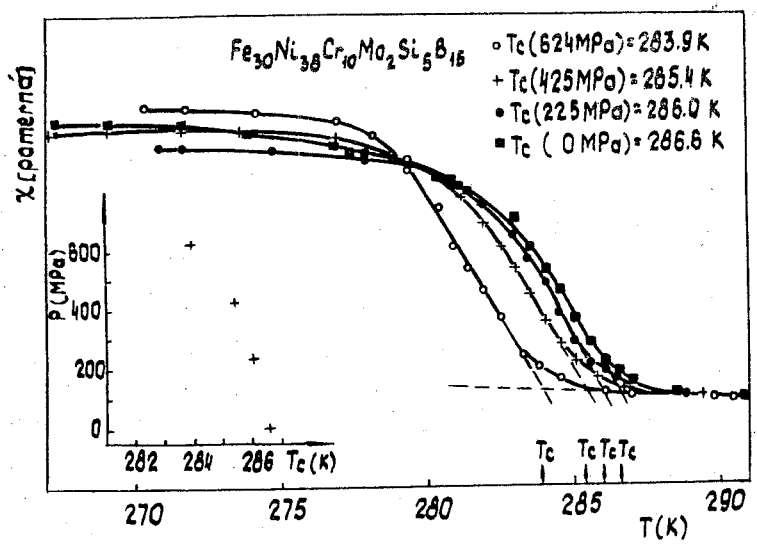

Fig.3. The temperature dependence of the initial susceptibility of unirradiated sample. T_c shifts to smaller values nonlineary with the pressure.

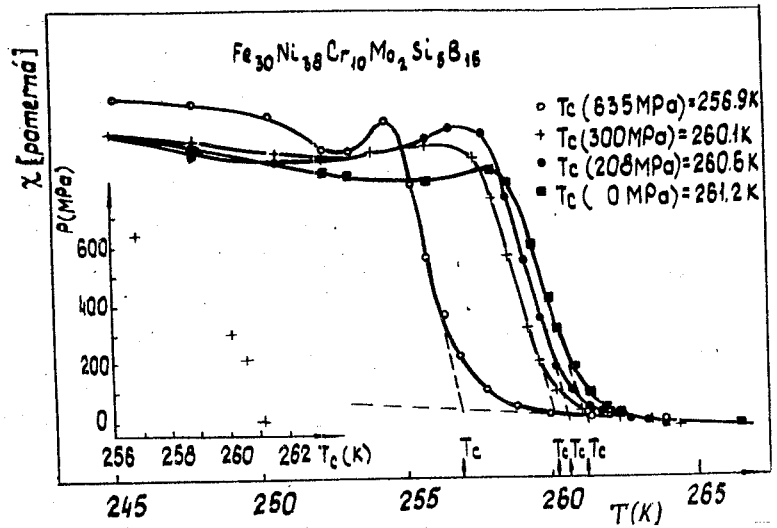

Fig.4. The temperature dependence of the initial susceptibility of sample irradiated with dose $5x10^{18}$n cm^{-2}.

In addition, hydrostatic pressure (up to 700 MPa) was applied to the samples in beryllium-bronze pressure cell filled with silicon oil using a piston-cylinder device. Manganin pressure sensor was used to the pressure determination. The Curie temperature was measured by the transformer method described in details by Leger et al./6/. The temperature was measured by calibrated thermocouple Cu-constantan.

Results and discusion. The dependence of T_c on the Cr content, on the annealing temperature /5/ and the doses of neutron irradiation is presented in Fig.I. The increase of the value of the annealing temperature leads to an increase of T_c, on the other hand the addition Cr and the neutron irradiation lead to a decrease of the Curie temperature.

Curves of magnetization versus field at liquid nitrogen temperature are shown in Fig.2. Curve (a) gives the magnetization of the annealed sample (523 K/I hour), curve (b) is for the unirradiated sample and curve (c) is for the sample irradiated with $5xI0^{I8}$n cm^{-2}. It can be seen from this Figure that the magnetization of irradiated sample is proportional to the magnetic field H at higher field. The magnetic isothermals can be therefore expressed by:

$$M(H,T) = \lambda_{hf} H + M(0,T)$$

where M(H,T) is the magnetization at temperature T and field H. The decrease of M(0,T) can be also attributed to the spatial inhomogenities (due to the irradiation procedure) in the magnetization.

It is evident from the Figs.3,4 that the decrease of T_c with an increase of the pressure is nonlinear. It seems that in the amorphous inhomogenous ferromagnets with relatively small sensitivity of the Curie temperature to the pressure, the reorganization of the amorphous structure, due to the neutron irradiation procedure, leads to an increase of the shift of T_c with pressure.

References

I. I.Škorvanek, A.Zentko:Phys.Stat.Sol./a/ 99, 275 (I987)
2. A.Zentko, M.Timko, P.Duhaj: Phys.Stat.Sol./a/ 66,KI25,(I98I)
3. M.Timko, A.Zentko, T.Tima: Acta Phys.Slov.35, 330 (I985)
4. M.Mihalik et al.: Czech.J.Phys. B 35 (I985) I053
5. M.Mihalik et al.: Czech.J.Phys. B 37 (I987) I6
6. J.M.Leger, C.Loriers-Susse, B.Vodar: Phys.Rev. B6 (I972) 4250.

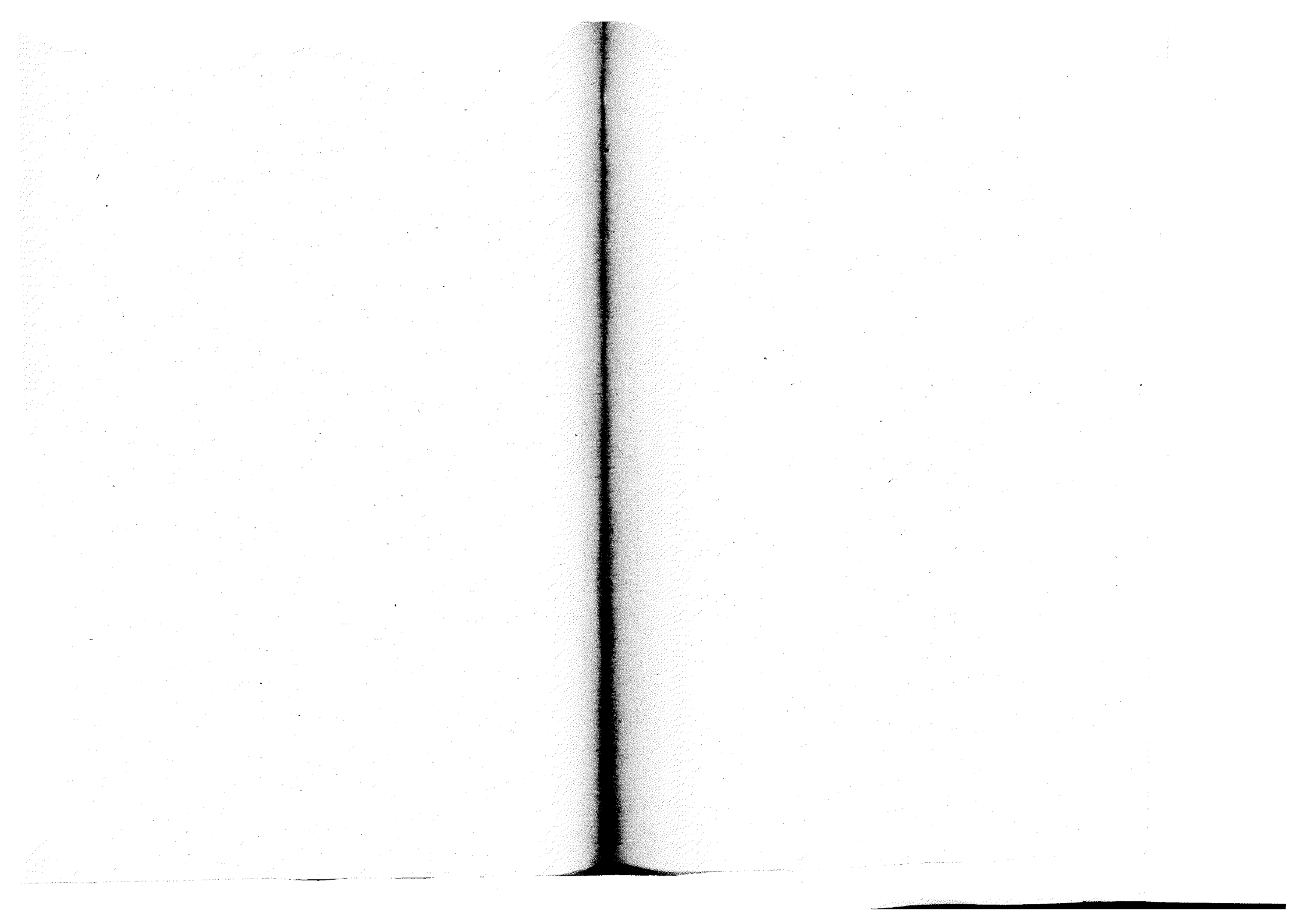

nal systems pressure influence would be felt first of all through a change of hybridization g. Calculation of the Hamiltonian's (3) total energy with the probe function was performed through variation of η, y, y_o parameters. These parameters were determined by minimization of values of λ and g.

It is obvious that the ground state, described by the function (4) has unmatching bond alternation $y \neq y_o$ for the electron subsystem and the lattice under $U \neq 0$. Moreover, there is a monotonical increase of y with an increase of U value, this reflecting the trend of the system to dissipate into molecules. In contrast to y, the displacement of atoms is proportional to y_o and has a maximum under further U increase. It is interesting that in the limit of absolutely rigid lattice ($\lambda = 0$, $y_o = 0$) there remains energetically favourable presence of bond alternation in the electron subsystem $y \neq y_o$. It is necessary to note that investigation of Hubbard chain /4/ reveals terms of order $U^2 y^2 \ln^3 y$ in E_{cor} in the U^2 approximation. In this sence our analysis has a qualitative character, however it allows to discuss a more complete system and to account for the gap y unmatching with the lattice dimerisation $\sim y_o$.

References

I. Barabanov A.F., Mikheenkov A.V. Variational method for ground state of one-dimensional Hubbard model. Fiz.Tverd.Tela (Leningrad), I986, 28, No 4, p.988-I004.

2. Kivelson S., Chapman P. Polyacene and a new class of quasi-one-dimensional conductors. Phys.Rev., I983, B28, No I2, p.7236-7243.

3. Baeryswil D., Maki K. Electron correlation in polyacetylene, Ibid, I985, B3I, No I0, p.6633-6642.

4. Krivnov V.Ya., Ovchinnikov A.A. Peierls instability in weakly nonideal one-dimensional systems, Zh.Eksp.Teor.Fiz. I986, 90, No2, p.709-723.

EFFECT OF PRESSURE ON BAND MAGNETISM

Mohammad Yousuf, P.Ch. Sahu, K.Govinda Rajan
Indira Gandhi Centre for Atomic Research, Kalpakkam 603 I02
India

Abstract

Pressure coefficient of electrical resistivity (PCR) undergoes a change in the sign and of the magnitude across the Curie temperature. However, the situation in iron is quite normal. We show that the anomalous behaviour of nickel is connected to a substantial band structure change during the magnetic transition.

Electrical resistivity of a band magnet shows a T dependence for $T < T_c$ and a T depending for $T > T_c$. Mott conjectured that the kink at T_c is due to substantial Fermi surface (FS) change. Considering the fact that the pressure coefficient of resistivity, $\partial \ln \rho / \partial P$ is a sensitive function of the band structure, and if there is a large change in the FS across T_c, then $\partial \ln \rho / \partial p$ is expected to be different on either side of the T_c /I/. Figs.I and 2 represent the data taken on nickel and iron. Obvious point to note is the clear cut change in the behaviour of the ρ of nickel just below and just above the T_c. We observe that the quantity of our interest $\partial \ln \rho / \rho P$ changes sign and magnitude if we compare the values at $T < T_c$ and $T > T_c$. In Fig.3 we plot the calculated and the observed resistivity as a function of temperature and at a fixed pressure (=50 kbar). It is noticed that above T_c, the calculated values do not reproduce even qualitatively the observed behaviour of nickel, it is clear that a significant feature must be missing from it. Mott's conjecture on the change of band structure across T_c provides an elegant solution to this anomaly /2/. Using this conjecture, we suggest, in the following, a qualitative account of the anomalous behaviour of paramagnetic nickel under pressure. In the high temperature phase of nickel, the situation can be described as follows:

I. The spins are relatively free, that is, the spin-spin coupling is fairly weak; and the magnetic moments are comparatively localised.

2. During the electron-ion scattering, spin flip is possible.

3. The strength of this spin flip scattering depends on the magnitude of the exchange splitting energy.

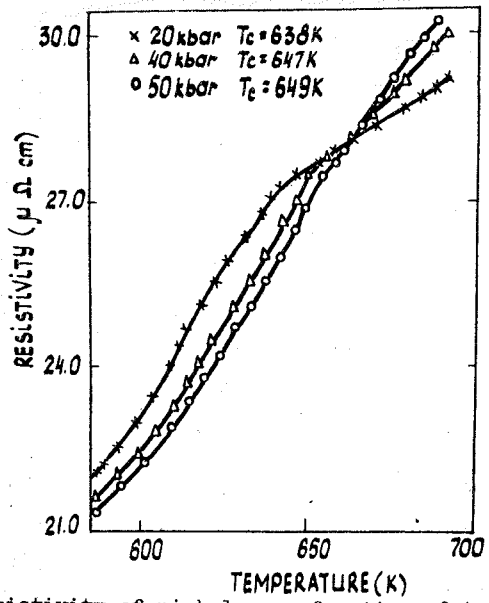

Fig.I. Resistivity of nickel as a function of temperature and pressure. The reversal in the behaviour of resistivity across T_c can be seen.

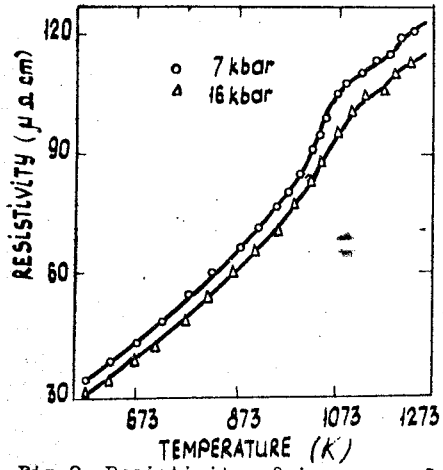

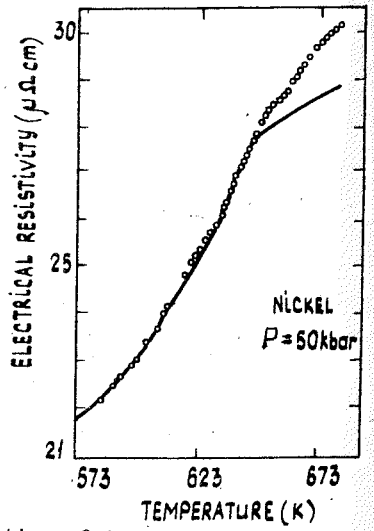

Fig.2. Resistivity of iron as a function of temperature and pressure. The pressure coefficient of electrical resistivity remains always normal and negative.

Fig.3. Electrical resistivity of nickel vs temperature and pressure = 50 kbar. ○ represents the data and the continuous curve is obtained from the expression for resistivity /I/.

It is worth noting that the scattering cross section per magnetic spin in paramagnetic phase is proportional to the square of the exchange interaction term. Since, the short range exchange interaction overlap of wavefunctions increases with pressure, this can lead to an increase in resistivity. This is precisely the situation in paramagnetic nickel.

Moving to the pressure results in paramagnetic iron, since, the exchange splitting energy is quite large here, spin flip scattering is not a dominant contribution. The usual processes leading normally to a decrease in resistivity can still dominate even in the paramagnetic phase.

We are thankful to Padmabhushan Shri C.V. Sundaram and Dr. P.Rodriguez for their constant encouragement.

References

I. A comprehensive review of this work can be found in Mohammad Yousuf, P.Ch.Sahu and K.Govinda Rajan, "High pressure and high temperature electrical resistivity of ferromagnetic transition metals: nickel and iron, Phys.Rev., 1986, B34, II, 8086.

2. Mohammad Yousuf, P.Ch.Sahu and K.Govinda Rajan, Evidence for a change in the FS of nickel across the magnetic transition, Phil.Mag. 1986, B54, 3, 241.

THE EFFECT OF PRESSURE ON GALUANOMAGNETIC PROPERTIES OF ELECTRON IRRADIATED $Pb_{1-x}Sn_xSe$

E.P.Skipetrov, V.P.Dubkov, E.A.Ladigin
Moscow State University, Moscow, USSR

Undoped IV-VI compounds and alloys ($Pb_{1-x}Sn_xTe$, $Pb_{1-x}Sn_xSe$) have a high density of native defects due to deviation from stoichiometry. The type and concentration of carriers in these materials are determined by the density and ionization state of point defects in metal and chalcogen sublattices. Electron irradiation generates point defects uniformly in the volume of the sample. This allows us to change the balance of defect densities and thus to control galvanomagnetic properties of alloys /1/. According to the theoretical data /2-4/, levels of native point defects in the lead chalcogenids are resonant with valence or conduction bands. Chalcogen vacancy levels are the nearest levels to the forbidden gap and lie in the conduction band close to the band edge. However, when the tin concentration in $Pb_{1-x}Sn_xTe(Se)$ alloys increases the chalcogen vacancy level will move down and at certain alloy composition it may be situated in the forbidden gap /4/.

In this work the effect of pressure ($P \leq 16$ kbar) on galvanomagnetic properties of n-$Pb_{1-x}Sn_xSe$ ($x=0.125$, 0.25), irradiated with electrons ($T \simeq 300$ K, $E = 4 \div 8$ MeV, $\Phi \leq 3.5 \cdot 10^{17}$ cm^{-2}), have been investigated.

Electron irradiation causes certain changes of galvanomagnetic properties of $Pb_{1-x}Sn_xSe$ alloys and the character of this changes depends on alloy composition. It was found that in $Pb_{1-x}Sn_xSe$ ($x = 0.125$) concentration of electrons remains unchanged or slightly decreases under electron irradiation.

Resistivity and Hall coefficient at $T = 4.2$ K of irradiated $Pb_{1-x}Sn_xSe$ ($x = 0.125$) samples increase under pressure (Fig.1), indicating the reduction of electron concentration in the conduction band. Extrapolation of n(P) curve shows, that at $P^* \simeq 10$ kbar electron concentration becomes zero and metal-insulator transition occures. At pressure $P \simeq 12$ kbar Hall coefficient at $T = 4.2$ K changes drastically and its sign reverses. In the upper pressure region ($P > 12$ kbar) resistivity and Hall coefficient at $T = 4.2$ K reach their saturation values. In the low pressure range ($P \lesssim 6$ kbar) temperature dependences of resistivity and Hall coefficient are characteristic for undoped crystals of $Pb_{1-x}Sn_xSe$. However,

at higher pressures character of dependences of resistivity changes and activation dependence on ρ (1/T) curve, that corresponds to existence of the deep local level in the forbidden gap of alloy, appeares. The activation energy $\Delta E_t = E_c - E_t$, evaluated from temperature dependence of resistivity, rises monotonically under pressure at a rate $d\Delta E_t/dP \simeq dE_g/dP$.

Experimental results obtained in this work may be explained assuming that band edges of $Pb_{1-x}Sn_xSe$ ($x = 0.125$) move with respect to each other under pressure, accompanied with the pinning of the Fermi level in irradiated samples by the local level E_t, associated, probably, with selenium vacancies (Fig.2). Under pressure band inversion and increase of forbidden gap take place, inducing a flow of electrons from the conduction band to the local level E_t. At $P = P^*$ local level transverses the bottom of conduction band and metal-insulator transition takes place. In dielectric phase the main low temperature transport mechanism is provided by the hole conductivity through localized states.

In $Pb_{1-x}Sn_xSe$ ($x = 0.25$) samples with $n = (4 \div 5) \cdot 10^{17}$ cm^{-3} electron irradiation produces reduction of the electron concentration with the initial rate $dn/n\Phi \approx 8$ cm^{-1}. Extrapolation of $n(\Phi)$ curve, obtained by Hall effect measurements at $T=4.2$ K, allows us to conclude, that at $\Phi^* \simeq 8 \cdot 10^{16}$ cm^{-2} electron concentration in conduction band becomes zero and metal-insulator transition takes place. While electron fluence reaches Φ^* absolute value of R_H at $T = 4.2$ K decreases and its sign reverses with increase of magnetic field. The sign reversal point shifts to the lower magnetic field with irradiation and at $\Phi > \Phi^*$ Hall coefficient at $T = 4.2$ K is positive in the investigated range of magnetic fields.

Reduction of the electron concentration and metal-insulator transition, induced by electron irradiation, may be explained assuming that the electron irradiation creates deep local level, associated with selenium vacancies, in the forbidden gap of $Pb_{1-x}Sn_xSe$ ($x = 0.25$). Generation of selenium vacancies under electron irradiation causes electron concentration reduction due to a flow of electrons from the conduction band to the local level. In dielectric phase the activation dependence on $\rho(1/T)$ curve, corresponding to creation of deep local level, appeares. Its activation energy is $\Delta E_t = E_t - E_v \simeq 0.025$ eV and is practically independent of pressure. Positive sign of Hall coefficient in dielectric phase indicates that the main transport mechanism is the hole conductivity through localized states.

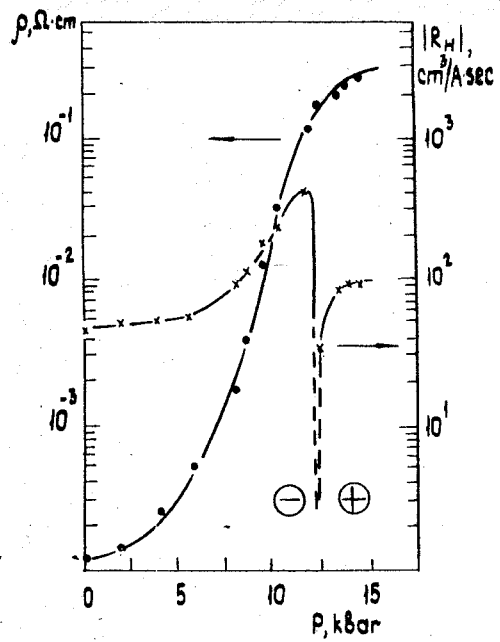

Fig.1. Pressure dependences of resistivity and Hall coefficient for sample $Pb_{1-x}Sn_xSe$(x = 0,125), irradiated with electrons ($\Phi = 1.6 \cdot 10^{17} cm^{-2}$), at T = 4.2 K.

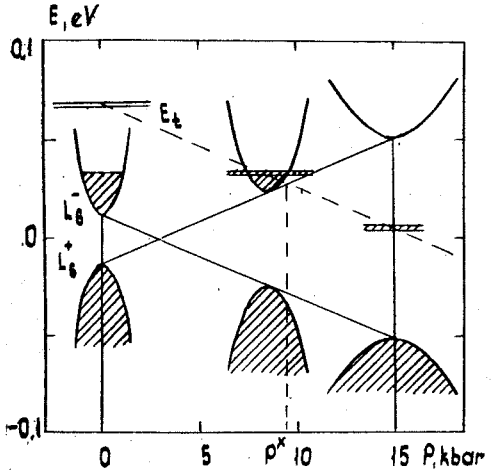

Fig.2. Alteration of the energy spectrum of $Pb_{1-x}Sn_xSe$ (x = = 0.125), irradiated with electrons, under pressure.

References

1. Zlomanov V.P., Ladigin E.A., Piregov B.P., Skipetrov E.P. Effect of electron irradiation on galvanomagnetic properties of $Pb_{1-x}Sn_xSe$. - Fiz. Tekh. Poluprov., 1985, v.19, N1, p.53-57.

2. Parada N.J., Pratt G.W. New model for vacancy states in PbTe.- Phys. Rev. Lett., 1969, v.22, N5, p.180-182.

3. Parada N.J. Localized defects in PbTe.- Phys. Rev.B., 1971, v.3, N6, p.2042-2055.

4. Volkov B.A., Pankratov O.A. Electronic structure of point defects in A^4B^6 semiconductors. - Zh. Eksper. Teor. Fiz., 1985, v.88, N1, p.280-292.

ELECTROPHYSICAL PROPERTIES OF SEMIMAGNETIC SEMICONDUCTORS $Hg_{1-x}Mn_xSe$ UNDER HIGH PRESSURE

V.A.Koulbachinskii, S.M.Chudinov
Moscow State University, Moscow, USSR

Oscillations of transverse and longitudinal magnetoresistance - effect of the Shubnicov-de Haas (SdH) - were investigated in single crystals n-type of semimagnetic semiconductor $Hg_{1-x}Mn_xSe$ under hydrostatic pressure up to P=1.6 GPa in magnetic field B up to 6.5 T in temperature range 0.2+15 K. Concentration of Mn in the samples was x=0.032 (inversion energy spectrum under atmospheric pressure, concentration of electron $n=4.5\cdot10^{18}$ cm^{-3}, Fermi energy E_F=390 meV) and x=0.07 (direct energy spectrum under atmospheric pressure, concentration of electrons $n=3.5\cdot10^{18}$ cm^{-3}, Fermi energy E_F=285 meV).

Oscillatory part of transverse magnetoresistance of the sample x=0.032 is given in Fig.1 for different temperatures, pointers show the positions of different nodes. In Fig.2 you can see temperature dependence of the second (a) and the third (b) nodes at different pressures. When pressure increases nodes go to the region of a weak magnetic field, as like when temperature increases. As transitions to cluster spin a glass observed in $Hg_{1-x}Mn_xSe$ with $x < 0.1$ when temperature $T < 1$ K /1/, then measurements of oscillations correspond to low temperature linear region in dependence of magnetic susceptibility χ^{-1} on T. In weak magnetic field at low temperature magnetic susceptibility is described by Curie-Weiss law, but with fitting parameters θ^* and x^*, where x/x^* means average quantity of magnetic atoms in a cluster. Let's suppose that if concentration of magnetic atoms is not large then interactions between them is small and mean value of spin $\langle S_z \rangle$ in magnetic field direction depends on temperature and magnetic field as well as in paramagnetic: $\langle S_z \rangle = -SB_S(y)$, where $B_S(y)$ - Brillouin function, S - maximum value of spin, $y = 2\mu_B SB/kT$. Oscillation amplitude is proportional to $\cos(\pi g^*/2)$, where g^* - effective g-factor. Exchange interaction leads to change of g-factor from constant to function of temperature and magnetic field and in nodes it is equal to an odd number. Interaction of magnetic moments in the theory of molecular field can be taken into account by change of argument Brillouin function on $y'=2\mu_B SB/k\cdot(T-\theta^*)$. Using x^* and θ^* as fitting parameters and values of ma-

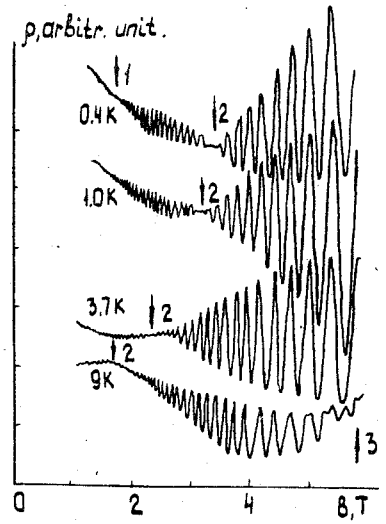

Fig. 1. Oscillations of transverse magnetoresistance ρ in sample with x=0.032 at different temperatures (shown in picture) at atmospheric pressure. Pointers show positions of different nodes.

trix elements of exchange interaction HgMnSe at atmospheric pressure /2/ one can calculate the position of nodes at each pressure and compare it with experimental data. As a result a dependence $\theta^*(P)$ is obtained, which for sample with x=0.032 is shown in Fig.3, x/x^* being equal 2.5, that is clusters consist from 2 or 3 atoms of Mn. Pressure dependence θ^* (Fig.3) corresponds to transition from antiferromagnetic to ferromagnetic interaction.

The surprising effect was discovered in HgMnSe under pressure decreasing of carrier concentration (which was calculated from SdH effect). This effect can be explained with assumption about transition of electrons from conduction band to acceptor band, born by deep admixture level, generated from conduction band, for example in L-points. Energy difference between L and Γ points $\varepsilon_{\Gamma L} \simeq 3.0$ eV. From experimental data using Pidgeon-Brown model was calculated change of E_F under pressure, which are practically linear: $|\partial\varepsilon_F/\partial P| = |\partial_{\Gamma L}/\partial P| = 0.09$/GPa for both samples.

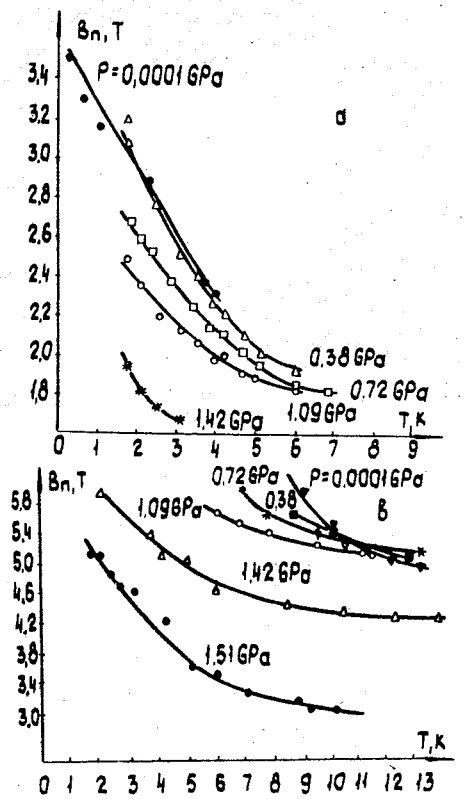

Fig. 2. Temperature dependence of the nodes positions B_n at different pressures (shown in picture) in sample with x=0.032 for node N°2 (a) and N°3 (b).

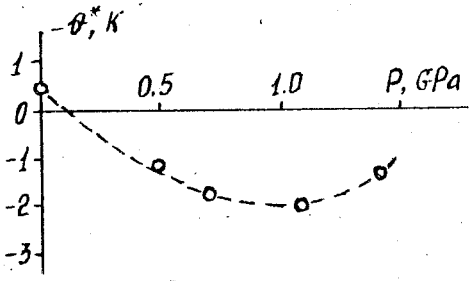

Fig.3. Pressure dependence parameter θ^* for x=0.032.

Exchange interaction in HgMnSe may be connected with superexchange of Bloembergen and Rowland, virtual transitions across zero energy gap of Bastard and Lewiner and in less degree with RKKI interaction but in frame work solid solutions of HgMnSe had electron concentration about $5 \cdot 10^{18}$ cm^{-3}, which correlates with normal, classical spin-glasses with RKKI interactions.

At the same time in the sample with x=0.07 under pressure $P \geq 0.6$ GPa there is no dependence of the nodes positions on temperature. The pressure $P \simeq 0.6$ GPa corresponds to the increase of direct energy gap up to value $\simeq$ 100 meV. Decreasing of exchange interaction under pressure if $P > 0.6$ GPa means disappearance of Bastard-Leviner mechanism.

References

1. Brandt N.B., Ismailov G.T., Koulbachinskii V.A. et al. Magnetic phase diagram of $Hg_{1-x}Mn_xSe$ //Sov.Phys., Low Temp. Phys., 1986,v.12, N12,p.215-217.
2. Takeyama S., Galazca R.R. Band Structure of $Hg_{1-x}Mn_xSe$ from anomalous Shubnicov-de Haas effect// Phys.Stat.Sol. (B) 1979, v.96, N 2, p.413-423.

THE EFFECT OF PRESSURE ON PHASE TRANSITIONS AND SUPERPROTONIC CONDUCTIVITY IN HYDROSULFATE CRYSTALS

V.V.Sinitsyn[I], A.I.Baranov[2], L.A.Shuvalov[2]

[I]Institute of Solid State Physics, USSR Academy of Sciences, USSR

[2]Institute of Crystallography, USSR Academy of Sciences Moscow, USSR

As has been shown in papers /I,2/, structural phase transition to a state with superionic conductivity takes place in a number of hydrosulfate crystals (hydroselenates) with the general formula $MeHAO_4$ (where Me=Cs, NH_4, Rb; A=S, Se). Such high-conductivity arises because static system of hydrogen bonds is broken and a dynamic one is formed /3/. Therefore, it would be of interest study the effect of pressure on both the phase transitions with such a type of the position disorder in the proton subsystem and the proton conductivity. In our paper the investigation has been carried out on an example of hydrosulfate crystals.

In $CsHSO_4$(CHS) and $CsDSO_4$(CDS) crystals the phase P-T diagrams (Fig.I) turned out to be wholly identical, except for the III⟶ II transition, which is not intrinsic in CDS. At the pressures P > I.0 GPa the P-T-diagram displays two new high-temperature (VI and VII) and two new low-temperature (IV and V) phases. Conductivity σ in phases IV and V was $\sim 10^{-8} \div 10^{-9}$ $Ohm^{-1}\cdot cm^{-1}$ ($T \approx 300$ K), and on transition to phases VI and VII it reached the values of $\sim 10^{-4} \div 10^{-2}$ $Ohm^{-1}\cdot cm^{-1}$. It should be noted that up to P ≈ I.0 GPa the superionic transition temperature, T_{si}, was almost independent of pressure ($dT_{si}/dp = 15 \pm 3$ deg/GPa), whereas the rate of change of the melting temperature, T_m, was quite noticeable ($dT_m/dp \approx 150$ deg/GPa).

In $MeHSeO_4$ crystals (Me=Cs, NH_4, Rb) with increasing the cation radius (Cs⟶ NH_4⟶ Rb), the superionic transition temperature elevates (127 °C ⟶ 144 °C ⟶ 173 °C) /2/. On the other hand, the superionic phase in $MeHSO_4$ crystals is realized in CHS only, and in crystals with a less radius, for instance, in NH_4HSO_4(AHS) and $RbHSO_4$(RHS), no superionic state exists up to T_m, though the low-temperature phases are identical. Note that the process of melting in AHS and RHS differes significantly from that of common ionic crystals. The solid body-melt phase transition for such hydrosulfates occurs within some temperature range (~ 10°) and is characterized by slow motion of the crystal-melt boundary. This feature of melting is also displayed for an anomalously low value of $(dT_m/dp)_{p=p_{at}} \approx$ 30 deg/GPa /4/.

Proceeding from these results and the empirical rule,which states that hydrostatic pressure is qualitatively analogous to an increase in the cation (anion) radius, one may expect for superionic phase transitions to arise in AHS and RHS crystals. Indeed, an analysis of the phase P-T diagram of AHS /4/ shows that phase VI, arising at $p \gtrsim 0.4$ GPa, is superionic. Pressure $p \gtrsim 0.28$ GPa induces a superionic phase for RHS as well (Fig.2). The temperature of superionic phase transition I⟶ IV decreases with pressure ($dT_{si}/dp = 80 \pm 10$ deg/GPa), that indicates a higher density of phase IV, as compared to phase I. However, the temperature of superionic transition III⟶ IV in RHS, as well as in CHS and AHS /4/, is almost independent of pressure ($dT_{si}/dp = 20 \pm 5$ deg/GPa).

The effect of pressure on conductivity in superionic and low-conductivity phases of hydrosulfate crystals differs both quantitatively and qualitatively (Fig.3). In superionic phases of CHS, AHS and RHS crystals conductivity decreases with pressure, whereas in the low-conductivity phase of CDS (with an accuracy of ±5%) it is independent of pressure.

The effect of pressure on the ionic transport is usually characterized by the activation volume V_a, which can be determined experimentally from pressure dependences of the ionic conductivity σ :

$$V_a = -T\left(\frac{\partial \ln \sigma}{\partial p}\right)_T + T\left(\frac{\partial \ln A}{\partial p}\right)_T \approx -T\left(\frac{\partial \ln \sigma}{\partial p}\right)_T$$

where A is the conductivity prefactor in the Arrhenius law.

In superionic phases of CHS, AHS and RHS crystals the values of V_a turned out to be equal to 1 ± 0.5 cm^3/mole, 1.1 ± 0.5 cm^3/mole and 2.5 ± 0.5 cm^3/mole, respectively. The qualitative difference of these values from $V_a = 0$ in low-conductivity phases indicates essential change in the mechanism of proton conductivity upon transition to a superionic state.

References

I. Baranov A.I., Shuvalov L.A., Schagina W.M. Superionic conductivity and phase transition in $CsHSO_4$ and $CsHSeO_4$ crystals.- Pis'ma Zh.Eksp.Teor.Fiz., 1982, 36, 381-384.

2. Moskvich Yu.N., Sukhovskii A.A., Rozanov O.V. Ion motion and high-temperature phase transition in NH_4HSeO_4 and $RbHSeO_4$ crystals. -Fiz.Tverd.Tela, 1984, 26, 38-43.

3. Merinov B.V., Baranov A.I., Shuvalov L.A., Maximov B.A. Crystal structure of the superionic phase of $CsDSO_4$ and phase transitions in cesium hydro- and deuterosulphates (selenates). - Kristallografiya, 1987, 32, N 1, 86-92.

4. Baranov A.I., Ponyatovskii E.G., Sinitsyn V.V., Fedosyuk R.M., Shuvalov L.A. Hydrostatic pressure-induced superionic conductivity in a crystal NH_4HSO_4. - Kristallografiya, 1985, 30, N 6, 1121-1123.

5. Gesi K., Ozawa K. - J.Phys.Soc.J., 1975, 38, 459-462.

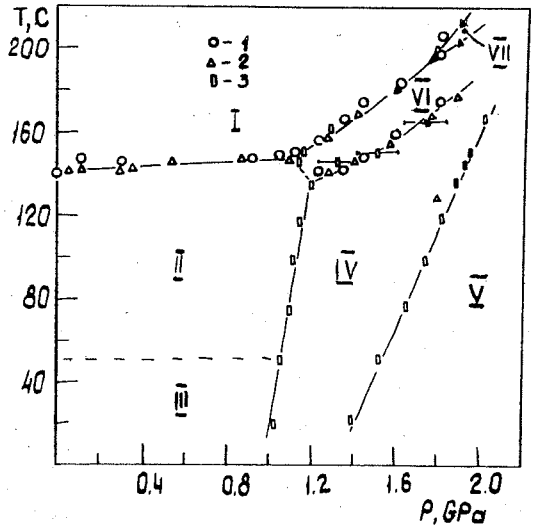

Fig.1. Pressure-temperature phase diagram of a $CsHSO_4$ crystal constructed from the following data: 1 - conductivity; 2 - pressure-temperature curves; 3 - piezometry.

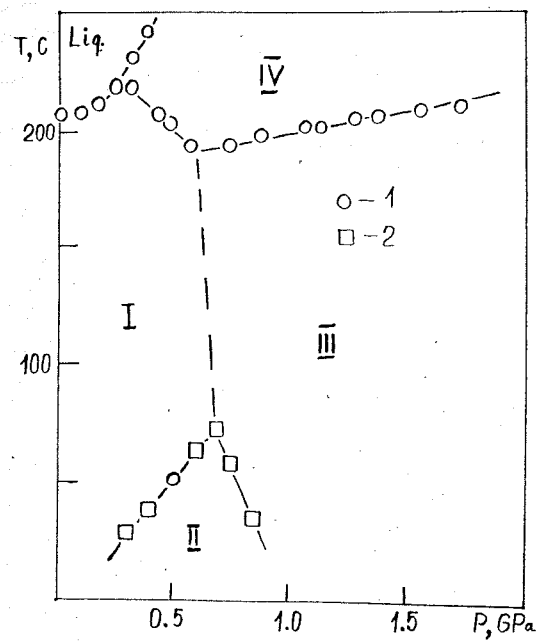

Fig.2. P-T phase diagram of a $RbHSO_4$ crystal: 1 - present work; 2 - /5/.

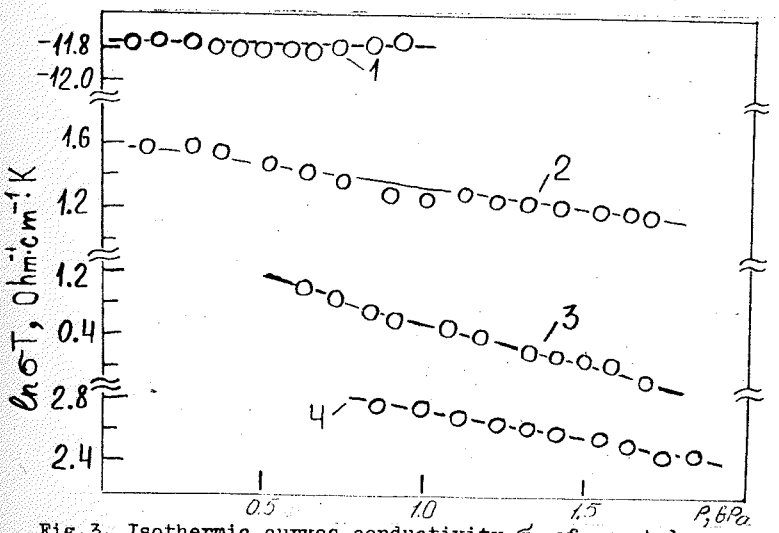

Fig.3. Isothermic curves conductivity σ of crystals: 1 - $CsDSO_4$ (T=400 K); 2 - $CsHSO_4$ (T=450 K); 3 - $RbHSO_4$ (T=497 K); 4 - NH_4HSO_4 (T=487 K).

CYCLOTRON RESONANCE AND IMPURITY LEVELS IN TELLURIUM IN SUBMILLIMETER REGION UNDER HYDROSTATIC PRESSURE

S.G.Lyapin[1], M.I.Eremets[1], A.M.Shirokov[1], E.A.Vinogradov[2], S.V.Demishev[2], Yu.V.Kosichkin[2], R.Herrmann[3], H.-U.Müller[3], F.Ludwig[3].

[1]L.F.Vereshchagin Institute of High Pressure Physics of the USSR Academy of Sciences, Troitsk, USSR

[2]The Institute of General Physics of the USSR Academy of Sciences, Moscow, USSR

[3]The Humboldt University, Berlin, GDR

We were the first to realize under hydrostatic pressure the submillimeter high resolution magnetospectroscopy /1/ - one of the most informative tool of band structure and impurity states investigation in semiconductors.

Subject of our inquiry was Sn-doped Te with $p \sim 2 \cdot 10^{14} cm^{-3}$. Transmission and photoconductivity were studied at magnetic field up to 6 T and under P up to 3.4 kbar at the helium T. Wave back tubes and submillimeter laser were used as radiation sources.

Pressure dependence of the hole effective mass was determined with the high accuracy from the cyclotron resonance (CR) line position in transmission spectra (Fig. 1a):

$$m_p^*(P) = m_p^*(P_o) \cdot \exp(-a \cdot P)$$

where $m_p^*(P_o) = (0.112 \pm 0.001) \cdot m_o$, $a = (5.6 \pm 0.1) \cdot 10^{-2}$ kbar^{-1}.

In photoconductivity spectra we observed impurity lines which were focused in three different values of zero magnetic field transition energy: E_B = 1.2 meV - F and C lines, E_D = 1.8 meV - E and D lines, E_X = 2.0 meV - B and X lines. From the circularly polarized radiation investigation we conclude that F and C lines correspond to transitions from the ground "bonding" state of hydrogenlike impurity to $2p_{\pm}$ states.

The pressure shift of lines originating from E_B transition had another sign and value than the shifts of lines originating from E_D and E_X (Fig.2). F and C lines were slightly shifted to the low magnetic field in a linear fashion. D, X, B lines were sharply shifted to the high field; the shift being nonlinear attained a saturation at P > 1.5 kbar.

The pressure dependece of the hydrogenlike impurity binding

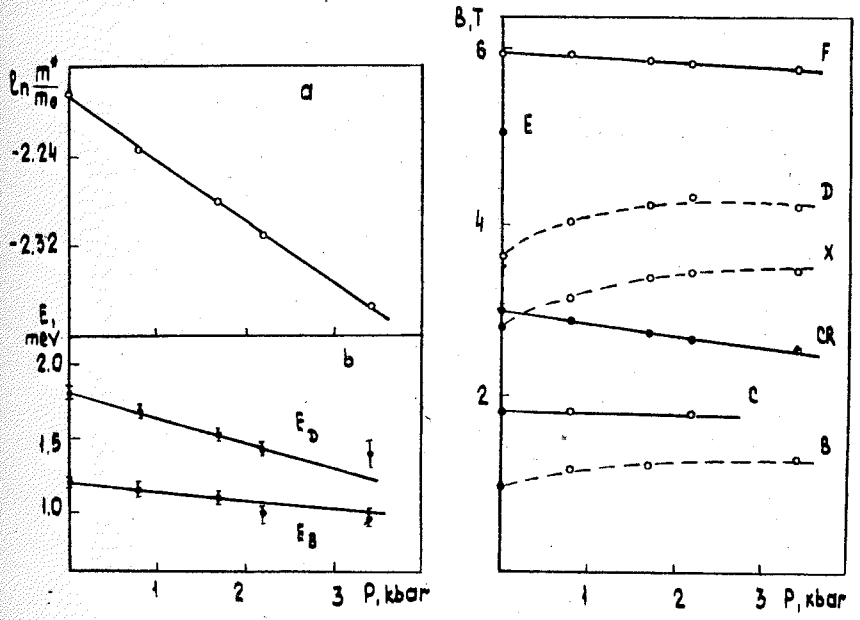

Fig. 1. Pressure effect on the hole effective mass (a) and impurity transition energies (b).

Fig. 2. Pressure effect on the magnetic field position of impurity lines and CR: T=1.6 K, λ =394 μm.

energy (which agrees with E_B accurate up to $kT \sim 0.15$ meV, Fig.1b) is more sharp than one determined from galvanomagnetic data /2/ and does not exhibit nonmonotonic behaviour predicted in /3/.

From more sharp pressure dependence of E_D and E_X energy in comparison with E_B we conclude that transitions E_D and E_X were from a ground level and a short-range potential played a large role in its formation. Therefore B,X,D,E lines are unlikely to be explained by transitions between exited states of heliumlike impurity. Thus a defect responsible for E_D, E_X transitions has quite different nature than hydrogen- and heliumlike impurities.

To determine electron effective mass m_n^* data about which are inconsistent we investigated CR of nonequilibrium charge carries. Transmission change ΔTr induced by the interband illumination (He-Ne laser, 3.39 μm) was recorded over the range 2-100 K (Fig.3). The circularly polarized submillimeter radiation was used to separate electron hole contributions.

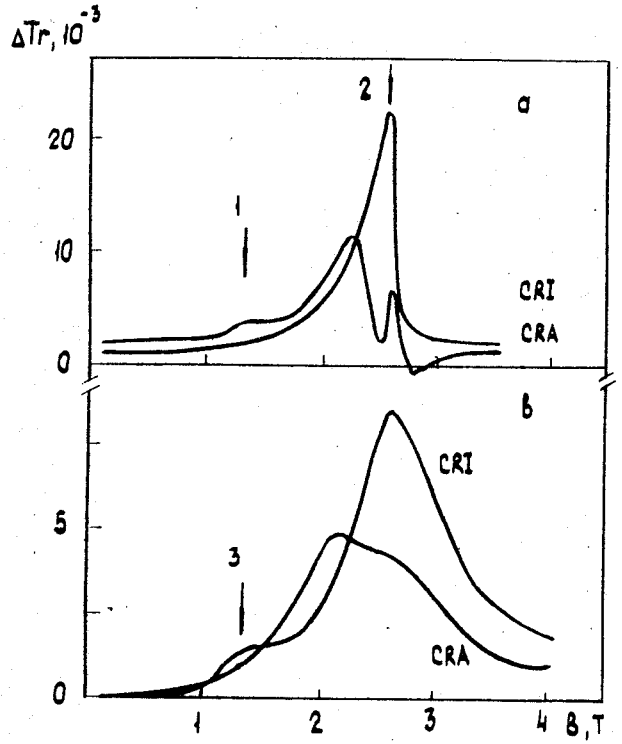

Fig. 3. Change of transmission of submillimeter circularly polarized radiation induced by interband illumination: a-T=2 K, b-T=25 K; λ=470 μm.

In the active sence of circular polarization CRA typical at the low temperature W-shaped curve ΔTr was transformed to V-shaped curve at the high temperature. The shape of the curve ΔTr and its change were well described by hole absorption only /4/.

The line 1 observed at 2K in CRA corresponds to one of impurity lines in photoconductivity spectra.

In the inactive sence of circular polarization CRI the strong line 2 was revealed over all temperature range. Its temperature dependence, the different position with respect to CR of holes did not furnish an explanation of the line 2 by hole absorption induced for example by depolarization effects. A special sample surface preparation decreasing accumulation layer depth resulted in decreasing of the line 2 amplitude by a factor of ten. Therefore the line 2 appears to be attributed to nonequilibrium electrons with $m^*_{ns}=0.115\cdot m_o$ localized near (0001) surface.

The line 3 arised in some temperature range in CRI. T~ 25K was the optimal T for its observation. Corresponding $m^*_n=0.06\cdot m_o$ well agrees with calculation /5/ for bulk electrons. The temperature behaviour of line 3 agrees with results of /6/ in accordance to which changes of electron mobility and lifetime over the range 2-100 K must cause an existance of some temperature being optimal for electron CR observation. It seems that CR of bulk electrons at low temperature was observed for the first time.

References

1. Steigenberger U., Eremets M.I., Lyapin S.G., Shirokov A.M., Vinogradov E.A. FIR-detection in the presence of high hydrostatic pressure - In: Proc. Conf. Infrared and Millimetre Waves, Miami, 1981.
2. Tani T. and Tanaka S. Pressure effect on the impurity state and impurity conduction in tellurium - In: Proc. Int. Conf. Phys. Selenium and Tellurium, Königstein, 1979. Berlin-Heidelberg-N.-York, 1979, p.142-152.
3. Thahn D. and Suffczinski M. Acceptor ground state in tellurium under hydrostatic pressure - Sol. State Commun. 1972,v.11, No 1, p.189-191.
4. Vinogradov E.A., Demishev S.V., Kosichkin Yu.V., Lyapin S.G., Polyakov Yu.A., Shirokov A.M. Characteristic properties of cyclotron resonance of nonequilibrium charge carries in tellurium at low temperature - Fiz. i tekh. poluprov., 1986, v.20, No 9, p.1629-1634.
5. Volkov B.A., Pankratov O.A., Pakhomov S.V. Deformation theory of the energy spectrum of tellurium - Zh. eksper. i teor. fiz., 1984, v.86, No 6, p.2293-2303.
6. Vinogradov E.A., Demishev S.V., Kosichkin Yu.V., Polyakov Yu.A. Recombination of photoexited charge carries in tellurium at low temperature - Fiz. i tekh. poluprov., 1985, v.19, No 8, p.1479-1487.

SUPERCONDUCTIVITY OF HIGH PRESSURE PHASES OF a-Si AND a-Si:H

I.V.Berman, E.A.Cohen, I.L.Romashkina, V.I.Sidorov, D.P.Utkin
Moscow State University, Moscow, USSR

We have studied the SC properties of amorphous a-Si and a-Si:H at high pressures. Crystallization pressure of amorphous silicon can exceed substantially the metallization pressure /I/. It permits to study the features of SC transition temperature T_c as the crystallization pressure is approached and also in crystalline phases that arise at higher pressures.

The samples of a-Si with the thickness D < 5 μm were produced by the vacuum deposition technique. The films of a-Si:H with the thickness D≈ I-5 μm were prepared by the glow-discharge decomposition of silane and contained up to 20 at.% of hydrogen.The thin films (D < 0.I μm) of a-Si:I0% H have also been studied.

Pressure induces an insulator-metal transition accompanied by a drop in the electrical resistance R by seven to ten orders of magnitude in the a-Si and a-Si:H systems. The distinct increase in transition pressure P_o with the enhancement of hydrogen content X is observed (Fig.I). We haven't succeeded to transform the a-Si:20%H sample into metallic state by applying the pressure at least up to 220 kbar. Transition pressure $P_o \sim 220$ kbar for thin films (D < 0.I μm) of a-Si:H is significantly higher than that of the films with the thickness more than I μm and the same hydrogen content.

There are a number of features in temperature dependences of R(T) of a-Si and a-Si:H samples. The R(T) dependence of the samples with D > I μm is metallic in the temperature range from 300 K to T_c. The dependences of R upon T and behaviour of T_c for thin a-Si:H films are completely different from the corresponding dependences for the thick films. The R decreases by 4-5 % down to its minimum at ~ 50 K and increases by 2 % in cooling down to 4 K. The onsets of SC transitions are observed at T≈ 2 K.

The value of T_c of a-Si:H films with D > I μm falls off linearly with the pressure enhancement at the pressure range $P_o(X) < P < I40$ kbar (metallic amorphous phase (Fig.2, curve I)). According to X-ray analysis /I/ for evaporated a-Si at this pressure range the crystalline peaks appear over the amorphous background and high-pressure phase of a-Si below I50 kbar can be reversed to the amorphous state after the compression. The situation in a-Si:H appears to be similar. This suggestion agrees with experimentally observed reversibility of T_c at the motion along the curve I (Fig.2). The amorphous metallic phase of a-Si with T_c values corresponding to the curve I persists up to pressures I80-200 kbar (Fig.2b).

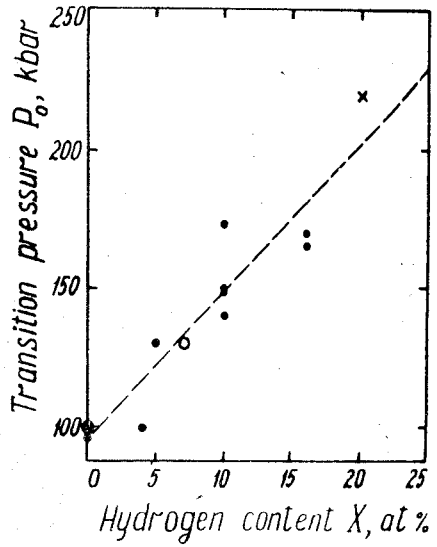

Fig.I. Semiconductor-metal transition pressure P_o dependence on hydrogen content X of the amorphous silicon films with the thickness D > I μm. White circles are the data of ref./I/. Present work data are marked by black symbols. The cross labels the pressure at which a-Si:20%H films weren't metallized yet.

The complete crystallization of a-Si takes place at pressures ~ I70 kbar /I/. The dependence of T_c on P of crystallized phases of a-Si:H in the form of the curve with the maximum near I75 kbar (Fig.2, curve II) has been shown primarily in /2/. This curve is completely reversible. Maximum near P=I50 kbar which was observed in the work /3/ on the crystalline c-Si in the pressure range I40<P<250 kbar agrees with the character of T_c on P dependence (curve II). In accordance with X-ray data /4/ this dependence is connected with the coexistence of two phases at P~I40 kbar and with complete transition of the sample into ph-

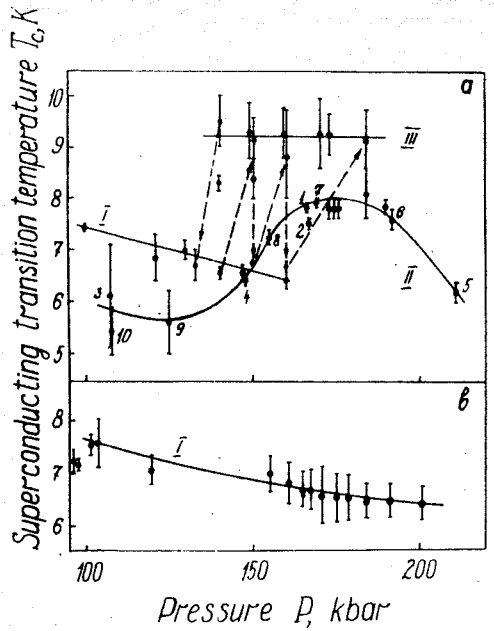

Fig.2. Change T_c of a-Si:H (a) and a-Si (b) films under pressure. Curve I is equilibrium T_c values of amorphous metallic phase, II is T_c values of crystallized phases of a-Si:H, III is T_c nonequilibrium phase of a-Si:H. The sequence of state changes of the same a-Si:IO%H sample are marked by digits I-IO.

-phase at P > I50 kbar /3/. Disappearance of the superconductivity at P < I00 kbar seems to be connected with enhancing the concentration of semiconducting bcc phase. The attention should be given to the fact that the thicknsss and producing conditions play a significant role in behaviour of a-Si and a-Si:H films under pressure. The results obtaining for thin a-Si:H films appear to point out the enhancing role of the electron localization effects as D decreases, which lead to the change of the curves R(T) and to the suppression the superconductivity.

In the pre-crystallization range of a-Si:H at intermediate pressures I40 < P < I80 kbar the following interesting phenomenon is revealed: a small pressure increase causes substantial (up to 3 K) increase in T_c (Fig.2, curve III). The state with the higher T_c persists for 2-3 h at room temperature. After a long annealing, this state is desrupted, the system going into either an equilib-

rium metallic amorphous state (at P < I60 kbar) with T_c corresponding to curve I or a crystalline state with T_c corresponding to curve II. After a complete crystallization of the sample (at P > I80 kbar) this effect disappears.

The increase observed in T_c near the crystallization threshold seems to be most closely related to the decrease in T_c for superconducting glasses during annealing of freshly quenched samples in nonequilibrium state.

References

I. Minomura S. Pressure-induced effects and phase transitions in amorphous semiconductors. - Amorphous Semicond.: Technol. and Devices, Tokyo e.a., Amsterdam e.a., I98I, p.245-254.

2. I.V.Berman, N.B.Brandt, I.L.Romashkina et al.Anomalies of the superconducting properties of amorphous hydrogenated silicon at high pressures. - Pis'ma ZETF, I985, v.4I, N7, p.288-290.

3. Mignot J.M., Chouteau G. and Martinez G. Properties of superconducting high-pressure phases of silicon. - Phys.Rev., I986, B 34, N5, p.3I50-3I55.

4. Jing Zhu Hu, Larry D.Merkle, Carmen S. Menoni and Ian L.Spain. Crystal data for high-pressure phases of silicon. - Phys.Rev., I986, B 34, N7, p.4679-4684.

RESONANT IMPACT IONIZATION IN Bi-Sb ALLOYS UNDER UNIFORM COMPRESSION AND STRONG UNIAXIAL DEFORMATION

E.V.Bogdanov, N.Ya.Minina
Moscow State University, Moscow, USSR

The resonant impact ionization effect which is caused by vertical Auger transitions at quantizing magnetic fields has been discovered in semiconducting bismuth-antimony alloys /1/. It is shown that the positions of the resonances are determined by an energy gap width and that the effect can be used for the determination of the energy spectrum change under applied external stress. Resistivity measurements in n- and p-type $Bi_{1-x}Sb_x$ semiconducting alloys ($0.10 \leq x \leq 0.16$) at high electric ($E \lesssim 50$ V/cm) and magnetic ($B \lesssim 5$ T) fields which are reported in this paper have been performed under uniform compression up to 1 GPa and strong uniaxial compressive deformations up to 0.2% at 4.2 K.

At normal conditions but at high breakdown electric fields (curve 1 in Figure 1) the resonance type minima appeared on magnetic field dependences of resistance in quantizing magnetic fields like it had been observed in Ref.1. The magnetic fields B_N of impact ionization resonances do not depend on the value of electric field or electric current and can be described quantitatively by the relation:

$$B_N = M \frac{cm_o}{e\hbar} \frac{E_{gL}^2}{N} \qquad (1)$$

where m_o is a free electron mass; M is a product of matrix elements which doesn't depend on strains; E_{gL} is the width of the energy gap at every L point of the Brillouin zone; N =1, 2,3 ... /1/.

Fig. 1 shows that the magnetic fields at which the resonances are observed decrease under the pressure. When the expression (1) is taken into account it is naturally to explain this effect by well-known /2/ decrease of direct energy gaps in $Bi_{1-x}Sb_x$ alloys ($x > 0.05$) under pressure. The position of the N=1 resonance was strictly fixed at the whole range of pressures. The amplitude of the N=2 resonance decreases repidly with pressure and its position moves to low magnetic fields where extremely large monotonic increase of the resistance doesn't permit to determine its position with sufficient precision. The dependence

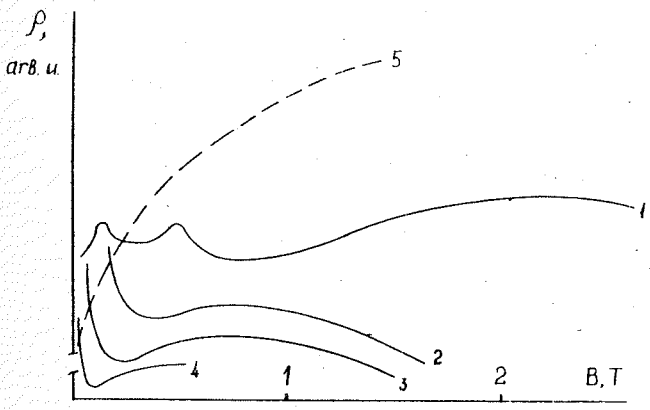

Fig.1. Dependence of the resistance ρ on the magnetic field B in n-$Bi_{0.89}Sb_{0.11}$ ($B \parallel j \parallel C_2$) at the following pressures p, GPa: 1.5-10^{-4}; 2-0.335; 3-0.56; 4-0.74 and the current density j, A/cm^2: 1÷4 - $4.5 \cdot 10^3$; 5-10.

of B_1 on the pressure value p is $B_1^{0.5} \sim -p$ (curves 1, 2 in Fig.2). This law can be easily obtained from (1) assuming the linear decrease of the energy gap with pressure and its poor response to the change of magnetic field /2/. The value $dE_{gL}/dp \simeq -17$ meV/GPa is obtained from the expression (1) and data on Fig.2 (curve 1, 2). This sufficiently agrees with result $dE_{gL}/dp \simeq -25$ meV/GPa known for $Bi_{1-x}Sb_x$ alloys /2/.

Fig.3 shows typical magnetic field dependences of the resistance under strong uniaxial compressive strain along C_1 axis. For low current density the resistance increases monotonously (Fig.3, curve 4). For high current densities, which correspond to electric fields above the threshold, minima like anomalies connected with resonant impact ionization appear. The resonance at B = 1.5 T results from the vertical Auger transitions in L_2 and L_3 equivalent valleys (N=1) /1/. Minimum at B=0.75 T is connected with transitions in L_1 (N=1) and in L_2, L_3 (N=2) because in this orientation the value of M for L_1 valley is half as large as for L_2,L_3 valleys /1/. Invariability of the resonance position at 1.5 T and absence of any minimum splitting at 0.75 T mean that direct energy gaps in all three L points of Brillouin zone are constant up to the highest obtained deformations. Under uniaxial

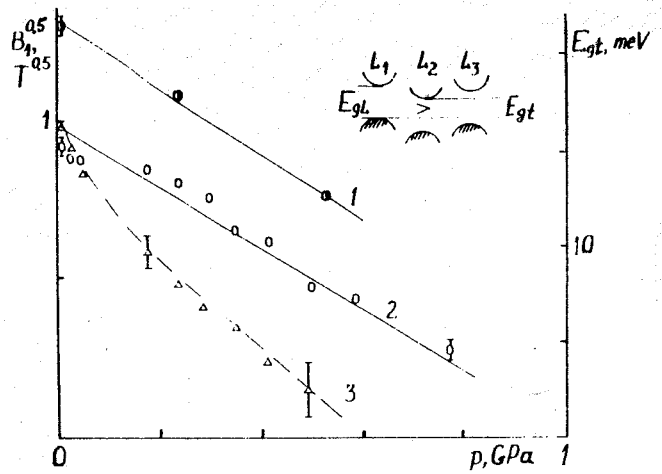

Fig.2. Dependences of $B_1^{0.5}$ (curves 1 and 2; left - hand scale) and the thermal energy gap E_{gt} (curve 3; right-hand scale) on the pressure p in n-$Bi_{0.84}Sb_{0.16}$(1) and n-$Bi_{0.89}Sb_{0.11}$ (2,3), $B \parallel j \parallel C_2$. The insert shows the schematic diagram of possible L band extrema displacements in Bi-Sb under pressure gradients in high-pressure chamber.

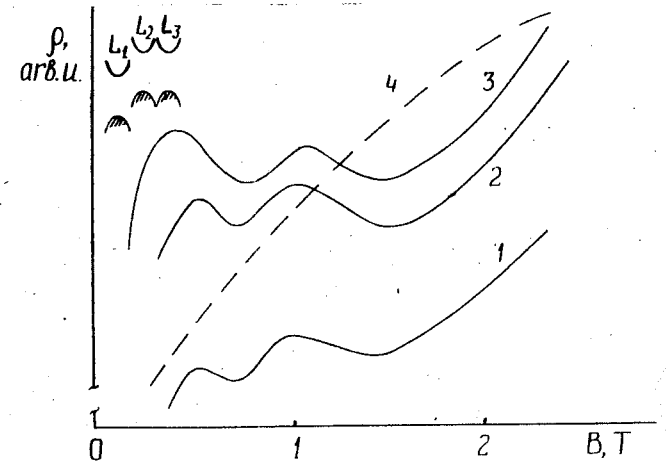

Fig.3. Dependence of the resistance ρ on the longitudinal magnetic field B in p-$Bi_{0.88}Sb_{0.12}$ ($B \parallel j \parallel C_1$) at the following values of strain under uniaxial compression along C_1 axis - ε_{xx},%: 1.4-0;2-0.06; 3-0.12; current density j, A/cm^2: 1+3-400; 4-40. The insert shows the c schematic diagram of the L extrema positions in Bi-Sb under uniaxial compression along C_1 axis /3/.

compression along C_2 axis anomalies of the resistance are somewhat weaker but they have the same properties.

Absence of any essential change of direct energy gaps in Bi-Sb monocrystals under uniaxial compression which is established by the resonant impact ionization method is in perfect agreement with the results of calculations made on the basis of known deformation potentials /3/.

The method of the resonant impact ionization may be used for exploring influence of the external conditions on direct energy gaps of materials.

References

1. Bogdanov E.V., Brandt N.B., Manankov V.M., Eleyshman L.S. Resonant impact ionization in $Bi_{1-x}Sb_x$ semiconducting alloys.- JETF Lett., 1982, v.35, No.2, 75-77.
2. Brandt N.B., Chudinov S.M., Karavayev V.G. Investigation of the gapless state induced by a magnetic field in bismuth-antimony alloys. - JETF, 1976, v.70, No.6, 2296-2317.
3. Brandt V.B., Yegorov V.B., Lavrenyouk M.Yu., Minina N.Ya., Savin A.M. Some properties of the thermal e.m.f. and resistance in electron topological transitions in bismuth and its alloys. - JETF, 1985, v.89, No.6(12), 2257-2269.

THE EXTREMALE HIGH UNIAXIAL ELASTIC DEFORMATION INDUCED INVERSION OF THE ENERGY BANDS IN n-Ge UNDER CONDITION OF METAL - INSULATOR TRANSITION (THE MOTT-TRANSITION)

P.I.Baranskii, V.N.Ermakov, V.V.Kolomoets, P.F.Nasarchuk
Institute of Semiconductors, Academy of Sciences of the Ukrainian SSR, Kiev, USSR

It is well known that characteristic features of metal - insulator (MI) transitions due to the change of wavefunctions overlap-degree are caused mainly by the transformation of impurity states and impurity bands /1/. Conductance band parameters remain the same as in lightly doped crystals.

Recently it was experimentally obtained that in n-Ge <Sb> the $L_I - \Delta_I$ - inversion of the type of absolute minimum of conductance band may occur, it may cause the transformation of shallow donor states due to the change of band parameters resulting from transformation of germanium-type conduction band into silicon-type conductance band under uniaxial pressure $X \parallel [00I]$ /2/.

Account the essential change of impurity states ionization energy during $L_I - \Delta_I$ - inversion M-I transition may occur in larger interval of concentrations corresponding to metallic conductivity than in the case of MI transition due to deformation induced change of the wavefunctions overlapdegree resulting from the decreasing of valley-orbit splitting /3,4/.

Furthermore since the ionization energy of shallow impurity donors essentially increases at the $L_I - \Delta_I$ - inversion /2/ (in the contraty to deformation-induced transition insulator-metal in n-Ge <As> and n-Si <P>) the latter may cause the metal-insulator transition in n-Ge<Sb>.

The results of automatic recording of resistivity of n-Ge<Sb> crystals at T=4.2 K and $X \parallel [00I] \parallel \vec{E}$ are shown in Figure.

The experiments were performed on n-Ge<Sb> crystals with the impurity concentration below (curve I, see Figure) and above (curves 2 and 3) the critical concentration corresponding to MI transition.

It was shown that at T=4.2 K the resistivity of crystals I increases due to $L_I - \Delta_I$ - inversion by more than seven orders of magnitude and that of crystals 2 increases approximately by six orders of magnitude.

It is well known that in general case conductivity of crystals with intermediate level of doping may be written as:

$$\sigma = \sigma_{01} \exp\left(-\frac{\varepsilon_1}{kT}\right) + \sigma_{02} \exp\left(-\frac{\varepsilon_2}{kT}\right) + \sigma_{03} \exp\left(-\frac{\varepsilon_3}{kT}\right)$$

Since the uncompensated crystals with the impurity concentration below critical concentration of MI-transition exhibit the ε_2-conductivity at T=4.2 K /3-5/, the strain change of conductivity caused by $L_I - \Delta_I$ - inversion depends on variation of activation energy ε_2, i.e.:

$$\frac{\sigma^L}{\sigma^\Delta} = \frac{\sigma^L_{02}}{\sigma^\Delta_{02}} \exp\left(\frac{\varepsilon^\Delta_2 - \varepsilon^L_2}{kT}\right)$$

This expression permits to evaluate the conductivity variation at $L_I - \Delta_I$ inversion in the vicinity of MI doping level transition. Thus taking into account that ionization energy of shallow donors in Ge increases by a factor of four at $L_I - \Delta_I$-inversion /2/ and assuming that the increase of activation energy ε_2 is approximately the same (i.e. $\varepsilon^\Delta_2 \simeq 4\varepsilon^L_2$) one obtaines for example that for the sample with activation energy $\varepsilon^L_2 = 2$ meV the increase of resistivity due to the inversion of germanium c-band into silicon -type band is equal to:

$$\frac{\sigma^L_2}{\sigma^\Delta_2} \sim \exp\left(\frac{\varepsilon^\Delta_2 - \varepsilon^L_2}{kT}\right) \approx 1.5 \cdot 10^7$$

Low-temperature transition to activation conductivity and corresponding deformation-induced increase of resistivity of the sample which exhibits metal conductivity in the unstrained state would, evidently, occur if:

$$\varepsilon^\Delta_2 - \varepsilon^L_F > kT \qquad (1)$$

where ε^Δ_2 is the activation energy for the transitions in the second impurity band, which was separated from the c-band due to $L_I - \Delta_I$-inversion, ε^L_F is the Fermi energy of degenerated electron gas in the initial state.

For the initially degenerated samples the increase of crystal resistivity is given by expression:

$$\frac{\rho_\infty}{\rho_0} = \frac{\sigma_0}{\sigma_\infty} = \frac{ne\mu_F}{\sigma^\Delta_{02}} \exp\left(\frac{\varepsilon^\Delta_2 - \varepsilon^L_F}{kT}\right) =$$

$$= A \exp\left(\frac{\varepsilon^\Delta_2 - \varepsilon^L_F}{kT}\right) \qquad (2)$$

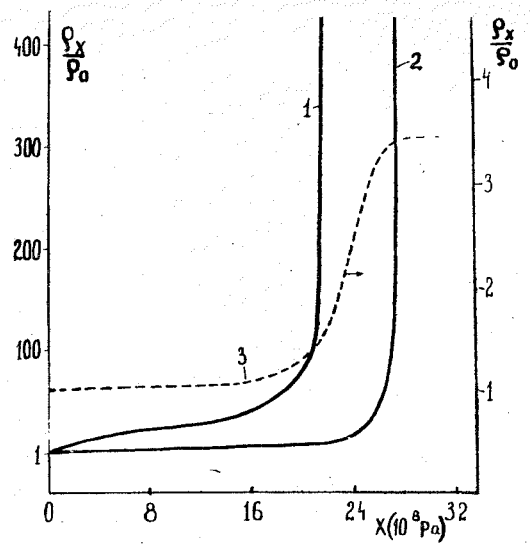

Dependences $\rho_x/\rho_o = f(X)$ for Sb-doped n-Ge crystals ; the concentrations of Sb are:
1 - $N_{Sb} = 6.6 \cdot 10^{16}$ cm^{-3} ; 2 - $N_{Sb} = 1.77 \cdot 10^{17}$ cm^{-3} ;
3 - $N_{Sb} = 2 \cdot 10^{18}$ cm^{-3}. T = 4.2 K. $X \parallel \vec{E} \parallel [001]$.

Taking into account the deformation induced increase of resistivity of sample 2 (which at T=4.2 K and X=0 exhibit the metal conductivity) by more than six order, one may conclude that in this crystal ε_2^{Δ} is essentially larger than ε_F^{L} (see (I) and (2)).

In the case of strong degeneracy (Figure, curve 3) $L_I - \Delta_I$ - inversion does not cause MI transition. Probably, in this case the shift of impurity band does not exceed the Fermi energy and according to (2) the activation-type conductivity will not occur. The increase of resistivity of strongly degenerated crystal is caused by the transition of carriers from L_I- to Δ_I-valleys. In this case Fermi level remains in c-band.

Thus,we have experimentally observed MI transition caused by the conductance band transformation due to $L_I - \Delta_I$-inversion of $X \parallel [001]$. This inversion of band minima causes the transformation of impurity states and impurity bands, leads to the separation of impurity band from c-band and to the activation-type conductivity.

It is experimentally observed that at T=4.2 K and $X \parallel [001]$ the MI transition in Sb doped n-Ge takes place at donor concentration which is 2 times larger than in unstrained crystals.

References

1. Mott N.F. Metal-Insulator Transitions.- M. ; Nauka, 1979.- 342 p.
2. Baidakov V.V., Ermakov V.N., Grigorev N.N., Kolomoets V.V., and Kudykina T.A. Breakdown of Impurity States As and Sb in Germanium at Uniaxially Compression $P \parallel [001] \parallel \vec{E}$. - Phys. Stat.Sol. (b) - 1984, v.122, N2, p.K 163 - K 167.
3. Fritzsche H. Effect of Uniaxial Compression on Impurity Conduction in n-Type Germanium. - Phys.Rev.-1962, v.125, N5, p.1552-1560.
4. Sugijama K. and Kobajashi A. Piezoresistance and Magnetoresistance in Impurity Conduction of Germanium. - J.Phys.Soc. Japan, 1963, v.18, N2, p.163-174.
5. Gerschenson E.M., Litvak-Gorskaja L.B., Lugovaja G.Ja. The influence of the compensation on the impurity conductivity of n-Ge in the intermediate doping region.- Fir.Tekh.Poluprov. 1981, v.15, N7, p.1284-1292.

HIGH-FREQUENCY PROPERTIES OF ANTIFERROMAGNET $(C_2H_5NH_3)_2CuCl_4$ AT HIGH UNIFORM AND AXIAL PRESSURE

V.Vasyukov, V.Telepa
Donetsk Physico-Technical Institute of the Ukrainian Academy of Sciences, Donetsk, USSR

The symmetry group of paramagnetic phase of antiferromagnetic (AFM) $(C_2H_5NH_3)_2CuCl_4$ is D_{2h}^{15} /I/. Magnetic cell coincides with crystallographic one.

Investigations of static magnetic properties of the given AFM performed in /2/ showed that at $T < T_N(T_N=10.2\ K)$ Cu^{2+} ions located within crystallographic planes parallel to (ab) plane are ferromagnetically ordered. At zero external field (H=0) magnetizations of adjacent layers with ferromagnetically ordered Cu^{2+} ions are oriented along the magnetization easy axis $\vec{a}$ and opposite with respect to each other.

The present paper is aimed to study the pressure effect on the anisotropy of magnetics. The investigation was performed by antiferromagnetic resonance (AFMR) at liquid helium temperature (T=4.2 K).

The frequency-field dependence of the spectrum is studied by means of the AFMR spectrometer with the running wave spiral as a resonator. The study was made over the frequency range from 300 MHz to 2.5 GHz.

Uniform pressure was created in the "piston-cylinder"-type chamber with two microwave frequency electric inputs in the shutter. Axial pressure was created by the bellows press and applied along the $\vec{c}$-axis of the crystal. Axial pressure effect on the AFMR spectrum was studied on cylindrical specimens 3 mm in diameter and 2.5 mm high.

According to papers /3,4/ description of the AFMR acoustic branches of $(C_2H_2NH_3)_2CuCl_4$ can be restricted to a two-sublattice model. From the symmetry considerations energy density can be presented in the form of

$$\mathcal{H}/M_o = -H_E(\sigma_A^2+\sigma_B^2)/2 + H_E'\vec{\sigma}_A\vec{\sigma}_B + H_Y(\sigma_{AY}^2+\sigma_{BY}^2)/2 + H_Y'\sigma_{AY}\sigma_{BY} + H_Z(\sigma_{AZ}^2+\sigma_{BZ}^2)/2 + H_Z'\sigma_{AZ}\sigma_{BZ} - H_d(\sigma_{AY}\sigma_{AZ}-\sigma_{BY}\sigma_{BZ}) - H(\sigma_{AX}+\sigma_{BX}) \quad (I)$$

$\vec{\sigma}_A=\vec{M}_A/M_o$; $\vec{\sigma}_B=\vec{M}_B/M_o$; $\vec{M}_A, \vec{M}_B$ are the magnetizations of A and B sublattices.

Both uniform pressure and axial one applied along the symmetry axis $\vec{c}$ do not change the symmetry group of the crystal therefore in expression (I) there are no additional terms of lower symmetry. Changes in the magnetic properties of the crystal caused by the external pressure can be described by the pressure dependence of the parameters of Hamiltonian (I).

Behaviour of the frequency-field dependence of the AFMR spectrum of the specimen subjected to the uniform pressure is shown in Fig.I. Strong dependence of the AFMR spectrum of $(C_2H_5NH_3)_2CuCl_4$ on the magnitude of uniform pressure is revealed. Such characteristics of the spectrum as spin-flop transition field H_{SF} and acoustic branch activation frequency ν_c decrease with the increase of the uniform pressure. Dependences of H_{SF} and ν_c on the uniform pressure magnitude are given in Figs.2,3.

$$dH_{SF}/dP = -(24\pm4)\cdot10^{-6}\ T/MPa$$
$$d\nu_c/dP = -(100\pm10)\cdot10^{-2}\ MHz/MPa \quad (2)$$

At 670 MPa a pressure-induced orientational phase transition of the Morin-type occurs /5/. As a result of this transition easy magnetization direction passes from $\vec{a}$-axis to $\vec{b}$-axis. At further increase of uniform pressure H_{SF} (at $\vec{H}\parallel\vec{b}$) and ν_c monotonously increase. Within the measurement error limits this dependence is of linear nature and

$$dH_{SF}/dP = +(73\pm15)\cdot10^{-6}\ T/MPa$$
$$d\nu_c/dP = +(240\pm40)\cdot10^{-2}\ MHz/MPa \quad (3)$$

Maximum axial pressure applied to the specimen did not exceed 25 MPa. Within this pressure all changes in the AFMR spectrum were completely reversible and no noticeable broadening of resonance lines caused by the axial pressure non-uniformity was observed.

Shift of the AFMR spectrum resonance line ($H_I=240\cdot10^{-4}$T) of the collinear phase on 575.6 MHz frequency caused by external axial pressure is shown in Fig.4, the shift of resonance lines of the spin-flop phase ($H_2=0.1295$ T) and ferromagnetic phase ($H_3=0.1637$ T) on 1.765 GHz frequency is given in Fig.5.

Solving equations of motions for irreducible operators we obtained expressions for AFMR resonance frequencies for all three

phases under considerations. Expressions for resonance frequencies were used to determine sensitivity constants of resonance fields with respect to parameters included in Hamiltonian (I) describing magnetic properties of $(C_2H_5NH_3)_2CuCl_4$ crystals.

Shifts of the spectrum resonance lines on these frequencies of the microwave frequency field are determined by the change of the interlayer exchange and anisotropy fields. Interlayer exchange is characterized by the Hamiltonian parameter H'_E. Of all parameters H_y, H'_y, H_z, H'_z characterizing the AFM anisotropy only $H_y+H'_y$ and $H_z+H'_z$ made considerable contribution to the change in the AFMR spectrum on these particular frequency of the microwave frequency field.

For resonance fields H_1, H_2, H_3 numerical values of the sensitivity parameters are given in relationship (4)

$$dH_1/dP_{\parallel c}=0.08dH'_E/dP_{\parallel c}+3.2d(H_Y+H'_Y)/dP_{\parallel c}$$

$$dH_2/dP_{\parallel c}=0.96dH'_E/dP_{\parallel c}-0.55d(H_Y+H'_Y)/dP_{\parallel c}-0.025d(H_Z+H'_Z)/dP_{\parallel c} \quad (4)$$

$$dH_3/dP_{\parallel c}=2.0dH'_E/dP_{\parallel c}-0.85d(H_Y+H'_Y)/dP_{\parallel c}-0.15d(H_Z+H'_Z)/dP_{\parallel c}$$

Change in resonance field H_1 is mainly due to change in anisotropy field in the (ab) plane $H_y+H'_y$. Anisotropy change in the (ac) plane $H_z+H'_z$ the most vividly manifests itself in resonance fields H_2, H_3.

Substituting experimentally obtained numerical values $dH_1/dP_{\parallel c}=-0.15\cdot10^{-4}$ T/MPa; $dH_2/dP_{\parallel c}=1.0\cdot10^{-4}$ T/MPa; $dH_3/dP_{\parallel c}=0.5\cdot10^{-4}$ T/MPa one can determine the magnitude of the contribution of the change of each parameter of the Hamiltonian to the resonance field change and distinguish axial pressure dependence of each parameter individually

$$dH'_E/dP_{\parallel c}=1.4\cdot10^{-4}\ \text{T/MPa}$$

$$d(H_Y+H'_Y)/dP_{\parallel c}=-0.08\cdot10^{-4}\ \text{T/MPa} \quad (5)$$

$$d(H_Z+H'_Z)/dP_{\parallel c}=16\cdot10^{-4}\ \text{T/MPa}$$

The obtained results show that in the presence of the axial pressure applied along the crystallographic $\vec{c}$ axis the anisotropy

field in the (ac) plane changes much more drastically than the interplane exchange one.

References

1. Willet R.D. Crystal structure of $(NH_4)_2CuCl_4$// J.Chem.Phys.-1964. -41,N8.-P.2243-2244.
2. Jongh L.J., Amstel W.D. de,Miedema A.R. Magnetic measurements on $(C_2H_5NH_3)_2CuCl_4$. Ferromagnetic layers coupled by a very weak antiferromagnetic interaction//Physica.-1972.-58,N2.-P.277-304.
3. Pashkevich Yu.G., Sobolev V.L., Telepa V.T. Symmetric analysis of static and high frequency properties of $CuCl_2\cdot2H_2O$ and $CuCl_2.2D_2O$//Fiz.Nizk.Temp.-1982.-8,N7.-P.705-711.
4. Peculiarities of antiferromagnetic resonance in rhombic antiferromagnets with Dzyaloshinskii interaction $(C_2H_5NH_3)_2CuCl_4$/ V.N.Vasyukov, A.V.Zhuravlev, S.N.Lukin et al.//Fiz. tverd. Tela.-1984.-26, N5.-P.1297-1305.
5. Orientational transitions in rare-earth magnets/K.P.Belov, A.K.Zvezdin, A.M.Kadomtseva, V.Z.Levitin.-M.Nauka, 1979.-436pp.

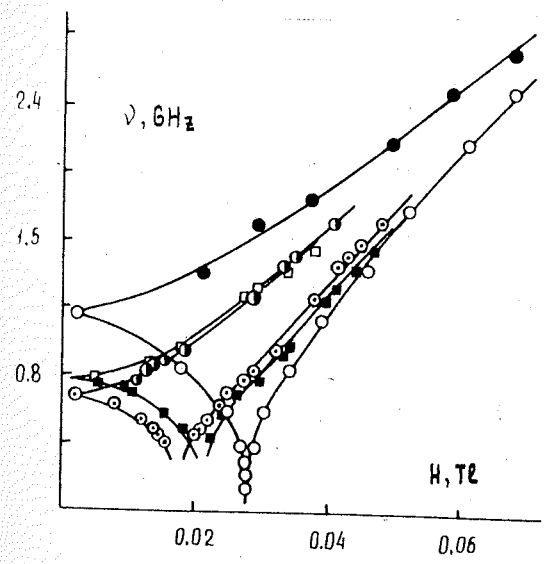

Fig.1. Frequency-field dependence of the AFMR spectrum: P=0 (○ – $\vec{H}\parallel\vec{a}$, ● – $\vec{H}\parallel\vec{b}$); P=4.6·10^2 MPa (⊙ – $\vec{H}\parallel\vec{a}$, ◉ – $\vec{H}\parallel\vec{b}$); P=7.5·10^2 MPa (■ – $\vec{H}\parallel\vec{b}$, □ – $\vec{H}\parallel\vec{a}$).

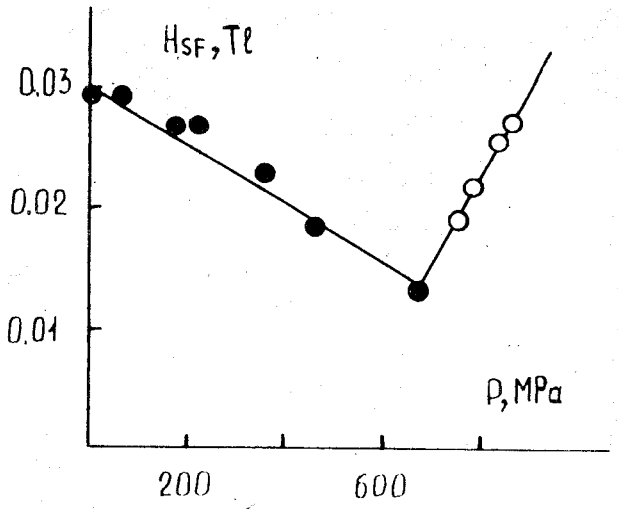

Fig.2. Spin-flop transition field as a function of the uniform magnitude: • - $\vec{H} \parallel \vec{a}$, o - $\vec{H} \parallel \vec{b}$.

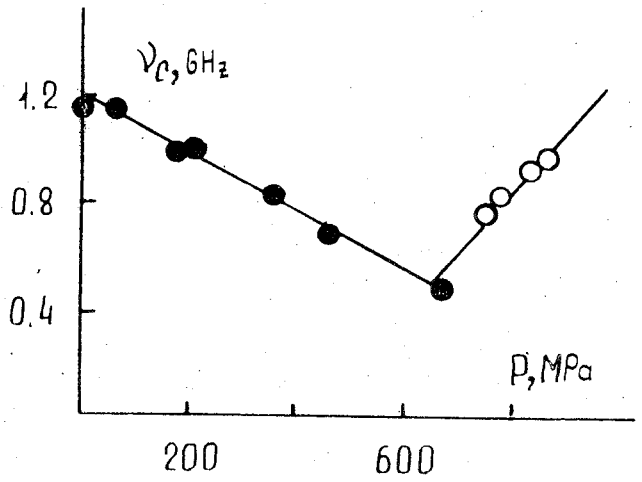

Fig.3. AFMR spectrum acoustic branch activation frequency as a function of uniform pressure magnitude: • - $\vec{H} \parallel \vec{a}$, o - $\vec{H} \parallel \vec{b}$.

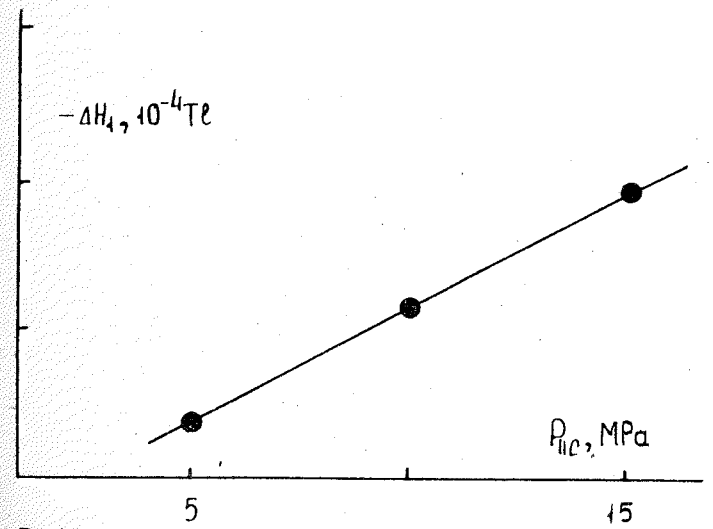

Fig.4. Position of the AFMR resonance line of the colinear phase as a function of the axial pressure magnitude. ν =575.6 MHz.

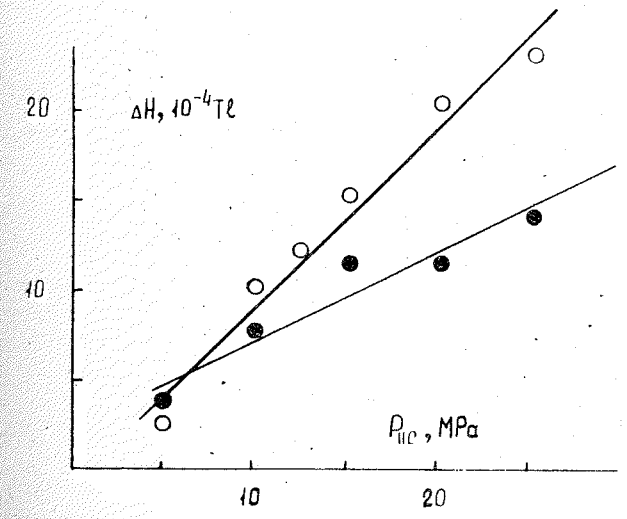

Fig.5. Positions of resonance lines of the spin-flop phase (o) and ferromagnetic phase (•) as a function of axial pressure magnitude. ν =I.765 GHz.

PRESSURE EFFECT ON THE $R(Fe_{I-x}Cu_x)_2$ COMPOUNDS FORMATION AND THEIR MAGNETIC PROPERTIES

A.V.Tsvyashchenko[I], L.N.Fomicheva[I], V.E.Makhotkin[2], V.A.Fradkov[2]

[I]L.F.Vereshchagin Institute of High Pressure Physics, Troitsk, USSR

[2]Institute of General Physics of the USSR Academy of Sciences, Moscow, USSR

The crystallization of the compounds R_6Cu_{23} (Th_6Mn_{23}-type structure) has been investigated in earlier work* where it was assumed that the copper was divalent (Cu^{+2}). This assumption led us to investigate the pseudobinary RFe_2-RCu_2 systems with the aim of obtaining compounds of composition RFeCu.

The synthesis of a stoichiometric mixture of the elements was carried out by application of high temperature at a constant pressure of 7.7 GPa in a chamber constructed by Khvostantsev et al.

The structure of the compounds was detected by X-ray diffraction, using a Debye-Scherrer camera II4 mm in diameter and nickel-filtered Cu K_α radiation.

The magnetization measurements were done on polycrystalline samples using vibrating-sample magnetometers. An electromagnet was used for fields below I0 kOe in the temperature range 4.2 - 700 K while a superconducting coil was used at 4.2 K for fields up to 67 kOe.

The X-ray powder data for RFeCu (where R=heavy rare earth) and $Yb(Fe_{I-x}Cu_x)_2$ (where $0 \leq x \leq 0.5$) were indexed in the basis of the cubic unit cell of the $MgCu_2$-type (CI5) structure and space group Fd3m. All light rare earth phases of composition RFeCu, except CeFeCu, form compounds with the hexagonal $MgZn_2$-type (CI4) structure. The X-ray powder data for the $YbCu_2$ alloy were indexed on the basis of the hexagonal unit cell (CI4-type) with the following parameters: a=5.260(5) Å and c=8.567(8) Å. The $\bar{V}$ increases continuously with increasing copper content. However, a strong negative deviation from Vegard's law is observed. From that it

* Tsvyashchenko A.V. High pressure synthesis of RE_6Cu_{23} compounds (RE=Tb, Dy, Yb, Lu). -J.Less.Common Met., I984, v.99, N°I, pp.L9-LII.

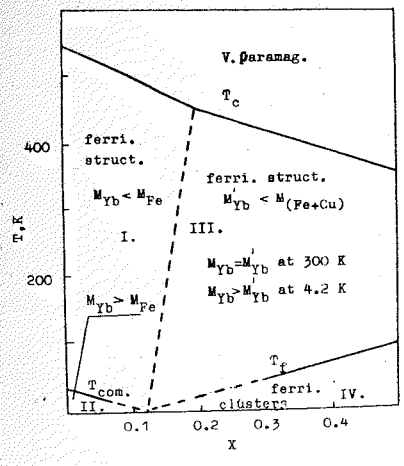

Magnetic phase (T,C) diagram for the $Yb(Fe_{I-x}Cu_x)_2$ system.

follows, that in the cubic Laves phase (CI5) the ytterbium is trivalent and copper has the $3d^9 4s^2$ configuration.

The results of our magnetic measurements may be summarized as follows. Up to 50 at.% Cu the alloys have a spontaneous magnetization clearly indicative of ferromagnetism for YFeCu and ferrimagnetism for RFeCu (see Table). The (Fe, Cu) sublattice magnetization determined from the M-H curve for the YFeCu and GdFeCu alloys is sufficiently high. For the YFeCu alloy, assuming that the iron moment is equal to about I.3 μ_B as in YFeAl, one finds that the magnetic moment of copper is equal to about 0.2 μ_B. For the GdFeCu alloy, taking the moment of gadolinium equals 7.I μ_B (as in $GdAl_2$) and assuming that the iron moment equals I.6 μ_B as in $Gd(Fe,Al)_2$ and that the (Fe, Cu) moments couple antiparallel to the gadolinium moments, one finds that the copper moment is equal to about 0.5 μ_B. That is to say the (Fe, Cu) sublattice magnetization behaviour in these alloys is similar to the cobalt magnetization behaviour in the RCo_2 alloys.

The low field magnetization against temperature curves show the existence of freezing temperatures T_f for $x \geq 0.3$.

The magnetic behaviour of $Yb(Fe_{I-x}Cu_x)_2$ alloys is illustrated in Figure by the magnetic phase (T,C) diagram, which consists of five fields. In fields I and II the magnetic structure is co-

Structure, lattice constants a(c), mean atomic volume $\bar{V}$, Curie temperatures T_c, compensation temperatures T_{com}, saturation magnetization M_s

RReCu	Structure	a, Å	c, Å	$\bar{V}$, Å^3	T_c, K	T_{com}, K	M_s, μ_B/f.e.
Ce	CI5	7.350(7)		I6.54	50-70		0.54
Pr	CI4	5.3I(I)	8.74(3)	20.54			
Nd	CI4	5.34(I)	8.7I(3)	20.70			
Sm	CI4	5.27(I)	8.59(3)	I9.88			I.54
Gd	CI5	7.426(7)		I7.06	699		5.00
Tb	CI5	7.375(5)		I6.7I	588		6.87
Dy	CI5	7.335(5)		I6.44			
Ho	CI5	7.330(5)		I6.4I	499		7.33
Er	CI5	7.293(5)		I6.I6			
Tm	CI5	7.26I(5)		I5.95		I20	3.03
Yb	CI5	7.277(5)		I6.06	358	~4.2	0.48
Lu	CI5	7.233(5)		I5.77			
Y	CI5	7.374(5)		I6.7I	38I		I.50

linear below all the ordering temperatures and orbital contribution freezing of the ytterbium moment does not yet occur. In fields III and IV the copper atoms bear a magnetic moment, at low-temperatures the ytterbium moment is reduced and ferrimagnetic clusters appear.

HIGH-PRESSURE STUDY OF IMPURITY RESONANCE SCATTERING MECHANISM IN Cr-Fe BASE ANTIFERROMAGNETIC ALLOYS

V.Yu.Galkin
Central Research Institute for Iron and Steel Industry
Moscow, USSR

The impurity resonance scattering (IRS) model has recently been developed for antiferromagnetic (AF) Cr-rich alloys. According to this model the spin polarized impurity states are formed in the energy gap occuring in AF Cr-rich alloys /I/. If the Fermi level E_F approaches that of the impurity state E then the amplitude of the conduction electron scattering increases sharply. The contribution of IRS to the total resistivity $\rho(T)$ is written in the form:

$$\rho_{res}(T) = \frac{I}{\pi N_r(0)} \left[I + \frac{(E-E_F)^2}{\gamma^2} + \frac{\pi T^2}{3\gamma^2} \right]^{-I} \qquad (I)$$

where γ is the resonance level width, $N_r(0)$ is the density of state in the electron reservoir.

The experimental evidence that supports the validity of the IRS model for AF Cr-Fe alloys was obtained by studying the effect of Mn and V doping on $\rho_{4.2}$ of $(Cr_{I00-x(y)}Mn_x(V_y))$ - 2.7 at% Fe alloys /I/. It is known that the addition of Mn to Cr or Cr-rich alloys results in E_F increase while the addition of V results in its decrease. According to (I) a sharp increase of $\rho_{4.2}$ at x_{res} = =0.4 at% Mn and y_{res}=0.45at% V was believed to result from the superposition of E_F and the impurity levels with E_0^+ and E_0^- energies correspondingly.

As has been pointed out previously /2/ the application of high pressure to Cr alloys results in E_F decrease. Therefore it is expected to get new and valuable information about IRS mechanism from the resistivity measurements under high pressure. In this paper we are presenting the results of $\rho(T)$ investigation of $(Cr_{I00-x(y)}Mn_x(V_y)$ - 2.7 at% Fe alloys on application of high pressure up to 2 GPa and at atmospheric pressure. The obtained results as well as $\rho(T)$ data for Cr-Fe /3/ alloys are discussed from the viewpoint of the IRS model.

The sample preparation methods and the experimental techniques for measuring resistivity have been described previously /I/. The high pressure was generated in berillium bronze pressure

vessel. A mixture of propane and transformer oil was used as a pressure transmitting medium.

The pressure dependences of $\rho_{4.2}$ of the studied alloys are shown in Fig.I. We suppose that the observed drastic difference in the behaviour of Mn- and V-doped alloys is connected with the different E_F positions relative to the impurity level with energy E_0^- and can be explained from the viewpoint of the IRS model. Since E_F in 0.25 at% Mn-doped alloy is higher than E_0^- level /I/ the value of $(E_0^- - E_F)$ parameter should decrease on application of pressure, go to zero when the resonance condition is fulfilled and then increase again. Owing to this, the $\rho_{4.2\ res}(P)$ dependence should also be non-monotonous, which seems to be the reason of the experimentally observed non-monotonous $\rho_{4.2}(P)$ dependence (curve I, Fig.I). The observed maximum in the $\rho_{4.2}(P)$ curve at $P \approx I$ GPa is supposed to be the result of E_F and E_0^- superposition. In both V-doped alloys E_F is lower than E_0^- level, therefore $\rho_{4.2\ res}$ should decrease on application of pressure, which is supported by the experiment as well (curves 2, 3, Fig.I).

Fig.2 shows $\rho(T)$ curves for $(Cr_{99.75}Mn_{0.25})$ - 2.7 at% Fe alloy at various pressures correspondingly. The addition of V causes similar changes in $\rho(T)$ behaviour that can be explained in terms of IRS model.

It follows from (I) that at low temperatures in case of $E_F \approx E_0^-$, ρ_{res} should decrease with temperature, which can cause the appearance of minimum in $\rho(T)$ curve (ρ_{min}). This idea has been supported experimentally. In both cases low temperature minimums appear when the resonance condition is fulfilled ($Y \approx Y_{res}$, $P \approx P_{res}$).

The value of the energy gap 2Δ in AF Cr alloys is known to decrease with temperature. Since the value of the impurity level energy is proportional to Δ /I/ and the origin of the scale is taken in the middle of the gap then $E_i^-(T)$ curves should have the analogous temperature dependences as $\Delta(T)$. The value of E_F decreases with the increase of y and P. In case of $Y < Y_{res}$ and $P < P_{res}$ the intersection of $E_{Fi}(T)$ and $E_i^-(T)$ will take place. According to (I) $\rho_{res}(T)$ has its maximum close to the intersection point. This is supposed to cause maximums in $\rho(T)$ curves for alloys with y=0.3 and 0.45 at% V. Since $\rho_{res}(T)$ depends on $(E^- - E_F)$ (I) then if $y > y_{res}$ or $P > P_{res}$, ρ_{res} should decrease with temperature and if $y < y_{res}$ or $P < P_{res}$ for $T < T_{max}$, ρ_{res} should increase with temperature. Such $\rho_{res}(T)$ dependence in the

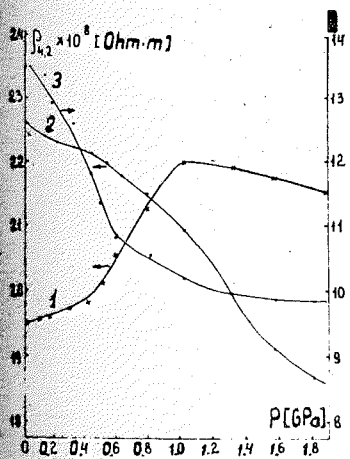

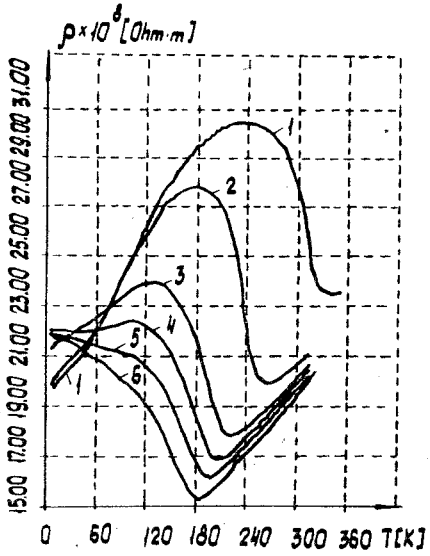

Fig.I. The electrical resistivity at 4.2 K of $(Cr_{100-x(y)}Mn_x(V_y))$-2.7 at% Fe alloys containing: I - x=0.25 at% Mn; 2 - y=0.5 at% V; 3 - y=2 at% V as a function of pressure.

Fig.2. The electrical resistivity of $(Cr_{99.75}Mn_{0.25})$-2.7 at% Fe alloy as a function of temperature for various pressures (GPa): I - 0; 2 - 0.53; 3 - 0.88; 4 - I.09; 5 - I.35; 6 - I.59.

first case is believed to be the reason of anomalous ρ increase with decreasing temperature for $T < T_N$ (curves 5,6, Fig.2) and in the second case-the reason of anomalous high ρ decrease for $T < 10$ K.

The existence of the resistivity minimum in AF Cr-Fe alloys is usually explained in terms of the Kondo effect /3/. However, there is a number of experimental data that makes the validity of this theory to AF Cr-Fe alloys very doubtful. We think that the appearance of minimums as well as other anomalies in the $\rho(T)$ curves of AF Cr-Fe alloys is due to IRS. Since the addition of Fe to Cr causes E_F increase, then by decreasing Fe concentration (C_{Fe}) in Cr-Fe alloys relative to C_{Fe}=2.7 at%, one can achieve the fulfilment of the resonance condition $(E_F - E_0^-) \to 0$ as in

the case of application of pressure and addition of V. Knowing the rate of the change in E_F per I at% Fe and I at% V /I/ it is easy to estimate Fe concentration ($C^{-}_{Fe\ res} \approx$ I.3 at% Fe) at which this condition is fulfilled. As it has been pointed out the fulfilment of the resonance condition results in ρ_{min} appearance. This statement is true for Cr-Fe alloys as well, because in these alloys ρ_{min} is observed for $C_{Fe} \approx C_{Fe\ res}$ /3/. Besides, the resistivity of Cr-Fe alloys containing I and I.5 at% Fe exhibits both a minimum and a maximum ($T_{max} < T_{min}$). The latter, according to our idea, indicate that at $T \approx T_{max}$ $E_F = E^{-}$. The reason of ρ_{min} disappearance in Cr-Fe alloys for $C_{Fe} >$ I.6 at% Fe /3/ and the anomalous high decrease of ρ with decreasing temperature for $T < 8$ K is easy to explain on the basis of the IRS model, because this case ($C_{Fe} > C^{-}_{Fe\ res}$) according to this model is analogous to the previously discussed ($y < y_{res}$ or $P < P_{res}$). The appearance of these $\rho(T)$ anomalies has not been explained in terms of the Kondo effect. Besides the appearance of ρ_{min} in Cr-2.7 at% Fe alloy with the addition of normal V impurity and on application of pressure is rather difficult to explain on the basis of the Kondo effect.

References

I. V.Yu.Galkin, V.V.Tugushev, T.E.Tugusheva. Resonance impurity scattering in dilute Cr-Fe-M (M=Mn, V) alloys . Fiz.Tverd.Tela (USSR), I986, 28, N 8, 2290-2298.

2. J.Mizuki, Y.Endoh, Y.Ishikawa. Pressure Effects on Spin Density Wave in Cr Rich Cr-Al, Si, Mn, Fe and Co Alloys . J.Phys. Soc.Jap., I982, 5I, N II, 3497-3503.

3. S.Katano, N.Mori. Resistivity Minimum in Antiferromagnetic Cr-Fe Alloys . J.Phys. Soc. Jap., I979,46, N 4, I265-I272.

THE INFLUENCE OF PRESSURE ON THE ELECTRON EFFECTIVE MASSES IN ZINC AND CADMIUM

A.G.Budarin, V.A.Ventsel, A.V.Rudnev

The Institute of High Pressure Physics, USSR Academy of Sciences, Troitsk, USSR

The conducting electron effective masses in metals are the important differential characteristics of the energy spectrum which depend on the Fermi - liquid properties of quasi - particles. There are two experimental methods for measuring effective masses: the Azbel'- Kaner cyclotron resonance /1/ and the de Haas - van Alphen (dHvA) effect /2/. The cyclotron resonance measurements demand excellent surface conditions of the sample and precise magnetic field alignment to the sample surface. Both these conditions are unattainable in a high pressure chamber. DHvA oscillations are a volume effect and may be measured under pressure. The effective masses is found from oscillation amplitude dependence on temperature.

At pressures up to 10 kbar the effective mass may change from 1+10% and this puts severe restrictions to measurement precision. By the apparatus in High Pressure Physics Institute (IFVD) /3,4/ effective masses can be measured with precision up to $\pm$1% thanks to the high precision of measuring and maintaing the temperature and the magnetic field (0.1%) during the time of the experiment. At high pressures a massive pressure vessel worsens the experimental conditions. The solenoid producing the modulation magnetic field can be placed in or out of the vessel. If this solenoid is placed into the vessel the Joule heat increases the temperature of the sample over the temperature of the helium bath and the precision of the temperature determination is distorted. The use of superconductive solenoid of such small dimension is limited by the critical fild and it cannot be winded because of the rigid superconductive wire. If the modulation solenoid is placed externally on the vessel the Joule heat is absorbed by the helium bath, but the sample can be heated by eddy currents, generated in the mass of the vessel and in the sample itself. Therefore the measurements were conducted with modulation frequency not more than 33 Hz. Such low modulation frequency decreased the signal to noise ratio and the error in the effective masses determination increased to $\pm$(3+5)%.

To increase the pressure hydrostaticity at low temperatures the pentan - oil mixture 1:1 was used as pressure transmitting medium, and the pressure vessel was cooled very slowly not more than K/min at all temperature. Preliminary effective mass measurements were made in the vessel at a pressure up to 1 kbar and the measured effective masses coincided with those in precise measurements without pressure /4/.

Pressure dependence of effective masses was measured for zinc and cadmium, but the increase of measurement errors in the pressure vessel did not allow to set good results for those parts of Fermi surface where the oscillation's frequency change under pressure is small. These parts are the lens in the third Brillouin zone and some monster cross sections in the second zone. For zinc the greatest pressure coefficient is known for the needle and the monster waist β . For the waist cross section β the frequency changes by $42 \cdot 10^{-3} \text{kbar}^{-1}$ and the effective mass may also change significantly. It was found that $\frac{d\ln m^*}{dp} = (9 \pm 4) \cdot 10^{-3} \text{kbar}^{-1}$. In cadmium pressure dependence of the effective mass for the pocket cross section α in the first Brillouin zone was measured on a sample with the axis lying in the $(11\bar{2}0)$ plane and inclined by 50° to $\langle 0001 \rangle$. It was found that $d\ln m^*_\alpha / dp = -(6 \pm 4) \cdot 10^{-3} \text{kbar}^{-1}$, the pressure dependence of the frequency F_α is $d\ln F_\alpha / dp = 10 \cdot 10^{-3} \text{kbar}^{-1}$ /5/. The pressure dependence of the electron-phonon interaction coefficient λ may be found from the pressure dependence of effective masses on that purpose the zone mass and its pressure dependence must be calculated with precision better than 1%.

The precise effective mass measurement under pressure led to an interesting conclusion. The effective mass of the new Fermi surface cross section, which appears in the cadmium monster at pressures beyond 5-6 kbar /6/ may not coincide with the extreme effective mass. For the specific Fermi surface cross sections, like monster cross section σ in zinc, the extremal effective mass may be not equal to the effective mass of the extremal cross section. This was found by comparing the masses of lens and monster cross sections β and σ in zinc, measured precisely by cyclotron resonance and by dHvA effect.

References

1. Azbel M.Y., Kaner E.A., JETP, 1957, 32, p.896.
2. Lifshits I.M., Kosevitch A.M., JETP, 1955, 29, p.730.

3. Budarin A.G., Ventcel V.A., Voronov O.A., Rudnev A.V. Izmeritelnaya tehnica, 1982, N4, p.66.
4. Budarin A.G., Ventcel V.A., Voronov O.A., Rudnev A.V., Stepanov A.N. JETP, 1983, 84, p.1511.
5. Ventcel V.A., Voronov O.A., Likhter A.I., Rudnev A.V. JETP, 1976, 70, p.1706.
6. Bud'ko S.L., Voronovsky A.N., Gapotchenko A.G., Itskevich E.S. JETP, 1984, 86, p.778.
7. Budarin A.G., Ventcel V.A., Rudnev A.V.,LTP, 1986, 12, p.312.

THE STUDY OF SUPERCONDUCTIVITY OF SULFUR UNDER STRESS IN MAGNETIC FIELDS UP TO 15 T

G.N.Stepanov

Institute of High Pressure Physics, USSR Academy of Sciences, Troitsk, USSR

Abstract. The temperature dependence of a resistance of the compound system consisting of anvils layer of sulfur (A-S-A) was investigated in magnetic fields up to 15 T. It was supposed that superconductive transition of sulfur under stress was a reason of low temperature resistance drop of A-S-A system. The maximum critical temperature $T_{c,m}$ was $\sim$ 30 K if load to anvils was applied at low temperatures. $T_{c,m}$ was decreased to $\sim$ 15 K in magnetic field 15 T.

Introduction. Under pressure $\sim$ 50 GPa sulfur transformed to metal /1/. For a several years there has been some interest in study of resistance of sulfur under high stress at low temperatures. Accordingly to results reported in 1980 /2/ the critical temperature of hypothetical superconductive transition of sulfur under stress was $\sim$ 30 K if the stress state of sulfur was created at low temperatures. The displacement of critical temperature in magnetic fields is a fundamental property of superconductivity. Earlier /2/ a resistance of A-S-A at low temperatures had been investigated in magnetic fields to 5 T. The displacement of critical temperature was not enough, about 2-3 K.

Experimental procedure. High stress and deformation of sulfur was got by rounded cone (R $\sim$ 0.1 mm) and flat anvils manufactured from synthetic polycrystalline diamond /3/. The current was coming through network of conducting channels formed at diamomd synthesis and sample (Fig.1). The load was applied at room temperature and at low temperature $\sim$ 4 K by screw press. Magnetic fields were generated by Bitter's solenoid.

Results. Fig.2 shows dependence of potential differences between anvils on temperatures at load 10^3 N, current 10 μA, in magnetic field up to 15 T. Critical temperature $T_{c,m}$ was estimated with "beginning of transition" (Fig.2). The results presented on Fig.2,a,were got after producing of stressed sulfur at room temperature. Fig.2,b shows temperature dependence of potential difference after applying the load at $\sim$ 4 K. After these last mea-

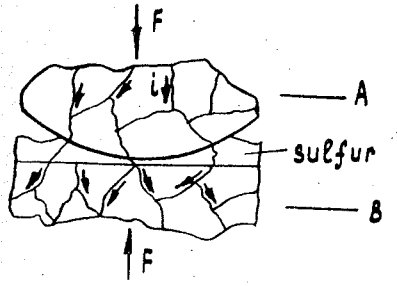

Fig.1. Scheme of high stress chamber.

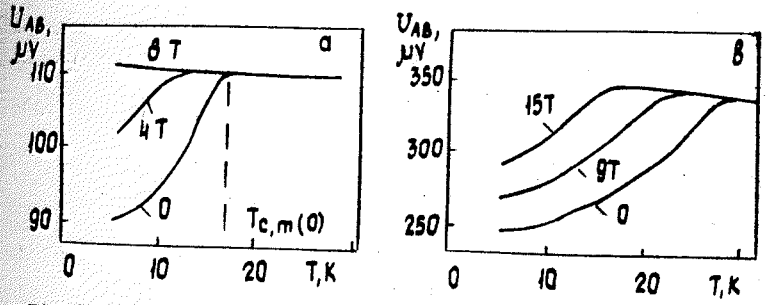

Fig.2. Temperature dependence of potential differences between anvils.

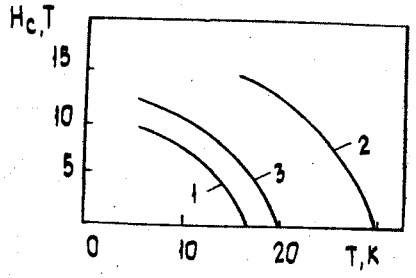

Fig.3. $H_c(T)$ after generating of stresses in sulfur 1 - at 300 K, 2 - at 4 K, 3 - at 4 K and after annealing at 300 K in the course of 5 days.

surements the A-S-A system was kept at the same load at room temperature in the course of several days. This annealing had as result the reduction of $T_{c,m}$. Fig.3 shows experimental information processing.

Discussion. The working hypothesis using for interpretation of low temperature resistance drop of A-S-A system is the superconductive transition of sulfur under stress. This hypothesis gives a chance to explain all experimental results. Namely, the interval of values of $T_{c,m} \sim 26 \div 31$ K, qualitative character of dependence $T_{c,m}(F)$ were reproduced using of different anvils, cryostates, low temperature presses. The large change of resistance of A-S-A system in magnetic field was observed only at $T < T_{c,m}$. $T_{c,m}$ was decreased in magnetic field, $H_c(0)$ was smaller for smaller $T_c(0)$ (see Fig.3). Unusual behaviour of $T_c(P)$ was discovered later for phosphorous /4/. As it was observed for sulfur, T_c phosphorous was increased about 100% if the pressure was generated at low temperature as compared with pressure generation at room temperature. The study of S and P under pressure may be valuable for advantage of high temperature superconductivity problem.

References

1. Dunn K.J., Bundy F.P. Electrical behavior of sulfur up to 600 kbar - metallic state. J.Chem.Phys., 1977, 67, N11, 5048-5053.
2. Степанов Г.Н., Яковлев Е.Н. Сверхпроводимость серы при высоком давлении. Письма в ЖЭТФ, 1980, 32, №11, 657-660.
3. Верещагин Л.Ф., Яковлев Е.Н., Степанов Г.Н., Бибаев К.Х., Виноградов Б.В. Давление 2,5 Мбар в наковальнях, изготовленных из алмаза типа карбонадо. Письма в ЖЭТФ, 1972, 16, №6, 240-243.
4. Kawamura H., Shirotani I., Tachikawa K. Anomalous superconductivity and pressure induced phase transitions in black phosphorous. Solid State Communs, 1985, 54, N9, 775-778.

PRESSURE DEPENDENCE OF ELECTROPHYSICAL AND PHOTOELECTRICAL InSb PARAMETERS

K.Yu.Guga, V.K.Malyutenko, V.P.Kisliy

Institute of Semiconductors, Academy of Sciences of the Ukrainian SSR, Kiev, USSR

Investigations of the effect of pressure (P) on the InSb photoelectrical properties have been carried out only in the low temperature range (~ 77 K) where the nonequlibrium processes in electron-hole plasma are characterized by Shockly-Read recombination at defect levels. We present the results of the radiative and Auger band-to-band recombinations investigations in InSb under hydrostatic P at T=300 K for the first time. The dependence of carrier lifetime τ on P by the steady-state photoconductivity method in crystals with different impurity concentrations ($10^{20} \leq N_a - N_d \leq 10^{23}$ m^{-3}) has been studied. The influence of P on the InSb conductivity in crossed electric and magnetic fields (magnetoconcentration effect - MCE) including the negative differential conductivity of N-type (N-NDC) at MCE has been studied also. The experimental data were compared with the theoretical calculations of τ made for both Auger - τ_A and radiative - τ_R recombination processes. We have used the well-known expressions for τ_A and τ_R /1,2/ corrected for the P dependences of the band gap E_g, intrinsic carrier concentration n_i and effective mass m^*. As calculations show, compression of i-InSb crystals with $N_a - N_d < 2 \cdot 10^{22}$ m^{-3} results in the increase of radiative processes contribution and at $P > 0.6$ GPa it became predominating. Such a behaviour may be understood taking into account that InSb has a positive pressure coefficient of E_g ($\frac{dE_g}{dP} = 0.15 \frac{eV}{GPa}$) and the value of n_i decreases with increasing P. At the same time, the experimental values of τ_e doesn't agree with calculated effective $\tau_{AR} = (\tau_A^{-1} + \tau_R^{-1})^{-1}$ (Fig.1) especially in crystals with large $N_a - N_d \geq n_i \approx 2 \cdot 10^{22}$ m^{-3}. Naturally to suppose that the τ decrease observed is due to appearance of some additional channel of recombination. This is most probably due to Shockly-Read recombination, although under atmospheric P the contribution of this recombination is negligible. Such a conclusion is confirmed by calculations of $\tau_\Sigma = (\tau_A^{-1} + \tau_R^{-1} + \tau_{SR}^{-1})^{-1}$. Here τ_{SR} is the lifetime of Shockley-Read recom-

bination for onelevel model. At the same time, the general behaviour of τ_e, τ_{AR} and τ_Σ with increasing P agrees with well-known dependence of τ on crystals "extrinsivity" $P_H = \frac{N_a - N_d}{n_i}$ /2/, which changed from $10^{-2} \div 10$ at atmospheric P to $10^{-1} \div 10^2$ at P_{max}. As a result, in semiconductors with extrinsic conductivity the dependence of τ on P has a maximum which is defined by P_H.

Reduction in contribution of the nonlinear recombination processes has been also observed in the investigation of N-NDC. N-NDC and relative high frequency (HF) current oscillations at MCE arise when the initial crystal conductivity is stimulated by the high mobility carriers ($U_n n_o > U_p p_o$, p-type) and the transversal redistribution of carriers lead to appearance of depletion and accumulation region and the current decreases in the depleted region more rapidly than it increases in the accumulated region /3/. The existence of N-NDC region is defined by the values of P_H, $S_{\pm}$, $\frac{U_n}{U_p}$, $\frac{d}{L_d}$. Here $S_{\pm}$ is the rate of surface recombination at the opposite crystal surface, U_n and U_p are the mobilities of intrinsic carriers, d is the crystal thickness and L_d is the diffusion length. It is important, that the larger P_H and L_d or the smaller d, the less the magnitude of the governing field necessary to achieve N-NDC. It is found experimentally the increase under P the typical values of fields corresponding to the threshold of HF current oscillations, their disappearance and maximum (Fig.2). That doesn't agree with the model of N-NDS dependence on P_H and $\frac{d}{L_d}$ described in /3/ but is in a good agreement with the recombination mechanisms, because the decrease of nonlinear recombination processes rate results in the shift of the N-NDC region to the higher governing fields /4/.

The increase in sensitivity of current-voltage characteristic (CVC) to the magnitude of magnetic field at MCE under carrier accumulation condition (CAC) may serve as an additional proof of the reduction of nonlinear recombination rate. At CAC in InSb at T~300 K and atmospheric P the CVC is sublinear which is due to the high Auger recombination rate /5/. Under P the CVC became linear or even superlinear that are typical for the band-to-band radiative and Shockley-Read recombination respectively /6/. Thus, the results obtained give conclusive evidence of a possibility to control the recombination mechanisms in narrow-gap semiconductors such as InSb by changing the P applied.

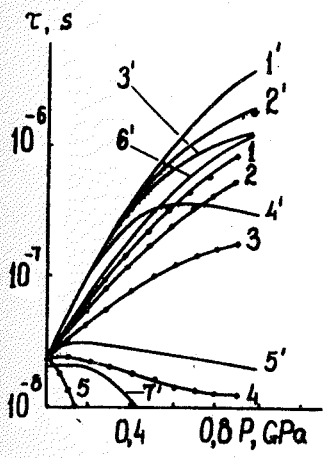

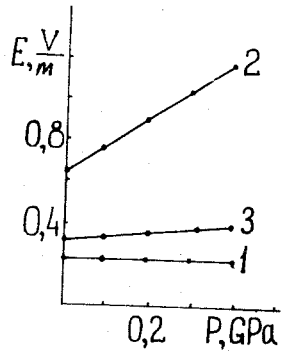

Fig.1. Pressure dependence of electron-hole pairs lifetime for InSb crystals with different impurity concentration: 1-5 - experiment - τ_e; 1'-7' - calculation : 1'-5' - τ_{AR}, 6', 7' - τ_Σ; $(N_a - N_d) \cdot 10^{-21} m^{-3}$: 1,1', 6'- 0.17; 2,2'- 3; 3,3' - 5,4 ; 4,4' - 20; 5,5', 7' -35.

Fig.2. Pressure dependence of distinctive fields of threshold (1), the end (2) and maximum (3) current oscillations by N-NDC at MCE

References

1. Gelmont B.L. - Fiz.Tekh.Poluprov., 1980, vol.14, N10, p.1913-1917.
2. Blakmore J.S. Semiconductors statistics, N.Y., 1962.
3. Akopyan A.A., Gribnikov Z.S., Guga K.Yu., Malozovskij Yu.M., Malyutenko V.K. - Fiz.Tekh. Poluprov., 1979, vol.13, N11, p.2111-2119.
4. Guga K.Yu., Malozovskiy Yu.M., Malyutenko V.K. - Fiz. Tekh. Poluprov., 1982, vol.16, N10, p.1858-1861.
5. Malyutenko V.K., Guga K.Yu., Malozovskiy Yu.M. - Phys.Stat. Sol., (a), 1981, vol.65, N1, p.131-140.
6. Malyutenko V.K., Bolgov S.S., Malozovskiy Yu.M. - Phys.Stat. Sol., (a), 1978, vol.50, N2, p.723-731.

ELECTRONIC STATES OF IMPURITIES AND DEFECTS IN SYNTHETIC DIAMONDS

V.K.Bazhenov, A.G.Gontar, V.E.Gorbachev, D.L.Kardashev
Odessa Institute of Marine Engineers, Odessa, USSR

The properties of an isolated vacancy in diamond are determined by electrones on the broken bonds /1/. These electrones can form bonds between the nearest atoms resulting in their local displacements. Nevertheless the calculations of undistorted vacancies are very important as they usually precede those of the diamond lattice local distortions in the vicinity of an impurity or a defect.

We use the full system of localized orbitals $|mk\rangle$, where m shows the orbital symmetry type and k defines the numbers of all the atoms of a perfect crystal /2/. $G^{kk'}_{mm'}(\epsilon)$ Green's operator matrix components of a crystal having an impurity or a defect meet the requirements of Dyson's equation system

$$G^{kk'}_{mm'}(\epsilon) = g^{kk'}_{mm'}(\epsilon) + \sum_{k''k'''m''m'''} g^{kk''}_{mm''}(\epsilon)\, U^{k''k'''}_{m''m'''}\, G^{k'''k'}_{m'''m'}(\epsilon), \qquad (1)$$

where $g^{kk'}_{mm'}(\epsilon)$ are the Green operator matrix components of a perfect crystal, $U^{kk'}_{mm'}$ are the matrix components of a vacancy or a defect potential, $\epsilon = E + i0^{+}$, and E is the electronic energy.

Let us assume that a vacancy in a diamond is formed by the k=1 atom removal. Then the vacancy potential matrix can be constituted of the components:

$$U^{kk'}_{mm'} = \delta_{k1}(1-\delta_{k'1})\, U^{1k'}_{mm'} + (1-\delta_{k1})\,\delta_{k'1}\, U^{k1}_{mm'} + W^{kk'}_{mm'}, \qquad (2)$$

where δ_{k1} is the Cronecker symbol and the two first constituents describe the semiconductor bicentered exitations caused by a vacancy.

Taking into consideration the orthonormality of the local orbital system and neglecting $W^{kk'}_{mm'}$ constituent (eqn 2) for the time being, one can easily obtain

$$G^{kk'}_{mm'}(\epsilon) = g^{kk'}_{mm'}(\epsilon) + \delta_{mm'}\,\frac{\delta_{k1}\,\delta_{k'1}}{\epsilon - \epsilon^{1}_{m}} - \sum_{m''}\frac{g^{k1}_{mm''}\, g^{1k'}_{m''m'}}{g^{1}_{m''}(\epsilon)}. \qquad (3)$$

We see that the bound and resonant state spectrum of an undistorted vacancy in diamond is determined by zeros of Green's local function $g^{1}_{m}(\epsilon)$. The levels with ϵ^{1}_{m}-energies belong to a removed atom.

We used an octaband tight-binding hamiltonian for diamond /1/. The $I_m g^{1}_{s}(\epsilon)$ and $I_m g^{1}_{p}(\epsilon)$ functions were calculated with the help of the random point selection from the irreducible part of Brillouin's zone, and the Guilbert's conversion was applied to calculate the $Reg^{1}_{s}(\epsilon)$ and $Reg^{1}_{p}(\epsilon)$ functions. These functions for diamond are given in the Figure in the energy fields of the valence and forbidden bands of a perfect crystal.

We can see that the $Reg^{1}_{s}(\epsilon)$ zeros correspond to the energy of -22.6 and -0.15 eV; and the $Reg^{1}_{p}(\epsilon)$ zeros correspond to the energy of -6.5 and 2.35 eV. According to eqn 3 that means the undistorted vacancy induces in diamond the a_1-superdeep resonant state at -22.6 eV; the a_1- and t_2-resonant states at -0.15 eV and -6.5; and the t_2-bound state at 2.35 eV.

Now we can consider the $W^{kk'}_{mm'}$ constituent (eqn 2) if we assume that minima and maxima of the ideal diamond energy bands are in the centre of Brillouin's zone. Then according to Luttinger and Kohn /4/ the following system of equations for $f_n(\vec{r})$ envelope functions can be obtained:

$$\left(\frac{\hat{p}^2}{2m} + \mathcal{E}_n - \mathcal{E}\right) f_n(\vec{r}) + \sum_{n'}\left[\frac{1}{m}\vec{P}_{nn'}\cdot\vec{p} + U_{nn'}(\vec{r})\right] f_{n'}(\vec{r}) = 0, \qquad (4)$$

where $\vec{p} = -i\hbar\vec{\nabla}$ is the impulse operator; m is the mass of a free electrone; E_n is the energy of an electrone in the semiconductor n-band in the centre of Brillouin's zone; $\vec{P}_{nn'} = \langle U_n|\vec{p}|U_{n'}\rangle$; and $U_n(\vec{r})$ is Bloch's wave function in the centre of Brillouin's zone.

The states of upper valence bands having degeneracy points in the centre of Brillouin's zone make the dominating contribution to the electronic states of shallow acceptors in diamond /1/. We assume here that upper bands contribution can be allowed for with the help of a single $f_v(\vec{r})$ envelope. As the electronic state energies of the shallow acceptors $E \gtrsim E_v$, all the other envelopes can be expressed in the form of

$$f_n(\vec{r}) = -\left[\vec{P}_{nv}\vec{\nabla} + \frac{U_{nv}(\vec{r})}{E_n - E_v}\right] f_v(\vec{r}). \qquad (5)$$

Thus we obtain the equation for the $f_v(\vec{r})$ envelope from (4):

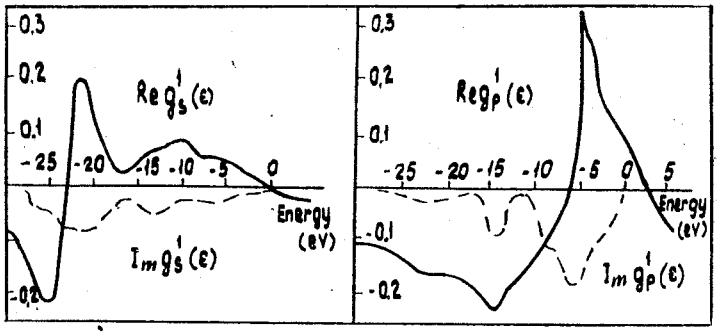

$Re\,g^1_{s,p}(\epsilon)$ and $Im\,g^1_{s,p}(\epsilon)$ functions for diamond.

where
$$\Big[\sum_{\alpha,\beta}(-i\nabla_\alpha)D_{\alpha\beta}(-i\nabla_\beta)+V(\vec r)\Big]f_\nu(\vec r)=(E-E_\nu)f_\nu(\vec r), \qquad (6)$$

$$D_{\alpha\beta}=\frac{\hbar^2}{2m}\delta_{\alpha\beta}+\sum_n (E_\nu-E_n)r^\alpha_{n\nu}r^\beta_{\nu n}\,; \qquad (7)$$

$$V(\vec r)=U_{\nu\nu}(\vec r)+\sum_{n\neq\nu}\Big[\vec r_{\nu n}\cdot\vec\nabla+\frac{U_{\nu n}(\vec r)}{E_\nu-E_n}\Big]U_{n\nu}(\vec r). \qquad (8)$$

Equation 6 coincides with a standard effective mass equation with the corresponding $V(\vec r)$ potential type /4/.

Replacing (5) with the more exact relation we have

$$f_n(\vec r)=-\varphi(\vec r)\cdot\Big[\vec r_{n\nu}\cdot\vec\nabla+\frac{U_{n\nu}(\vec r)}{E_n-E_\nu}\Big]f_\nu(\vec r), \qquad (9)$$

where $\varphi(\vec r)$ is not equal to 1 for small distances only. Instead of (7) and (8) we obtain:

$$\tilde D_{\alpha\beta}=\frac{\hbar^2}{2m}\delta_{\alpha\beta}+\varphi(\vec r)\sum_n(E_\nu-E_n)r^\alpha_{\nu n}r^\beta_{n\nu} \qquad (10)$$

and

$$\tilde V(\vec r)=U_{\nu\nu}(\vec r)+\varphi(\vec r)\sum_{n\neq\nu}\Big[\vec r_{\nu n}\cdot\vec\nabla+\frac{U_{\nu n}(\vec r)}{E_\nu-E_n}\Big]U_{n\nu}(\vec r). \qquad (11)$$

In this case the effective mass of a charge carrier in a kinetic energy operator is the function of a space coordinate. It is only natural to choose the $\varphi(\vec r)$ so that $\tilde V(\vec r)$ should correspond to $V(\vec r)$ from the effective mass equation /4/. The solution obtained is the sensitive function of the short-range constituents of the impurity potential and of the electronic structure of an ideal

crystal. The stronger corrugation of the hole isoenergetic surfaces as well as stronger local lattice distortions in the vicinity of impurities are characteristic of diamond in comparison with silicon.

References

1. Баженов В.К., Викулин И.М., Гонтарь А.Г. Синтетические алмазы в электронике. – ФТП, 1985, т.19, в.8, с.1345-1364.
2. Смирнов В.П., Эварестов Р.А. Локализованные орбитали в кристаллах и зонные представления пространственных групп. – ФТТ, 1983, т.25, в.11, с.3261-3267.
3. Баженов В.К., Кардашев Д.Л., Нахабин А.В. Электронные уровни нейтральных вакансий в $A^{III}B^{V}$ полупроводниках. – ФТП, 1986, т.20, в.1, с.113-117.
4. Бир Г.Л., Пикус Г.Е. Симметрия и деформационные эффекты в полупроводниках. – Л., Наука, 1972, 584с.

INVESTIGATION OF THE PHASE TRANSFORMATIONS OF THE RARE-EARTH METALS La, Pr AND Nd AT HYDROSTATIC PRESSURES UP TO 9 GPa AND TEMPERATURES UP TO 800 K, THERMOPOWER AND ELECTRORESISTANCE

N.A.Nikolaev
L.F.Vereshchagin Institute of High Pressure Physics
Troitsk, USSR

Introduction

For trivalent rare-earth metals from La to Lu the semiempirical generalized P-T phase diagram was constructed in /I/. In the lanthanides the crystal structures of the metals are varied in the sequence: hcp → Sm-type → dhcp → fcc with increasing pressure or reducing an atomic number of the series. It is established that the sequence is caused by s → d electronic transition /2,3/. In /4/ it had been given the theoretic justification about a possible occurence of a critical point at s → d transition in the metals at isomorphological transition. So far in the metals of period only Ce was found to have the critical point on the P-T plane at the electronic $\gamma - \alpha$ transformation /5/.

On the generalized phase diagram /I/ La, Pr and Nd take up a limiting right position. From a linear extrapolation of the dhcp-fcc phase boundary for La one can expect that on the temperature axis Pr and Nd will be undergone the phase transition accordingly at 560 and 690 °C /I/. However the fcc phase of Pr or Nd is not exist at the barometric pressure /6/.

To study the P-T diagrams and a features of the phase transitions of La, Pr and Nd we have measured the electroresistance and the thermopower of the metals. It was investigated the modification of the phase transition hysteresis with the temperature and pressure. The background results were presented in /7,8/.

Results and discussion

The behaviour of the kinetic coefficients of La, Pr and Nd is found to be like. Fig.I shows the hydrostatic pressure dependence of the thermopower of the metals at about room temperature. The transitions from dhcp phase to the high pressure phase occur in the row La, Pr and Nd at pressures of 2.05, 4.0 and 7.0 GPa. These values correlate with the initial magnitudes (its differences) of the thermopower of the metals - S^o_{La}=I.9 μV/K, S^o_{Pr} =-I.45

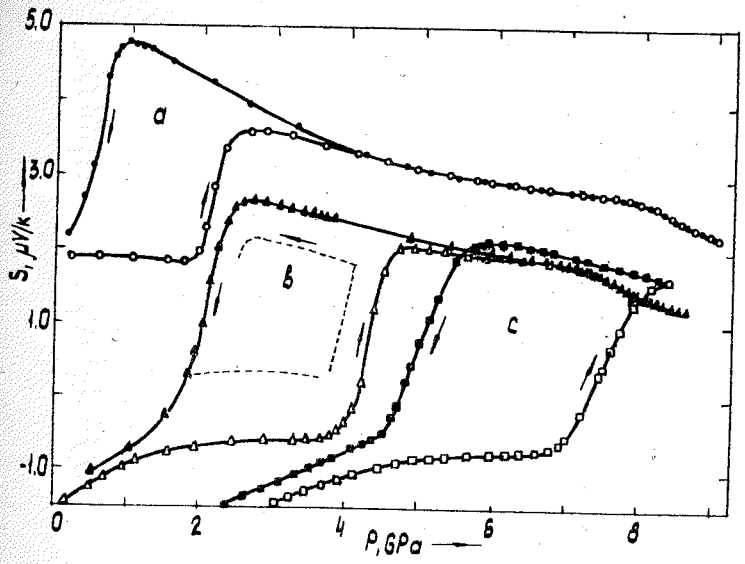

Fig.I. Hydrostatic pressure dependences of the absolute thermopower for a - La, T=32 °C, b - Pr, T=27 °C, c - Nd, T=27.2 °C at increasing ○, △, □ and decreasing ●, ▲, ■ pressure. Dash line - partial cycling of the transformation in Pr.

μV/K, S^o_{Nd}=-3.0 μV/K. The circumstance carries evidence to electronic nature of the transformation when the occupancy of the d-like electron state determines the crystal structure /3/ and gives a positive partial contribution to the thermopower of the metals.

On the dependences of the kinetic coefficients (Fig.I, Fig.I /7/) at the fcc-dist.fcc phase transition in La and Pr the thermopower of the metals reveals a very small anomaly compared with the electroresistance. The results can not validate the expectation on electron-topological character of the transition or the s-d electronic transition. The coming into being of the softing mode dominantly effected on a scattering process of the s-like electrons may explain the changes of the kinetic coefficients at the transition in question.

The fact of common analogy between the kinetic coefficients of La, Pr and Nd under pressure, i.e., a pronounced elevation of thermopower and a drop of electroresistance at the dhcp → fcc phase transition, a small variations in thermopower at the fcc→

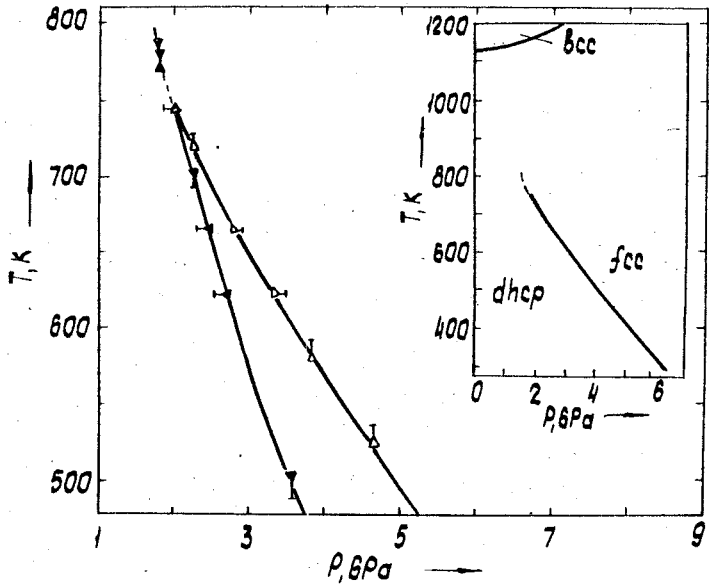

Fig.2. P-T diagram of phase transitions in Nd under hydrostatic pressure: Δ and ▲ (or Δ and ▼) - locations of direct and reverse transitions respectively at increasing and decreasing pressure (or temperature). Transitions in extent are recorded by sections. Fragment of hypothetical equilibrium P-T diagram is shown.

dist.fcc transition, a closeness of the thermopower of the metals in the high pressure phases, testifies to the absence of 4f--electrons influence on the transport phenomena in Pr and Nd at pressures up to 9 GPa.

High temperature investigations of Pr and Nd by means of developed method allow us to locate the position of direct dhcp → → fcc and reverse fcc → dhcp phase boundaries in the P-T diagram. Fig.2 shows a modification of the dhcp-fcc phase transition hysteresis of Nd at high temperatures. The data confirm completely those obtained early by investigation of Pr (Fig.5 /7/). The experimental bring out details of the dhcp-fcc transition in Pr and Nd consist in the following: the rectilinear course of a phase transition boundary in the P-T diagram is ended at the high temperatures, the hysteresis of the transformation approaches zero in the vicinity of particular points. As follows from Fig.3

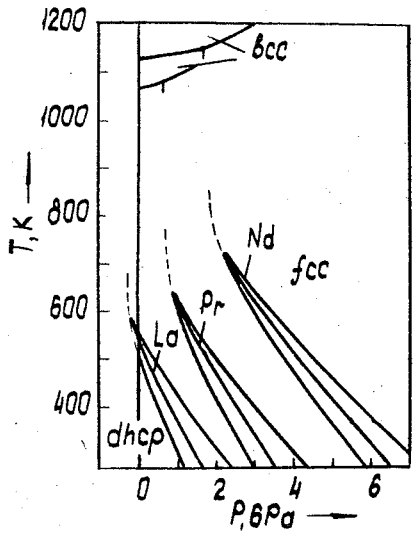

Fig.3. The phase diagrams of La, Pr and Nd with the dhcp-fcc transformation. Thin lines correspond to the beginning of the experimentally observed transitions. Dash lines are hypothetical lines of the phase transitions.

the indicated type feature may lie at negative pressures for La. In spite of the essential difference between phase transformations under pressure in Pr, Nd and Ce the electronic character of the transitions may unite the observed phenomena at high temperatures.

References

1. Johansson B., Rosengren A. Phys.Rev.B, 1975, II, 2836.
2. Duthie J.C., Pettifor D.G. Phys.Rev.Lett., 1977, 38, 564.
3. Skriver H.L. Phys.Rev.B, 1985 31, 1909.
4. Arkhipov R.G. Zh.eksper.teor.Fiz., 1965, 49, 1601.
5. Ponyatovskii E.G. Dokl.Akad.Nauk SSSR, 1958, 120, 1021.
6. Zinovjev V.E. Kineticheskie Svoistva Metallov pri vysokikh Temperaturakh. M.:Metallurgiya, 1984.
7. Nikolaev N.A., Khvostantsev L.G. Zh.eksper.teor.Fiz., 1987, 92, 358.
8. Nikolaev N.A., Khvostantsev L.G., Zinovjev V.E., Starostin A.A. Zh.eksper.teor.Fiz., 1986, 91, 1001.

HIGH PRESSURE SUPERCONDUCTING PHASE OF TITANIUM HYDRIDES: ELASTIC AND INELASTIC NEUTRON SCATTERING

A.I.Kolesnikov[1], I.Natkaniec[2], V.K.Fedotov[1], I.O.Bashkin[1], E.G.Ponyatovsky[1], S.Habrylo[2]

[1]Institute of Solid State Physics, the USSR Academy of Sciences, USSR

[2]Joint Institute for Nuclear Research, Dubna, USSR

Recently a number of metastable phases of metal hydrides (Ti-H; Zr-H; Hf-H, etc.) have been produced by quenching under pressure up to 60 kbar /1/ or low-temperature hydrogen implantation /2/, which have, like stable PdH_x and Th_4H_{15} hydrides, a higher transition temperature (T_c) into superconducting state compared to the starting metals. Phonon spectra of superconducting hydrides have been measured only for PdH_x /2/ and Th_4H_{15} /3/. The first results on the study of the hydrogen local modes in the metastable superconducting ε-phase of $TiH_{0.71}$ have been published in /4/. The present paper is a further step in the investigation of the phonon spectra of TiH_x (x=0.71; 0.81 and 0.86) and TiD_x (x=0.72 and 0.86) attempted with the purpose to elucidate the effects of isotopic substitution D→H as well as x-concentrations on the phonon spectra (as to the production of hydrides, see Ref./1/).

It is found /5/ that the ε-phase of the hydrides studied is a superconductor, with the inverse isotope effect taking place for T_c (T_c^{Ti-H}=4.3 K < T_c^{Ti-D}=5.0 K). For Ti, T_c=0.4 K, the superconductivity of α, γ, γ', δ and ω phases of titanium hydride has not been observed down to 1.2 K. The ε-phase of Ti-H(D) was obtained by quenching under 60 kbar /1/. After heating the ε-phase to T > 110 K the latter transformed into the δ-phase (FCT structure). Subsequent annealing for 5 hs at T=440 K resulted in the transition to the ($\alpha+\gamma$)-phase (HCP and FCC structures, respectively).

Neutron scattering experiments were performed at the Joint Institute for Nuclear Research (Dubna) using the KDSOG-M spectrometer /6/ installed at the IBR-2 reactor. The diffraction and inelastic neutron scattering (INS) spectra were measured simultaneously by the time of flight technique.

It follows from the diffraction spectra that the ε-phase lattice for all Ti-H(D) samples is close to the FCT with the parameters a=4.29 Å and c=4.02 Å (c/a=0.937). The elastic neutron

spectrum obtained exhibit in addition to the ε-phase peaks also the δ-phase lines (20%) for TiH_x (x=0.81 and 0.86) and the γ-phase lines (10%) for $TiD_{0.86}$. The analysis of the ε-phase reflex intensities shows that the hydrogen (deuterium) occupies mostly the O-sites of the metal lattice.

A rather large metal-hydrogen distance for the O-sites of ε-phase (R_{Me-H}=2.15 Å and 2.01 Å) as compared with that in the T-sites (1.88 Å for δ-phase and 1.91 Å for γ-phase) gives rise to optical low-frequency modes ω_1 in the INS spectra of the ε-phase. Fig.1 illustrates the functions of weighted density of vibrational states, $G_H(\omega)$, /7/ for ε-phase in $TiH_x(D_x)$ which were obtained in one-phonon approximation. The second peak ω_2 is caused by the vibrations of H(D) in the T-sites as well as by the processes of two-phonon and multiple scattering of neutrons on the ω_1-mode and by the contributions of the second harmonic of this vibration (since $\omega_2 \simeq 2\cdot\omega_1$). In the case of two-phase samples ε +(δ or γ) the contribution to the intensity of this peak is made by hydrogen vibrations in the T-sites of the second phase.

It should be noted that the halfwidth of the ω_1-peaks ($\Delta_1 \simeq$40 meV) is rather large (the spectrometer resolution in the region of H(D) vibrations in O-sites is about 6 meV; in T-sites about 17 meV). This is indicative of a strong dispersion of H(D) vibrations in the O-sites. Moreover, the stresses and distortions in the lattice produced by quenching should lead to extra broadening of local modes. The results obtained for the ε-phases of titanium hydride are similar to those obtained for other superconducting hydrides. Low-energy optical vibrations of hydrogen atoms with a considerable dispersion are observed in these systems.

In the $G_H(\omega)$ plots of nonsuperconducting δ and ($\alpha+\gamma$)-phases of titanium hydride (see Fig.2) the peaks are conditioned by the H(D) vibrations only in the T-positions (the first, second, etc. harmonics). It is seen that the energy ω_1 in the δ-phases is higher than in the ($\alpha+\gamma$)-phases approximately by 7 meV for TiH_x and by 2 meV for TiD_x (it will be recalled that $R^{\delta}_{Me-H} < R^{\gamma}_{Me-H}$). The halfwidth of the first peak of the ($\alpha+\gamma$)-phase in $TiH_{0.71}$ is much larger than that in the δ-phase. This points to the fact that the dispersion of local modes in the γ-phase (which is richer in hydrogen) is higher due to the increased H-H interaction.

Our results show that hydrogen predominantly occupies the O-sites at the titanium hydride transition to the superconducting ε-phase, and the phonon spectra exhibit a local low-energy mode

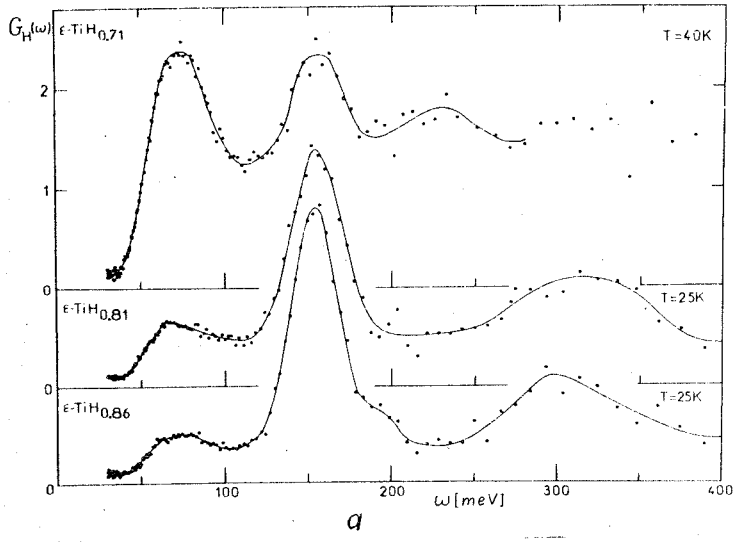

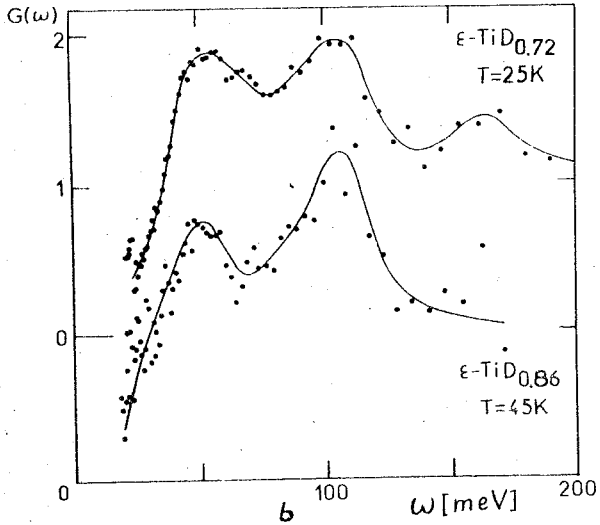

Fig.1. Generalized frequency spectrum $G_H(\omega)$ for optical vibrations in $\mathcal{E}$ -phases: a - TiH_x; b-TiD_x.

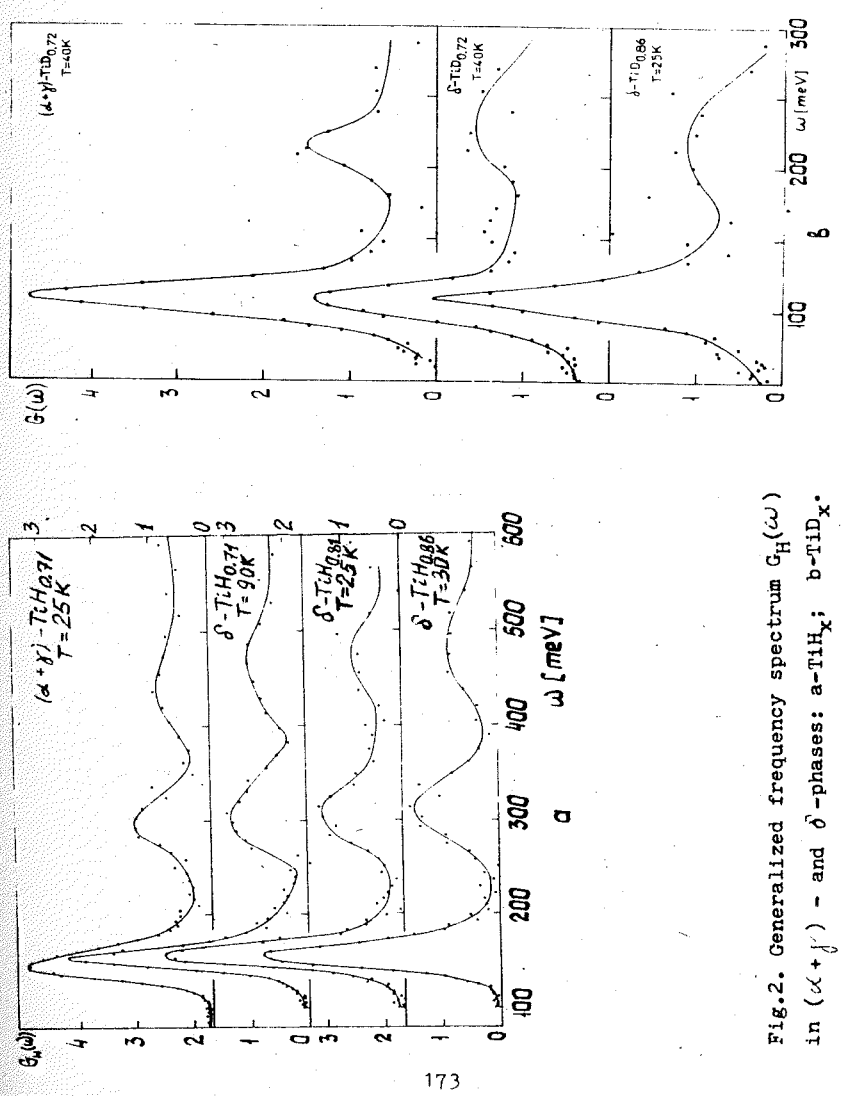

Fig.2. Generalized frequency spectrum $G_H(\omega)$ in $(\alpha+\beta')$ - and δ-phases: a-TiH_x; b-TiD_x.

with high dispersion. When hydrogen occupies only the T-sites, no superconductivity is observed in Ti-H.

References

1. Ponyatovsky E.G., Bashkin I.O., Degtyareva V.F. et al. Fiz.Tverd.Tela (Leningrad) 1985, 27, N11, 3446-3448.
2. P.V.Geld, R.A.Ryabov, L.P.Mohracheva "Hydrogen and physical properties of metals and alloys". Moscow: "Nauka", 1985, 232 p.
3. Dietrich M., Reichard W., Rietschel H. Phonon densities of states of the thorium hydrides. Solid State Commun., 1977, 21, N6, 603-605.
4. Kolesnikov A.I., Fedotov V.K., Natkaniec I., et al. "Hydrogen transition to octahedral lattice sites in the superconducting phase of titanium hydride". Pis'ma v ZhETF, 1986, 44, N8, 396-398.
5. Bashkin I.O., Malyshev V.Yu., Rashchupkin V.I., Ponyatovsky E.G. "Composition and superconductivity of high pressure phases in titanium hydrides" to appear in Fiz.Tverd.Tela (Leningrad).
6. Baluka G., Belushkin A.V., Bragin S.I. et al., "Inverted geometry spectrometer KDSOG-M on a IBR-2 reactor". JINR, P13-b4-242, Dubna, 1984.
7. Izymov Yu.A., Ozerov R.P. "Neutron spectroscopy". Moscow: Energoatomizdat, 1963, 328 p.

PRESSURE EFFECT ON CONDUCTIVITY OF ORGANIC CONDUCTOR (BMDT-TTF)-I

V.A.Bondarenko, K.I.Pokhodnya, Yu.V.Sushko
Institute of Semiconductors, Ukrainian Academy of Sciences, Kiev, USSR

Low dimensional organic compounds exhibit extremely wide variety of electrophysical properties including metallic and semiconducting as well as superconducting and recently discovered (in (BEDT-TTF)$Ag_{I.8}I_{2.9}$ /I/) superionic features. Hydrostatic pressure can substantially change the properties of these compounds. It also can affect the phase transitions in these crystals and elucidate the nature of the phase states.

In the present paper we have investigated single crystals of (BMDT-TTF)-I (iodid of bis(methylenedithio)tetrathiafulvalene), obtained by electrochemical oxidation of BMDT-TTF in nitrobenzene in the presence of $(n\text{-}Bu_4N)I_3$ as supporting electrolyte.

The temperature dependence of resistivity of the samples studied at ambient pressure is of metallic type in 300-I00 K range the $R_{300}/R_{I00\ K}$ being approximately equal to 2 (Fig.I, curve I). Below I00 K R(T) curve is of insulator type with activation energy of conductivity E ≈I70 K.

Hall effect studies at room temperatures have shown p-type conductivity (the temperature dependence of Hall-factor R_H at P=I bar and B=5 T is shown at Fig.2, curve 3), the Hall mobility and carrier density being $\mu_H \simeq 0.5\ cm^2V^{-1}s^{-1}$ and $p \approx I0^{2I}cm^{-3}$, respectively. The p-type conductivity was also confirmed by thermopower measurement at room temperatures.

With the lowering of T the type of major carriers changes: electrons replace the holes at T≤ I00 K. With the lowering of T in the temperature region below I00 K the carriers concentration essentially decreases with the activation energy 230 K; this value is somewhat larger than the activation energy of conductivity in this temperature region.

High pressure studies were performed in pressure bomb of clamp-cell type with a help of silicon oil.

The hydrostatic pressure (up to 8 kbar) causes the increase of (BMDT-TTF)-I conductivity, - under room temperature $\partial[\sigma(P)/\sigma(P=I\ bar)]/\partial P \approx +I5$ % kbar. This value is a typical one for synthetic metals. Besides, as evidenced by Fig.I, the incre-

Fig.1. Temperature dependence of resistivity for (BMDT-TTF)-I under different pressures: I - P=I bar; 2 - P=4 kbar;3 - P=6 kbar.

Fig.2. Temperature dependence of resistivity under different pressures (I - P=I bar; 2 - P=6 kbar) and Hall-factor (3 - P=I bar) for (BMDT-TTF)-I.

ase of the pressure leads to substantial decrease of metal-to--insulator transition temperature, T_{MI}, the $\partial[T_{MI}(P)/T_{MI}(P=Ibar)]/\partial P \sim -I2$ %/kbar and causes substantial decrease of conductivity activation energy to I40 K at 6 kbar. Note, that R(T) curve is changed under the pressure in the vicinity of metal-insulator transition. The rate of resistivity decrease in the temperature range $30\ K < T < 70\ K$ increases with lowering T at P=6 kbar while it decreases in the appropriate part of the R(T) curve at P=I bar.

The obtained change of conductivity type may be caused by complicated electronic spectrum of material under investigation. The complicated form of the Fermi-surface may facilitate nesting /2/ in some parts of this surface which usually yields the Peierls instability causing the charge density wave (CDW). Hydrostatic pressure can vary the commensurability of initial and distorted lattices in such systems and cause transitions of commensurate CDW - incommensurate SDW type. Besides the lowering of the metal-insulator (semiconductor) transition temperature the pressurization can cause the abrupt increase of conductivity before the transition /3,4/. Probably such mechanism is responsible for observed peculiarity of R(T) dependence at P=6 kbar.

The authors thank Tanatar M.A. for the assistance and fruitful discussions, and Baram G.O. for the samples presented.

References

I. Суперионная проводимость в $(BEDT\text{-}TTF)_3Ag_xI_8$/М.А.Танатар, Г.О.Барам, В.А.Бондаренко, К.И.Походня, В.А.Стародуб, Ю.В.Сушко // Тезисы докладов II Всесоюзного симпозиума "Неоднородные электронные состояния". Новосибирск.-I987.-С.II8-II9

2. Л.П.Горьков. Физические явления в новых органических проводниках // УФН.-I984.-Т.I44, вып.3.-С.38I-4I3

3. Б.М.Гореlов, В.Н.Лаухин, И.Ф.Шеголев. Влияние нестехиометричности и давления на фазовый переход металл-диэлектрик в иодидах тетратиотетрацена //ЖЭТФ.-I98I.-Т.80, вып.6.-С.2403-2408

4. A.Andrieux, Schulz H.I., Jerome D et al. Fluctuation conductivity in I-d conductor TTF-TCNQ //J.de Phys.Lett.-I979.-V.40, N I5,-P.385-389

PRESSURE DEPENDENCE OF THE T_c OF HIGH TEMPERATURE SUPERCONDUCTORS

A.Driessen[I], R.Griessen[I], H.Hemmes[I], N.Koeman[I], J.Rector[I], P.H.Kes[2]

[I]Natuurkundig Laboratorium der Vrije Universiteit, De Boelelaan 1081, 1081 NV Amsterdam, the Netherlands

[2]Kamerlingh Onnes Laboratory, University of Leiden, P.O.Box 9606, 2300 RA Leiden, the Netherlands

Abstract

The pressure dependence of the transition temperature of high temperature superconductors has been measured in the diamond anvil cell using a resistometric method. Our measurements on $Y_1Ba_2Cu_3O_7$ up to 170 kbar reveal only a small pressure effect in agreement with data in literature at lower pressure. A comparison is made with literature data on the M-La-Cu-O system (M=Ba, Sr), which has a strong pressure dependence. The phase diagram of Chakraverty for T_c as a function of the electron-phonon coupling parameter is used for a qualitative explanation of the observed pressure effects.

Introduction

In general high pressure is considered as an important parameter in the study of the new class of high T_c superconducting ceramic materials. Already in some of the first papers on the Ba-La-Cu-O system pressure was used to increase the transition temperature /1,2/. But in contrast to this a later study on Y-Ba-Cu-O showed nearly no pressure dependence of T_c /3/. For this alloy the application of pressure seems to be not the way to get drastically enhanced T_c. But on the other hand, pressure should be an important experimental parameter, which can probably bring more insight in the mechanism of superconductivity in this class of materials, or at least, could exclude some currently available theoretical models. We therefore decided to do high pressure studies of the ceramic superconductors in our diamond anvil cell, which was originally designed for the measurement of superconducting properties of metal hydrides /4/.

Experiment

Our diamond anvil cell, which is nearly completely made from

hardened BeCu 25, can be operated in the temperature range from 1.5 to 300 K with a maximum force of 30 kN on the diamonds. For rapid cooling, a liquid nitrogen or helium flow system is attached to the cell. The whole is placed inside an optical helium bath cryostat. During the experimental run pressure can be determined in situ at all temperatures with the aid of the ruby fluorescence method /5/. Fig.1 shows the geometry of the sample space. Because of the four electrical leads connected to the electrodes, the brass gasket and isolated from it a second thin brass foil, only the contact between sample and brass ($<$ 1 Ohm) adds to the resistance of the sample.

Fig.2 shows the result of applying a pressure of 157 kbar on $La_{1.8}Sr_{0.2}CuO_4$, which at zero pressure has a superconducting transition at 36 K. The curve exhibits no superconducting behavior down to 1.8 K, but instead a strong, reproducible increase of the resistance at low temperature. Similar behavior is often found in this class of materials, which Bednorz et al./6/ interpret as the onset to a localization transition. As there are no data points in the intermediate pressure range, we can draw no further conclusions about this qualitative change of the resistance curve at high pressure. With this measurement, however, the reliability of the resistance measurements in the gasket geometry as shown in Fig.1 is demonstrated.

In a second experiment we studied $Y_1Ba_2Cu_3O_7$, which was prepared by standard solid state reaction. In the experiment with the same gasket configuration as before we were able to follow the transition temperature up to 170 kbar. In agreement with the data of Hor et al./3/, only a weak pressure dependence could be detected /7/.

Discussion

In order to clarify, whether the observed pressure effects, strong pressure dependence in the La-Cu-O based alloys and nearly vanishing effects in the Y-Ba-Cu-O class of materials, are real physical effects, we give in Table a summary of all available data for dT_c/dp. With the relation:

$$\frac{d(\ln T_c)}{d(\ln V)} = -\frac{B\, dT_c}{T_c\, dp}$$

and the bulk modulus B=1.7 Mbar, taken from Salomons et al. /16/,

we can determine the volume derivative of T_c, which is the quantity needed for theoretical considerations. Fig.3 gives this value as a function of T_c. The La based alloys, with exception of pure La_2CuO_4, follow one curve and show in general a strong pressure dependence. The Y-Ba-Cu-O class of superconductors, all with a T_c around 90 K, show a very weak pressure dependence with only a slight scatter around zero. The pressure measurements are also in agreement with "chemical pressure" data, i.e. changes of T_c by substituting part of the constituents with atoms of different atomic radius. The La based alloys are very sensitive to it /I7,I8/, whereas the Y-Ba-Cu-O class shows nearly no effect /I9/. The overall agreement of all data give evidence for dealing with a real physical effect.

Pressure and volume dependence of the onset temperature T_{co}. The pressure range for each experiment is indicated in the column P. The symbols are used in Fig.3

Sample	T_c (K)	dT_c/dp (K/kbar)	$dlnT_c/dlnV$	P P (kbar)	Symbol	Ref.
$La_{0.8}Ba_{02}CuO_{3-y}$	32	0.64	-34	0-I3	△	/I/
$La_{0.85}Ba_{0.I5}CuO_{4-y}$	35.2	0.3I	-I5	0-I9	+	/8/
$La_{I.85}Sr_{0.I5}CuO_4$	36	0.28	-I3.2	0-5	x	/9/
$La_{I.8}Sr_{0.2}CuO_4$	37	0.26	-II.9	0-6	o	/I0/
$La_{I.8}Ba_{0.2}CuO_{4-y}$	39	0.82	-35.7	0-I7	▲	/2/
$La_{I.8}Sr_{0.2}CuO_4$	39.2	0.I8	-7.8	0-I2	●	/I0/
La_2CuO_4	40	I	-42.5	0-I0	▽	/II/
$La_{I.8}Sr_{0.2}CuO_{4-y}$	50	0	0	20-42	◐	/I0/
$YBa_2Cu_3O_7$	90	$<$ 0.I2	$>$ -2.3	0-I7	□	/I2/
$Y_{0.4}Ba_{0.6}CuO_{3-y}$	90	$<\pm$0.I2	$>\pm$2.3	I-8	◇	/I3/
$Y_IBa_2Cu_3O_7$	9I	0.043	-0.8	0-I70	■	/7/
$Y_{0.325}Ba_{0.675}CuO_{2.3}$	92.2	0.I7	-3.I	0-I0	◧	/I4/
$Y_{0.35}Ba_{0.65}CuO_{2.3}$	93	0.I	-I.8	0-I0	◨	/I4/
$Y_{I.2}Ba_{0.8}CuO_{4-y}$	93	0.043	-0.8	0-I9	⊗	/3/
$Y_{0.4}Ba_{0.6}CuO_y$	93.2	0.045	-0.8	0-I20	•	/I5/
$Y_{0.425}Ba_{0.575}CuO_{2.3}$	93.5	0.09	-I.6	0-I0	◒	/I4/

In ref./20/ the consequence of the observed pressure effects for some theoretical models for the superconducting mechanism are discussed. We will not repeat this discussion, instead we try to find a possible explanation on the basis of a phase diagram for superconductors as proposed by Chakraverty /2I/, (Fig.4). In this diagram, T_c is given as a function of the electron-phonon coupling parameter λ. For small λ one has the standard BCS superconductivity with:

$$T_c \sim \exp\left(-\frac{I+\lambda}{\lambda}\right)$$

and for large λ the bipolaronic superconductor, which with even more increase in λ transforms to a bipolaronic insulator. Nevertheless the lack of knowledge about the exact nature of the superconducting mechanism in between, there is a continuous transition from one region to the other (see Nasu /22/), which should exhibit at least one maximum. At this maximum predicts Chakraverty /2I/ a metal-insulator transition for temperatures higher than T_c. This could explain the experimental observation that the highest T_c values for oxides occur near a metal-insulator transition /2/.

We tentatively suggest the position of the two classes of superconducting alloys as indicated in Fig.4. Changing λ, by real or chemical pressure, will have a strong influence on La-Ba-Cu-O, but only a very weak one in the case of Y-Ba-Cu-O, in agreement with the experimental results. Also the diminishing pressure dependence with rising T_c (Fig.3), can qualitatively be explained as T_c approaching the flat region by varying λ with pressure. It is interesting to note that Yomo et al./I0/ find a saturation behavior in the pressure dependence of $La_{I.8}Sr_{0.2}CuO_4$ at pressures above 20 kbar, which could be interpreted as λ having reached the position of the maximum in Fig.4. A similar saturation behavior at high pressure was already found for the same material by Chu et al./2/.

Conclusion

As conclusion we can say:

I. The observed pressure effects on T_c measured by several groups on different samples are in good agreement.
2. Further experimental data as a function of pressure, especially in the region where effects nonlinear in pressure could be expected,

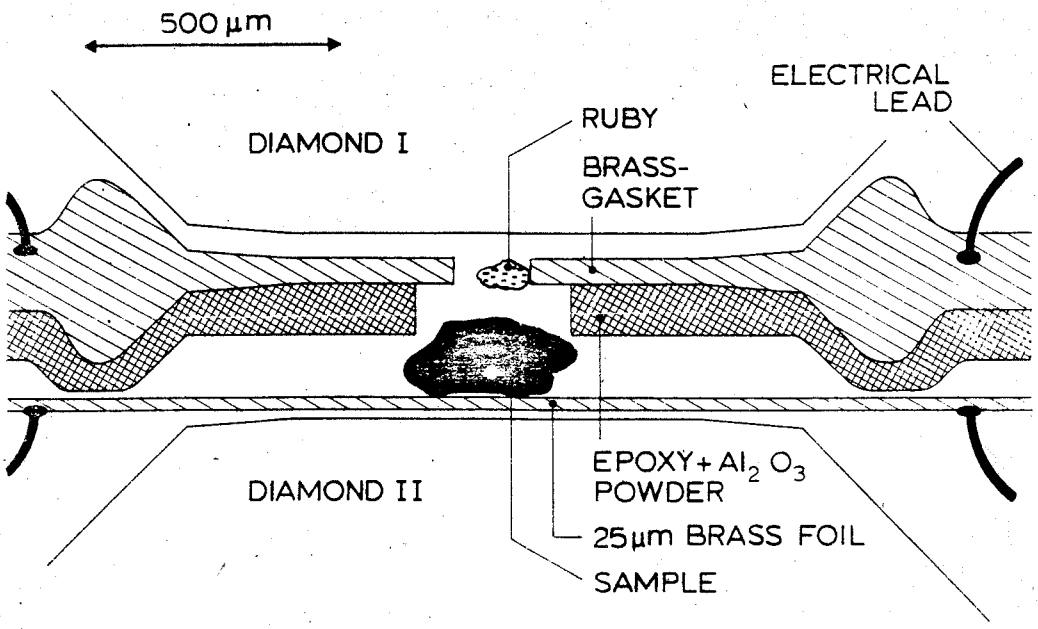

Fig.I. Schematic representation of the pressure chamber of the diamond anvil cell. For clarity it is shown in the situation before pressurizing the sample into the gasket/epoxy hole.

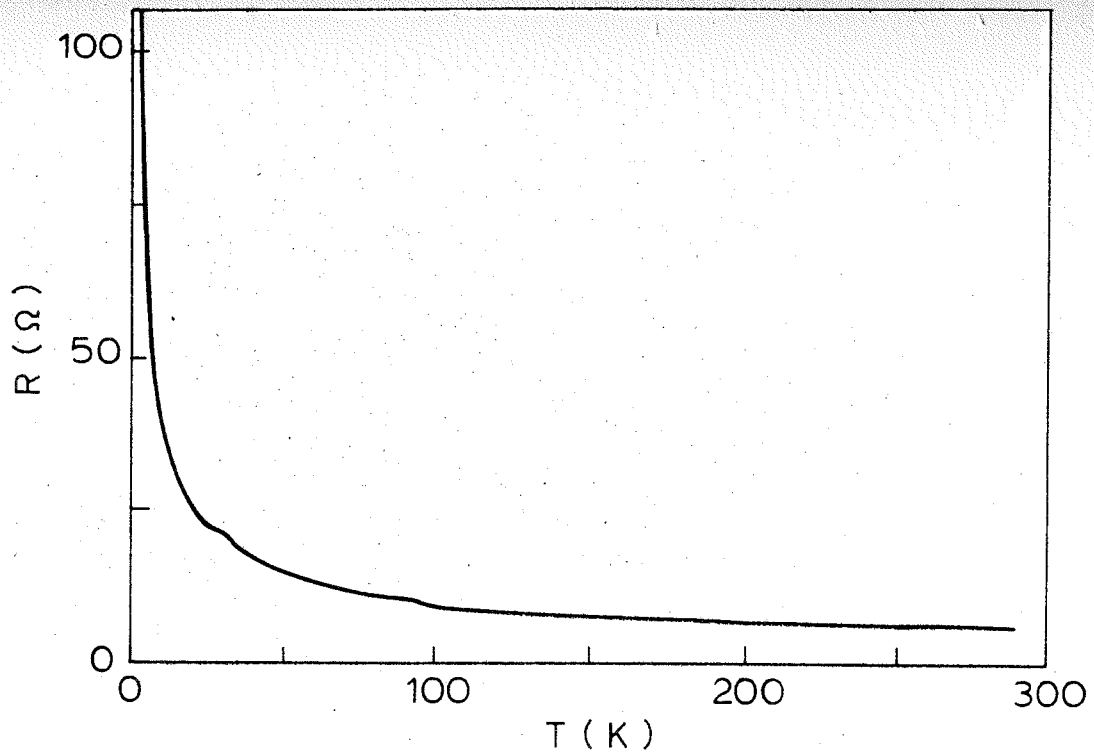

Fig.2. The resistance of $La_{I.8}Sr_{0.2}CuO_4$ as a function of temperature at a pressure of I57 kbar.

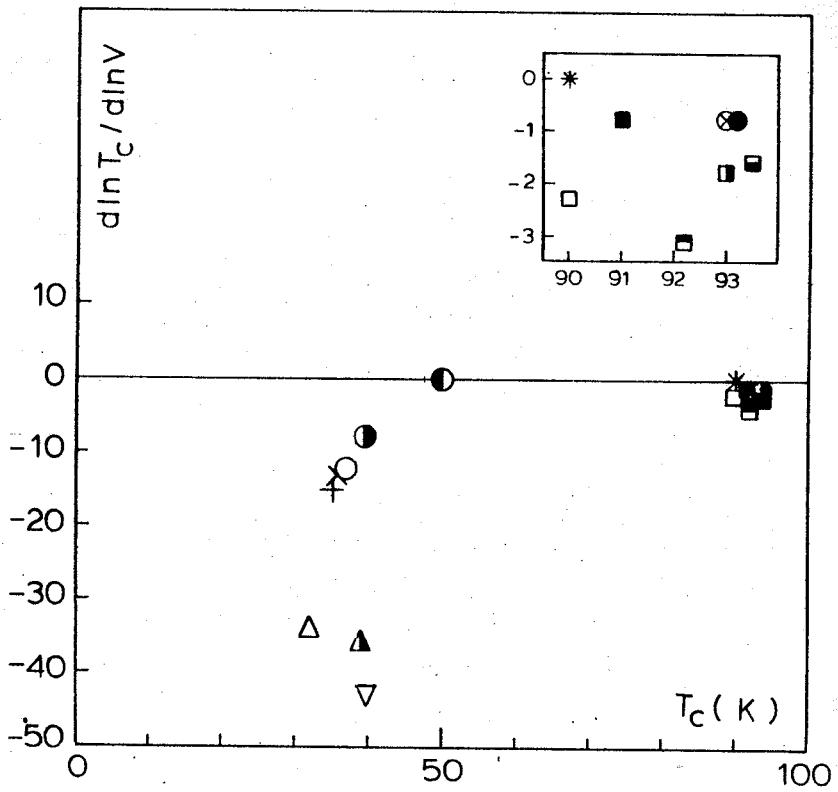

Fig.3. Relative volume dependence of the onset temperature T_{co} as a function of T_c. The symbols are defined in Table. For more clarity the data points of the Y-Ba-Cu-O system are given on an enlarged scale in the inset.

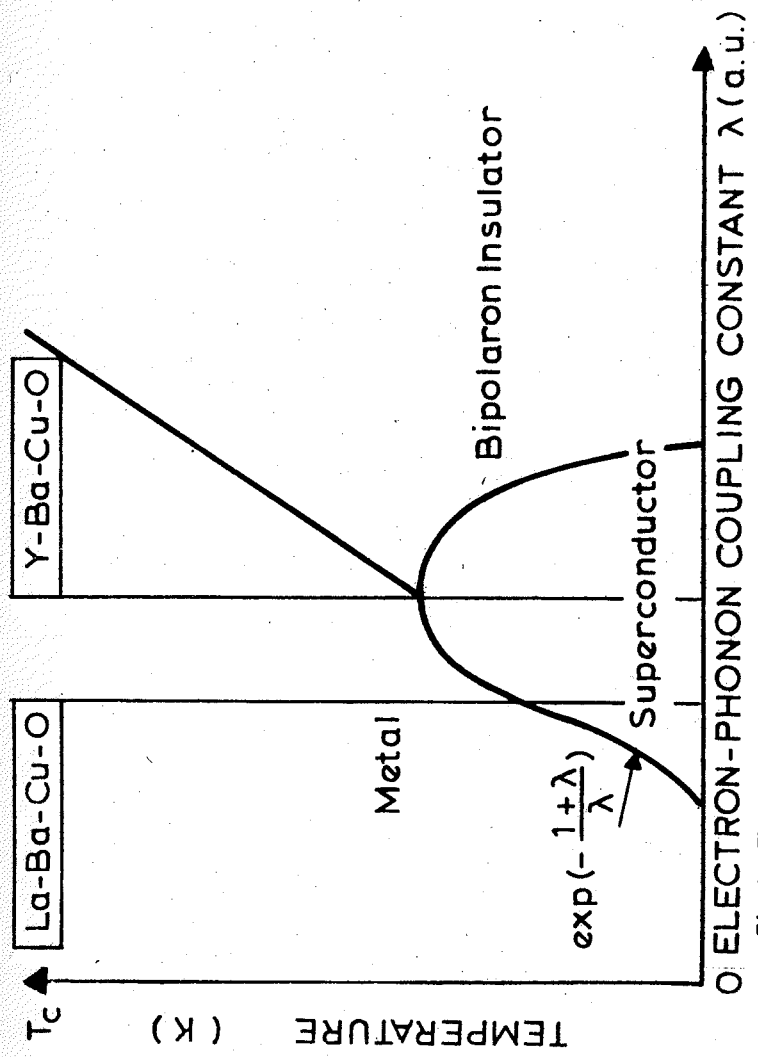

Fig.4. The phase diagram as a function of electron-phonon coupling strength as proposed by Chakraverty /21/. For more explanation see text.

are desirable for developping theories about the mechanism of the high T_c superconductivity.

References

I. C.W.Chu, P.H.Hor, R.L.Meng, L.Gao, Z.J.Huang and Y.Q.Wang, Phas.Rev.Lett. 58 (I987) 405.

2. C.W.Chu, P.H.Hor, R.L.Meng, L.Gao, Z.J.Huang, Science 235 (I987) 567

3. P.H.Hor, L.Gao, R.L.Meng, Z.J.Huang, Y.Q.Wang, K.Forster, J.Vassilious, C.W.Chu, M.K.Wu, R.J.Ashburn and C.J.Torng, Phys.Rev.Lett. 58 (I987) 9II

4. H.Hemmes, A.Driessen and R.Griessen, to be published

5. A.Jayaraman, Rev.Mod.Phys. 55 (I983) 65

6. J.G.Bednorz, M.Takashige and K.A.Mueller, Europhys. Lett.3 (I987) 379

7. A.Driessen, R.Griessen, N.Koeman, E.Salomons, R.Brouwer, D.G.de Groot, K.Heeck, H.Hemmes and J.Rector, to be published

8. M.Kurisu, H.Kadomatsu, H.Fujiwara, Y.Maeno and T.Fujita, Jpn. J.Appl. Phys. 26 (I987) L36I

9. C.Allgeier, J.S.Schilling, H.C.Ku, P.Klavins and R.N.Shelton, EMSR-Conference, Strasbourg, June 3, I987; Phys.Rev.B, to be published

I0. S.Yomo, C.Murayama, H.Takahashi, N.Mori, K.Kishio, K.Kitazawa and K.Fueki, Jpn.J.Appl.Phys. 26 (I987) L603

II. P.M.Grant, S.S.P.Parkin, V.Y.Lee, E.M.Engler, M.L.Ramirez, J.E.Vasquez, G.Lim, R.O.Jacowitz and R.L.Greene, Phys.Rev. Lett. 58 (I987) 2482

I2. Y.Akahama, S.Endo, S.Noguchi and K.Okuda, Jpn J. Appl. Phys. 26 (I987) L87I

I3. K.Murata, H.Ihara, M.Tokumoto, M.Hirabayashi, N.Terada, K.Senzaki and Y.Kimura, Jpn.J.Appl.Phys. 26 (I987) L47I

I4. H.Yoshida, H.Morita, K.Noto, T.Kaneko and H.Fujimori, Jpn. J. Appl.Phys. 26 (I987) L867

I5. B.Okai, K.Takahashi and M.Ohta, Jpn.J.Appl.Phys. 26 (I987) L820

I6. E.Salomons, H.Hemmes, J.J.Scholtz, N.Koeman, A.Driessen, D.G. de Groot and R.Griessen, to be published

I7. R.B.van Dover, R.J.Cava, B.Battlog and E.A.Rietman, Phys.Rev. B35 (I987) 5337

I8. K.Kishio, K.Kitazawa, N.Sugii, S.Kanbe, K.Fueki, H.Takagi and S.Tanaka, Chem.Lett. (I987) 635

I9. P.H.Hor, R.L.Meng, Y.Q.Wang, L.Gao, Z.J.Huang, J.Bechtold, K.Forster and C.W.Chu, Phys.Rev.Lett. 58 (I987) I89I

20. R.Griessen, to be published

2I. B.K.Chakraverty, J.de Phys.-Lettres 40 (I979) L99

22. K.Nasu, Phys.Rev. B35 (I987) I748

ELECTRON SPECTRUM SINGULARITIES IN SUPERCONDUCTION CHARACTERISTICS OF UNORDERED SYSTEMS UNDER PRESSURE

T.Ignat'eva, A.Velikodnyj

Kharkov Institute of Physics and Technology, the Ukrainian Academy of Sciences, Kharkov, USSR

As indicated in the early paper by Makarov and Bar'yakhtar /1/, a study of the superconducting transition temperature (T_c) of alloys under pressure makes it possible to determine singular points (ε_c) in the electron spectrum of a metal. These singular points are indicated by an extremum in $\partial T_c/\partial$(P, C at.%).

It is known that the Fermi energy (ε_F) variation of the metal under the action of impurities and pressure can cause the electron transition if ε_F reaches the ε_c value. At the transition point the density of electron states has the singularity $\delta\nu(\varepsilon)\sim(\varepsilon_F-\varepsilon_c)^{1/2}$. This singularity shows up as a nonlinearity in kinetic and thermodynamic characteristics of a metal or alloy, while $\partial T_c/\partial$(P,C %) and the thermopower $\propto$(P,C %), being proportional to the derivative $\partial\nu(\varepsilon)/\partial\varepsilon(\varepsilon)$, give extreme points.

Transition metals and alloys with a complex electronic structure are known to have some peculiar physical properties, e.g., the alloys of some transition metals have high T_c values. To elucidate the nature of these high transition temperatures, it is of importance to study the singularities of the electron spectrum of transition metal alloys. One of these alloys is Mo-Re, which has a wide range of the solid solution with the bcc lattice (up to $\sim$ 30 at. %). The Mo lattice constant changes insignificantly with the addition of Re.

We have investigated T_c(C at.%) and $\partial T_c/\partial$P(C %) in alloys of Mo-Re, Mo-Re-Nb. The results obtained are illustrated in the figure. The Re addition has been found to cause the growth of T_c from 0.9 K for pure Mo up to $\sim$ 10 K for Mo-Re 26 at.% (see the figure). The derivative $\partial T_c/\partial$P(C %) has an extremum for $\sim$ 11 at.% Re, this corresponding to Ne = 6.11 outer electrons/atom (curve 1). The anomaly observed in $\partial T_c/\partial$P(C %) correlates with a nonlinear growth of T_c(C %) and of the electron specific heat /2/, with the anomalous thermopower /3/, etc. for the same Re concentrations.

The singularities observed can be related to the appearance of new electron groups of the Fermi surface as soon as the Fermi

energy reaches $\mathcal{E}_c$. According to the available theoretical calculations of the electron spectrum for Mo, at an energy ~ 0.2 eV above $\mathcal{E}_F$ there is a critical point $\mathcal{E}_c$ in the NH direction of the Brillouin zone. The addition of Re causes the $\mathcal{E}_F$ increase and at ~ 10-11 at.% Re the Fermi energy reaches the value corresponding to the bottom of a new zone, which results in the electron transition. It follows from the experiments that $\mathcal{E}_F - \mathcal{E}_c$ amounts up to ~ 0.15 eV /3/.

The investigation of ternary Mo-Re-Nb alloys based on the alloys of Mo-Re with a variable Nb content has indicated the relation between the high T_c values of Mo-Re and the electron transition.

We have investigated the ternary alloys using the alloys of Mo-Re ~ 17 at.% and Mo-Re ~ 27 at.% as a base. In the Mo-Re alloys with impurities exceeding ~ 10 at.% the Fermi energy is above the critical one ($\mathcal{E}_c$), at which a new electron group can arise. The addition of Nb to such alloys reduces $\mathcal{E}_F$ and leads to the disappearance of the new electron groups of the Fermi surface. This corresponds to the extremum in $\partial T_c/\partial P$(C at.% Nb) in the Mo-Re-Nb systems for Ne ~ 6.1 outer el./at. (this electron concentration corresponds to Mo-Re ~ 17 at.%-Nb 7 at.%, curve 2). The superconducting transition temperature in the Mo-Re-Nb alloys nonlinearly decreases as Nb is added, closely following the T_c(C at.%) variation for Mo-Re in the backward direction (lower curve, clear points). This correlation of the T_c(C at.%) variation with the extremums in $\partial T_c/\partial P$(C %) of the Mo-Re, Mo-Re-Nb alloys gives an experimental evidence of the connection between changes in T_c and the electron transitions. It is of interest to note that the extremum in the alloys of Mo-Re, Mo-Re-Nb occurs for one and the same concentration but different residual resistivities. At the extreme point of $\partial T_c/\partial P$(Ne outer el./at.) the residual resistivity was found to be $\rho_1 = 0.39$ for Mo-Re and $\rho_2 = 0.88$ for Mo-Re-Nb ($\rho = R_{4.2K}/R_{300K} - R_{4.2K}$). This enables one to estimate the effect of the processes of scattering on the electron-topological transition. The amplitude of the anomaly in Mo-Re-Nb decreases by a factor of ~ 1.4, which is due to the decrease of the quasi-particle lifetime $\tau \sim 1/\Gamma$ in scattering by impurities. The results presented above show that the ratio of the anomaly amplitudes of binary alloys to those of ternary alloys varies as $\sim \sqrt{\frac{\rho_2}{\rho_1}} \sim \sqrt{\frac{\Gamma_2}{\Gamma_1}}$. This indicates that the scattering processes in the electron-topological transition manifest themselves similarly both in the superconducting and normal characteristics of the alloys.

References

1. Makarov V.I., Bar'yakhtar V.G. On temperature anomalies of the superconducting transition under pressure. - Zh.Ehksp. Teor.Fiz.1968, v.8, p.1717-1722.
2. Morin F.J. and Maita J.P. Specific heats of transition metal superconductors. - Phys. Rev. 1963, v.129, p.1115-1120.
3. Velikodnyj A.N., Zavaritskij N.V., Ignat'eva T.A. Yurgens A.A. Thermopower and electron topological transition in the $Mo_{1-x}Re_x$ system. -Zh. Ehksp. Teor. Fiz. Pis'ma 1986, v.43, p.397-399.

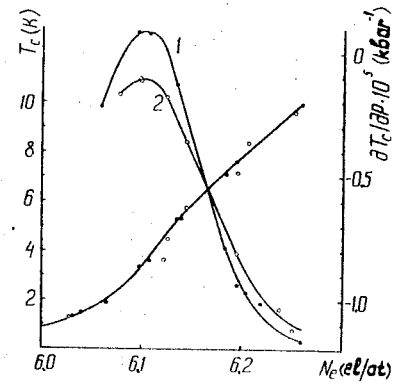

Temperature of the superconducting transition (T_c) versus the number of outer electrons (Ne el./at.) ● - Mo-Re; ○ - Mo-Re-Nb.
Pressure derivative of the superconducting transition temperatures ($\partial T_c/\partial P$) versus the number of outer electrons (Ne el./at.) Curve 1 - Mo-Re; curve 2 - Mo-Re-Nb.

NITROGEN AT VERY HIGH PRESSURE

W.J.Nellis
Lawrence Livermore National Laboratory, P.O. Box 808,
Livermore, California 94550, USA

Abstract

High-pressure results for nitrogen are reviewed and discussed in terms of phenomena that occur at extreme conditions.

I. Shocked Molecular Phase

Nitrogen is one of the most thoroughly investigated materials at high pressure because of its importance to condensed matter physics, planetary science, and chemical explosives.

Equation-of-state data have been measured in the molecular fluid phase by the shock compression of liquid nitrogen /I-4/. The molecular range extends up to about 30 GPa on the principal Hugoniot shown in Fig.I. These pressure-volume data and data for other small molecules were successfully explained by a theory which scales the spherically-symmetric exponential-six pair potential of Ar by critical-point parameters, assumes rotational degrees of freedom are fully excited, and assumes that molecular vibrational levels are equally spaced in energy, as in the gas phase, and populated according to a Maxwell-Boltzmann distribution /5/. This theory calculates a pressure-volume (P-V) curve in excellent agreement with the shock data up to about 30 GPa and 7000 K /5/ and provides evidence that the N_2 molecule persists to these extreme conditions. The excellent agreement also means that molecular vibrational equilibrium is achieved in a time of $\sim$ I ns, the time resolution of the shock velocity measurement of the equation-of-state experiments. If vibrational equilibrium were not achieved on an ns time scale, then relatively more internal shock-compression energy would be distributed into thermal energy and the measured shock-compression P-V curve would be stiffer than observed /5/. The relaxation time for energy transfer from translational to vibrational degrees of freedom was calculated recently to be $\sim$ 0.5 ns for fluid N_2 at conditions comparable to 30 GPa shock pressure /6/. The scaled theory /5/ also calculates shock temperatures in good agreement with experimental data /7,8/. Recent pulsed coherent anti-stokes Raman scattering (CARS) spectra for liquid N_2 single-shocked up to I6 GPa and double-shocked up

to 34 GPa show that the spacings between vibrational levels of N_2 are constant within the uncertainties of the experimental data, close to gas-phase values and that excited vibrational states are populated in $\leq$ 50 ns, an upper-bound on the vibrational equilibration time consistent with the ns discussed above /9/.

2. Shock-Induced Dissociation

Nitrogen undergoes a continuous, dissociative phase transition in the fluid state above 30 GPa, 2 g/cm^3, and 7000 K, based on several experimental observations. The comparison of the shock-compression curves for liquid N_2, isoelectronic CO, and theory for the molecular fluid phase of each suggested dissociation as the mechanism causing deviations from the molecular-phase Hugoniot of N_2 above 30 GPa /I0/. Dissociation is a logical phenomena by which dense molecular nitrogen could respond to high density and temperature. By taking the radial positions of the zeros in the repulsive pair potentials for the N_2 - N_2 /5/ and N - N /II/ interactions as an estimate of the effective hard-sphere diameters in the dense fluid, a significant volume decrease is obtained for two N atoms relative one N_2 molecule. The densites at which the phase transition is observed are close to where theory suggests that monatomic solid nitrogen might be metastable at 0 K /I2/. High temperatures can drive this transition to the monatomic state in the shock experiments.

Double-shock equation-of-state data lie above the principal Hugoniot /I0/ and show that $(\partial E/\partial P)_V < 0$ in the phase transition region. These data are shown as the symbols with error bars in Fig.I. The average Grüneisen parameter $\gamma = V(\partial P/\partial E)_V$, calculated using the principal Hugoniot and the double-shock equation-of-state data, is plotted vs molar volume in Fig.2. The negative γ's are indicative of a phase transition, which occurs in a relatively narrow range of volume near II cm^3/mol (V_o=35 cm^3/mol).

The fact that $(\partial E/\partial P)_V < 0$ predicted that $(\partial T/\partial P)_V < 0$ /I0/. Double-shock temperature experiments verified this prediction, provided evidence for crossing isotherms, and most remarkably showed shock-induced cooling, as illustrated in Fig.3 /8/. Shock-induced cooling indicates that so much internal energy is absorbed in the phase transition at the higher pressure and density of the double-shock state that the temperature of the double-shock state is actually lower than that of the first-shock state.

The electrical conductivity, plotted in Fig.4, rises rapidly with pressure between I9 and 27 GPa (4000-7000 K) and increases

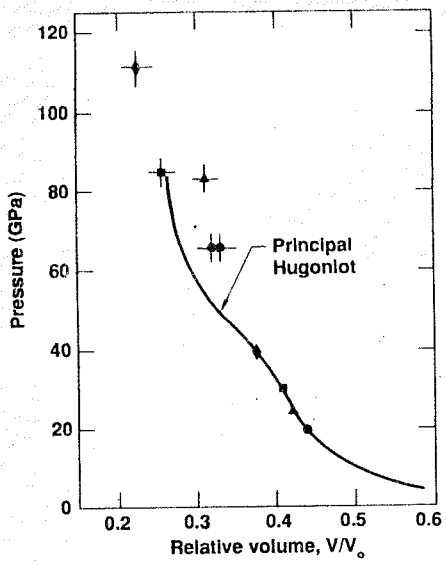

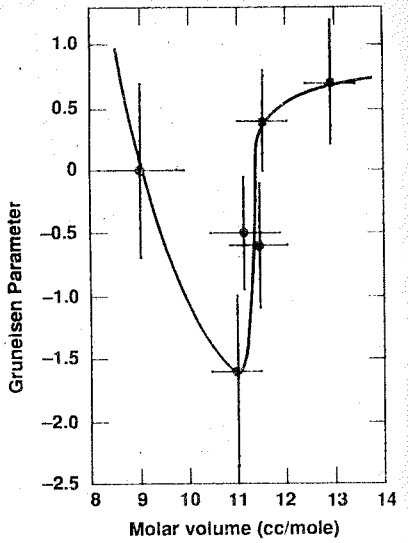

Fig.I. Principal Hugoniot (solid curve) and double-shock points for liquid nitrogen initially at 77 K. Symbols without error bars are first-shock states and corresponding symbols with error bars are second-shock states (Reference I0).

Fig.2. Average Grüneisen parameters for nitrogen calculated from Hugoniot of Reference I0 and double-shock data of Reference I0 (solid circles) and Reference 4 (solid squares) vs molar volume (V_o=35 cc/mole).

more slowly between 34 and 6I GPa (8000-I2000 K) /8/. Electrons are probably the dominant carriers by virtue of their high mobility relative to ions. The high densities and temperatures suggest that electron scattering probably occurs with a mean-free path of the order of a molecular diameter over the entire range of the data. Above 30 GPa, where substantial amounts of dissociation occurs, electrons are probably ionized primarily from N atoms. The excited electronic states of the N atom are at significantly lower energies than for the N_2 molecule. At the high densities achieved, these levels would be expected to broaden into bands with the monatomic states lower than the diatomic ones. The calculated fraction of dissociated N_2 molecules /8/ is also plotted vs pressure in Fig.4 and shows that the electrical conductivity is approximately proportional to the concentration of N

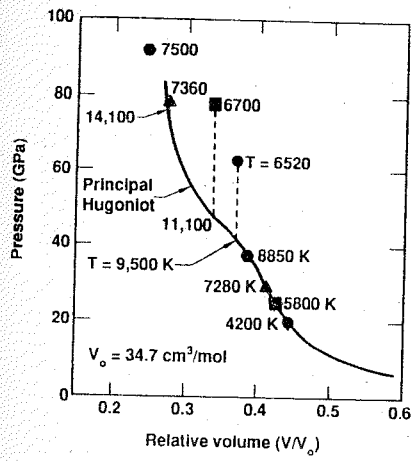

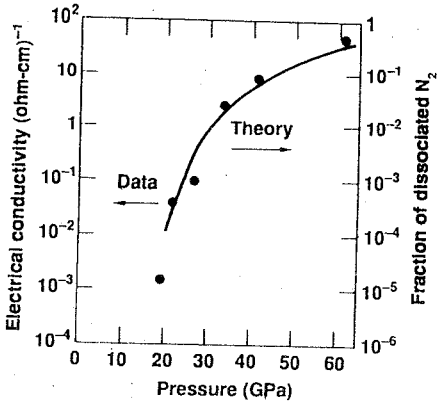

Fig.3. Principal Hugoniot is solid curve. Each pair of identical symbols corresponds to single- and double-shock temperatures measured in same experiment. This figure shows $(\partial T/\partial P)_V < 0$ in phase transition region, shock-induced cooling (hexagons), and crossing isotherms at 80 GPa (Reference 8).

Fig.4. Electrical conductivity and calculated dissociated fraction of N_2 vs shock pressure (Reference 8).

atoms, which is consistent with the picture that the conductivity is dominated by electrons ionized from dissociated N atoms.

Effective dissociation energies and rates in dense fluid N_2 have recently been estimated /8,I3/. These results show that the effective dissociation energy decreases with increasing pressure and density and that the order of magnitude of the reaction time for dissociation decreases with pressure, approaching the time resolution of the shock experiments and reaching a few percent at the pressures where the effects of dissociation are observed in the experimental data.

3. N_2 at High Static Pressure

The observation of a phase transition above 30 GPa in shocked liquid nitrogen led to a theoretical prediction that at 0 K solid N_2 might transform to a monatomic phase at pressures possibly below I00 GPa /I4/. Static high-pressure Raman-scattering experiments at 300 K in a diamond anvil cell up to I30 GPa showed that solid N_2 retains its diatomic nature up to this pressure, al-

though three transitions to new structures are observed /I5/. The fact that N_2 dissociation occurs in the dynamic experiments and not in the static ones shows that higher shock temperatures drive this transition.

The melting curve of N_2 has been measured to I8 GPa and 900 K in a diamond anvil cell /I6/. The lowest shock temperature measurement of 2000 K at I0.6 GPa /7/ is well above the melting temperature of 600 K at this pressure, showing that the shock compression data for liquid nitrogen are well into the fluid phase.

Acknowledgements

Work performed under the auspices of the U.S. Department of Energy by the Lawrence Livermore National Laboratory under contract number W-7405-ENG-48, with partial support from the U.S.National Aeronautics and Space Agency under contract PR I0-39083.

References

I. V.N.Zubarev and G.S.Telegin, "The impact compressibility of liquid nitrogen and solid carbon monoxide", Dokl.Akad.Nauk SSSR I42 (I962) 309 /Sov.Phys.Dokl. 7 (I962) 34/.
2. R.D.Dick, "Shock wave compression of benzene, carbon disulfide, carbon tetrachloride, and liquid nitrogen", J.Chem.Phys. 52 (I970) 602I.
3. W.J.Nellis and A.C.Mitchell, "Shock compression of liquid argon, nitrogen, and oxygen to 90 GPa", J.Chem.Phys. 73 (I980) 6I37.
4. G.L.Schott, M.S.Shaw, and J.D.Johnson, "Shocked states from initially liquid oxygen-nitrogen systems", J.Chem.Phys. 82 (I985) 4264.
5. M.Ross and F.H.Ree, "Repulsive forces of simple molecules and mixtures at high density and temperature", J.Chem.Phys. 73 (I980) 6I46.
6. B.L.Holian, "Simulations of vibrational relaxation in dense molecular fluids", J.Chem.Phys. 84 (I986) 3I38.
7. M.Voskoboinikov, M.F.Gogulya, and Yu.A.Dolgoborodov, "Temperatures of shock compression of liquid nitrogen and argon", Dokl.Akad.Nauk SSSR 246 (I979) 579 /Sov.Phys.Dokl. 24 (I979) 375/.
8. H.B.Radousky, W.J.Nellis, M.Ross, D.C.Hamilton, and A.C.Mitchell, "Molecular Dissociation and shock-induced cooling in fluid nitrogen at high densities and temperatures", Phys.Rev. Lett. 57 (I986) 24I9.
9. S.C.Schmidt, D.S.Moore, and M.S.Shaw, "Vibrational spectroscopy of fluid N_2 up to 34 GPa and 4400 K," Phys.Rev. B 35 (I987) 493.
I0. W.J.Nellis, N.C.Holmes, A.C.Mitchell, and M.van Thiel, "Phase transition in fluid nitrogen at high densities and temperatures", "Phys.Rev.Lett. 53 (I984) I66I.
II. F.H.Ree, D.F.Calef, M.van Thiel, and D.C.Hamilton, "High-pressure high-temperature phase changes in chemically reactive mixtures", these proceedings.

I2. M.Ross and A.K.McMahan, The metallization of some simple systems, in: Physics of Solids under High Pressure, eds.J.S. Schilling and R.N.Shelton (North-Holland, Amsterdam, I98I) pp.I6I-I68.
I3. D.F.Calef and F.H.Ree, "An estimate of the barrier to and rate of dissociation of dense nitrogen under shock conditions", Phys.Rev.B (in press).
I4. A.K.McMahan and R.LeSar, "Pressure dissociation of solid nitrogen under I Mbar", Phys.Rev.Lett. 54 (I985) I929.
I5. R.Reichlin, D.Schiferl, S.Martin, C.Vanderborgh, and R.L.Mills, "Optical studies of nitrogen to I30 GPa", Phys.Rev. Lett. 55 (I985) I464.
I6. D.A.Young, C-S.Zha, R.Boehler, J.Yen, M.Nicol, A.S.Zinn, D. Schiferl, S.Kinkead, R.C.Hanson, and D.A.Pinnick, "Diatomic melting curves to very high pressure", Phys.Rev.B 35 (I987) 5353.

STUDIES ON THE ELECTRON STRUCTURE RECONSTRUCTION IN INTENSE SHOCK WAVES

E.N.Avrorin, B.K.Vodolaga, V.A.Simonenko
Chelyabinsk State University, Chelyabinsk, USSR

Shock-wave studies have made it possible to obtain data on the compressibility of more than 200 materials at standard conditions, in solid, liquid and gaseous states, including about 50 metals /I,2/. It has been found that the functions of atomic volumes of elementary substances versus the atomic number have a periodic forms. This periodicity is related with the electron shell structure of atoms. A flattening of curves versus a pressure increase and a growth of compressibility of substances with large atomic volumes are observed. This phenomenon is related with the reconstruction of the electron structure: the atoms are drawing together under compression and the energy exchange is increasing. It leads to broadening and overlapping of electron energy levels. The pressure range up to several megabars has been studied in detail under laboratory conditions. At these pressures electron structure changes of substances having an inverse population may take place. Transitions of outer S-electrons onto vacant D-levels are the most prevailing ones under compression. Closed internal configurations characterized by an essentially lower compressibility appear. The treatment of shock-wave experiments results has shown the inflections of shock adiabats at pressures of some hundred kilobars in some cases /I/, which was related with the completion of above-mentioned transitions. There are contradictions in this interpretation of measurement results. So most of metals of the fourth group are characterized by the most closely packed atoms structures and therefore it is impossible to explain a sharp reduction of the compressibility with respect to transition to the close-packed phases; we have failed to find the hypothesis-predicted bend on the shock-wave adiabat of kalium. Furthermore most of inflections have not been confirmed by later experimental researches /3/. According to /3/ the inflections of three materials are expressed considerably weaker and not at the same values of particle velocity as compared with /I/. In the procedure of the treatment of experimental results /I/ there is inconsistency which is typical for many early researches. In our opinion this inconsistency has led to an appearance of the shock adiabat inflactions for some substances. We shall explain the abovesaid in detail now.

Experiments on measuring the material compressibility by shock waves are based on relations that bind kinematic parameters shock velocity D and particle velocity behind its front U - with thermodynamic values (density, pressure and internal energy). Simultaneous measuring of D and U in the experiments makes it possible to determine thermodynamic values without using model considerations. So the shock-wave adiabats of comparatively few number of substances have been studied. Such adiabats of Al and Fe have been studied in more details than that of other materials by the Soviet researchers.

In widespread experiments shock velocities in both contacting materials are measured. One of the materials of the pair is a material studied during experiments with simultaneous measuring D and U (the reference). The traditional treatment of experiments in contacting materials is carried out by means of P-U diagrams method (see, for example, /4/) and requires using model considerations; for the consequent treatment we must know not only the shock-wave adiabat of one-stage compression but also isentropes or shock-wave adiabats of two-stage compression of the reference material. Available experimental techniques ensure a high accuracy in measurements of only the shock-wave adiabat of one-stage compression. Other characteristics can be obtained with the help of model considerations the validity and the applicability of which it is necessary to verify. The situation is essentially simplified only in the low pressure range where the shock-wave adiabats and the isentropes are weakly different from the cold compression curve and the appropriate transitions from one dependence to the other are weakly sensible to the model choice. In this case it is sufficient to know the shock-wave adiabat of one-stage compression of the reference material. Over the high pressure range the discrepariciés between above-said curves increase and the appropriate substitutions lead to appreciable error in determining a mass velocity of a sample. And the mass velocity obtained by plotting curves with a reflected shock-wave adiabat is less than the true one.

The treatment of experiments using a reflected shock-wave adiabat is widely used, in particular the authors /I/ used it.

The following regularity attracts our attention: experimental data on metals with the inflection on the shock-wave adiabat are obtained in the low pressure range mainly concerning aluminium while in the high pressure range concerning ferrum. In cases when we used one reference material over the whole range of stu-

died pressures (kalium was among these metals) the inflection has not been observed on the dependence curves. One should not exclude the possibility of the fact that the inflections in /I/ were due to the application of the reflected shock-wave adiabats at the treatment and possible inconsistencies in the used shock--wave adiabats of aluminium and ferrum. The results of our treatment have confirmed this assumption. The shock-wave adiabats of metals in D-U-coordinates have a rather complex form and, only in a rather limited pressure range can be approximated by means of linear and quadratic expressions with high accuracy. According to /I/ metals having inflections on the shock-wave adiabats in form of D-U dependences are not distinguished among others.We associate the shading and the flattening of electron transition, which take place in this pressure range, with the effect of a high (some electron-volts) temperature accompaning the shock-wave compression that leads to a strong smearing of energetic zones. This gives rise to a marked broadening of the pressure range in which the electron structure reconstruction takes place. Therefore such reconstructions on shock-wave adiabats are expressed far weaker than on curves of the cold compression.

At the further increase of the shock-wave amplitude the electron structure reconstructions are due to the thermal ionization process. Up to the present this pressure range has not been studied experimentally and the effect of these reconstructions on thermodynamic parameters was studied by using various theoretical models. Statistical models are not valid for this investigation because they use the model of continuous electronic states. Calculations on models taking the shell electron structure into account give the wavy or even the step-wise form of curves in the behaviors of thermodynamic values, the oscillation position and amplitude of various models differ strongly. It was impossible to exclude the presence of such areas in the region of thermodynamic variables where $(\partial^2 P/\partial V^2)_S \leq 0$ which, as it is known, is the cause of the anomalous behavior of materials during dynamic processes: rarefaction takes place in a shock-wave regime while the compression is accomplished smoothly (see, for example, /4/). The necessity of calibrating up-to-date theoretical models of a substance, the determination of the oscillation values, the verification of the fulfilment of a condition of the thermodynamic stability made the problem of obtaining experimental data in the pressure range of about I00 Mbars urgent.

The elimination of uncertainties in the region of the discrepancy results of various theories claims to the accuracy of experimental data, in particular wave velocities should be measured with an error not more than 0.5-I.0%. As applied to porous sample studies these claims do not change as it was found in the calculations with changing a porosity coefficient in the range I-50.

Experimental studies in the wide pressure range have been carried out with the necessary accuracy in /5/ for aluminium and lead. These measurements have produced the first and reliable confirmation of a manifestation of shell effects on the shock-wave adiabats of metals. The value of the oscillation amplitude and its decreasing versus the atomic number growth agree well with predictions according to the model of a self-consistent field (SCF) /6/ in which widths of energetic zones responsible for the thermodynamics are calculated in a quasi-zone approximation, which is fairly close to the assumption accepted in statistical models on smearing the electronic shells. If we also take the prediction of SCF for the oscillation amplitudes of other thermodynamic parameters the condition of the thermodynamic stability as calculations have indicated, is valid over the entire region necessary for applications.

References

I. Al'tshuler L.V., Bakanova A.A., Dudoladov I.F. et al. Shock--Wave Adiabats of Metals. New Data, Statistical Analysis and General Regularities. - AMTP, I98I, N 2, p.3-2I.

2. Trunin R.F. Compressibility of Various Materials at High Pressures of Shock Waves. - Physics of the Earth, I986, N 2, p.26-43.

3. Gust W.H., Royce E.B. New Electronic Interactions in Rare-Earth Metals at High Pressure. - Phys.Rev.B., I973, v.8, N 8, p.3595-3609.

4. Zel'dovich Ya.B., Raiser Yu.P. Physics of Shock Waves and of High Temperature Hydrodynamic Phenomena. Moscow, Science, I966, 688.

5. Avrorin E.N., Vodolaga B.K., Voloshin N.P. et al. Experimental Confirmation of Shell Effects on the Shock Adiabats of Aluminium and Lead. - Pis'ma Zh.Eksp.Teor.Fiz. I985, v.43, N5, p.24I-244.

6. Sin'ko G.V. Calculation of Thermodynamic Function of Elementary Substances on the Basis of Equations of a Self-Consistent Field- From Numerical Methods of Mechanics of Continuous Medium, v.IO, N I, publ.ITAM, S.D.A.S. Novosibirsk, I979, p.I24-I36.

EQUATIONS OF STATE AND ELECTRON STRUCTURE OF COMPRESSED METALS

L.V.Al'tshuler[I], S.E.Brusnikin[2]
[I]VNIIOFI, Moscow, USSR, [2]NEE PFP, Minsk, USSR

At present time in various dynamical and statical investigations large informations are collected, it gives priority for thermodynamical model and bounds for quantum-statistical descriptions of elements with metallic properties.

Main equations of states components are potentials of atom interaction at zero absolute temperature, which are determined by their electron structure. Shell-structure effects are demonstrated in periodical variations of density and compressibility with atomic number at normal conditions, but for some elements it gives nonmonotonic static and dynamic compression curves. Such effects were discovered for elements of the 3d-5th periods, and were systematized by /I/. This elements are disposed on falling branches of atomic curve and have specific configuration of shock Hugoniot adiabats (Fig.I), which lag on two linear lines with different derivatives in D-u variables /D,u - wave and mass velocities of shock wave/. For alkaline-earth metals large compressibility at the beginning of adiabats and nonmonotonic increasing of elastisity is explained by transition outer-shell s-electron on empty d-levels and formation of noncompression electron configurations.

Information about the nature of more complicated electron reconstructions for rare-earth metals /REM/ are received from quantum-mechanical calculations /2,3/ of energetic spectra and electron distributions on s,p,d,f-harmonics. Two-fold compression of Pr increases d-electron number from I.33 to 2.I8, i.e. to /s,p/-d transition, but for light REM it gives /s,p/-d transition, which increases electron numbers in f-states for Ne from 2.II to 3.6 and for La - from 0.I5 to 0.63. Delocalization of f-electrons, which gives phase transition, is found for static compression of Pr /4/.

In a wide range of density variation "cold" components of equations of state are received for 25 elements with smooth shock adiabats. Traditionally shock pressures are devided on heat and "cold" components according to dynamic experimental curves,

which were found on strict hypothesis about Grüneisen functions.

New approach /5/ is a search for equation of normal isentropes, which are close to zero isotherms, from coefficients $D(u)=a_0 + a_I u$ or $D(u)=a_0 + a_I u + a_2 u^2$. This coefficients determine isentropic moduli of volumetric compression $\varkappa_{os} = \rho_0 a_0^2$ and its derivatives $\varkappa_{Is} = 4a_I - I$ for normal states. Such isentropic compression curves in Born-Mayer form after introducing small Debye corrections fixed site of zero-degree and normal isotherm until two-, three-fold compression. Relative situation curves $p_x(\rho)$ and Hugoniot adiabats $p_h(\rho)$ are determined heat components EOS, which are anomalously large /5/ for transition metals.

Constructed in this paper equations of states for 7 metals /Pb, Cu, Cd, W, Be, Fe, Mo/ adequately describing absolute and relative measurements of compression are received by interpolational connection of regional EOS, which are true at temperatures $T \lesssim 5$ev and $T \gtrsim I0$ev. Regional EOS are distinguished by it's heat electron components, but have identical zero-degree isotherms, received by approximation of experimental and quantum-statistical compression curves, and same components, represented free energy of heat nuclear motion in form /7/.

At "low temperature" EOS electron members /8/ parameters are found from experimental values, in high temperature EOS are taken from quantum-statistical calculations. Values for 5 metals are taken from TFP model /6/, it's for Fe, Mo from Thomas-Fermi model because of high heat components for transition metals. In Figs.2 and 3 solid lines are shock adiabats, calculated in accordance with regional models, another lines are calculations on quantum-mechanical models "SSP" /9/ and MXFS /I0/ and are results of relative measurements at TPa pressures.

Good coincidence of calculations with experiments confirms the adequacy of description of thermodynamics of metals by quantum-statistical models with "corrected" semiempirical curves of cold compression. But quantum-mechanical calculations according to MXFS theory contradict the compression results on metals /Fig.2/ and according to CCP theory contradict the site shock adiabats for Cu and Cd /Fig.3/.

For Al laboratory determinations of dynamic compression /Fig.I/ fix with high precision /I,5/ the low monotonic part of shock adiabat. Under pressures of about I.8MBar, as it's shown by experiments /II/, /I5/, the metal undergoes predicted /I6/ interrupted increase in dynamic compression "because of the existence

of the range of negative electron Grüneisen coefficients and bend in cold compression curve."

The whole experiment of aluminum gigabaric range /Fig.4/ is satisfactorily described by semiempirical model "SSP" and by statistical adiabat suggested in /I8/ which implicitly takes into account the zero isotherm original configuration.

References

I. Al'tshuler L.V., Bakanova A.A., Dudoladov I.P., Dienin E.A., Trunin R.F., Chekin B.C. Shock Hugoniot adiabats. New data, statistical analysis and total relationships. PMTF, I98I, N 2, p.3-34.

2. Al'tshuler L.V., Voropinov A.I., Gandel'man G.M. et al. Particular structure of electronic spectra for rare metals at high pressures. FMM, v.5I, N 5I, p.76-80.

3. McMahan A.K., Skriver H.L., Johansson B. The s-d transition in compressed lanthanum. Phys. Rev. B, v.23, N IO, p.50I6-5029.

4. Mao H.K., Hazen R.M., Bell P.M. Evidence for 4f-shell delocalization in praseodymium under pressure. J. Appl. Phys., I98I, v.52, N 7, p.4572-4574.

5. Al'tshuler L.V., Brusnikin S.E., Kuz'menkov E.A. Zero-degree isotherm and Grüneisen parameters for 25 metals. PMTF, I987, N I, p.4-30.

6. Kalitkin N.N., Kuz'mina L.V. Tables of thermodynamical properties of substances at high energies. Preprint IPM AS USSR, I975, N 35.

7. Kormer S.B., Funticov A.I., Urlin V.D. et al. Dynamical compression of metals and equation of state with changing heat at high temperatures. JETF, I962, N 3, p.686-702.

8. Sapozhnikov A.T., Pershina A.V. Equation of state of metals for wide-range densities and temperatures. VANT, I979,N4, p.47-56.

9. Sin'ko G.V. Some results of calculations of thermodynamical functions for aluminum, iron, copper, cadmium and lead. CMMSS, I98I, v.I2, N I, p.I2I-I30.

IO. Novikov V.G. Shock compression of litium, aluminum and iron in model MXFC. Preprint IPM AS USSR, I985, N I33.

II. Al'tshuler L.V., Kalitkin N.N., Kuz'mina L.V., Chekin B.C. Shock Hugoniot adiabats at high pressures. JETF, I977, v.72, N I, p.3I7-324.

I2. Trunin R.F. Compression of some materials at high pressures. JETF, I977, v.72, N I, p.26-43.

I3. Ragan Ch.E. III, Silbert M.G., Diven B.C. Shock compression of molybdenum to 2 TPa by means of the nuclear explosion. J. Appl. Phys., I977, v.48, p.2860-287I.

I4. Ragan Ch.E. III, Shock-wave experiments at three-fold compression. Phys. Rev. A., I984, v.29, N 3, p.I39I-I402.

I5. Bushman A.V., Prochorov A.M., Ternovoi B.I., Fortov V.E. et al. Dynamical compression and thermodynamics of density of plasma of aluminum for megabars pressures. Pis'ma JETF,I985, v.39, N 8, p.34I-343.

I6. Simonenko V.A., Boloshin N.P., Vladimirov A.S. et al. Absolute measurements of shock compression of aluminum for pressures P≳I TPa. JETF, I985, v.88, N 4, p.I452-I459.

I7. Avrorin E.I., Vodolaga B.K., Voloshin B.K., Kuropatenko V.F., Simonenko B.A. et al. Experimental confirmation of shell-structure effects in shock compression of aluminum and lead. JETF, I986, v.30, N I, p.I3II-I320.

I8. Voropinov A.I., Gandel'man G.M., Podval'ni V.G. Electron energetical spectra and equations of state of solids at high pressures and temperatures. UFN, I970, v.I00, N 2, p.I93-224.

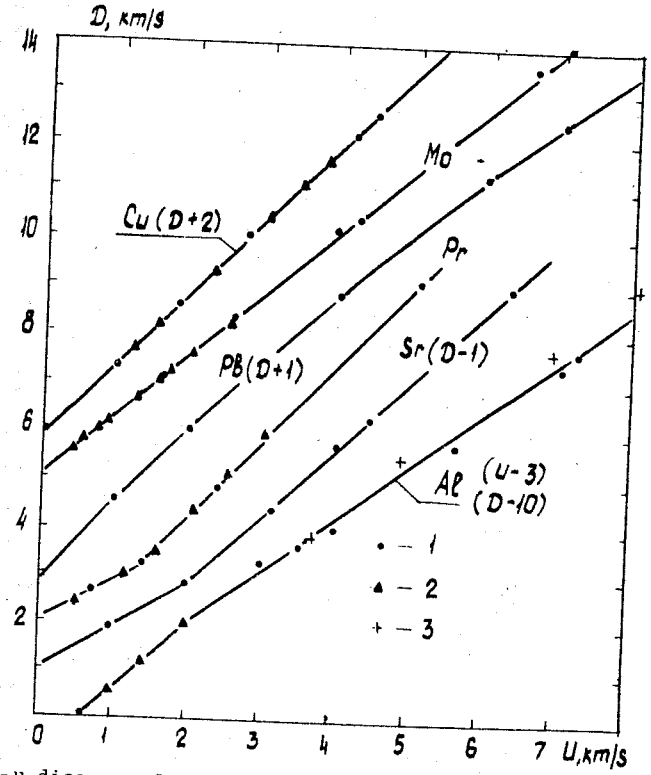

Fig.I. D-u diagrams for elements with smooth (Cu, Mo, Pb) and nonmonotonic (Sr, Pr, Al) Hugoniot adiabats:
I,2 - absolute measurements of Soviet /I/ and foreign /2/ authors; 3 - data from /I5/ for Al.

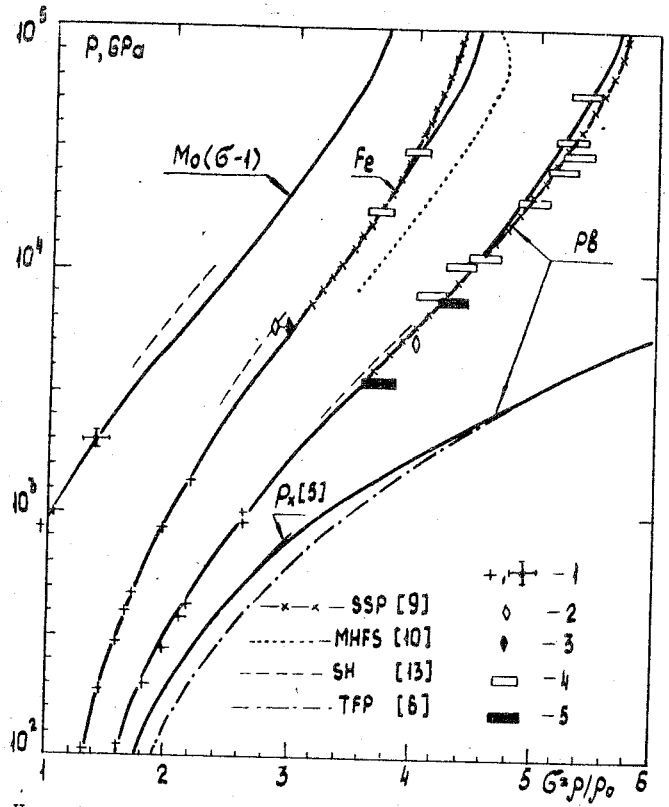

Fig.2. Hugoniot adiabats for Pb, Mo, Fe:
I - absolute measurements /I/, /II/, /I2/; 2 - relative measurements /I3/; 3 - the same but processed by the authors; 4,5 - relative measurements /I4/, /I5/ and /II/.

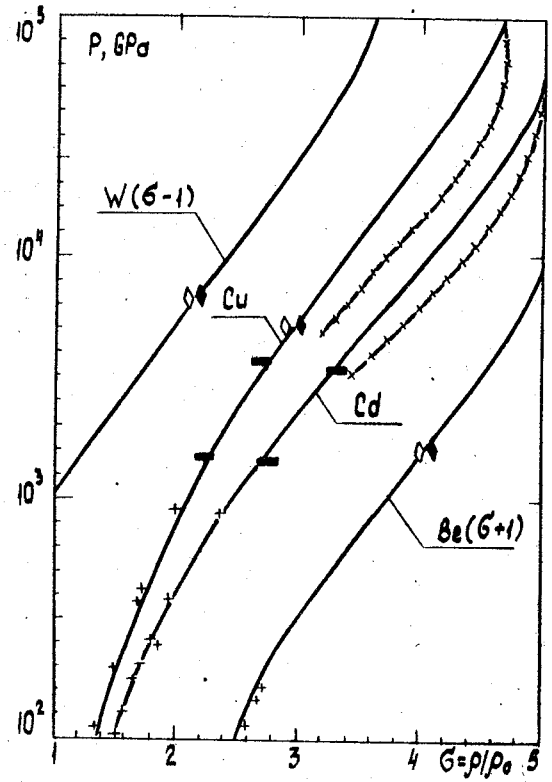

Fig.3. Hugoniot adiabats for W, Cu, Cd and Be. Designation from Fig.2.

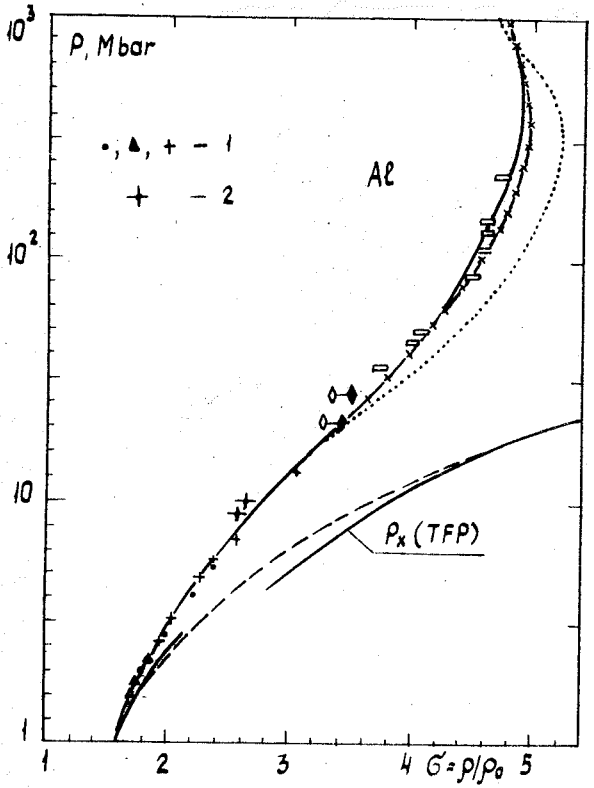

Fig.4. Hugoniot adiabats for Al:
I - absolute measurements of Soviet /I/, /II/, /I5/ and foreign authors; 2 - data from /I7/. The remaining designation from Fig.2.

THE WIDE-RANGE EQUATION OF STATE

G.V.Shpatakovskaya[I], E.A.Kuz'menkov[2]

[I]The Keldysh Institute of Applied Mathematics, USSR Academy of Sciences, Moscow, USSR

[2]All-Union Research Institute of Optical and Physical Measurements, Moscow, USSR

A quasiclassical simple model (QM) of equation of state is proposed for an electron component of the matter /I-3/. The QM is valid over a wide range of densities and temperatures, connecting the regions of the traditional employment of Saha-model and statistical Thomas-Fermi (TF) model with exchanges and quantum corrections (TFK or TFC /4/). The QM describes from the first principles typical step behaviour of the ionization state and energy, as a result of succeeded ionization of the ion's shells with the temperature increase. Also QM naturally includes the effects of electron-ion interaction with the density increase.

The model treated is based on the Thomas-Fermi model. A role of quantum, exchange and shell effects is considered additively by the appropriate corrections. To incorporate the effects of shell structure in TF theory an analytical quantization condition /5/ was used. This condition has a true asymptotic behaviour: in the region of strong binding it transforms to Bohr-Zommerfeld condition, and in the region of weak binding it describes a band energy structure and a change to the continuous spectrum.

The quantum-exchanges terms are calculated as in the TFK-model /4,6/. The shell corrections to the pressure and to the internal energy we obtain from the general view for a correction to the free energy /6/ $\delta F_{shell}=-\int_{-\infty}^{\mu} d\mu' \delta N_{shell}(\mu')$. If a variation of the self-consistent field is assumed to be small $\delta U_{shell}=0$ one can have:

$$\delta P_{shell}=\rho(R)\,\delta\mu_{shell},\quad \delta\mu_{shell}=-\frac{\delta N_{shell}}{\int\frac{\partial\rho}{\partial\mu}d\vec{r}},$$

$$\delta E_{shell}=\left[\frac{3}{2}Z-\int\frac{\partial\rho}{\partial\mu}(\mu-U(\vec{r}))d\vec{r}\right]\delta\mu_{shell}$$

$$\delta N_{shell}=\frac{2}{\pi\delta\mu}\sum_{k=1}^{\infty}\left[\frac{2\pi k\frac{\partial\tilde{\pi}\lambda_{max}}{\partial\mu}T}{sh\left(2\pi k\frac{\partial\pi\lambda_{max}}{\partial\mu}T\right)}\cdot\frac{\cos 2\pi k\lambda_{max}}{k^2}-\right.$$

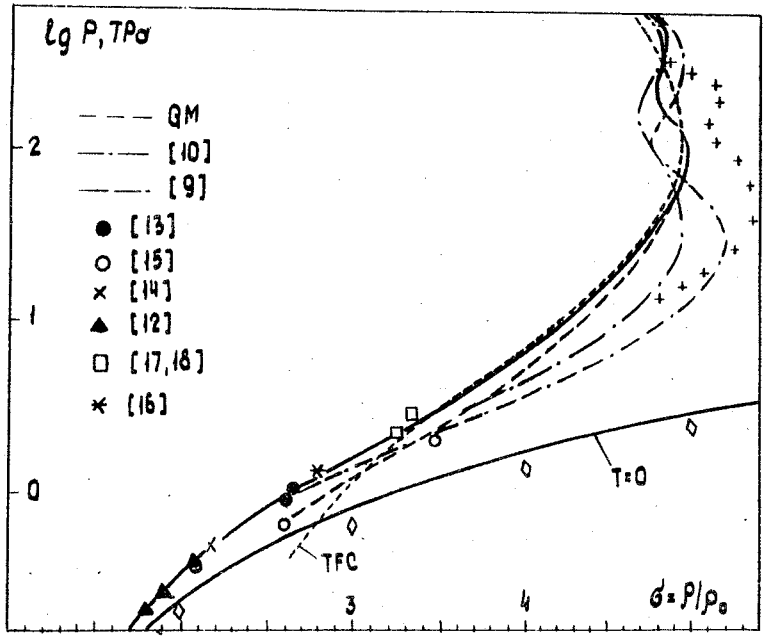

A theoretical and experimental shock Hugoniots for Al: —— QM with interpolated zero Kelvin isotherm; + - INFERNO of Liberman from /II/.

Zero Kelvin isotherms: —— interpolated one; ◊ - APW from /II/.

$$\left. - \frac{2\pi\kappa\tau_\mu T}{\mathrm{Sh}(2\pi\kappa\tau_\mu T)} \frac{\cos 2\kappa S_\mu}{\kappa^2} \right] I_\kappa(\varphi_\mu),$$

$$I_\kappa(\varphi) = \frac{(-1)^\kappa}{2}\left[P_\kappa(2\varphi^2-1) - P_{\kappa-1}(2\varphi^2-1)\right], \quad \varphi_\mu = \mathrm{tg}\left(\frac{\pi}{8} + \frac{1}{2}\mathrm{arctg}\left(\mathrm{th}\frac{\chi}{4}\frac{\mu}{\sqrt{\chi\rho(R)}}\right)\right),$$

P_k - the Legendre polynomial, S_μ and τ_μ - the classical action and time of the electron's motion with an energy equal to the TF chemical potential μ and zero orbital moment in the TF potential $U(r)$, λ_{max} - maximal orbital moment $l+\frac{1}{2}$ for the energy μ, $\delta_\mu = -\partial^2 S_{\mu\lambda}/\partial\lambda^2|_{\lambda=0}$. The function $I_k(\varphi_\mu)$ governs decay of the temperature shell oscillations: for nondegenerate plasma $\mu < 0$, $|\mu| \gg 1$, $\varphi_\mu \to 0$, $I_k^{\pm}(\varphi_\mu) \to 1$; for degenerate matter $\mu \gg 1$, $\varphi_\mu \to 1$, $I_k^{\pm}(\varphi_\mu) \to 0$.

Clearly the model outlined above, based on the TF-model, can not adequately describe the equation of state under the normal conditions because of the improper 0 K isotherms in the TF- and TFK-models. Therefore to expand the area of application of the model treated QM 0 K isotherm is replaced with a semi-empirical curve /7/, extrapolated to QM under the high densities.

For demonstration of QM-abilities Hugoniot curve of Al is shown in Figure, where the QM-curve is compared with the other theoretical models and the available experimental data. The semi-empirical 0 K isotherm is also given. In our calculations of Hugoniot curve nuclear motion term based on the one-component plasma theory according to the ref./8/.

References

1. Shpatakovskaya G.V. The shell effects in the thermodynamics of the nondegenerate plasma. Teplofiz.Vysok.Temp., 1985, v.23, No.1, pp.42
2. Kuz'menkov E.A., Shpatakovskaya G.V. Semi-consistent semi-classical thermodynamics of the nondegenerate plasma. Moscow, Inst.Appl.Mathem., the USSR Acad. of Sci., 1985. Preprint No.93.
3. Kuz'menkov E.A., Shpatakovskaya G.V. The extention of the semi-classical thermodynamics to the low-temperature plasma. Moscow, Inst.Appl.Mathem., the USSR Acad. of Sci., 1986, Preprint No.206.
4. Kalitkin N.N., Kuz'mina L.V. The tables of thermodynamic functions under the high concentration of energy. Moscow, Inst. Appl.Mathem., the USSR Acad. of Sci., 1975, Preprint No.35
5. Shpatakovskaya G.V. To semi-classical description of the electron spectrum structure in one- and three-dimensional crystal.

Moscow, Inst.Appl.Mathem., the USSR Acad. of Sci., 1985, Preprint No.28

6. Kirzhnits D.A., Lozovik Yu.E., Shpatakovskaya G.V. The statistical model of the matter. Usp.Fiz.Nauk,1975,v.117,No.1,p.3

7. Al'tshuler L.V., Brusnikin S.E., Kuz'menkov E.A. The isotherms and Grüneisen functions of 25 metals. Prikl. Mech. and Tehn. Fiz., 1987, No.1, p.134

8. Kopyshev V.P. To the nucleus thermodynamics of the one-atomic matter. Moscow, Inst.Appl.Mathem., the USSR Acad. of Sci., 1978, Preprint No.59.

9. Nikiforov A.F., Novikov V.G., Uvarov V.B. The Modified Hartree-Fock-Slater model for the matter under given temperature and density. Voprosy atom.nauki i tehniki, Ser. "Metodiki i programmy", 1979, No.4(6), p.16

10. Syn'ko G.V. Application of the semi-consistent field method for a calculation of thermodynamic electron functions in the simple substances. Teplofiz. Vysok. Temp., 1983, v.21, No.6

11. Young D.A., Wolford J.K., Rogers F.J., Holian K.S. Theory of aluminium shock equation of state to 10^4 Mbar. Phys.Lett., 1985, v.108A, No.3, pp.157-160

12. Bushman A.V., Krasyuk I.K., Pashinin P.P. et al. The dynamic compressibility and thermodynamics of the dense aluminium plasma under Mbar-pressure. Pis'ma Zh.Eksp.Teor.Fiz., 1984, v.39, No.8, p.341

13. Simomenko V.A., Voloshin N.P., Vladimirov A.S. et al. The absolute measurements of aluminium shock compressibility under pressure P~ 1 TPA. Zh.Eksp.Teor.Fiz., 1985, v.88, No.4, p.1452

14. Kormer S.B., Funtikov A.I., Urlin V.D., Kolesnikov A.N. The dynamic compression of porous metals and equation of state with a variable heat capacity under the high temperatures. Zh.Eksp.Teor.Fiz., 1962, v.42, No.3, p.686

15. Al'tshuler L.V., Chekin B.S. The metrology of the impulse pressure. In coll. reports I All-Union symp. on the impulse pressure. Moscow, VNIIFTRI, 1974

16. Nellis W.J. Shock waves in condensed matter. Amsterdam-New York-Tokyo, 1983, pp.81-84

17. Ragan C.E. III, Shock compression measurements at 1 to 7 TPA. Phys.Rev., 1982, v.25A, No.6, pp.3360-3375

18. Ragan C.E. III, Shock-wave experiments at three-fold compression. Phys.Rev., 1984, v.29A, No.6, p.1391

EQUATION OF STATE OF SOLID NEON FROM X-RAY DIFFRACTION MEASUREMENTS TO 110 GPa

R.J. Hemley[1], A.P. Jephcoat[1], C.S. Zha[1], H.K. Mao[1], L.W. Finger[1], and D.E. Cox[2]

[1]*Geophysical Laboratory, Carnegie Institution of Washington, Washington, DC 20008 USA*

[2]*Brookhaven National Laboratory, Upton, NY 11973 USA*

The properties of condensed gases at ultrahigh pressures continue to attract much experimental and theoretical attention as these systems provide critical tests of theoretical models of bonding in solids. Neon has been the subject of considerably fewer experimental and theoretical studies than other rare gases. The first high-pressure studies of condensed gases in general [1], and solid neon in particular [2,3], were low-temperature studies limited to below 1.0 GPa. Later, single-crystal x-ray diffraction studies were performed on neon to 14.4 GPa, as well as argon to 8.2 GPa, at room temperature [4]. From a theoretical point of view, there does not yet appear to be a consensus on the role of many-body forces in the solid. Indeed, the determination of an accurate Ne-Ne pair potential has been fraught with difficulties [5-7]. Both statistical electron and band-structure calculations have been performed to predict the properties of the solid at ultrahigh pressures, including the P-V equation of state [8,9]. The band-structure calculations indicate that the electronic structure is only weakly perturbed over a wide range of pressures; the pressure-induced insulator-metal transition is predicted to occur at extreme pressures above 100 TPa [9]. One may surmise from these results that a simple pair-wise description of the interatomic forces should accurately represent the properties of the solid in the 100 GPa range.

The last several years have seen the development of static compression techniques based on the diamond-anvil cell in which gases have been contained and pressurized above 100 GPa [10]. Few detailed structural studies, however, have been carried out on gases in this pressure regime. Structural studies with con-

ventional x-ray diffraction techniques are particularly difficult for weakly scattering (i.e., low-Z) materials. In the present experiments neon gas, together with powdered tungsten and ruby, was loaded at room temperature in a megabar-type diamond-anvil cell with bevelled anvils [10]. The x-ray diffraction was measured at room temperature at the National Synchrotron Light Source, Brookhaven National Laboratory (beamline X13A) operating at 2.5 GeV and 50-120 ma. The incident x-ray beam from the synchrotron was collimated to a width of 20-40 μm, and the diffraction was measured by energy dispersive scattering techniques [11,12]. Pressures of the sample in the diamond-anvil cell were measured *in situ* by x-ray induced ruby fluorescence [12]. The recently determined quasihydrostatic ruby

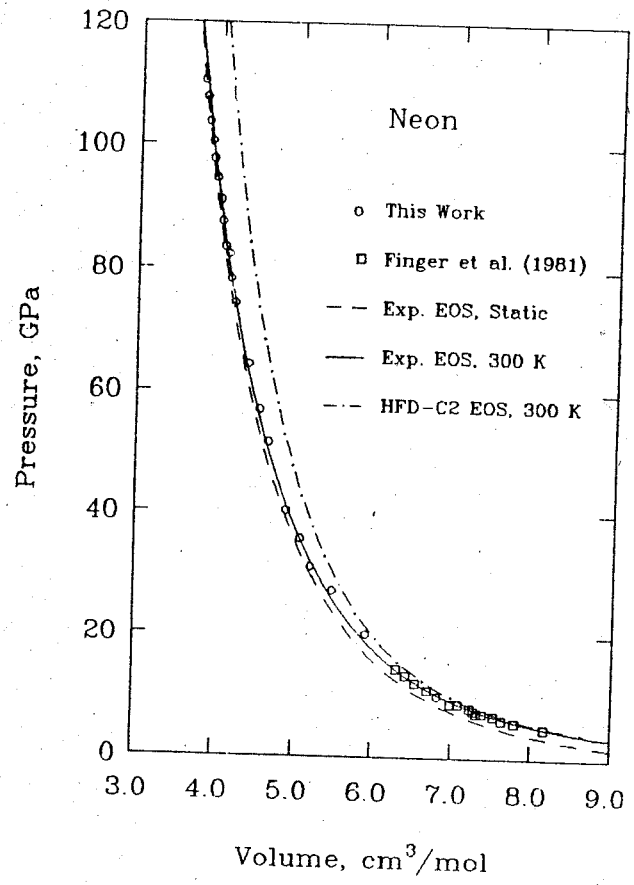

pressure scale was used [13]. The pressure was also checked against that calculated from the x-ray diffraction pattern of the tungsten by the use of the tungsten P-V isotherm [12].

The (111) and (200) lines of solid Ne in the fcc structure were observed to the maximum pressures. In the lower pressure range below 30 GPa, however, an irregular variation in the relative intensities of the two Ne bands was observed with each change in pressure. This effect is attributed to partial recrystallization of neon micro-crystals with preferred orientation with increasing pressure [4]. The molar volume calculated from the diffraction pattern is plotted as a function of pressure in Fig. 1 along with the results of the earlier single-crystal study at low pressure. Very good agreement with the earlier study is indicated. The results of a least-squares fit using a third-order Birch-Murnaghan finite-strain equation of state [14] are also shown. The fit was performed by first reducing the 300 K data to 0 K in order to use the low-temperature zero-pressure volume V_0 and bulk modulus K_0 in the fit, as described in the figure caption.

Fig. 1. Pressure-volume data and calculated equations of state for solid neon. The solid line was calculated assuming $P(V,T) = P_S(V) + P_{ZP}(V) + P_{TH}(V,T)$, where P_S (dashed line) and P_{ZP} are the static lattice and zero-point pressures, respectively, which are functions of volume only, and P_{TH} is the thermal pressure (at 300 K), which is a function of both volume and temperature. The latter two terms were calculated in the Debye approximation; viz, $P_{ZP} = (9\gamma/8V)R\,\Theta(V)$ and $P_{TH} = (3RT\gamma/V)D(\Theta/T)$ where R is the gas constant Θ is the Debye temperature, and D is the Debye function. γ is the Gruneisen parameter, which was calculated assuming the $\gamma = (V/V_0)\,\gamma_1 + 1/2$, where $V_0 = 13.394$ cm³/mol and $\gamma_1 = 2.05$ (Refs. [2,4]). The T = 0 K isotherm $P(V, 0\text{ K}) = P_S(V) + P_{ZP}(V)$ was then fit using the Birch-Murnaghan finite-strain expansion, in terms of the nomalized stress F as, $F(f) = P(0\text{ K})/[3f(1 + 2f)^{5/2}] = K_0(1 + af)$, where $f = (1/2)[(V_0/V)^{3/2} - 1]$ and $a = (3/2)(K_0 - 4)$. K_0 and K_0' are the bulk modulus and its pressure derivative. In this calculation K_0 was set equal to 1.097 GPa (Ref. [14]), and the value for K_0' was determined by least-squares fit to be 9.23(3). The dash-dot line was calculated from the HFD-C2 pair potential of Ref. [5], with the P_{ZP} and P_{TH} contributions calculated from quasiharmonic lattice dynamics (see Ref. [1], and to be published).

Also shown in Fig. 1 is the equation of state calculated from the pair potential recently determined by Aziz et al. [5]. In this calculation the thermal contribution was determined by quasiharmonic lattice dynamics. At lower pressures it is generally believed that the triple dipole dispersion terms contribute. In addition, anharmonicity of the crystal is believed to be significant and thus a Monte Carlo or molecular dynamics calculation must be performed to determine accurately the properties at low pressures [1]. Despite these approximations, good agreement with experiment is observed at low pressures. At higher pressures, however, a significant departure from the predictions of the pair potential model is apparent; i.e; the compression is strongly underestimated. Moreover, the use of other pair potentials from Ref. [5] show worse agreement with the new P-V data.

The experimental equation of state is compared with theoretical results of theoretical predictions in Fig. 2. The calculation of Boettger [9] is a band-structure approach using a LCGTO basis for the static lattice. At lower pressure (below 34 GPa) the calculation appears to underestimate the pressure. It is likely that the principal source of error is associated with limitations of the theoretical method for expanded volumes, as discussed by Boettger [9]. It is therefore encouraging that excellent agreement is observed at higher pressures and densities where such complications in the theoretical method do not obtain. There is also good agreement with the isotherm determined by Zharkov and Trubitsyn [8], which was calculated by interpolation between the results of quantum statistical calculations at ultrahigh pressures and the early experimental data at low pressures (< 1 GPa).

The overestimation of the pressure (or volume) in the pair-potential calculation may reflect inadequacies of the form of the repulsive part of the potential. Indeed, the determination of the entire potential for neon has been a difficult problem in the last few years (see Ref. [7]). The HFD-C2 potential was adjusted to fit both exchange-coulomb-type potentials and the high-energy molecular beam data of Rol (see Ref. [5]). The Rol data appear to represent the best estimate of the pure two-body interaction potential high on the repulsive wall. Thus, it is also possible that the deviation of the measured high-pressure data and the prediction of the HFD-C2 potential arises from the effects of many-body forces in the compressed

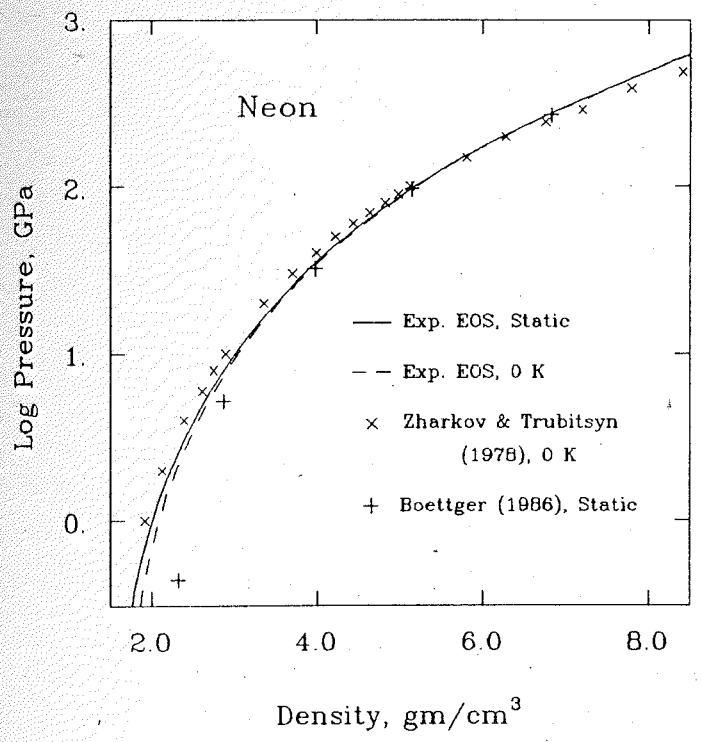

Fig. 2. Comparison of the temperature-reduced (T = 0 K) and static-lattice experimental and theoretical equations of state for neon at high pressures and densities. The calculation of Zharkov and Trubitsyn [8] is semiempirical: it was determined by interpolation from low-pressure experimental data and the results of quantum statistical calculations at high pressures. Boettger [9] employed local density functional methods using a linear-combination of gaussian-type orbital (LCGTO) basis.

solid. As discussed by Meath and Aziz [15], at high densities many-body exchange terms are believed to represent the largest many-body contribution. This term tends to soften the repulsive forces in the solid, causing a decrease in the pressure. The extent to which overlap effects will serve to diminish this contribution in the compressed solid, however, is not yet clear [16].

In conclusion, new x-ray diffraction techniques involving the use of synchrotron radiation in conjunction with the megabar-type diamond-anvil cell have been applied to determine the structure and and pressure-volume equation of state of solid neon in 100 GPa range. The maximum compression, corresponding to a relative volume $V/V_0 = 0.28$ at 110 GPa, appears to be the largest measured yet by x-ray diffraction techniques. Neon remains an insulator with the fcc structure over this pressure interval. The measured P-V isotherm at high pressure is in excellent agreement with the results of electronic structure calculations but is incorrectly described by pair potentials recently developed for neon.

This research was supported in part by the Carnegie Institution of Washington, NASA (contract NAGW214), and U.S. Department of Energy, Division of Materials Sciences (contract DE-AC02-76CH00016).

References

1. Klein, M.L., and Venables, J.A., *Rare Gas Solids* (Academic, New York, 1976), vol. 1, 607 p.

2. Fugate, R.Q., and Swenson, C.A, Specific heats of solid natural neon at five molar volumes and of the separated neon isotopes at P = 0, J. Low Temp. Phys., 1973, **10**(3/4), 317-343.

3. Batchelder, D.N., Losee, D.L., and Simmons, R.O., Measurements of lattice constant, thermal expansion, and isothermal compressibility of neon single crystals, Phys. Rev., 1967, **162**(3), 767-775.

4. Finger, L.W., Hazen, R.M., Zou, G., Mao, H.K., and Bell, P.M., Structure and compression of crystalline argon and neon at high pressure and room temperature, Appl. Phys. Lett. **39**(11), 892-894 (1981).

5. Aziz, R.A., Meath, W.J., and Allnatt, A.R., On the Ne-Ne potential energy curve and related properties, Chem. Phys., 1983, **78**, 295-309.

6. LeSar, R., Electron-gas plus damped dispersion model for intermolecular forces. The rare-gas and H_2-He, H_2-Ne, and H_2-Ar potentials, J. Phys. Chem., 1984, **88**, 4272-4278.

7. Aziz, R.A., Interatomic potentials for rare-gases: pure and mixed interactions, in *Inert Gases*, Springer Series in Chemical Physics, Vol. 34, edited by Klein, M.L. (Springer, New York, 1984), pp. 5-86.

8. Zharkov, V.N., and Trubitsyn, V.P., *Physics of Planetary Interiors*, (Pachart, Tucson, Arizona, 1978) 388 p.

9. Boettger, J.C., Equation of state and metallization of neon, Phys. Rev. B, 1986, **33**, 6788-6791.

10. Bell, P.M., Mao, H.K., and Hemley, R.J., Observations of solid H_2, D_2, and N_2 at pressures around 1.5 Mbar and 25° C, Physica 1986, **139 & 140B**, 16-20.

11. Baublitz, A., Arnold, V., and Ruoff, A.L., Energy dispersive x-ray diffraction from high pressure polycrystalline specimens using synchrotron radiation, Rev. Sci. Inst., 1981, **52**(11), 1616-1624.

12. Zha, C.S., Mao, H.K., Jephcoat, A.P., Finger, L.W., Hemley, R.J., and Cox, D.E., in preparation.

13. Mao, H.K., Xu, J., and Bell, P.M., Calibration of the ruby pressure gauge to 800 kbar under quasi-hydrostatic conditions, J. Geophys. Res. 1986, **91**(B5), 4673-4676.

14. Birch, F., Isotherms of the rare gas solids, J. Phys. Chem. Solids, 1977, **38**, 175-177.

15. Meath, W.J., and Aziz, R.A., On the importance and problems in the contruction of many-body potentials, Mol. Phys., 1984, **52**(1), 225-243.

16. Barker, J.A., Many-body interactions in rare gases, Mol. Phys., 1986, **57**(4), 755-760.

COMPRESSIBILITY OF POROUS METALS IN SHOCK WAVES

R.F.Trunin, A.B.Medvedev, G.V.Simakov, Yu.N.Sutulov
Institute of Chemical Physics, USSR Academy of Sciences, Moscow, USSR

Experimental results

The new results of compressibility measurements of porous tantalum and additional data for nickel and molybdenum concerning mainly the non-studied range of states are given in accordance with this aim.

The specimens under test (cylindrical pellets 12-15 mm in diameter and 3-5 mm in hight) were fabricated with the metal powders pressing to the required values of initial density $\rho_{oo} = \frac{\rho_o}{m}$ (where ρ_o is the crystallographic density of metal, m is a porosity). The least density (maximal porosity) was reached by the sublimation of light organic component from preliminary prepared homogeneous mixture of fine-dispersed metal powders with this additive.

Electrocontact technique of wave velocity measurements was used /1/; with the pressures less than 10 GPa as a temporary pickups the piezoelectric ceramics was used.

The resulting experimental data are shown in Figs.1-4. In Fig.1 one can see the dependence of wave velocity (D) on the porosity (m) for molybdenum. These are so-called the "lines of one charge" - i.e. the dependences that allow to costruct the adiabats of any porosities in Δm experimentally investigated interval. Just the same dependences were received for other metals.

It should be noted that for molybdenum (as well as for other studied metals) beginning from some "m" (m-2.0-2.5 in our case) with the same screen material (in the most our tests aluminium) and their initial states the values of wave velocity in porous specimens have a linear dependence on the initial specimen density.

The experimental data totality in the kinematic D-U variables is shown in Fig.2. In example of nickel analysis of D-U diagrams shows:

1. The initial adiabat sections of porous metals represent a fan of diverging straight linescentered to the small region $\Delta D(U=0)$ adjacent to the origin.

2. The most initial D'_u slope in this fan has the adiabats with the low "m" values; the adiabat slope decreases with "m" increase. For some adiabats with the maximum porosity the linear extrapolation of D-U dependences on high D,U parameters to U=0 leads formally to the negative values of sound velocities and accordingly at some $U < U_c$ values to the negative wave velocities. It is in contrast with the conservation laws: $D > U$ is the necessary condition of the shock wave existence. This adiabat's investigation in the region of boundary D=U straight line shows inverse convexity for the D-U dependence (as compared for the adiabats with small "m" values).

On the equation of state

In practical application of equations of state the most widely distributed are the equations where the relation between heat pressure and energy expresses in terms of $\gamma = V(\frac{\partial P}{\partial E})_V$ Grüneisen coefficient. In /2/ the construction of equation of state the $\eta = P(\frac{\partial V}{\partial E})_P$ factor that supposed to depend only on the pressure was taken as a basis. The equation of state used in our study is based on the approach that represents the combination of two above mentioned ones. As it is seen from γ and η definition both factors represent the specific z derivative:

$$z = \frac{\partial (PV)}{\partial E} /_f \qquad (1)$$

In this expression $f\,(= \frac{dP}{dV})$ is a tangent of slope angle of direction in P-V coordinates. If, for instance, z is estimated with $V = \mathrm{Const}(f = \infty)$, then $z = \gamma$ if with $P = \mathrm{Const}$ $(f = 0)$, then $z = \eta$. In common case z value depends on the direction where the derivative is estimated, i.e. on f. Let's stipulate to find such direction in the arbitrary point of P-V plane that is characterized by the tangent of slope angle $f\,(= \frac{dP}{dV})$ along which the equality

$$\frac{\partial (PV)}{\partial E} /_{f=\frac{2}{3}} \qquad (2)$$

is fulfilled.

The differentials of numerator and denominator of the left-hand side of equation are equal to

$$d(PV) = PdV + VdP \qquad (3)$$

$$dE = (\frac{\partial E}{\partial V})_P dV + (\frac{\partial E}{\partial P})_V dP \qquad (4)$$

The $(\frac{\partial E}{\partial P})_V$ derivative expresses in terms of γ and ρ density as follows:

$$(\frac{\partial E}{\partial P})_V = \frac{1}{\gamma\rho} \qquad (5)$$

Just after some transformations $(\frac{\partial E}{\partial V})_P$ may be written as

$$(\frac{\partial E}{\partial V})_P = \frac{\rho C^2}{\gamma} - P \qquad (6)$$

where C is sound velocity. Hence we get the expression for γ:

$$\gamma = \frac{(\rho C^2)\ (\frac{2}{3} - \frac{5}{3}\frac{\gamma \cdot P}{\rho C^2}}{\gamma - \frac{2}{3}} \qquad (7)$$

Then we assume some supporting curve. As this curve we choose here the shock adiabat of solid (m=1) substance as the most thoroughly experimentally studied. Label the quantitives on this curve by "Γ" index. Draw a straight line in P-V coordinates with tangent of slope angle determined by the expression (7) from arbitrary point on the supporting curve

$$P = P^\Gamma + \gamma^\Gamma (V - V^\Gamma) \qquad (8)$$

Along this straight line expand PV in series till the first-order term with respect to E.

So far as according to γ^Γ determination along the straight line (9) in the point of its intersection by the supporting curve the $\frac{\partial (PV)}{\partial E}\Big/_{\gamma^\Gamma} = \frac{2}{3}$ equality is fulfilled, the expansion in series gives the next relation

$$PV - P^\Gamma V^\Gamma = \frac{2}{3}\ (E - E^\Gamma) \qquad (9)$$

The equation of state is determined by (8), (9) and (7) expressions. In the $V \gg V^\Gamma$ limit takes the following form

$$P \cdot V = \frac{2}{3} E \qquad (10)$$

Thus, the transition to the ideal gas is guaranteed.
The shock adiabats from /3/ work are used as the supporting curves for the studied metals where they are represented in D-U coordinates either linear or squarely. The V^Γ, P^Γ, E^Γ values are expressed in terms of conservation laws under the shock compression.

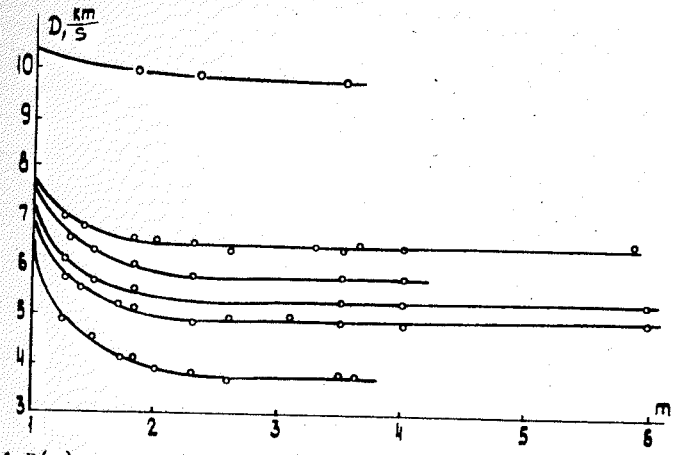

Fig.1. D(m) experimental dependence for molybdenum. Each curve was obtained for the fixed states of shock wave in screen - "lines of one charge" (so-called).

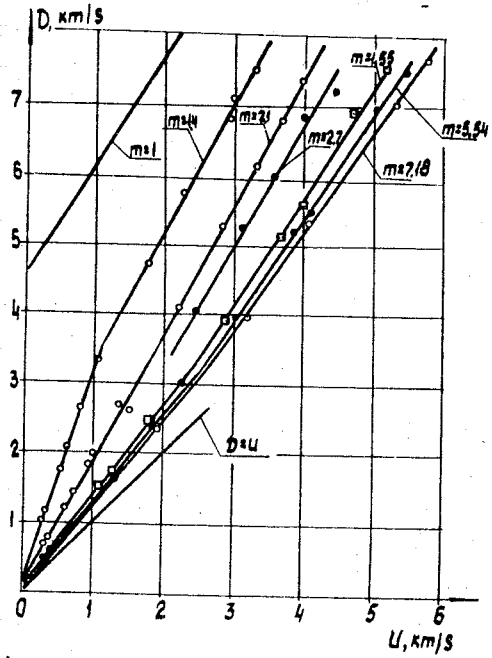

Fig.2. D-U diagram of nickel: O, ● , □ - experimental data.

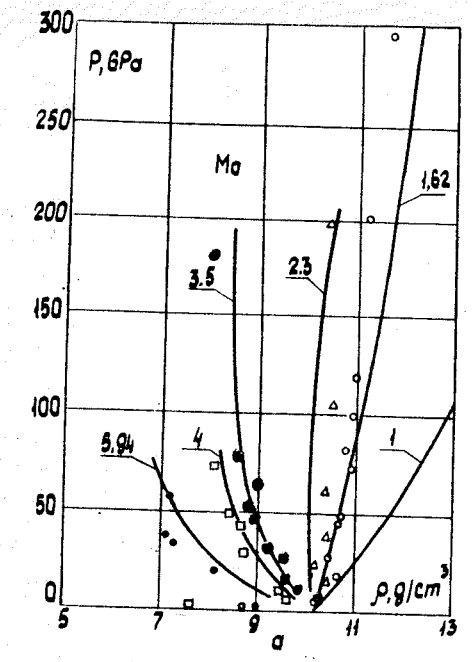

Fig.3. P-ρ diagrams of molybdenum and tantalum. O, ●, Δ, □ - experimental data.

The estimated shock adiabats and experimental data are correlated in Fig.3, a,b in P-ρ coordinates. It is seen that in pressure region where the strength influence is small the experiments and calculations are in good agreement.

References

1. Al'tshuler, K.K.Krupnikov, M.I.Brazhnik. Dynamic compressibility of metals at pressures from four hundred thousands to four millions atmospheres. JETP, v.34, n.4., 1958, p.886.

2. V.N.Zubarev, M.A.Podurets, L.V.Popov, G.V.Simakov, R.F.Trunin.Shock compressibility and the equation of state of copper in high pressure region. Col. Detonation. Critical phenomena. Physical-chemical transformations in shock waves. USSR Academy of Sciences, Department of the Institute of Chemical Physics. - 1978.

3. L.V.Al'tshuler, A.A.Bakanova, A.B.Bushman, L.P.Dudoladov, E.A.Dinin, R.F.Trunin, B.S.Chekin. Shock adiabats of metals. New data, statistical analysis and common laws. J.of Applied Mathematics and Technical Physics, n.2, 1981, p.3-33.

HIGH PRESSURE PROPERTIES OF KRYPTON: EQUATION OF STATE AND ELASTIC MODULI

A. POLIAN[1], J.M. BESSON[1], W.A. GROSSHANS[2] AND J.P. ITIE[3].

[1]Physique des Milieux Condensés - (U.A. 782) - Université Paris VI, T13, E4, 4 place Jussieu F-75252 Paris Cédex 05.

[2]Experimentalphysik, Gesamthochschule - D-4790 PADERBORN

[3]LIMHP-(LP 1311) Avenue J.B. Clément - F-93430 VILLETANEUSE.

Abstract

High pressure properties of solid krypton have been measured at room temperature by energy dispersive x-ray diffraction, x-ray absorption and Brillouin scattering up to 30 GPa. The equation of state and the elastic constants are deduced. The approach of a phase transition is deduced from these results.

I Introduction

We present results on solid krypton obtained under pressure at room temperature, by various techniques: Energy Dispersive x-ray diffraction (EDX), Extended x-ray Absorption Fine Structure (EXAFS) in the dispersive mode and Brillouin scattering. The experiments were performed in diamond anvil cells (DAC) up to 30 GPa. From these experiments the room temperature equation of state (EOS) is deduced as well as limiting values for the three elastic constants. These results suggest the approach of a phase transition which is theoretically predicted around 60 GPa [1].

II Experimental

The EDX experiments were performed using the synchrotron radiation source of DESY (Hamburg - FRG) using the experimental setup already described in Ref. [2]. The DAC was of Syassen-Holzapfel type [3].

The EXAFS experiments were done at the energy dispersive EXAFS port of LURE (Orsay - France). The dispersive mode [4] is very convenient for use in conjunction with a DAC mainly because of the focussing of the polychromatic x-ray beam and of the stability of the beam due to the lack of any mechanical motion.

Brillouin scattering was performed in the back-scattering geometry using a five pass piezoelectrically scanned Fabry-Pérot interferometer. The exciting light was the 514.5 nm line of a single moded argon ion laser. In both last experiments a Block-Piermarini type DAC [5] was used.

III Results and discussion

A - EDX

Between five and seven diffraction peaks were followed as a function of pressure. The experimental EOS was then deduced from these data up to 32 GPa. The experimental data were fitted with a first order Murnaghan EOS:

$$\rho = \rho_0 \left(1 + \frac{B_0 P}{B'}\right)^{1/B'} \qquad (1)$$

where ρ and ρ_0 are the densities at P and room pressure respectively, B_0 and B'the bulk modulus at P=0 ant its first derivative with respect to pressure. The best fit parameters are:

$$\begin{aligned} \rho_0 &= 2.37 \pm .005 \ g/cm^3 \\ B_0 &= 1.71 \pm .005 \ GPa \\ B' &= 4.15 \pm .1 \end{aligned} \qquad (2)$$

ρ_0 is only a fit parameter. These results are shown in Fig. 1 where the points are the experimental results and the continuous line represent the Murnaghan EOS.

B - EXAFS

Only preliminary results are yet obtained. Above the absorption edge, one get EXAFS oscillations. The amplitude of the Fourier transform of these oscillations shows peaks for the successives neighbours distances which allow to deduce an EOS. The variation of the intersity of these peaks is directly related to the Debye-Waller factor. The analysis of the height of the nearest neighbour peak shows that the Debye-Waller decreases when the pressure increases. Quantitative analysis of this phenomenon will be done elsewhere [6].

C - Brillouin scattering

Raw results of Brillouin scattering versus pressure are shown in Fig. 2 On this figure the scattering of the points is due to the fact that various crystalline orientations were explored: when the pressure is changed reorientations may happen, and each time that a new crystal is grown, a new orientation is tested.

In backscattering, the frequency shift in cm^{-1} measured by Brillouin scattering is related to the sound velocity v by:

$$\Delta\sigma = \frac{2nv}{\lambda c} \qquad (3)$$

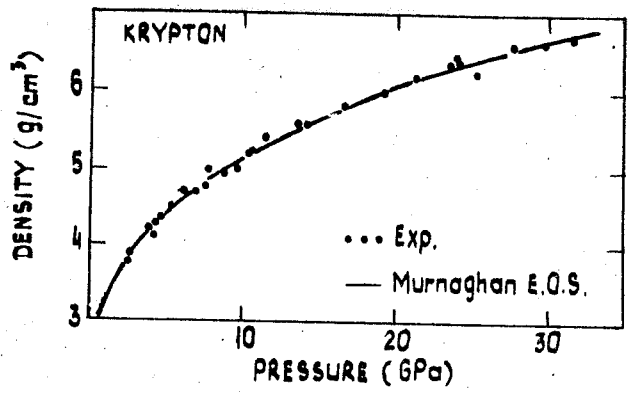

Fig. 1: Experimental (points) and fitted (continuous line) EOS of solid krypton.

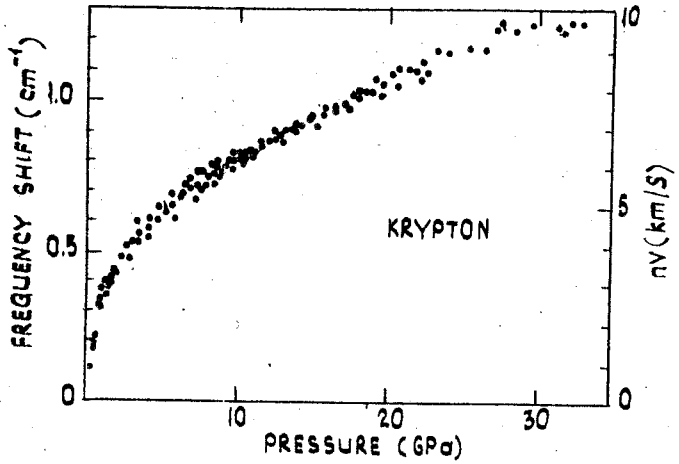

Fig. 2: Frequency shift (left hand scale) and product nv (right hand scale) obtained from Eq. 3 versus pressure.

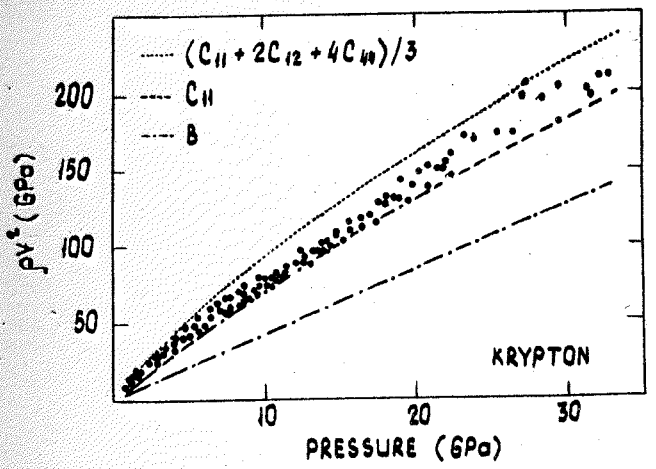

Fig. 3: Elastic moduli and bulk modulus of krypton vs. pressure (see text)

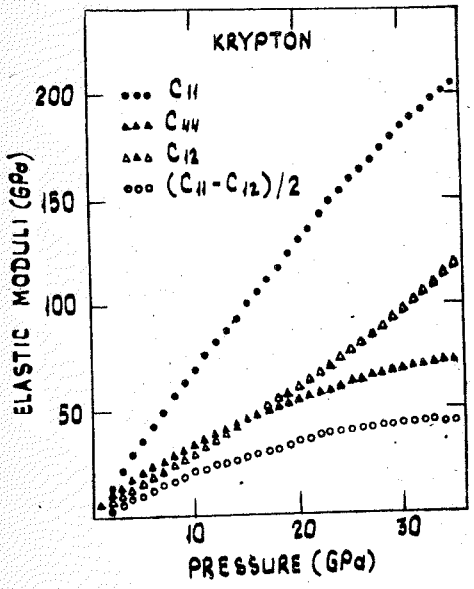

Fig. 4: Complete set of elastic constants of solid krypton.

where n is the refractive index, λ and c the wavelength and the velocity of light. The sound velocity is related to the elastic constants by:

$$C = \rho v^2 \qquad (4)$$

where C is a linear combination of elastic constants depending on the relative orientation of the phonon and the crystallographic axes and ρ the density.

The refractive index was calculated using the same procedure as already used for argon [7]. From the values of $\Delta\sigma$ shown in Fig. 2 the sound velocity was calculated (Eq. 3) and using the Murnaghan EOS fitted on the EDX data, the elastic constant was calculated (Eq. 4). In cubic crystals the elastic constants have extremum in the [100] and in the [111] directions. From low temperature measurements[8], it is known that C is minimum in the [100] direction ($C = C_m = C_{11}$) and maximum in the [111] direction ($C = C_M = (C_{11} + 2C_{12} + 4C_{44})/3$). Moreover, $B = (C_{11} + 2C_{12})/3$. Fig. 3 shows the experimental C (points), C_M (dotted line), C_m (dashed line) and B (point-dashed line). From C_M, C_m and B one deduce limiting values for the various C_{ij} which are shown in Fig. 4. It is easy to show that C_{11} is an upper value and C_{12} and C_{44} lower values. $(C_{11} - C_{12})/2$ is an upper value and begin to decrease at 30 GPa. This may indicate the approach of the fcc - hcp phase transition which is predicted to happen around 60 GPa [1].

IV Conclusion

The study of solid krypton under pressure by various techniques allowed us to determine the room temperature EOS and limiting values for all the elastic constants. The approach of the fcc - hcp phase transition is deduced from the analysis of the evolution of a transverse elastic constant with pressure.

Referenoes

1. P. LOUBEYRE: to be published
2. W.A. GROSSHANS, E.F. DUESING and W.B. HOLZAPFEL: High Temp. - High Pres. 16, 539 (1984)
3. K. SYASSEN and W.B. HOLZAPFEL: Europhys. Conf. Abstr. 1A, 75 (1975)
4. E. DARTYGE, C. DEPAUTEX, J.M. DUBUISSON, A. FONTAINE, A. JUCHA and G. TOURILLON: Nucl. Inst. Methods: A246, 452 (1986)
5. G.J. PIERMARINI, S. BLOCK, J.D. BARNETT and R.A. FORMAN: J. Appl. Phys. 46, 2774 (1975)
6. A. POLIAN, J.M. BESSON, J.P. ITIE, E. DARTYGE, A. FONTAINE and G. TOURILLON: to be published.
7. M. GRIMSDITCH, P. LOUBEYRE and A. POLIAN: Phys. Rev. B33, 7192 (1986)
8. B.P. STOICHEFF: in "Rare gas solids" ed. by J.A. VENABLES and M.L. KLEIN (Academic Press, New York 1976), p. 979

BIRCH'S LAW FOR FLUID METALS*

J. W. Shaner, R. S. Hixson, and M. A. Winkler
Los Alamos National Laboratory
Los Alamos, NM, 87545, USA
and
D. A. Boness and J. M. Brown
Graduate Program in Geophysics, University of Washington,
Seattle, Washington, 98195, USA

By comparing acoustic velocities in fluid metals over a very wide range of densities we have established Birch's Law as an approximate representation over the entire liquid range. For a given liquid metal the acoustic velocity is close to linear in density, with a slope determined by the atomic weight. The measurements include isobaric expansion to less than half normal density, ultrasonics on molten metals at 1 atmosphere, and shock melted metals to greater than twice normal density.

1. INTRODUCTION

In an attempt to identify what materials lie deep in the earth from seismic velocities, Birch proposed an empirical law that bulk and elastic wave velocities should scale linearly with density and inversely as the square root of the atomic weight [1]. This law was based on elastic constant measurements on rocks to 10 kbar [2], representing a density change of only 10%, and some early shock wave data from which rarefaction velocities were calculated or measured [3]. Since Birch's original work, several people have tried to explain the linear density dependence as an approximation over a limited density range to more general solid state models [4].

*This work performed under the auspices of the U.S. Department of Energy.

Over the past few years we have used the optical analyzer technique to measure the pressure at which shocked materials lose their ability to support longitudinal elastic waves [5]. At higher shock pressures, the release wave moves into a fluid-like material at the bulk wave velocity. Above the shock melting pressure we then have measurements of the acoustic velocity of the fluid. New data for liquid lead, obtained by this technique, are presented by Boness, et al. [6].

Another method of measuring thermodynamic properties of fluid metals is the isobaric expansion experiment (IEX). In this experiment, a metal wire is heated in a gas pressure vessel quickly enough so normal hydrodynamic instabilities play no role in the heating dynamics, but slowly enough so that isobaric conditions apply, and the electrodynamic skin effect is insignificant [7]. The function of the gas pressure is to stabilize a homogeneous fluid phase over the widest density range possible. After heating the wire to 5000-10,000 K in several tens of microseconds, we often find a stable liquid column for 10 microseconds, during which time we can perform detailed optical pyrometry or an acoustic velocity measurement.

The acoustic velocity measurement consists of a stress pulse induced by a Q-switched ruby laser pulse of ~0.1 J in 20 nsec, focussed to a spot roughly 0.1 mm on the central portion of the fluid column. This pulse propagates at the bulk sound velocity across the diameter of the wire and initiates a stress wave in the gas at a point diametrically opposite from the laser focal spot. The gas stress wave is detected by Schlieren photography with a streak camera. The velocity is simply the diameter divided by the time interval between the exciting laser pulse and the initiation of the gas stress wave. This technique has allowed us to make measurements of acoustic velocity in lead, for example, expanded to almost one third normal density [8].

The combination of acoustic velocity and a track on the equation of state (EOS) surface in the form of a (P,V,T) isobar, or a Hugoniot, allow one to determine two orthogonal derivatives of the EOS. Swenson, et al. [9] show how to obtain the Grüneisen gamma,

$$\gamma = V \left(\frac{\partial P}{\partial E}\right)_V \quad , \tag{1}$$

from the Hugoniot and acoustic velocity. This derivative is, up to a simple metric, orthogonal to the isothermal bulk modulus. With isobaric expansion data, one can obtain the Grüneisen gamma from

$$\gamma = \left(\frac{\partial V}{\partial H}\right)_P c^2 \quad , \tag{2}$$

where H is the enthalpy, the electrical energy input at constant pressure, and c is the acoustic velocity. Temperature measurements along the Hugoniot permit an experimental determination of the isothermal bulk modulus by straightforward but tedious arithmetic [10]. Along the isobar, the isothermal bulk modulus, B_T, can be determined from

$$C_p = C_v + \alpha^2 V T B_T \quad ,$$

and

$$c^2 = V B_T \, C_p / C_v \quad , \tag{3}$$

where α is the volume thermal expansion coefficient and $C_{P,V}$ are the heat capacities. Everything is measured experimentally in Eq. (3) except C_V and B_T.

2. EXPERIMENTAL DATA

We present acoustic velocity data for expanded liquid lead and tantalum in Fig. 1. The lead data at high temperatures and expansions show no pressure dependence. Since the P,V isobars separate at high temperatures we can say that the acoustic velocity is only weakly temperature dependent, at least at high expansions. These isobaric expansion data show the normally observed linear de-

pendence of acoustic velocity on density, but to much higher expansions than are usually obtained for metals [11].

The combination of data presently available for acoustic velocity in metals in expansion, shock compression, and at the one-atmosphere melting point is shown in Fig. 2, including the recent data of Boness, et al. [6] The N_2 data are from molecular dynamics calculations [12]. It is important to realize that in the shock compression regions the density derivative of the temperature is positive, while it is negative in the expansion region, so any temperature dependence might tend to skew the data with respect to a straight line fit. In principle one should plot isotherms of c vs density, but under the extreme energy density conditions of these experiments, well defined thermodynamic data are limited.

3. DISCUSSION

The data of Fig. 2 show that the Birch's law suggestion that c is linear in density works reasonably well, even over a density range of three to five, for metals in the liquid range. The change of slope in the Pb data from expansion to compression is, however, well outside experimental error. The average slopes decrease monotonically with atomic mass. At low densities the linearity must break down as one approaches the ideal gas limit, which is independent of density.

For a linear shock velocity vs. particle velocity, $U_s = C + SU_p$, the pressure derivative of the isentropic bulk modulus is given by $B' = 4S-1$. Thus, for a simple two parameter equation of state, B_s should scale like density to the 4S-1 power, or

$$c = (B_{s/\rho})^{1/2} \sim \rho^{(2S-1)} \quad . \tag{4}$$

Since most Hugoniots have S between 1 and 1.5, one expects c to scale between linear and quadratic in density, at least in the compression range. Our data show that this scaling extends to significant expansions as well.

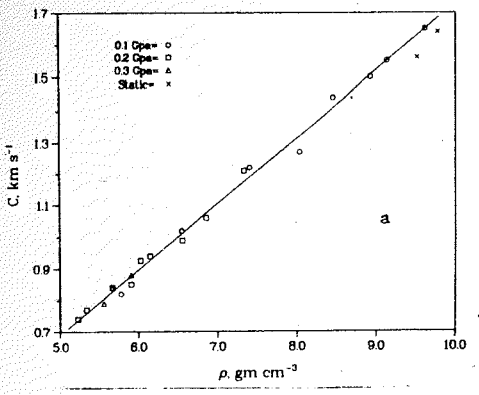

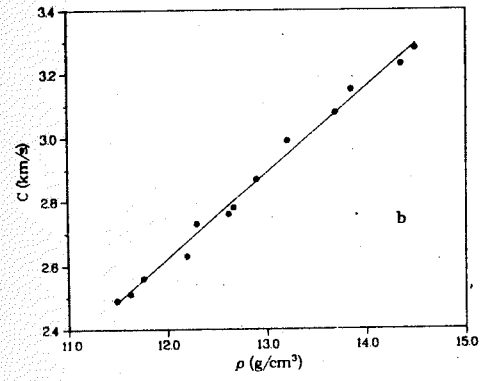

Fig. 1. Acoustic velocity in heated, expanded liquid metals: a) lead (Ref. 8); b) tantalum (Ref. 10).

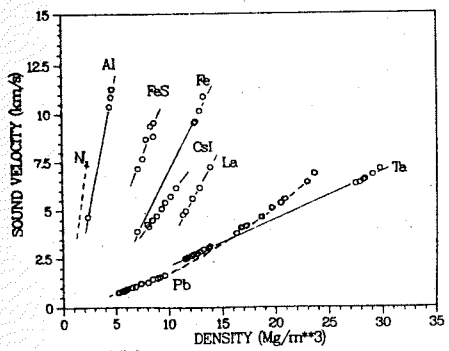

Fig. 2. Density dependence of sound velocity for liquid metals.

Grüneisen's gamma shows unexpected behavior for Pb when plotted against density. The data of Boness, et al. [6] show $\rho\gamma$ to be weakly density dependent. On the other hand, the IEX data show γV to be roughly constant.[8] Therefore, the slope of $\gamma(\rho)$ changes sign around normal density. This can be explained simply by a temperature dependent γ in the fluid phase. In fact, using the soft sphere model, which has been applied to the IEX data [13], one obtains an explicitly temperature dependent γ, and the observed shape of the $\gamma(\rho)$ curve [14]. Recognition of an explicitly temperature dependent γ is of particular importance in calculating isothermal compression curves from Hugoniot data extending well into the liquid.

References

1. F. Birch, Phys. Earth and Planet. Interiors 1, 141 (1968).
2. F. Birch, J. Geophys. Res. 65, 1083 (1960).
3. F. Birch, Geophys. J. Royal Astron. Soc. 4, 295 (1961).
4. T. J. Shankland, J. Geophys. Res. 77 3750 (1972), D. H. Chong, Science 177, 261 (1972), and O. L. Anderson, J. Geophys. Res. 78, 4901 (1973).
5. R. G. McQueen, J. W. Hopson, and J. N. Fritz, Rev. Sci. Inst. 53, 245 (1982).
6. D. A. Boness, J. M. Brown, and J. W. Shaner, these proceedings.
7. G. R. Gathers, J. W. Shaner, and R. L. Brier, Rev. Sci. Inst. 47, 471 (1976).
8. R. S. Hixson, M. A. Winkler, and J. W. Shaner, Physica 139 & 140B, 893 (1986).
9. C. A. Swenson, J. W. Shaner, and J. M. Brown, Phys. Rev. B34, 7924 (1986).
10. R. S. Hixson, M. A. Winkler, and J. W. Shaner, High-Temp. High-Press. 18, 635 (1986).
11. J. W. Shaner, in Thermal Expansion 6, I.D. Peggs, ed. [Plenum Press (1979) [69].
12. R. LeSar, private communication.
13. G. R. Gathers, J. W. Shaner, and D. A. Young, Phys. Rev. Lett. 33, 70 (1974).
14. J. W. Shaner, to be published.

EQUATION OF STATE OF MATTER AT HIGH PRESSURES AND TEMPERATURES BY THE MODIFIED HARTREE-FOCK-SLATER MODEL

A.F.Nikiforov, V.G.Novikov, V.B.Uvarov

M.V.Keldysh Applied Mathematics Institute, Moscow, USSR

The equation of state of matter at extremely high pressures P ~10 - 100 Mbars and temperatures T ~ 5 - 50 eV has been very intensively investigated today /1,2/. The experimental determination of the matter properties in this region of parameters is very expensive while the theory meets with grave difficulties because the matter under these conditions represents a strongly coupled multicomponent nonideal plasma. In practice for calculations of the equation of state quasiclassical models are used, as those by Thomas-Fermi (TF) and Thomas-Fermi with corrections /3/. However they do not include the shell effects. Most consistently these effects can be taken into account by quantomechanical self-consistent models /4-7/.

The modified Hartree-Fock-Slater model (MHFS) /5/ is based on the Hartree-Fock approximation for the matter with given temperature and density, where some effective local approximation for the exchange effects is used. In addition the quasiclassical approximation is used to describe the electron states with great energy ($\varepsilon > \varepsilon_0$, where ε_0 is the effective boundary of continuum). It allows significant simplification of calculations without loss of accuracy.

Using these approximations for the internal energy and entropy of the system and applying the most general variational principle, requiring the great thermodynamic potential to be minimum we obtain the MHFS model equations and construct the thermodynamics for electrons /7/. In addition to the MHFS equations, using the variational principle yields the condition for the parameter ε_0. The physical sense of this condition is that the sum of all electron states with energy $\varepsilon > \varepsilon_0$ and $\varepsilon < \varepsilon_0$ must be constant for different temperatures and densities.

The MHFS equations describe the electron system with given position of nuclei. This multi-nuclei and multi-electron problem is impossible to solve, therefore one usually calculates the potential near some chosen nucleus, averaging it by all positions of other nuclei. Such an approach leads to calculation of the

selfconsistent potential in a spherical cell, which contains a single nucleus and Z electrons (Z is the charge of nucleus). The volume of the cell is assumed to be equal to an average volume per one atom of the matter.

The boundary conditions for wave functions must be established when we go over from the great volume of matter to the atomic cell. So that after averaging the result should not change with transition from one cell to another, the periodical conditions must be used, which leads to the Bloch conditions in quantomechanical models. The periodical conditions are used in the extremely packed approximation.

The MHFS equations give the descriptions of the electron component only. To describe ions the one-component plasma model /8/ is employed with some corrections for the ion size by using the hard sphere model /7/. Calculations of the equation of state for ideal and nonideal plasmas, the cold compression curves and Hugoniot curves for some elements have been carried out using the MHFS model.

The internal energy of lithium calculated by the TF, TFC, MHFS and Saha models for pressure of 1 kbar and different temperatures is shown in Fig.1. There is a good agreement with results of the MHFS and Saha models but there is a notable descrepancy with results of the TF and TFC models which coincide here. Note that the Saha model practically coincides with experiment.

The Hugoniot shock curves of aluminium by some models and experimental data /9-12/ are shown in Fig.2.

References

1. Ross M. Matter under extreme conditions of temperature and pressure. - Rep.Prog.Phys., 1985, v.48, p.1-52.
2. Bushman A.V., Fortov V.E. The equations of state models of the matter. - Uspekhi Physicheskikh Nauk, 1983, v.140, N2, p.177-232.
3. Kalitkin N.N., Kuzmina L.V. Quantum-statistical equation of state. Physica Plasmy, 1976, v.2, N5, p.858-868.
4. Rozsnyai B.F. Relativistic Hartree-Fock-Slater calculations for arbitrary temperature and matter density. - Phys.Rev.A, 1972, v.5, N3, p.1137-1149.
5. Nikiforov A.F., Novikov V.G., Uvarov V.B. Modified Hartree--Fock-Slater model for the matter with given temperature and density. The Questions of Atomic Science and Technology, 1979, N4 (6), p.16-26.
6. Nikiforov A.F., Novikov V.G., Uvarov V.B. The influence of the shell structure of atoms on the shock Hugoniot curves of aluminium and ferrum. - Doklady Akademii Nauk SSSR,1982, v.267, N3, p.615-618.

7. Nikiforov A.F., Novikov V.G., Uvarov V.B. Using the quasiclassical approximation in the modified Hartree-Fock-Slater model. Teplophysica Vysokikh Temperatur, 1987, v.25, N1, p.12-21.
8. Hansen J.P. Statistical mechanics of the dense ionized matter. Phys.Rev.A, 1973, v.8, N6, p.3096-3109.
9. Al'tshuler L.V. et al. The equation of state of Al, Cu and Pb for the region of great pressure. - JETP, 1960, v.38, N3, p.790-798.
10. Simonenko V.A. et al. Absolute measurements of shock compression of Al at pressures $P \gtrsim 1$ TPa.- JETP, 1985, v.88, N4, p.1452-1459.
11. Ragan Ch.E. III Shock-wave experiments at threefold compression. Phys.Rev.A, 1984, v.29, N3, p.1391-1402.
12. Avrorin E.N. et al. Experimental confirmation of the shell effects on the Hugoniot curves of Al and Pb.- Pis'ma v JETP, 1986, v.43. N5, p.241-244.

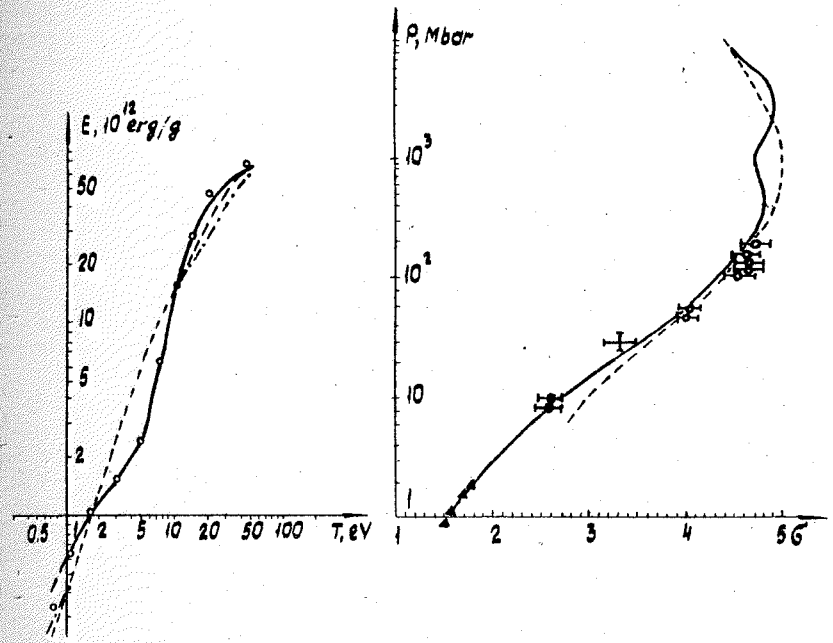

Fig.1. Internal energy of lithium for pressure of 1 kbar and different temperatures:
— MHFS; o - Saha; - - -TF; -·-·- TFC.

Fig.2. Hugoniot shock curves of aluminium:
— MHFS; - - - TEC. Experimental results: ▲ - /9/; ⊢⊣ -/10/; ⊢⊣ -/11/; ⊢o⊣ -/12/.

ON PLASMA PHASE TRANSITIONS

H.Hess and T.Kahlbaum

GDR Academy of Sciences
Central Institute of Electron Physics, Berlin, GDR

Nonmetal-metal transitions (Mott or plasma phase transitions) occur in very different systems as in metal vapours, metal-ammonia and metal-methylamine solutions, doped semiconductors, electron--hole systems, films of alkali-metal and rare-gas atoms, and in molecular and atomic gases. In rare gases, the plasma phase transition (PPT) is believed to be studied in its pure form, well-separated from the liquid-gas transition.

Recently, scaling relations were proposed for the critical parameters of the PPT /1/. Detailed model calculations in xenon now confirm these rough estimations and give more insight into the thermodynamics of the PPT. Our approach is based on an analytical formulation of the chemical potential of electrons, ions, and atoms which is a generalization of a model only applied to hydrogen and alkali metals up to now /2/ simply leading to a Saha equation and an equation of state. We treat Coulomb interaction of the charged particles most important for the PPT as well as van der Waals-like interaction of atoms most important for the liquid-gas transition and take into account the spatial extension of ions and atoms by corresponding hard core interactions /3/. The PPT critical values obtained are

T_c = 16.000 K, $n_c = 8 \times 10^{21}$ cm^{-3}, p_c = 2 GPa, and α = 0.9.

The critical pressure given here is lower by more than one order of magnitude compared with /7/ and in good agreement with /1/.

The second phase transition shown in Fig.1 at high pressure well-separated from the usual liquid-gas transition is the PPT which is characterized by a jump in density and ionization degree. The Livermore shock experiments /4,5/ are already located in the metallic region. Fig.2 gives a further idea of the relative location of the two transition regions. In Fig.3, crossing isotherms and the possibility of describing one point in the p-n diagram by two very different temperatures can be seen as it was reported for nitrogen in /6/. These measured effects should be connected with a PPT mixed with the dissociation process. Finally, in Fig.4 the sickle- or tongue-like shape of the PPT region can be noticed which leads to increasing densities at both sides of C_2 along

the coexistence-region boundary what is in contrast to the behaviour at C_1.

References

1. Hess, H., Proc. 8th ESCAMPIG, Ernst-Moritz-Arndt University, Greifswald 1986, 306-307.
2. Ebeling, W., and W. Richert, Phys.Stat.Sol. (b) 128 (1985) 467-474
3. Mansoori, G.A., N.F. Carnahan, K.E. Starling, and T.W.Leland, J.Chem.Phys. 54 (1971) 1523-1525.
4. Keeler, R.N., M. van Thiel, and B.J. Alder, Physica 31 (1965) 1437-1440.
5. Nellis, W.J.,M. van Thiel, and A.C. Mitchell, Phys. Rev. Lett. 48 (1982) 816-818.
6. Radousky, H.B., W.J.Nellis, M. Ross, D.C. Hamilton, and A.C. Mitchell, Phys.Rev.Lett. 57 (1986) 2419-2422.
7. Ebeling, W., H. Hess, A. Foerster, and W.Richert, ICTP preprint 86/271, Trieste 1986

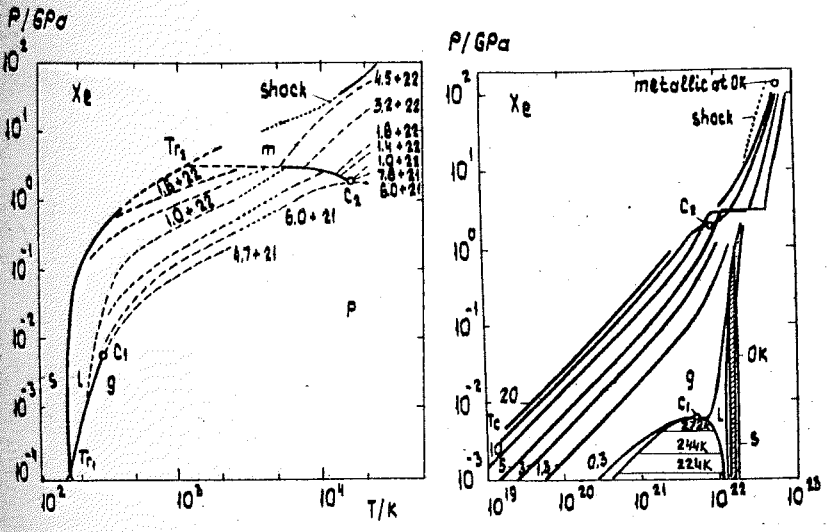

Fig.1. p-T diagram of xenon. $Tr_{1,2}$, $C_{1,2}$- tripel and critical point of the gas-liquid (1) and the plasma phase (2) transition. s - solid, l - liquid, g - gas, p - plasma, m - metal. The dashed lines are isochores the density of heavy particles along which is given by the numbers (6.0 + 21 read 6.0 x 10^{21} cm^{-3}). The dotted line labelled "shock": experiments from [4,5].

Fig.2. p-n diagram of xenon. T_c=16.000 K; shown are isotherms, the numbers give the temperature in 10^3 K.

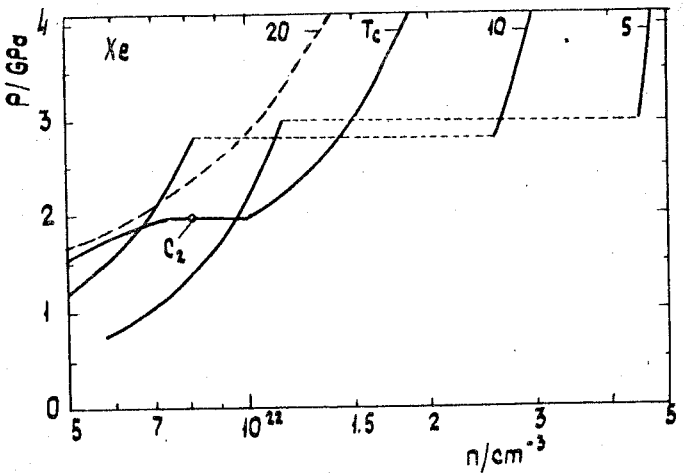

Fig.3.p-n diagram of xenon. Enlarged cut-out from Fig.2 around C_2. Shown are isotherms, the numbers give the temperature in 10^3 K. Critical point C_2 at the bottom of the coexistence region. Crossing isotherms can be seen as reported in 6 for nitrogen.

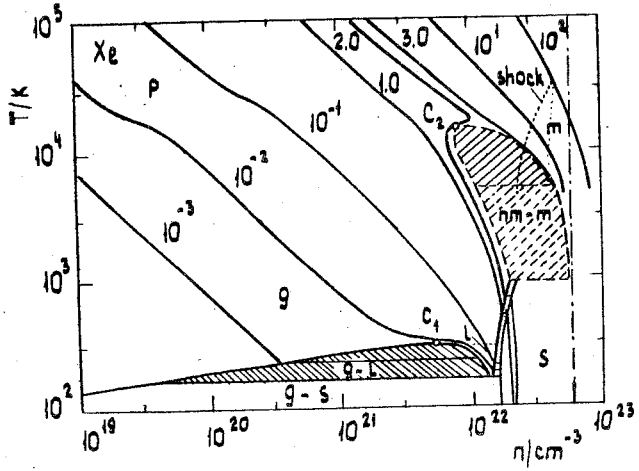

Fig.4. T-n diagram of xenon. Shown are isobars, the numbers give the pressure in GPa. The sickle- or tongue-like shape of the region of coexistence can be seen.

EQUATIONS OF STATE AND PECULIARITIES OF NUMERICAL MODELLING OF HIGH SPEED BODY INTERACTION PROBLEMS

V.M.Fomin
Institute of Theoretical and Applied Mechanics, Siberian Division of the USSR Academy of Sciences, USSR

In the report the works on numerical modelling of deformed bodies collision at high velocities and detonation products effect are considered. The principal question dealt with is connected with the choice of the equation of state and the influence of the latter on the interaction of bodies under large pressures and temperatures.

The given class of problems presents a set of complex phenomena including various physical processes, as, for example, the detonation of explosive substances, propagation of shock waves and the breakdown of substances which in the first place are characterized by a considerable heat release, high pressures and temperatures. A qualitative analysis of the principle physical processes which take place at the collision of solid bodies at high speeds carried out by K.P.Staniukovich /I/ and explained later with the help of numerical calculations in the framework of one-dimensional non-stationary approximations /2/ allowed to establish the boundary of collision velocity and accordingly, of the pressure and temperature, beginning with which there take place the phenomena, similar to explosion. In the interaction zone the crystal structure of the media is destroyed, and the substance passes into another phase or undergoes a mechanical crush with the subsequent scattering. The velocity at which the colliding bodies in the zone of impact reach the melting temperature and turn into compressible liquid or gas we will call threshold velocity, and it is equal $\mu_* = \frac{u_*}{a_*} \sim 0.75$, where u_* is a collision velocity, and a_* is a sound velocity in the obstacle.

Let us consider the peculiarities of body collision processes with velocities of meeting $\mu_* \geq 0.75$. Under these conditions inequalities of the form $P \gg \sigma_{ij}$ $(i \neq j,\ i,\ j = 1,\ 2,\ 3)$ are carried out, where the pressure $P = \frac{1}{3}\sum_{i=1}^{3}\sigma_{ii}$ and consequently, one can neglect the tangent components in the stress tensor, if compared with the normal ones. In this case the process in the interaction zone will be described by the system of Euler equations with a closure according to the thermodynamic equation of state of the

form $P=\varphi(\rho,e)$ where ρ is the medium density, and e is the internal energy. Consider, how the dependency $P=\varphi(\rho,e)$ influences the piercing of thin obstacles. Let us carry out the comparison according to the dimensions of the opening which is formed in the obstacle. The collision is carried out by the normal, and the dimensions of the opening are chosen using the impulse mechanism of destroying /3/. The solution is carried out numerically following the modified Harlow method /4/. The results of comparison by the diameter of opening D/d depending on the collision velocity u_o with the experimental data are given in Fig.I for the obstacles of aluminium alloy 2021-I3 and for aluminium strikers in the form of balls of the diameter $d \simeq 3.2$ mm. The calculations were carried out for the dependence $P=(\gamma-I)\rho e$ and for the Osborn equations. It is to be noted that thereat the finite dimensions of the opening coincide, but the calculation time on a computer at equal initial parameters in case of the Osborn equation is considerably smaller than in case of the ideal gas state equation. This fact is confirmed also for the cases when the obstacle materials are iron, nickel, copper and fabric-based laminate.

At the impact velocity in the interval $0.6 \leq \mu_o \leq 5$ the individual properties of the material do not influence the dimension of the diameter of the opening depending only on kinematic parameters. With the growth of the collision velocity the diameter of the opening in the obstacle decreases beginning with a certain critical impact velocity in the interval $D/d|_{u_o \to \infty} \to I$.

To model the processes when the collision velocity $\mu_o < 0.75$ is much more complicated. Thereat it is impossible to neglect shift components in σ_{ij}, i.e. the strength properties of the media are important. The question about the closure of preservation laws is reduced to setting the equation of the process and the thermodynamic equation. The detailed analysis of application of different models to the solution of the given class of problems is suggested in works /2,3,4/. By the results of comparison of numerical calculations and experimental data on the damping of the shock wave front in metals when they (the latter) are charged by the contact explosion or by the impact, the limits of the applicability of different models of a continuous medium are established. It is shown that the Prandtl-Rice elasto-plastic model satisfactorily describes the process in the given interval of the charging velocities. Further on it is recommended to use this rather simple model for the solution of the collision problems

in a multidimensional approximation. To solve the given class of problems the Wilkins method accompanied by the local reconstruction of the difference mesh in the process of calculation is used. The recoil of cylindrical and conical, homogeneous and multilayer bars of the finite lenght of absolutely solid obstacles /5/ is studied. The change of the resistance force of the striker when it penetrates thick multilayer obstacles depending on the choice of front and back layers and taking into account the formation and motion of cracks /6,7/ is elucidated.

On the basis of the phenomenological approach a mathematical model is proposed which allows to describe the behaviour of porous bodies affected by detonation products. The analysis of strong shock waves propagation in porous media /8/, and the comparison with the experimental data are given.

The analysis of the shell scattering with regard for destruction and escape of detonation products depending on the description of the behaviour of detonation products is carried out. In Fig.2 dependences $\alpha = \frac{u_\rho}{u_o}$ and $\varepsilon_\rho = \frac{a^+ - a^\circ}{a^\circ}$ on $\beta = \frac{\mu_{ea}}{\mu_{o\delta}}$, are presented where u_ρ is an average mass shell velocity with destruction and u_o without destruction, a^+ and a° is an external and initial shell radia, μ_{ea} and $\mu_{o\delta}$ is the mass of an explosive substance and the mass of the shell respectively. Thereat it turns out that in the interval $0.3 < \beta <$ I there exists a fall through in α from 0.97 up to 0.73, i.e. the shell velocity and degree of the absorbed energy decrease considerably.

References

I. Staniukovich K.P. Non-settled motion of a continuous medium.- Moscow, Nauka, I97I.

2. Fomin V.M., Khakimov E.M. Numerical modelling of compression waves and breakdown in metals.-PMTF, N 5, I979.

3. Fomin V.M., Sapozhnikov G.A., Deribas A.A. et al. Shock waves damping in metals when charging them by contact explosion. FGD, N 2, I979.

4. Fomin V.M., Nesterenko V.F., Cheskidov P.A. Damping of strong shock wave in laminated materials. PMTF, N 4, I983.

5. Fomin V.M., Gulidov A.I., Papirin A.N. et al. Experimental-theoretical study of short bars recoil of solid obstacle. PMTF, N 5, I982.

6. Fomin V.M., Gulidov A.I., Yanenko N.N. Numerical modelling of body penetration in elasto-plastic application. In: Problems of Mathematics and Mechanics. SO AN SSSR, Novosibirsk, I983.

7. Fomin V.M., Gulidov A.I., Shabalin I.I. Numerical modelling of breakdown by sound. In: Mechanics of Rapid Processes. IGL SO AN SSSR, Novosibirsk, I985.

8. Fomin V.M., Staver A.M., Cheskidov P.A. Strong shock waves structure in powders. In: Numerical Methods of Problems Solution of the Elasticity and Plasticity Theory. Materials of the 8th All-Union Conference, ITPM SO AN SSSR, Novosibirsk, 1984.

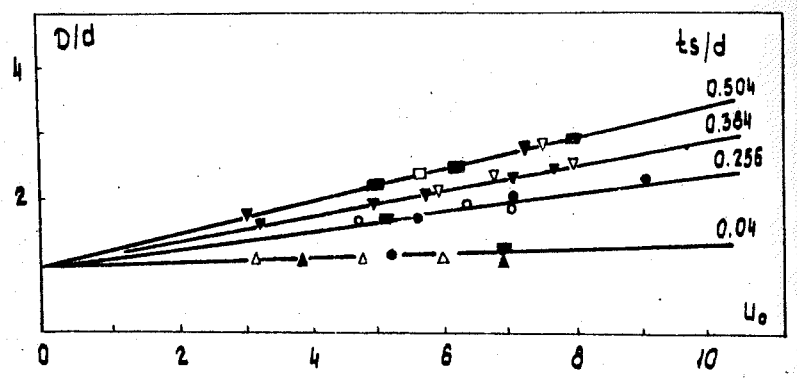

Fig.I. The results of comparison by the diameter of opening depending on the collision velocity: o, ▽, □ - experiment; —— - $D/d = 0.45\, U_o(ts/d)^{3/2}+0.9$; ■, ▼, ▲, ● - calculation.

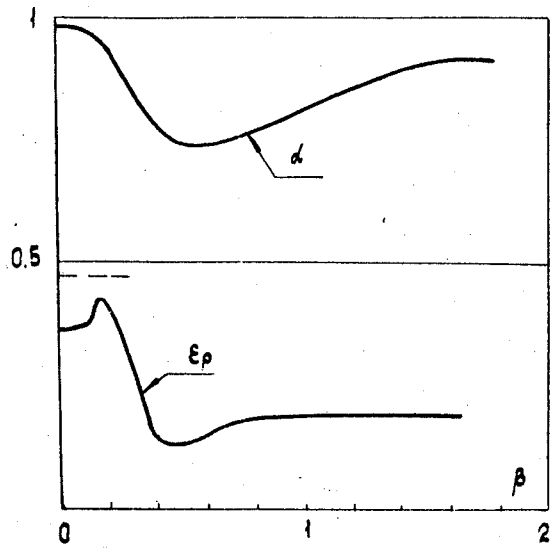

Fig.2. Dependences of α and ε_ρ on β.

SCALE EFFECTS BY SHELL PULSED FRACTURE

A.G.Ivanov, V.I.Tsypkin

Institute of Chemical Physics, USSR Academy of Sciences, Moscow, USSR

Recent years investigations in dynamic fracture of geometrically-like objects (tubes, vessels, material samples) /1/ showed the possibility of strong scale effects (SE) upon object fracture, disregarded in fact in present strength theories. This initiated the search of ways to depart from strong SE exhibition under dynamic loading and stimulated the study of dynamic reaction and composite shell fracture peculiarities under extreme pulsed loads.

In references /1,2/ strain and fracture of cylindrical glass-reinforced plastic shells including geometrically like ones, were experimentally tested. Shells, whose cavity was filled with water or air, were subjected to single and multiple loadings when the spherical explosive charges which are initiated at their geometrical centers. The measure of the shell specific load was a nondimensional parameter ζ - the ratio of explosive charge weight to the shell weight.

Experimental investigations permitted to determine the main features of dynamic reaction and glass-reinforced plastic shell fracture under extreme pulsed loading.

1. Shells deform elastically right up to the fracture. Elastic modulus (circumferential) of glass-reinforced plastic does not depend on the strain rate in the range of 10^{-1} - $1.5\cdot10^{3}$ 1/s.

For shells of different scales single dependences of maximum deformations and rates on ζ parameters were obtained, that is, the whole process of blast loading and dynamic reaction of shell in geometric simulation conditions is automodel.

2. Ultimate (on the fracture threshold) dynamic strain of axially symmetric shell tension in the first phase of expansion is $\gtrsim 4\%$ and does not depend on the pulsed loading nature (water or air medium filling the shell cavity), specific size (scale) and relative shell thickness.

3. Glass-reinforced plastic shells do not show appreciable sensitivity to defects. The existence of even rough defects (through-thickness cracks) in the shell does not result in considerable lowering of its strength by subsequent loading and in fact has no influence on the dynamic strain parameters.

4. The strength of glass-reinforced plastic shells under pulse loading is limited by dynamic compression strain. So, the shell cavity filled with water allowed the compressive strain restriction to $\lesssim 1\%$ and all the tested shells (with δ/R from 3.8% to 27%) did not lose their strength upon the strength up to 4%. If the shell vibrations would rather take place (the cavity filled with air) after pulse loading has occured, the shell loses its strength under significantly less strains ($\sim 2.5\%$ and $\sim 1.5\%$ at $\delta/R = 16\%$ and 5%), the fracture happening in the first or subsequent compressive phases and a relative shell thickness becoming an important parameter affecting its dynamic strength.

5. The dynamic strength of glass-reinforced plastic shells considerably depends on the loads number. The more intense strength reduction is observed by realization of free steel vibration. Thus, the increase of free shell pulsed loads number (from $\delta/R = 16\%$) up to 23 results in its breaking strain reduction by a factor of 2.5 (from 2.5% to 1%). In this case the logarythmic damping decrement of radial shell vibrations equal to ~ 0.05 with the first loading (at the strain level $\sim 1\%$), increases up to ~ 0.4 with the 20-th loading.

6. Glass-reinforced plastic shells have higher strength under blast loading compared with steel ones. This difference is particularly important for large-scale shells.

7. The development of the main-purpose structures, subjected to extreme pulse loading requires the sound knowledge of their safety margin. Unique character and high cost of the majority of such objects exclude the possibility of obtaining direct data on safety margin by reducing them to fracture. In this situation the extension of model test results to the full scale structures is possible only if reliable data on scale effects, disregard of which may cause the catastrophe, is present.

The nature of SE considering fracture (object separation) to be an act of work perform is a consequence of a more rapid growth of elastic tension energy EE in the object by its geometrically like enlargement compared with that of the work performed upon its fracture with the regard for this, the necessary fracture condition is particularly simple in writing for elastic strain region (where the left part is EE and the right one is the work performed by the object fracture):

$$\frac{\sigma^2 L^3}{2E} \geq A\lambda L^2 \qquad \sigma^2 \geq \frac{2E\lambda A}{L} \qquad (1)$$

where σ, E, λ, L and A are typical stress, material Young's modulus, specific fracture work per surface unit, typical object size, form and stressed state factor. For the two geometrically like objects the condition /1/ may be written as

$$\sigma_1/\sigma_2 = \sqrt{L_2/L_1} \qquad (2)$$

The results of some investigations by internal pulsed loading of geometrically like steel vessels and glass-reinforced plastic tubes are presented in Fig.1 and 2 in the process of their filling up with standard pressure air and water, respectively. Parameter τ is used as the quantity characterizing the loading rate (quasistatic pressure analogue).

Experimental results, given in Fig.1, showed that by filling vessels (tubes) with air the fifteenfold increase of vessels resulted in strong SE: the 15 reduction by a factor of 15.7 with a simultaneous transition of fracture into the elastic strain region. The similar increase of glass-reinforced plastic tubes by a factor of 9.3 accurate to the experimental error did not affect their strength in any way. The τ quantity remained invariable. When comparing the fracture of geometrically like vessels, that is high pressure boilers and glass-reinforced plastic tubes, filled with water, one can observe the analogous situation (see Fig.2).

What is the reason of the glass-reinforced plastic behaviour such as that? As has been emphasized above the main element of force in this material taking up load and responsible for the glass thread (fiber) of unalterable diameter (~ 10 μm). That is in formula (2) one and the same quantity - the glass thread diameter - must be adopted as the typical sizes L_1 and L_2. Really EE removed from the environment of the breakdown extended several thread diameters both with large and small objects, may be consumed to destruct (break-down) the thread. Then, according to (2) $\sigma_1 = \sigma_2$.

The conclusion of energic nature SE absence, responsible in some cases for unforeseen catastrophic fracture of objects made of steel is an important advantage of the discussed composite, but it does not rule out the possibility of statistical and technological manifestations of more weak compared with energetic SE of different nature.

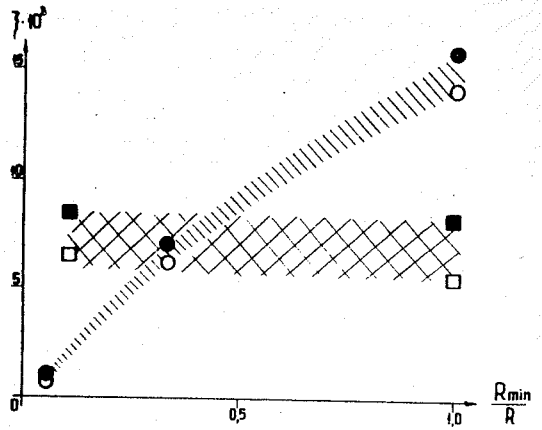

Fig.1. The strength geometrically like steel and glass-reinforced plastic shells filled with air as a function of scale (relative radius):

●●- steel 22 K, spherical vessels, δ/R=21.4%, R=50, 150, 750 mm, R_m=50 mm;

■■- glass-reinforced plastic tubes, δ/R=6%, R=75 and 700 mm, R_m=75 mm;

●■- fracture, ○□ - no fracture.

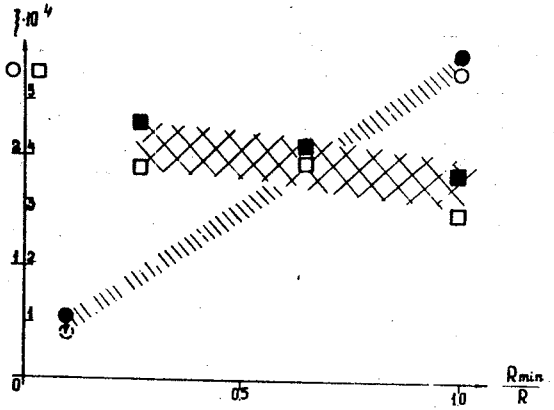

Fig.2. The strength of geometrically like steel and glass-reinforced plastic shells filled with water as a function of scale (relative radius):

●●- steel 22 K, elliptic high pressure boilers of different thickness, δ/R=10 ...20%, R=100 and 1000 mm; R_m=100 mm;

■■- glass-reinforced plastic tubes, δ/R=3.8%, R=100, 150 and 440 mm, R_m=100 mm;

●■-fracture, ○□ - no fracture.

The carried out review show significant advantages of glass-reinforced plastic in shell structures subjected to extreme pulsed loads.

References

1. Иванов А.Г., Новиков С.А., Синицын В.А., Цыпкин В.И. Прочность и разрушение материалов и простейших конструкций при интенсивных импульсных нагрузках. - Всесоюзн.межвузов. сб. Прикл. вопросы прочности и пластичности, Горький, 1985, вып.29, с.3-21.

2. Иванов А.Г., Цыпкин В.И. Деформация и разрушение стеклопластиковых оболочек при интенсивных импульсных нагрузках.- Механика композитных материалов, 1987, №3, с.475-487.

INVESTIGATION OF PRESSURE AND SHOCK COMPRESSION DURATION INFLUENCING THE RESISTANCE TO SPALL FRACTURE

S.V.Rasorenov, G.I.Kanel'

Institute of Chemical Physics, USSR Academy of Sciences, USSR

Spalling is a material failure produced by the action of tensile stresses developed in the interior of body, when two decompression waves collide /1,2/.

The most direct and authentic methods to determine the strength under conditions of spall fracture are those, based on continuous recording of velocity of free-surface samples /3/.

The samples of aluminium alloy AM$_2$6M, stainless steel X18H10T copper M2 and magnesium Ma1 1.8-15 mm-thick and more 80x80 mm^2 - cross size were loaded by the impact of flat projectiles 0.2-5 mm-thick or detonation explosive directly contacting the samples to change shock loading duration. In order to study the influence of shock compression amplitude on the spall strength the samples of aluminium alloys AM$_2$6M, AD1, titanium alloys BT5-1, BT8 and routine steel 4-10 mm-thick were loaded by aluminium plate 2 mm - thick with the impact-velocity from 660 m/s to 5300 m/s. The sizes of samples and impactors provided conditions of all experiments one-dimentioned.

A continuous recording of sample free surface velocity was carried with capacitor gauges /4/ or with the help of laser interferometer /5/. The time resolution of surface velocity growth in shock wave front is about 10 nc.

In the cases of aluminium and titanium alloys the temperature of unreversible shock heating of material after a shock compression and release under pick pressure reached 800 ^{o}K and 1100 ^{o}K, and summary deformation before the fracture was 65% and 50% accordingly.

Fig.1 shows a free-surface velocity - time profiles for titanium alloy BT5-1 samples 4 mm-thick. They were loaded by aluminium plates 2 mm-tnick, which have been accelerated to high velocities-660 m/s (1), 1900 m/s (2) and 5300 m/s (3) by explosive plane wave generators. The exit of elastic-plastic compression wave on free surface led to its rapid velocity growth. The further velocity drop is determined by the exit of rarefaction wave. A small precursor before the shock wave is caused by air wave before impactor (curve 3). Fracture of material by tensile stresses produces

further oscillations of surface velocity due to spall pulse appearance.

The measurement was not made under the peak impact velocity (5300 m/s) in aluminium samples, the pressure corresponded 64 GPa. The surface of loaded sample loses stability under this condition in the rarefaction wave because of aluminium melt /6/. The coefficient of light reflection is sharply decreased and data can't recorded.

The values of tensile stresses under spall condition σ^* were determined from the profiles of velocity W(t) as /7/:

$$\sigma^* = \frac{1}{2}\rho_o c_o(\Delta W + \delta W),$$

where ρ_o is initial density of material, c_o is sound velocity, ΔW is velocity difference between the first maximum and the first minimum, δW is the correction for the influence of elasto-plastic behavior of material.The values of spall strength under the same duration practically don't depend on the shock compression amplitude and were 4.16$\pm$0.06 GPa (6.5$\leq$P$\leq$77 GPa), for titanium BT8-σ^*=4.63$\pm$0.03 GPa (5.6$\leq$P$\leq$70 GPa), for aluminium alloys AM$_2$6M-σ^*=0.93$\pm$0.04 GPa (2$\leq$P$\leq$56 GPa), AD1-σ^*=0.85$\pm$0.05 GPa (3.3$\leq$P$\leq$44 GPa), and for routine steel-σ^*=2.9$\pm$0.1 GPa (6$\leq$P$\leq$90 GPa). The absence of the temperature influence on the resistance to dynamic fracture can be connected with the transition to activationless mechanisms of plastic deformation and fracture under high strain rates.

Fig.2 shows the results of the spall strength measurements under variation of shock wave duration and amplitude for alloy AM$_2$6M in the form a fracture stresses σ^* versus strain rate $\dot{V}/V_o$=-1/2 $\dot{W}_1/c_o$. In the boundary of the measurement error the experimental data is explained by the relationship:

$$\sigma^* = 0.093\ (\frac{\dot{V}}{V_o})^{0.2} \qquad (1)$$

The similar relationships were received for other metals /8/.

On the basis of the experimental data and the notions about incipient fracture by concentrator of stresses and by viscous growth of voids the semi-empiric kinetic relationship suitable for the calculations of spall fracture in wide range of shock loading parameters was obtained in form /9/

$$\dot{V}_T = K_1(|\sigma| - \sigma_o\frac{a}{V_T+a})(V_T + K_2\sigma^n)\ \mathrm{sign}\ (\sigma)\quad |\sigma| > \sigma_o\frac{a}{V_T+a}, \qquad (2)$$

where σ_0 is initial threshold of fracture between real break stress under static conditions and spall strength; $a \approx 0.01\ V_T$, K_1, K_2, n are constants. The initial fracture speed is $\dot{V}_T = K_1 K_2 \sigma^{n+1}$ and the constants n and the product of K_1 into K_2 can be obtained from the experimental relationship (1).

Fig.3 shows by the dashes calculated profiles of free-surface velocity, using a fracture kinetic in form (2). They are in good agreement with experimental profiles (continuous lines), thus a proposed fenomenological model of fracture provides a sufficiently good description of spall phenomena in wide range of strain rates.

Thus the value of spall strength increases less than two times under decrease of initial compression pulse duration by a factor of 100 and doesn't depend of loading intensity; the temperature and deformation before material fracture don't influence the spall strength value. It is determined, probably, by initial material state, that allows to construct a more simple models of material behavior under fracture.

The authors thank L.G.Ermolov, who made invaluable contributions to the experimental program.

References

1. Никифоровский В.С., Шемякин Е.И. Динамическое разрушение твердых тел. Новосибирск, Наука, 1979, 272 стр.
2. Meyers M.A., Aimone C.T. Dynamic fracture (spalling) of metals.-Progress in Material Science,1983,v.28, p.1-96.
3. Graham R.A., Asay J.R. Measurement of wave profiles in shock-loaded solids.- High Temperature-High Pressure, 1978, v.10, p.355-390.
4. Иванов А.Г., Новиков С.А. Метод емкостного датчика для регистрации мгновенной скорости движущейся поверхности. - ПТЭ, 1963, №1, стр.135-138.
5. Asay J.R., Barker L.M. Interferometric measurement of shock-induced internal particle velocity and spatial variations of particle velocity. -J.Appl.Phys., 1974, v.45, N6, p.2540-2546.
6. Бородулин С.А., Бричиков А.И., Волков К.В., Ольховский Ю.В. Рыбаков А.П. Рентгенографическое исследование процесса разлета легкоплавких металлов при выходе ударной волны на их свободную поверхность. - ФТТ, 1976, т.18, №9, стр.2814-2816.
7. Степанов Г.В. Откольное разрушение металлов в плоских упруго-пластических волнах нагрузки. - Проблемы прочности, 1976, №8, стр.66-69.

8. Канель Г.И., Разоренов С.В. Фортов В.Е. Откольная прочность металлов в широком диапазоне длительности нагрузки. - ДАН СССР, 1984, т.275, №2, стр.369-371.
9. Канель Г.И., Разоренов С.В., Фортов В.Е. Кинетика разрушения алюминиевого сплава АМг6М в условиях откола. - ПМТФ, 1984, №5, стр.60-64.

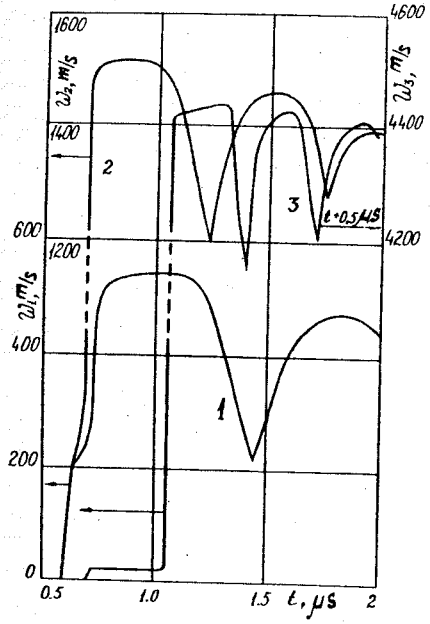

Fig.1. Free surface velocity-time profiles for titanium BT5-1. Zero time indication is the moment of impact, for curve 3 the time was increased by 0.5 μs.

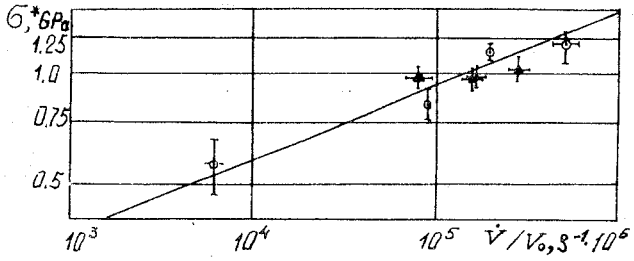

Fig.2. The depending of aluminium AM26M spall strength versus the strain speed under duration (⊙) and amplitude (▲) change on initial compression pulse.

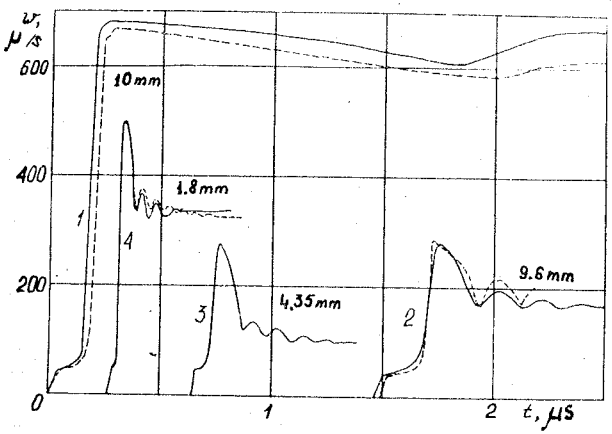

Fig.3. Profiles of free-surface velocity W(t) for aluminium samples AM26M under of pulse duration change. The conditions of loading were: explosive plate generator (1), impactor 0.4 mm-thick (2) impactor 0.19 mm thick (3,4).

TRANSPORT PROPERTIES OF NON-IDEAL GAS-PLASMA MIXTURES

N.N.Kalitkin, P.D.Shirkov
M.V.Keldysh Institute of Applied Mathematics, Moscow, USSR

High-pressure plasma is formed in capillary discharges, strong shock waves etc. Such plasma contains many components for molecular substance: moleculas, atoms of different elements, their ions and electrons. The charged particles interaction leads to strong non-ideality of plasma.

1. Transport coefficients calculations in such plasma need firstly to find plasma's composition, i.e. to solve the system of chemical and ionization equilibrium equations with non-ideality correction for ionization potentials. Extra-fast algorithms, which demand less than 200 arithmetic operations of any essential component of mixture and allow to use the same formulas for calculations in wide region of temperature and density, were developed /1/ for solving this problem. Those algorithms are based on: a) the range lowering of initial algebraical system; b) non-interrupting variables secretion and their beginning approximation; c) an effective iterative method using.

For real mixtures the lowering of the range of system for more than an order can be obtained by exclusion of the equilibrium reactions expressions from initial system of plasma composition.

Concentrations of ions with prevail charges in mixture are non-interrupting variables. The charges of prevailing ions and their beginning approximations for iterative method are defined by thermodynamic co-ordinated d e c o m p o s i t i o n model (CDM) /2/. This model have a 3% accuracy in the region of its physical application and allow to compute the chemical and ionization equilibrium by obvious formulas.

The iterative method based on decomposition of nuclear balance equations from charge balance equation /1/. In this case no more than 13 outside iterations by ionicity and 1-2 inside Newton's iterations by concentrations of prevail ions are required for composition calculation (for example, of nitrogen-oxygen mixtures) with 0.01% accuracy in wide region of temperature and density changing.

Those algorithms allow to use in calculations: a) molecular

and electronic energy levels excitations in particles; b) ionic potentiales correction and statistical summes limitation by charged particles interactions.

2. Semiclassical theory /3-5/ is good for electronic conductivity description in classical plasma with any non-ideality. This theory is based on linear Boltzmann equation for electrons and only use two-body interactions.

Charged particles scattering is described by Debay pseudopotential. Their cross-sections is calculated by quantum-mechanics rules, interference is allowed for electron-electron scattering (the first Born's approximation is enough for accuracy and use simple formulas). In contrast to classical theories (such as Spitzer theory, for example), there is no any integral divergencies in this case.

It is necessary to solve linear Boltzmann equation with accuracy. Well-known Chapmenn-Enskog method is more economical; usually already III-IV approximations gives errors less than 1%. However, there are some examples of bad convergence for this method. It is useful to take problem to Fredholm integral equation with one variable and then solve it with difference schemes /6/.

Electronic conductivity and electronic component of heat conductivity depend on scattering parameter $b=8D^2T$ (D-Debay's radius) for fully-ionized plasma, but not on non-ideal parameter $\Gamma=(DT)^{-1}$, which is always used in classical theories. The Fig.1 shows the coincidence of this theory with some expirements and other author's theories; it is obviously, that this theory is single which describes transport properties of plasma with strong non-ideality.

3. New method /7/ for reactive heat conductivity calculation of equilibrium mixture was developed in bound of kinetic theory. This method more fully describes processes of energy transmission by chemical reactions, particles dissociations and ionizations of mixture, excitations of their moleculas and electronics levels.

This method is less-labour-consuming than previously known. It based on gradients of concentration of mixture components definition; these gradients are calculated immediately from chemical and ionic equilibrium system. It's necessary to solve the linear equations system, which order is equal to quantity of elements from periodical table, compounding the mixture.

The Fig.2 shows the coincidens of such method with expire-

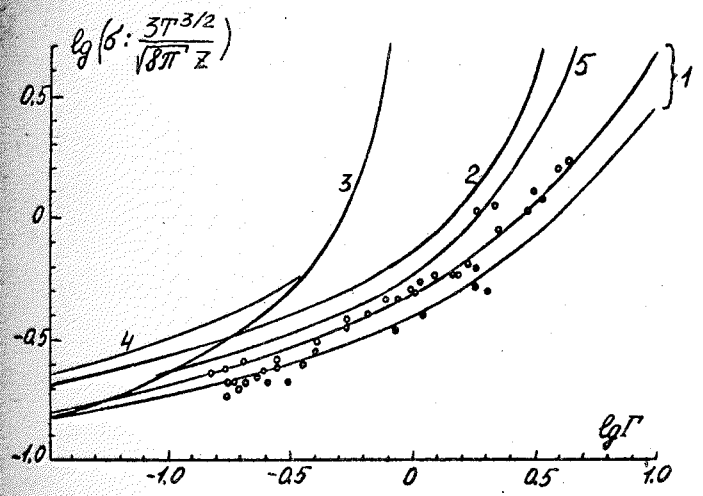

Fig.1. o - expirements of different authors: 1 - given theory for T=25000 K and T=12600 K; 2 - Spitzer; 3 - Gould, De Witt; 4 - Kihara, Aono; 5 - Dremin, Fortov.

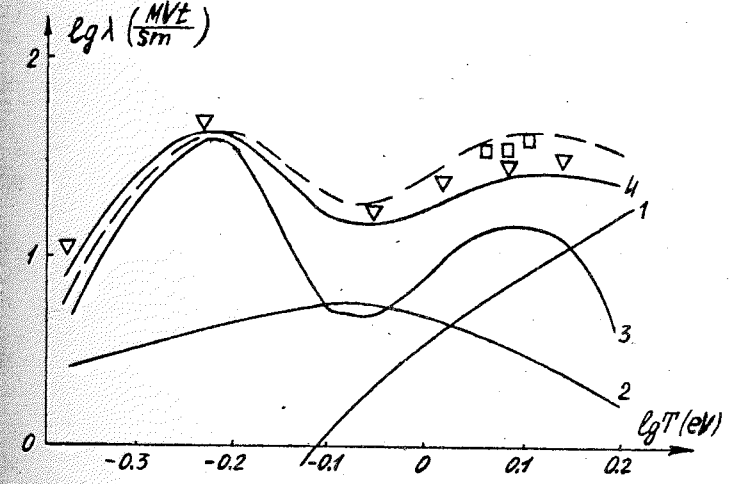

Fig.2. Heat conductivity and it's components of low-temperature nitrogen plasma for P=1 atm - given calculation: 1 - electronic component, 2 -conductive components, 3 - reactive component, 4 - their sum ; - - - Devoto calculation; expirements: □ - Asinovsky and ..., ▽ - Hermann, Schade).

ments and estimations of other authors for heat conductivity of nitrogen plasma.

References

1. Ritus I.V., Shirkov P.D. - preprint, Inst.Appl.Mathem., the USSR Academy of Sciences, 1986, n.118.
2. Shirkov P.D. - preprint, Inst. Appl. Mathem., the USSR Academy of Sciences, 1987, n.131.
3. Kalitkin N.N. - J. of High-Temperature Thermophysics, 1986, v.6, n.5 - 801 p.
4. Rogov V.S. - J. of High-Temperature Thermophysics, 1970, v.8, n.4 - 689 p.
5. Ermakov V.V., Kalitkin N.N. - J. of Plasma Physics, v.5, n.3, - 650 p.
6. Voloschenco O.A., Kalitkin N.N. - preprints, Inst. Appl. Mathem., the USSR Academy of Sciences: 1981, n.155; 1981, n.113; 1983, n.58.
7. Rogov V.S., Shirkov P.D. - Communication of the Joint Institute for Nuclear Research, Dubna, 1982, P5-82-293.

INTERACTION OF A LASER BEAM WITH A HIGH PRESSURE PLASMA AND SHOCK COMPRESSED SILICON

Yu.B.Zaporozhets, V.B.Mintsev

Institute of Chemical Physics, USSR Academy of Sciences, USSR

The experimental results of the laser beam (λ = I.06 μm) reflection from dense xenon plasma at high pressures and shock compressed silicon at a semiconductor-metal transition region are presented. Reflection characteristics and possibility of the estimation of the electron properties of the substance under high pressure are discussed.

Generation of the chosen states was carried out by the method of the shock wave compression and heating of the substance. Experiments were performed with the explosively driven generator of rectangular shock waves /I/. Laser beam was introduced into the explosive chamber with the aid of the special optical system and was fixed after reflection from the sample by the photomultipliers provided with the interference filters ($\Delta\lambda$= 200 A). The specific power of the laser beam was varied in the range 10^3-10^5 W/cm^2. Optical reflectivity factor R was determined by comparison of the probe and reflected radiation collected by the ring lens. In order to determine the parameters of the substance under shock compression the speed of the striker and the shock wave speed in the sample were measured in every experiment.

Measured values of the nonideal xenon plasma reflectivity are shown in Fig.I /2/. Measurements were carried out at pressures from I.6 GPa up to I7 GPa and plasma densities from 0.5 g/cm^3 up to 4 g/cm^3. Strongly heated ($T\sim 3\cdot 10^4$ K) plasma with considerable Coulomb interaction ($\Gamma = e^2 kT/r_D$ = 2-7) is realized under these conditions. For λ = I.6 μm electron density is higher than the critical one $n_c = 10^{21} I_{cm}^{-3}$ (look at the arrow in Fig.I). The three-dimensional structure analysis of ionizing shock wave shows /3/, that the photoionization of cold gas doesn't influence the emission propagation. Avalanche thermal ionization kinetics causes shock front three-dimensional structures with characteristic sizes I-2 orders of magnitude less than the laser wave length. These circumstances justify the employment of Frenel's equation: $R = \left|\frac{\sqrt{\varepsilon}-I}{\sqrt{\varepsilon}+I}\right|^2$, where ε - complex dielectric constant $\varepsilon = I - \frac{4\pi\sigma}{\omega}$. To estimate high frequency conductivity σ experimental data on static conductivity σ_0 /I/ of xenon plasma were used. The curve I

in Fig.I is calculated with the Drude's formula $\sigma = \sigma_0 (I - i\omega/\nu)^{-1}$. The curve 2 is the extrapolation to the high frequency region of the integral relation $\sigma \sim \sigma_0 \int (\nu - i\omega)^{-1} v^3 (-\frac{\partial f}{\partial v}) dv$, which describes high frequency conductivity more accurately in the case of the strong dependence of the electron collision frequency on the electron energy. The divergence of the theory and the experiment at low densities appears to be the indication of the existence of the additional mechanism of the electron scattering. It may be the scattering on thermal plasma vibrations /4/(curve 3). To estimate the value of the collision frequency the calculations at ν/ω = const approximation were made (dotted line in Fig.2). It's seen that the best agreement with the experimental data can be obtained at $\nu/\omega = 2$.

To explore silicon reflectivity we use p-type monocrystals with the specific resistance 40 Ohm·cm, thickness I.5 mm, diameter I5 mm. The lower side of the sample was cut out perpendicular to the [III] direction, while the upper side, to remove interference effects, was cut out at the angle 2.5° to the lower side.

The typical oscillograph record is shown in Fig.2. The initial radiation intensity I_0 corresponds to the laser beam reflection from the upper and the lower sides of the silicon crystal and polished culet. The shock wave having gone into the sample (moment t_0) laser beam reflection from the lower side disappears. Intensity I_I corresponds to the reflection from the upper side only (R ~ 30%). When the plastic waves reach the free surface (moment t_I), reflected radiation intensity increases up to the value I_2. Silicon reflectivity conserves during several microseconds up to the moment, when the temperature noise emission of the air shock waves masks reflected radiation.

Unloading silicon reflectivity versus shock wave pressure is presented in Fig.3. It is seen that silicon conserves its initial reflectivity R~30% at P≈I0 GPa. Over the pressure range P~I5-I8 GPa the reflectivity abruptly increases up to the value R~80%. The results of the silicon conductivity measurements obtained in dynamic (curve I) and static (curve 2) experiments are shown in Fig.3 also. We use these data for silicon reflectivity estimation (curve 3). It is seen that there is reasonable agreement with our experiment. This fact allows to determine the lower limit of the static conductivity values of the silicon in our conditions $\sigma_0 \geq 2 \cdot 10^4$ Ohm^{-1}cm^{-1}.

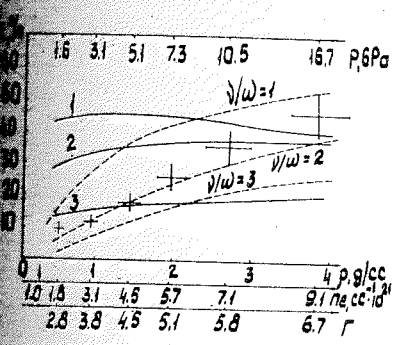

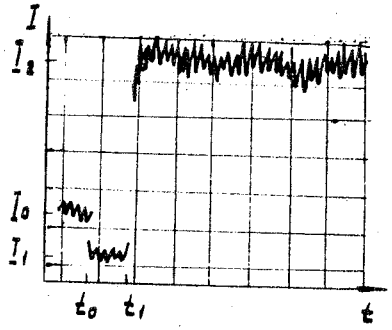

Fig.I. Xenon plasma reflectivity vs. plasma density.

Fig.2. Typical oscillograph record.

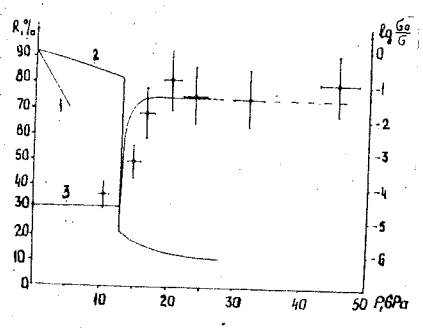

Fig.3. Unloading silicon reflectivity vs shock pressure.

Presented results show, that the silicon metallic phase with the charge carriers concentration $n \gtrsim 10^{21} cm^{-3}$ is formed under shock wave compression at $P \gtrsim 15$ GPa. This phase either conserves after adiabatic unloading, or transforms to a new metallic type phase.

References

1. Фортов В.Е., Якубов И.Т. Физика неидеальной плазмы. 1984.
2. Запорожец Ю.Б., Минцев В.Б., Фортов В.Е., Батовский О.М. Отражение лазерного излучения от ударно-сжатой плазмы ксенона высокого давления. Письма ЖТФ, 1984, т.10, №21, с.1339-1343.
3. Зельдович Я.Б., Райзер Ю.П. Физика ударных волн и высокотемпературных гидродинамических явлений. М.: Наука, 1966.
4. Валуев А.А., Куриленков Ю.К. Электропроводность плазмы в широком диапазоне плотностей зарядов. Теплофизика высоких температур, 1983, т.21, №3, с.591-594.
5. Запорожец Ю.Б., Минцев В.Б., Фортов В.Е. Образование металлической фазы при сжатии кремния ударными волнами. В сб.: Химическая физика процессов горения и взрыва. Детонация и ударные волны. 1986, с.82-85.

ON THE COMPRESSIBILITY OF CONDENSED GASES IN THE MEGABAR PRESSURE RANGE

A.P.Kalinin[1], V.B.Leonas[1], I.D.Rodionov[2], I.P.Rodionova[2]

[1]The Institute of Problems in Mechanics, Academy of Sciences of the USSR, Moscow, USSR

[2]M.V.Keldysh Institute of Applied Mathematics, Academy of Sciences of the USSR, Moscow, USSR

This paper is an attempt to fill the gap in the data on the megabar pressure range compressibility of condensed gases. The calculation of the data is based on reliable interatomic potentials V(R). The latter in turn were obtained from high energy molecular beam small angle scattering measurements. The conventional methods of compressibility determination (a shock-wave compression, an isentropic compression, a diamond anvil static compression) do not give reliable information on the low temperature (T=0,K) compressibility for the pressures P higher than 0.5 - 1 Mbar. At the same time the applicable theoretical models are well justified under the highest pressure and require for the independent check at the megabar pressure range. In this paper the results for helium and hydrogen are presented and discussed.

The high energy beam scattering data (reduced differential scattering cross-section $\rho(\tau)$ and integral cross-section $Q(\tau)$) Fig.1), were measured using the experimental set up for fast beam small-angle study. The measured ρ, Q vs τ dependences were inverted to derive the short range pair interaction potentials. By combining them with the thermal range measurements data we proposed the potentials covering the energy range 0.1-20 eV (Fig.2).

These potentials are compared with the available effective ones as obtained from the shock compression measurements /1,2/ and several empirical potentials /3, 4, 5/ (Fig.3). The close agreement of the effective potentials for He-He, H_2-H_2 from /1/,/2/ with our pair potentials allows to make an important conclusion that many-body interaction effect doesn't play a significant role in the investigated pressure range ($P \lesssim 1$ Mbar). This conclusion contradicts to the one made in /6/.

The potentials obtained in present work were used to calculate the high pressure compressibilities for a number of condensed gases. In this calculation we assume that for $P \gtrsim 0.5$ Mbar the structure can be taken as corresponding either to a close-packed

hexagonal or face-centered cubic lattice and that in order to find the energy of crystal E_t it is enough to perform summation over the pairs of N atoms within the first coordination sphere. Thus the total energy per one molecule is equal

$$E_t = \frac{1}{2N} \sum_{i \neq j}^{N} V(|R_i - R_j|) = 6\, V(d) \qquad (I)$$

where $d = 1.124\, V^{1/3}$ is the nearest neighbour distances, V - the single atomic cell volume. The assumption on the energy additivity (I) can be justified only when comparing with the independent data available. The (T=0,K) compressibility can be calculated from the formulae $P = -\partial E / \partial V$.

The calculated T=0, K compressibility curves for condensed He and H_2 as based on the empirical pair potentials of the present work are shown in Fig.3. For the comparison the other theoretical and experimental data are depicted in Fig.3 as well. For both the high and submegabar pressures these comparison displayed a gratifying close agreement between our calculated and independent compressibility data.

In summary, we have shown that the many-body interaction effect play negligible role in the discussed pressure range and it is possible to calculate the compressibility of condensed gases in the megabar pressure range on the bases of the pair interaction potentials. It is noteworthy that analogous agreement were obtained in the cases of neon, xenon, nitrogen, carbon oxide studied as well.

References

1. Ross M., Young D.A. Equation of state and melting curve of helium at high density //Phys.Rev.Let.A, 1986, v.118, n.9, p.463-466.
2. Ross M., Ree F.H., Young D.A. The equation of state of molecular hydrogen at very high density //J.Chem.Phys. 1983, v.3, p.1487-1497.
3. Feltgen R., Kirst H., Kohler K.A., Pauly H. Unique determination of the He_2 ground state potential from experiment by use of a reliable potential model //J.Chem.Phys.1982, v.76, N5, p.2360-2372.
4. Foreman P.B., Rol P.X., Coffin K.P. The repulsive $^1\Sigma_g^+ He_2$ potential obtained from total cross section //J.Chem. Phys. 1974, v.61, n.5, p.1658-1665.
5. Norman M.J., Watts R.O., Buck U. A spherical potential for hydrogen from solid state and scattering data /J.Chem.Phys. 1984, v.81, n.8, p.3500-3509.

6. Nellis W.J., Holmes N.C., Mitchell A.C. et al. Shock compression of liquid helium to 56 GPa (560 kbar) //Phys.Rev. Lett. 1984, v.53, n.13, p.1248-1251.
7. Калиткин Н.И., Кузьмина Л.В. Кривые холодного сжатия при больших давлениях// Физика твердого тела, 1971, т.13, №8, с.2314-2318.
8. Никифоров А.Ф., Новиков В.Г., Уваров В.Б. - в книге :Вопросы атомной науки и техники . Сер.: методика и программы численного решения задач математической физики, М., ЦНИИатоминформ, 1979, вып.4(6), с.16-26.
9. Григорьев Ф.В., Кормер С.Б., Михайлова О.Л. и др. Уравнение состояния молекулярного водорода. О фазовом переходе в металлическое состояние //Журнал экспериментальной и теоретической физики, 1978, т.75, вып.5, №11, с.1683-1692.
10. Silvera I.E. New Phases of Molecular and Atomic Hydrogen under Extreme Conditions //Europhys.News, 1982, v.13, p.4-6.

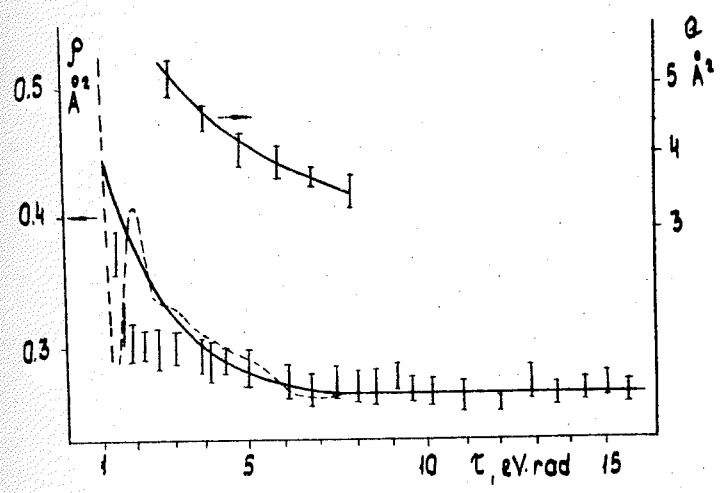

Fig.1. Reduced differential $\rho(\tau)$ (beam energy E=600 eV) and integral $Q(\tau)$ (beam energy E=600÷1600 eV) cross sections for He-He system. The experimental results are shown by vertical bars; solid line - the values calculated classically for the potentials proposed in this work; dot-line - the values for the quantum mechanical calculation.

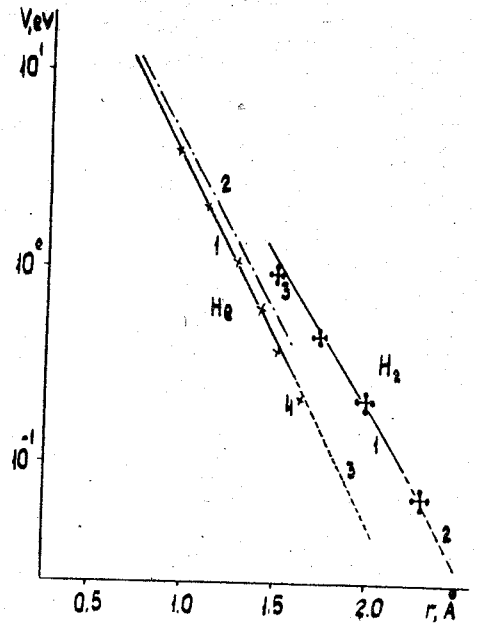

Fig.2. The interaction potentials for He-He and H_2-H_2: I - this work; 2 - thermal beams /3/, /5/; 3 - effective potentials from shock-wave experiments /I/,/2/; 4 - high energy beam /4/.

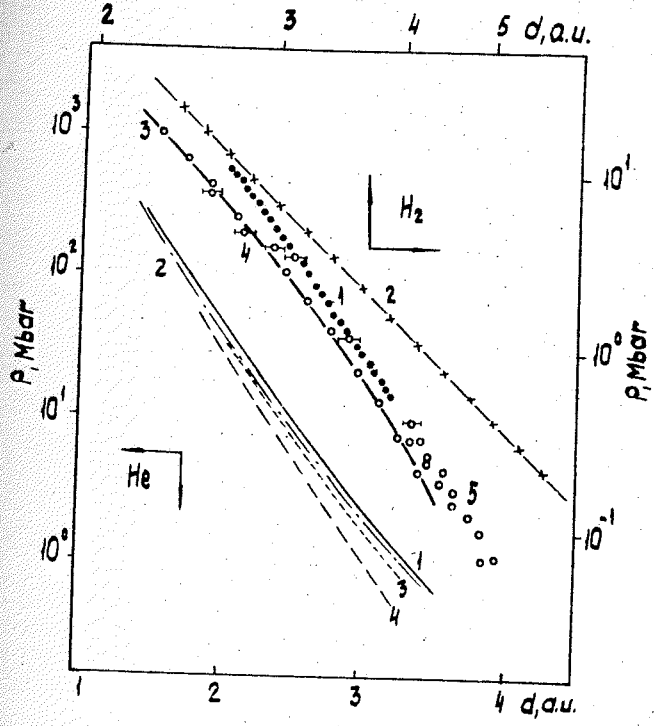

Fig.3.The zero-temperature compressibility of condensed helium and molecular hydrogen. He: I - on the basis of potentials from this work; 2 - from /7/; 3 - from /6/; 4 - from /8/. H_2 : I - on the basis of potentials from this work; 2,3 - from /7/; 4 - from /9/; 5 - from /5/, /IO/.

THERMAL EXPANSION, GRÜNEISEN PARAMETER AND DEBYE TEMPERATURE OF COESITE, STISHOVITE AND PERICLASE

A.M.Doroshev, V.M.Galkin, G.N.Kuznetsov
Institute of Geology and Geophysics, Novosibirsk, USSR

The knowledge of the thermal expansion of high pressure minerals is fundamental both in theoretical and experimental approaches to the clarification of the equation of state of the Earth interior. Adequate representation of the thermal expansion data as a function of temperature is necessary to provide the interpolation between the temperatures of the measurements and for the aim of high and low temperature extrapolation.

The use of equations formulated as power series in temperature for the representation of the temperature dependence on the thermal expansion is of common practice. However, similar expressions of thermal expansion may not be appropriate to predict or to extrapolate the expansion at the temperatures out of the measured range. It is desirable to use the equation based on the theory of thermal expansion to minimize the errors in such extrapolation.

Theory and calculation procedure. One of the objectives of the present work is to develope a new method of approximation of thermal expansion data based on the connection between thermal expansion and heat capacity by the thermodynamical value of Grüneisen parameter. In order to express heat capacity as a function of temperature with few unknowns we use Debye representation in the form $C_c=3R\nu D$ where D is defined by

$$D=3(T/\theta)^3 \int_0^{\theta/T} \frac{x^4 e^x}{(e^x-1)^2}\, dx, \qquad (1)$$

R is the gas constant; ν is the number of atoms in the molecule formula; θ is the Debye temperature. By substituting the equation for the heat capacity into Grüneisen relation $\gamma=\alpha K_T V/C_V$ and integrating it we obtain

$$V_T = V_{To}+3R\nu \int_{To}^{T} \frac{\gamma D}{K_T}\, dT, \qquad (2)$$

where K_T is the isothermal bulk modulus. To set up the function under the integral as a temperature function we specify Grüneisen parameter as $\gamma_T=\gamma_{To}(V_T/V_{To})^q$, (3)

where $q=[(\partial \ln\gamma)/(\partial \ln V)]_T$. The Debye temperature θ is considered to be only a function of volume ($\gamma=d\ln\theta/d\ln V$). Using Eq.3 Debye temperature is represented as

$$\theta_T=\theta_{To}\mathrm{EXP}((\gamma_{To}-\gamma_T)/q) \qquad (4)$$

Temperature dependence of K_T is evaluated from thermodynamical identity

$$(\partial K/\partial T)_p = -\alpha K_T(\partial K/\partial P)_T \qquad (5)$$

Taking the derivative $K'=(\partial K/\partial P)_T$ as constant upon integration of (5) we have

$$K_T=K_{T_o}(V_{T_o}/V_T)^{K'} \qquad (6)$$

After substituting Eq.(1), (3), (4) and (6) into (2) within the scope of the approximation (3) and (6) we have the precise expression of molar volume as a function of T, V_{T_o}, γ_{T_o}, θ_{T_o}, K_{T_o}, K' and q

$$V_T=V_{To}\,(1+\varphi\int_{To}^{T} D\,(1+\varphi\int_{To}^{T} D\,dT)^{K'+q}\,dT), \qquad (7)$$

where $\varphi=3R\nu\gamma_{To}/K_{To}V_{To}$

The fitting parameters to be calculated from a set of equations (7) are of explicit physical meaning: V_{To} = molar volume; γ_{To} = Grüneisen parameter; θ_{To}=Debye temperature. To define the unknowns the least squares technique and iteration procedure have been used on the truncated Taylor's series expansions of the function (7).

Experimental procedure. The phases under study were synthesized from analytical oxides. Coesite was produced at 1300 K, 5 GPa for two hours and stishovite was prepared at 1600 K, 12 GPa.

Thermal expansion was measured by the powder diffraction method using an X-ray diffractometer "DRON-3" equipped with heating and cooling systems and Cu radiation. Reflections used for the determination of the unit cell dimensions were obtained at a scanning speed at 1/4 or 1/2 per minute, using silicon as an internal standard.

Results. To check the accuracy of the measurements, thermal expansion of periclase was measured. The volume thermal expansion

data obtained for MgO in the range from 96 to 650 K were found to agree with that obtained by different methods /2,5/ within 0.05%.

Unit cell parameters of coesite and stishovite were determined in the same temperature range. Changes in the lattice parameters were fitted well with second degree of polynomials (Table 1).

Table 1. Coefficients for the equations $F=X_o+X_2T+X_2T^2$ relating unit cell parameters and temperature

$F/_X$	X_o	$X_1 \times 10^6$	$X_2 \times 10^8$	$\alpha(298) \times 10^6$
		C o e s i t e		
a,Å	7.1357(3)	5.3788(16)	2.4127(21)	2.77
b,Å	12.3678(4)	2.5679(26)	2.2133(36)	1.27
c,Å	7.1726(3)	-3.4116(17)	1.2061(23)	0.53
β,deg	120.355(1)	-50.94(32)	-19.743(44)	-0.14
V,cm^3/mol	20.5595(16)	13.2835(99)	-19.3681(14)	6.25
		S t i s h o v i t e		
a,Å	4.1777(4)	-6.2(3.4)	4.04(6.8)	4.27
c,Å	2.6661(5)	-8.6(4.1)	2.47(82)	2.28
V,cm^3/mol	14.0109(33)	-85.(29)	4.0(6)	10.8

Thermodynamical properties of the phases under study derived from Eq.(7) are listed in Table 2.

Table 2. Thermodynamical properties of periclase, coesite, stishovite

	Periclase	Coesite	Stishovite
K_S(GPa)	162.8 /1/	96.0 /3/	316.0 /4/
K'	3.8 /1/	8.4 /3/	4
q	1	1	1
V(cm^3/mol)	11.2478	20.5804(4)	14.0228(9)
γ	1.495(6)	0.303(15)	1.441(56)
θ (K)	750(18)	1021(68)	1169(82)
$\alpha_V(\times 10^6 K^{-1})$	30.78	6.25	12.62

The Debye temperatures of the phases obtained from the thermal expansion data agree with those calculated from heat capacity.

References

1. Sumino Y., Anderson O.L., Suziki I. Temperature coefficients of elastic constants of single crystal MgO between 80 and 1300 K. -J.Phys.Chem.Minerals, 1983, v.9, N.1, p.37-47.
2. Suziki I. Thermal expansion of periclase and olivine, and their anharmonic properties. - J.Phys.Earth, 1975, v.23, pp.145-159.
3. Levien L., Prewitt C.T. High pressure crystal structure and compressibility of coesite. - Amer.Mineral.,1987, v.66, pp.324-333.
4. Weidner D.L., Bass J.D. The single crystal elastic module of stishovite.- J.Geoph. Res., 1982, v.87, pp.4740-4746.
5. White G.K., Anderson O.L. Grüneisen parameter of magnesium oxide. - J.Appl. Phys., 1966, v.37, No1, pp.430-432.

VISCOSITY OF COPPER IN SHOCK WAVE FRONT

O.R.Osipova[1], S.V.Rasorenov[2]
[1]Institute of High Temperatures, Moscow, USSR
[2]Department of the Institute of Chemical Physics of the USSR Academy of Sciences, USSR

At deforming velocities to $10^3 s^{-1}$ the strain of metal flow is described by log dependence /1,2/.

$$\tau_T = \tau_{Tc} + \alpha \ln(\dot{\gamma}/\lambda) \qquad (1)$$

where τ_{Tc} is the flow strain at quasi-static deformation; $\dot{\gamma}$ is the deformation velocity; α, λ are the constants of the material. For analysis of impact wave evolution in metallic materials information is needed about resistance to deformation at more higher values of $\dot{\gamma}$. Extremal high velocities of deformation are developed in the impact wave front. Investigations of impact wave structure give information of material properties at $\dot{\gamma} >> 10^3 s^{-1}$. In this paper measurements of impact wave front width with an intensity to 10 GPa are carried out and copper viscosity is estimated at deformation velocities to $10^7 s^{-1}$.

Evaluation of impact wave front width with an intensity of >4 GPa have been carried out by determining the pressure pulse transmission completeness in Al barriers of different thickness. Al foils of a thickness of 7 to 200 μm were rolled on the polished surface of a copper specimen of 12 mm thickness. The velocities of foil barriers in vacuum impacted by an impact wave in the specimen were measured. As it is shown by simple analysis of wave interactions in coordinates pressure p - mass velocity u the Al barrier gains a higher velocity than the copper specimen surface because of dynamic elastance difference. However, if the barrier thickness is comparable with the impact transition width or is less than it the barrier velocity decreases on the contact boundary because of free surface influence on the process of impact wave reflection /3/.

Dependence of foil barrier velocity w on their thickness δ is obtained by using electro-contact transducers. Measurements showing experimental data spread are given in Fig.1 for an impact wave with amplitudes 6.6 and 10 GPa (solid curves). The experimental results demonstrate the velocity decrease of the foil barrier with decreasing in its thickness.

To determine copper elasticity characteristics a numerical

simulation of conducted experiments was carried out. The equation system describing mass conservation laws and the quatity of solid compressed medium was solved by the through technique according to the "cross" diagram in Lagrange /4/ coordinates, and we used the equation of medium condition, Hooke's law for the deviation component of the strain voltage tensor and the contact between voltage flow and elastic shear velocity.

$$\begin{aligned}
&\rho_0 \frac{\partial V}{\partial t} - \frac{\partial u}{\partial t} = 0,\\
&\rho_0 \frac{\partial u}{\partial t} + \frac{\partial \sigma_x}{\partial h} = 0,\\
&\sigma_x = p(V) + 4/3\tau,\\
&\frac{\partial \tau}{\partial t} = G(p)\left(-\frac{1}{V}\frac{\partial V}{\partial t} - \dot{\gamma}(\tau)\right),\\
&G = \frac{V}{V_0}\left(G_0 + 6b\,\frac{1-2\nu}{1+\nu}p\right).
\end{aligned} \qquad (2)$$

Here ρ_0 is the material density in the initial state; V is the specific volume; σ_x is longitudinal normal voltage stress; τ is maximum shear stress; c_0, b are linear expression indices for material impact adiabat; G is shear modulus; $\dot{\gamma}$ is maximum deformation velocity; ν - Poisson's factor. Stress and deformation are assumed positive under compression. According to /5/ for copper $\rho_0 = 8.93$ g/cm^3, $c_0 = 4$ km/s, $b = 1.5$; for Al $\rho_0 = 2.71$ g/cm^3, $c_0 = 5.34$ km/s, $b = 1.36$. Sound velocity measurements give for copper $G = 28.5$ GPa, $\nu = 0.407$; for Al $G = 22.7$ GPa, $\nu = 0.366$.

During numerical solution of the system (2) splitting due to physical processes was applied. At first mass velocity value changes, specific volumes and stresses at frozen elastic deformation, then stress relaxation as a result of elastic deformation at fixed values of specific volumes have been calculated on every time layer. As for determination of the structure of an impact wave a rather tiny step along the coordinate (≈1mm) must be used, the calculation was carried out within the boundaries of the mobile analytical layer, moving together with the impact wave. The analytical layer width varied in the process of calculation and in all cases it was chosen large enough to provide final parameter establishment behind the impact wave and to exclude influence of its boundaries on the reflection wave processes on contact and free surfaces.

Relationship of $\dot{\gamma}(\tau)$ is required and in some ranges it varied in the calculation. As the initial one we used the relationship (1) with indices $\alpha = 2$ MPa, $\lambda = 3 \cdot 10^{-3} s^{-1}$, determined according to the results of analysis of copper hardening curves in the range

of deforming velocities 10^{-3} - 10^{3} s^{-1}, shown in /6/. According to those data the quasi-static flow stress was determined as

$$\tau_{TC} = \beta\sqrt{\dot{\gamma}}$$

where β = 200 MPa. Preliminary calculations showed that when using the given indices in (I) the elastic impact wave front width appeared to be less than I μm, that is much lower than the results of estimations according to experimental data available. Thus dependence of elastic deformation velocity on stress for $\tau<\tau^*$ is described by the relationship (I), and for $\tau>\tau^*$ by the relationship

$$\dot{\gamma} = (\tau - \tau_0)/\eta_\ell$$

Values of τ^*, τ_0 are determined from the equations of stresses and their derivatives at the dead sector place.

Fig.I shows gained from calculation of dependence of Al barriers velocity on their thickness for impact waves with intensities of 6.6 and I0 GPa in copper (dashed curves). Values η_ℓ are given at curves in Pa·s. Analysis of preliminary calculation results showed that Al barrier velocity depends essentially on accepted parameter values of its elastic plastical deformation. In all cases the calculated relations $w(\delta)$ are arranged the lower the more resistance to Al deformation is assumed.

Comparison of calculated and experimental dependences $w(\delta)$ presumes to evaluate the values of viscosity endurance η_ℓ. For an impact wave with an amplitude of 6.6 GPa the η_ℓ value is near I0 Pa·s, for I0 GPa - 5 Pa.s.

These values in order of magnitude are in good accordance with the evaluation results (≃20 Pa·s) obtained from pore widening analysis when copper is chipped off /8/. At the same time in /9/ the upper evaluation of copper viscosity in impact waves (≃300 Pa·s) is significantly overestimated.

The authors are thankful to L.G.Ermolov for assistance in preparation and conducting of the experiments.

References

I. Campbell J.D. Dynamic plasticity: Macroscopic and microscopic aspects. - Mater.Sci. and Eng., I973, v.I2, N I, p.3-I5.

2. Rosenfield A.R., Hahn G.T. Numerical descriptions of the ambient low-temperature and high-strain rate flow and fracture behavior of plane. - ASM, I966, v.59, N 3, p.962-985.

3. Разоренов С.В., Канель Г.И. Измерение ширины фронта ударной волны в меди. - В сб.: Механика быстропротекающих процессов. Новосибирск: Наука, I984, с.92-97.

4. Самарский А.А., Попов Ю.П. Разностные схемы газовой динамики. - М.: Наука, I975, 350 с.

5. Маккуин Р., Марш С., Тейлор Дж. и др. Уравнение состояния твердых тел по результатам исследований ударных волн. - В сб.: Высокоскоростные ударные явления. М.: Мир, I973, 533 с.

6. Полухин П.И., Гук Г.Я., Галкин А.М. Сопротивление пластической деформации металлов и сплавов. Спр. - М.: Металлургия, I983, 35I с.

7. Gilman J.J. Resistance to shock-front propagation in solids.- J. Appl. Phys., I979, v.50, N 6, p.4059-4065.

8. Голубев В.К. О расширении пор в пластических металлах при отколе., ЖПМТФ, I983, № 6, с. I59-I65.

9. Chhabildas L.C., Asay J.R. Rise-time measurements of shock transitions in aluminum, copper and steel. - J. Appl. Phys., I979, v.50, N 4, p.2749-2756.

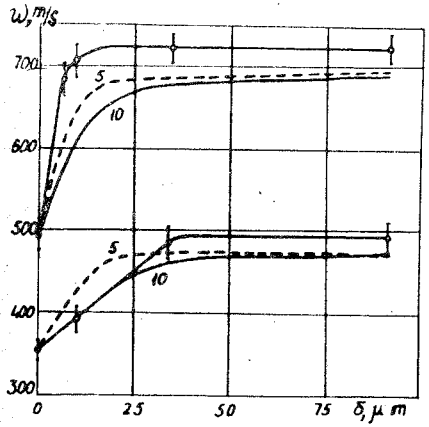

Fig.I. Dependence of foil barrier velocities on their thickness for impact waves.

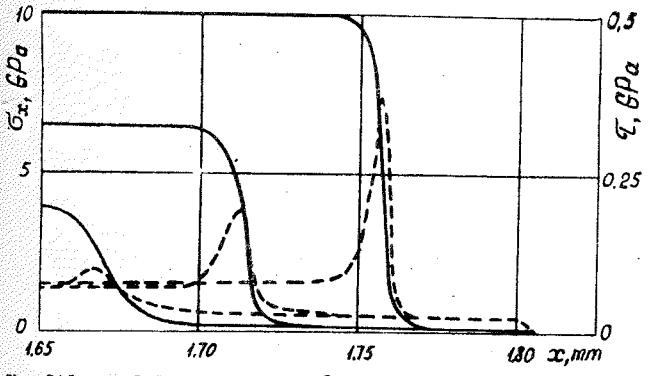

Fig.2. Profiles of longitudinal σ (x)(solid lines) and shifted τ(x)(dotted lines) stresses in copper at time momentum t = 0.4 μs for three intensities of impact waves at η_ℓ = I0 Pa·s.

QUASIZONE MODEL FOR THERMODYNAMICAL PROPERTIES OF DENSE PLASMA

N.N.Kalitkin
M.V.Keldysh Institute of Applied Mathematics, Moscow, USSR

Broadening and shift of spectral lines, induced by microfields in low-temperature non-dense plasma, were investigated theoretically and experimentally long ago /1/. It is interesting to use these ideas for plasma of enormous density comparable with condensed matter density.

Such plasma is multiply ionized. Ions are located in strong fluctuating electrical fields of neighbouring ions. The average potential and vector of the microscopic field strength and their mean square fluctuations are equal, according to the nearest neighbour model,

$$\langle\varphi\rangle \approx -z/R, \quad \langle\vec{\mathcal{E}}\rangle = 0, \quad \langle\mathcal{E}\rangle \approx z/R^2, \qquad (1)$$
$$\sqrt{D\varphi} \approx z/R, \quad \sqrt{D\mathcal{E}} \approx z/R^2.$$

Here z is the ion charge and R is the radius of an atomic cell (all formulae are reduced in the atomic system of units). An example of calculations for xenon according to the more accurate model is given in Table. These values differ from those in formulae (1), but not so strong.

Fluctuations of microfields results in a peculiar structure of spectrum of bound states - it is not discrete or zonal but quasi-zonal. The separate atom levels are shifted by a value determined by the microscopic field potential at a given point at a given time. Due to the field fluctuations these shifts are different for different ions. A set of similiar levels of different ion forms a quasi-zone with half-width $\sim\sqrt{D\varphi}$ (Fig.1). Table shows that this half-width may be equal to hundreds of electron-volts in dense plasma.

Stark-effect. The fields are moderate in nondense plasma, and Stark-effect is quadratic by the field strength; in dense plasma fields are so great that the effect become linear. The number of allowed transitions grows since the electrical field removes prohibition for the transitions with $\Delta l > 1$.

Such structure of electron spectra takes a considerable effect upon thermodynamical and optical properties of plasma. While

microscopic potentials of ionization are numbers, macroscopic potentials are stochastically distributed variables with half-width $\sim\sqrt{D\varphi}$. For ionization from different levels these distributions correspond to quasi-zones in Fig.1. It requires a respective generalization of the ionization equilibrium equations and leads to reducing the shell effects in the equation of state.

It may be seen from Fig.2, where the theoretical and experimental data on strong shock compression of aluminium are presented (figures near curves and points mean numbers of references). Quantum-statistical model /2/ supposes totally smoothed zones and doesn't take into account the shell effects. Zone model /3/ totally neglects the smoothing of zones, and pseudo-zone model /4/ takes this effect into account in part. The accurate experiments /5/ demonstrate that quasizone smoothing of shells is large enough and has to be taken into account /6/.

Distribution of ionisation potentials leads to a strong smearing of the photoeffect threshold with a characteristic width $\sim\sqrt{D\varphi}$ (Fig.3). The effect is appreciable in a nondense plasma too, where it manifests as a smearing of the continious spectrum boundary. In the dense plasma it is additionally intensified due to ions of both average and others multiplicities with somewhat different ionization potentials.

T, eV	2	2	1000
ρ, g/cm^3	0.01	1	1
n, cm^{-3}	4.6×10^{19}	4.6×10^{21}	4.6×10^{21}
P	230 bar	16 Kbar	330 Mbar
z	1+2	1	45 ± 5
$-\langle\varphi\rangle$, eV	1.1	3.0	250
$\sqrt{D\varphi}$, eV	0.9	2.0	100
$\sqrt{D\varphi}:\frac{z}{R}$	1.1	0.5	0.6
$\sqrt{D\mathcal{E}}$, MV/cm	2.1	9.5	1040
$\sqrt{D\mathcal{E}}:\frac{z}{R^2}$	0.43	0.09	0.23

Fluctuations in the Stark splitting values mean that the corresponding spectrum lines of different atoms and ions have dif-

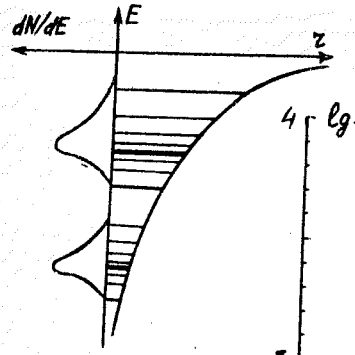

Fig.1.

Fig.2.

t
in a
S
and Stark
plasma fiel
ber of allowed
ves prohibition

Such structure
fect upon thermodynam

es mean that the
atoms and ions have dif-

23

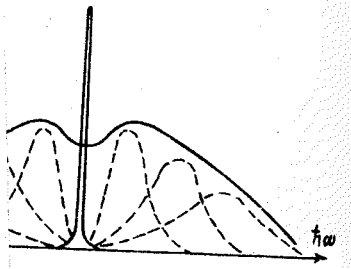

Fig.4.

ferent lengths. In a macroscopic volume of matter it it equivalent to a broadening of each multiplet line by a value on the order of its average shift. Since distancies between the lines are approximately the same, the result of such a broadening is that all the lines merge into a singl quasi-line with a great width equal to

$$\Delta(\hbar\omega) \sim R^{-2}\left[n(n-1) + n'(n'-1)\right]$$

under the linear Stark-effect. Here n and n' are the main quantum numbers of the upper and lower levels between which a transition takes place (Fig.4). Under the quadratic Stark-effect, i.e. in a nondense plasma, the quasi-line width is proportional to R^{-4}.

In recent publications /7,8/ on optical properties of dense plasma a hypotesis has been postulated about an anomalously big broadening of lines. However a physical nature of this phenomenon has not been explained.

References

1. Griem H.R. Spectral line broadening by plasma. - N.Y. & L., Academic press, 1974.
2. Kalitkin N.N., Kuzmina L.V. Quantum-statistical equation of state. - Soviet Plasma Physics, 1976, v.2, N6, p.858-868.
3. Nikiforov A.F., Novikov V.G., Uvarov V.B. Modified Hartree-Fock-Slater model for matter with given temperature and density. - Sov.Atomic Science and Technik Questions; methods and codes, 1979, N4(6), p.16-35.
4. Sin'ko G.V. Using of self-consistent field method for calculation of electron thermodynamical functions in simple substances. - Sov.Thermophysics of High Temperatures, 1983, v.21, N6, p.1041-1052.
5. Avrorin E.N., Vodolaga B.K., Voloshin N.P., Kuropatenko V.F., Kovalenko G.V., Simonenko V.A., Chernovoluk B.T. Experimental confirmation of shell effects on shock adiabats of aluminium and lead. - Sov. Pis'ma JETP, 1986, v.43, N5, p.241-244.
6. Kalitkin N.N. Quasizone electron spectrum, thermodynamical and optical properties of dense plasma. -M.: Inst.Appl. Math., 1986, preprint N107, -27 p.
7. Shalitin D., Stein J., Akiva R. Level and line broadening for Thomas-Fermi atoms at finite temperature. - Phys.Rev.A., 1984, v.29, N5, p.2789-2795.
8. Stein J., Shalitin D., Akiva R. Average-atom models of line broadening in hot dense plasmas.- Phys.Rev.A, 1985, v.31, N1, p.446-450.

EXPERIMENTAL EQUATION OF STATE OF SOLID HYDROGEN AT PRESSURES 2-27 KBAR

A.N. Utyuzh

Institute of High-Pressure Physics of the USSR Academy of Sciences, Troitsk, USSR

The improved piston-displacement technique was used to determine the pressure-volume relations for solid hydrogen at 4.2K in extended pressure range and at 77K with increased accuracy by extension of improved technique in temperature range higher than triple point. The final uncertainty in the determination of volume, in which the error in pressure determination is included, was ±0.4%. The volume of the solid hydrogen sample was 0.5-2 cm^3. The results were represented by Birch relation (I), with the mean square uncertainty δ and parameters shown in Table I.

$$P(V) = P_o + y^5 \sum_{n=1}^{2} A_n (y^2-I)^n \qquad (I)$$

$$\text{with } y = (V(P_o)/V(P))^{I/3}$$

The estimation of p-H_2 concentration and the calculation of quadrupolar pressure made it possible to treat, within the experimental error, the data obtained as V(P) for p-H_2. Our results at 4K are in good agreement (no worse than 0.2% in volume) with /I/. The T=0 isotherm of equation of state (EOS) /2/, obtained by treatment of various experimental data, at P> I0 kbar deviates seemin-

/3/ at 77K exceed the

77K isotherm, calcu-

?> I5 kbar.

accurately approxi-

lid hydrogen, in par-

ochores. We stated

herms, calculated from

5 kbar. In Table 2 EOS

ated using method /2/.

ere used as T=0 iso-

l data approximation

6/ were used for mel-

series of reduced te-

T_m are given. The va-

me, cm^3/mol; Θ_D and T_m,

isotherms in 4-300K

t

in a

S.

and Stark

plasma fiel

ber of allowed

ves prohibition

Such structur

fect upon thermodynam

es mean that the

toms and ions have dif-

23

Table I. Values of the parameters for the Birch equation (I) and mean square error δ for 4K and 77K

T, K	P_o, kbar	A_I, kbar	A_2, kbar	δ, cm^3/mole
4.2	I	II.523	I0.3I0	0.0I9
77.4	4.953	32.480	I8.674	0.0I3

Experimental data V(P) for solid hydrogen there are on isotherms 4K and 77K and along the melting line. Comparison of calculated from our EOS isotherm 77K with our experimental data demonstrated agreement within experimental accuracy. Comparison of available data for molar volumes of solid hydrogen on melting line $V_{ms} = V(T_m, P_m)$ are shown in Figure. Differences in volume in isobars are plotted with respect to molar volume at 4K. Values of V_{ms} computed on base of Silvera-Goldman potential /8/ and V_{ms} point from accurate measurements /I/, are in good agreement with line I. Values of V_{ms}, measured with a piston-displacement technique /4,5/ are in good agreement with line I within its stated substantial error bars.

Table 2. The equation of state of solid parahydrogen

T/T_m =				0.0	0.2	0.4	0.6	0.8	1.0
V	Θ_D	γ	T_m	P(V,T)					
16.00	209.99	1.839	53.39	2.250	2.251	2.263	2.308	2.400	2.537
15.00	236.04	1.791	65.80	3.280	3.281	3.301	3.372	3.510	3.708
14.00	266.69	1.749	81.15	4.755	4.757	4.789	4.901	5.105	5.386
13.00	303.11	1.706	100.24	6.895	6.899	6.951	7.123	7.421	7.815
12.00	346.82	1.661	124.23	10.05	10.06	10.14	10.40	10.81	11.39
11.00	399.94	1.615	154.81	14.81	14.82	14.96	15.35	15.98	16.75
10.00	465.45	1.568	194.55	22.19	22.20	22.42	23.02	23.92	25.01
9.50	504.12	1.544	219.01	27.37	27.39	27.68	28.41	29.50	30.80
9.00	547.66	1.520	247.39	33.99	34.02	34.38	35.30	36.62	38.18

Experimental results for V_{ms} of hydrogen were represented in /I,4,6/ by a relation of the form suggested by Kechin et al./4/:

$$V_{ms} = A - B \ln T_m \qquad (2)$$

with T_m - melting temperature; A = 37.989; 37.28; 35.8596, B =

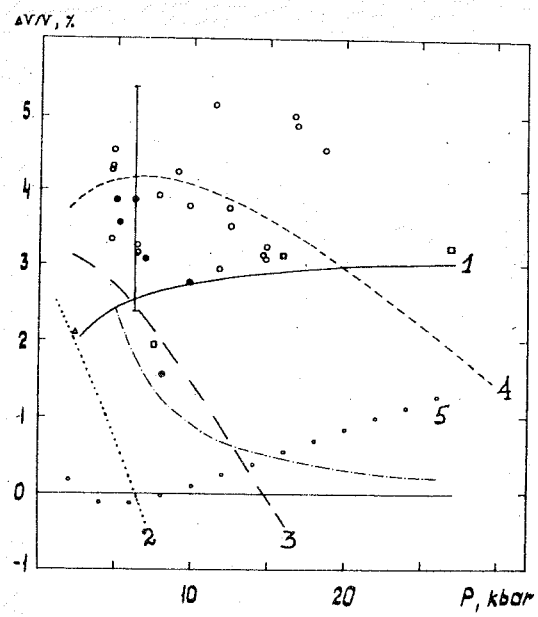

The change in volume of solid hydrogen on an isobar relative to our data for T=0. The symbols correspond to experimental and computational results for volume of solid H_2 at the melting

...nge and Swenson/I/; ● - Kechin et al. /4/; □
'. The lines corres-
isotherm, from the
ntation by equation
S /2/.

temperatures T_m, the
parameters from /I,4,6/
versus melting pres-
is used for melting
re plotted in Fig. I.
of hydrogen doesn't ag-
cause curves 2-4, dis-
ion of solid phase, be-
tersect experimental
spectively.

...23
...mean that the
...atoms and ions have dif-

S...
and Stark...
plasma fiel...
ber of allowe...
ves prohibition ...

Such structur... ...es
fect upon thermodynam...

References

1. Krause J.K., Swenson C.A. Direct measurements of the constant-volume heat capacity of solid parahydrogen from 22.79 to I6.I9 cm^3/mole and resulting equation of state.-Phys.Rev.B, I980, v. 2I, N 6, p. 2533-2548.
2. Driessen A., Silvera I.F. An improved experimental equation of state of solid hydrogen and deuterium.- J. Low Temp. Phys., I984, v. 54, N 3/4, p. 36I-385.
3. Kechin V.V., Pavlyuchenko Yu.M., Likhter A.I., Utyuzh A.N. Experimental dependence of the volume of solid normal hydrogen on the pressure up to 30 kbar at a temperature 77K.- Zh. Exsp. Teor. Fiz., I979, v. 76, N 6, p. 2I94-2I97.
4. Kechin V.V., Likhter A.I., Pavlyuchenko Yu.M., Ponizovsky L.Z., Utyuzh A.N. Melting curve for hydrogen up to I0 kbar.- Zh. Exsp. Teor. Fiz., I977, v.72, N I, p. 345-347.
5. Liebenberg D.H., Mills R.L., Bronson J.C. Measurements of P, V, T and sound velocity across the melting curve of n-H_2 and n-D_2 to I9 kbar.- Phys.Rev.B, I978, v.I8, N 8, p. 4526-4532.
6. Diatschenko V., Chu C.W., Liebenberg D.H., Young D.A., Ross M., Mills R.L. Melting curves of molecular hydrogen and molecular deuterium under high pressure between 20 and 373K.- Phys.Rev.B, I985, v. 32, N I, p. 38I-389.
7. Hemmes H., Driessen A., Griessen R. Thermodynamic properties of hydrogen at pressures up to I mbar and temperatures between I00 and I000K.- J.Phys.C. Solid State, I986, v. I9, N I9, p. 357I-3585.
8. Young D., Ross M. Theoretical calculation of thermodynamic properties and melting curves for hydrogen and deuterium.- J. Chem. Phys., I98I, v. 74, N I2, p. 6950-6955.

TECHNOLOGY AND EQUIPMENT FOR HYDROSTATIC TREATMENT OF MATERIALS

B.I.Beresnev, V.G.Synkov
Donetsk Physico-Technical Institute , Academy of Sciences of the Ukrainian SSR, Donetsk, USSR

The main requirements to the quality of products are the homogeneity of technological and service properties, the improved characteristics of strength and plasticity, endurance and brittle failure resistance. In recent years many investigations into developing the High Hydrostatic Pressure Technologies (HHPT) and equipment to meet these requirements have been carried out by scientific schools of Academicians L.F.Vereshchagin, G.V.Kurdyumov, A.I.Tselikov and A.A.Galkin in the USSR. Physical basis of these technologies is represented by the plastic deformation effects under high pressure: material plasticization /I/, strain ageing /2/, decrease of a carbide inhomogeneity /3/, use of a liquid as a machining tool /4/ etc. HHPT are widely spread and promising especially in metallurgy as the ferrous metals account for more than 96% of the total structural material consumption in machine building, while assortment of products is about 5000 profile sizes of bars, 30000 profile sizes of tubes, 50000 types of metalware.

Nowadays the hydrostatic pressing of a round billet may give I% of the total quantity of steel shapes (SS) mentioned above.Besides, the costs of process stage at transition to hydrostatic extrusion decrease only for the SS of the 6-9 complexity groups, while the shapes of the 8-9 groups are not yet extruded taking into account the equipment reliability /5/. Hydrostatic extrusion of the SS provides an expenses decrease by 63 roubles in metallurgy and 460 roubles per I ton of the shapes for a consumer /6/.

The hydrostatic extrusion (at reduction of 5-7%) of low-tempered martensite of the type CrNiMo, CrMoW, CrWAl medium-carbon steels provides the unique combination of strength, plasticity and impact strength at their practically uniform distribution all over the bar cross-section /7/. At a metallurgical work the rods of ...GSN2A steel, 28-30 mm in diameter and up to 2.5 m long we...th the values for σ_b =2040-2050 MPa, σ_s =I930-I950 MPa, ψ =54-56%, a_H=600-800 kJ/m^2 at the maximum work...ssure of 520 MPa. The material with these properties ...the highly loaded parts of mining tools, in the tran-

...port machine building, for producing needles and mandrels in the field of pipe rolling and drawing. The savings for a consumer when utilizing this metal is 300-I000 roubles per I ton /6/.

Hydrostatic extrusion of these steel types under the heat-mechanical pretreatment conditions at reduction of 25-35% in comparison with hot rolling improves the torsional fatigue strength by I.8-2.4 times. Besides there is an opportunity of the subsequent cold upsetting of the ends at deformation up to 60-70% /8/, decreasing labour expenditure by I0-I5% while producing shafts, axles and springs due to elimination of the shot cold-work hardening or the spinning with general effect of 630-7I5 roubles per I ton of parts.

Hydrostatic extrusion of the thick-walled and superthick-walled tubes ($D/s \leq 5$) eliminates longitudinal creases over the inner surface, the geometrical dimension accuracy corresponds to precision tubes (All-Union state standard 9567-75), involving the improvement of speed-torque characteristics. That saves more than 3 roubles per one ton of tubing in the heavy and chemical engineering /9/.

In the field of metallurgy the apparatuses with a vertical-horizontal design of working unit, pressure up to I500 MPa, the billet diameter up to 60 mm, an output up to I50 kg/hr, a grading area of I0-I5 m^2 are used.

The hydrostatic extrusion of wire and wire billet has become a component of the processing of heat-proof and refractory materials, bi-metallic and multistrand wire, high-strength metal and polymer fibre. It is especially effective while producing fine and superfine wire of high ductile materials, e.g. of aluminium A 999 0.I5-0.3 mm in diameter at single drawing up to 2500 /I0/.
The application of high hydrostatic pressure in machine building is related to the technologies of hydrostatic die forging and sheet-metal stamping. During production of the tubular parts with laterals (T-joints, pipe crosses) it has been found /II/ that at low output (up to 6000 pieces a year) hydrostatic extrusion is more effective than other pressure treatment types (die forging and sheet-metal stamping) with respect to the expenses amount.The most effective application it may find in the field of veloproduction substituting for the stamping-welding.

In the field of powder metallurgy the gasostatic sintering may be changed for the cold hydrostatic extrusion at a pressure of 600-800 MPa (density 87-9I%) of the preformed briquettes (den-

sity 65-76%) sintered in a vacuum furnace with their subsequent hot extrusion /I2/.

References

I. Bridgman P.W, Study in large plastic flow and fracture. - Moscow, Foreign Literature, 1955, - 444 p.

2. Certificate of invention 223I24 (USSR). Method of steel hardening/G.V.Kurdumov, L.V.Vereshchagin, R.I.Entin et al. -Published in Bulleten' izobreteniy, I968, N 24.

3. Certificate of invention 260670 (USSR). Method of processing high-speed steel/A.A.Galkin, U.F.Chernyi, V.S.Koviko et al.- Published in Bulleten' izobreteniy, I970, N 4.

4. Certificate of invention 287507 (USSR). Method of die forging of articles /E.D.Martynov, B.I.Beresnev, U.N.Ryabinin. - Published in Bulleten' izobreteniy, I970, N 35.

5. Estimation of possibility and necessity of the hydrostatic pressing utilization in ferrous metallurgy/G.A.Krivonos, B.V. Magaziner, A.I.Podgayetskiy. - Fizika i Technika Vysokih Davleniy, I984, 15, p.32-35.

6. Recommendations on methodology of determination of the hydrostatic pressing economical effectiveness (illustrated by an example of producing articles of ferrous metals). Edited by O.A.Romanova.-Sverdlovsk: IE USC of the Ac.Sci.of the USSR, I983.- 75 p.

7. Experience of the hydrostatic pressing application for steel hardening through the martensite strain ageing/ A.G.Batalov, A.P.Bashchenko, Y.B.Gurevich et al. - Fizika i Technika Vysokih Davleniy, I983, II, p.52-56.

8. The industrial experience of the hydrostatic pressing utilization while producing billets for high-loaded parts of structural steel/E.A.Konovihin, N.G.Aleksandrov, A.P.Lubchenko et al. -Proceedings of the IV All-Union Conference "Hydrostatic Treatment of Materials" (Donetsk, September IO-I2, I985). Abstracts of papers. Donetsk: Donetsk Physico-Technical Institute , I985, p.II9.

9. Apparatus for hydrostatic pressing of the thick-walled steel tubes/V.H.Kasyian, V.Y.Ostrenko, V.A.Nesterov, V.T.Dyachenko.- Fizika i Technika Vysokih Davleniy, I983, I3, p.23-25.

IO. Hydrostatic pressing of wire/V.P.Buryak.-Fizika i Technika Vysokih Davleniy, I98I, 3, p.75-83.

II. Bogoyavlenskiy U.N., Seryakov E.I., Kobyshev A.N., Voronina N.F. Production of the complex void shapes. Leningrad: Mashinostroeniye, I979,- 2I8 p.

I2. Compaction of porous briquettes of high-speed steel through hydrostatic treatment /B.I.Beresnev, V.Z.Spuskanyuk, V.S.Tyutenko et al. - Proceedings of the IV All-Union Conference "Hydrostatic Treatment of Materials" (Donetsk, IO-I2 September, I985): Abstracts of papers. Donetsk: Donetsk Physico-Technical Institute, I985, p.228.

INVESTIGATION AND DEVELOPMENT OF HYDROSTATIC EXTRUSION OF QUENCHED STEEL

A.G.Batalov, A.P.Bashchenko, A.D.Voloskov, Ya.B.Gurevich, V.V.Davydov, V.N.Dmitriev, E.V.Polyakov

Central Institute of Ferrous Metallurgy, Moscow, USSR

Strain aging of the martensite SAM is one of the contempora- methods for strengthening of construction steels.

Deformation of the martensite was suggested to be carried by the hydrostatic extrusion method /I/. This method pro- homogeneous deformation and the perfect fine structure of material. The Fig.I shows dependence of mechanical properties steel with martensite structure after hydrostatic extrusion rolling on deformation degree /2/. In the first case intensi- increase in yield stress and some increase in plasticity are obser- After rolling plasticity of the steel decreases sharply. The intensive strengthening of a quenched steel with the carbon content 0.3-0.4% occures at the deformation degree 4-6%. As a re- of hydrostatic extrusion, strengthening of a quenched steel accompanied by stress relaxation. This fact is confirmed by re- tion of the X-ray diffraction lines and precision measuring density. After hydrostatic extrusion the density is practi- the same. The density decreased about 0.0I g/cm^3 after with reduction of I5%.

Fig.2 shows the values of the yield stress and the impact toughness (Y.S and I.T) for quenched and annealed at 200 °C steels (CrNiMoSi) with different carbon content and after SAM un- rolling and hydrostatic extrusion at 3% deformation. As carbon content in the steel increases the strength increases too, the im- strength decreases but its values are essentially higher un- SAM at hydrostatic extrusion.

Due to OHT a rough martensite structure forms. The following methods for production the homogeneous and fine martensite struc- are known: high-temperature and low-temperature thermomecha- treatments; treating for production the superfine austenite grains (up to 2-3 μm). The complex methods had been carried out strengthening which combined previously mentioned method with the SAM /3/. The results show that high level of the mecha- properties can be reached when combination of the SAM under hydrostatic extrusion is being used in combination with the methods of strengthening. For instance, the steel CrNiMoSi

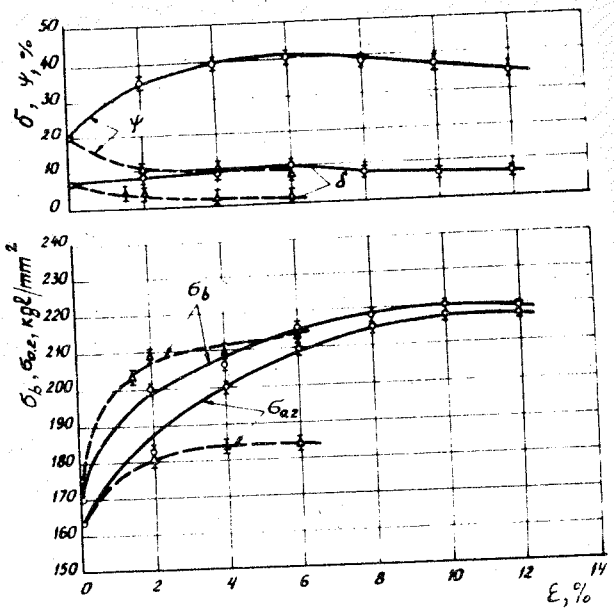

FigI. The mechanical properties of 45H3MC steel depending on deformation degree under hydrostatic extrusion (continuous lines) and under rolling (brocken lines) followed by the aging at 200 °C.

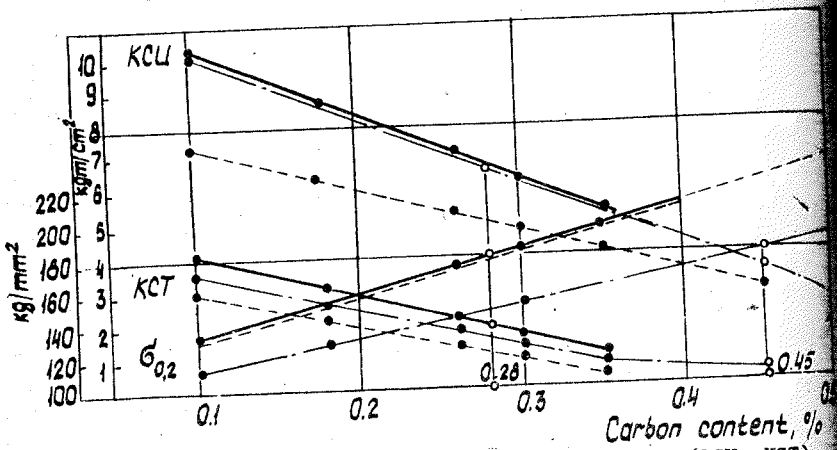

Fig.2. Dependence of the yield stress and toughness (KCU, KCT) of XH3MC steel on carbon content:
—— SAM under hydroextrusion; - - - SAM under rolling;
-.-.- thermal treatment.

(0.35% C) after HTTMT with the SAM has σ_b=2350 MPa, $\sigma_{0.2}$ = =2300 MPa, δ_5=8%, ψ=40% and steel CrNiMoSi (0.45% C): σ_b= 2860 MPa, $\sigma_{0.2}$=2695 MPa; δ_5=6%, ψ=35%, accordingly. Strengthening of CrMnSiNi(0.3%C) due steel to the process of HTTMN by rolling and SAM under hydrostatic extrusion were used to produce the rods 30 mm in diameter and 2.5 m in length /4/. The hydrostatic extrusion with reduction 5% had been carried out using the verticaly - horizontal plant. There had been obtained the following properties after such treating: σ_b=2000 MPa, $\sigma_{0.2}$=1890 MPa, δ_5=7%, ψ = =54%, KCV=70 kJ/m^2, HRC=52.

The plastic properties are increased after hydrostatic extrusion combined with back pressure. In the case of construction steel with carbon content 0.3-0.4% for production the rods 5.0--10.0 mm in diameter the combination of the HTTMT and SAM under hydrostatic extrusion with the back pressure 1000-1700 MPa and summary reduction 35-50% results in increasing the strength up to 2500-3500 MPa at the satisfactory plasticity.

Electronmicroscopic research shows that the deformation of quenched and low tempered steel by hydrostatic extrusion results in the following changes of the structure: the dislocation density increases from $5 \cdot 10^{10}$ cm^{-2} (initial condition is HTTMT) to 10^{11} cm^{-2}; almost all martensite crystals undergo elastic bending and the size of the distored microareas is being decreased, the deformation twins appears.

It was shown that deformation of the rods 8-30 mm in the diameter manufactured from a construction steel provided increase of the strength as much as 200-700 MPa and the resistance to stress corrosion at the satisfactory values plasticity and impact strength.

References

1. Patent N 223124, USSR, The method of strengthening of steel. G.V.Kurdyumov, L.F.Vereshchagin, R.I.Entin, et al. B.I., N24, 1968.
2. Strain aging of the martensite under hydroextrusion /G.V.Kurdyumov, L.F.Vereshchagin, R.I.Entin et al.,-F.M.M., 1970, v. 29, N4, p.172-176.
3. Possibility of improving mechanical properties of steel by using high hydrostatic pressures for martensite deformation/ Ja.B.Gurevich, V.N.Dmitriev, Yu.S.Konyaev et al. - In book: Problemy Metallovedenia i Fiziki Metallov.- M. Metallurgia, 1976, N3, p.149-156.
4. Experience of industrial hydroextrusion application for steel hardening by the martensitic strain aging method /Batalov A.G., Bashenko A.P., Gurevich Ya.B et al. - Fizika i Tekhnika Vysokih Davleny, 1983, NII, p.52-56.

METHOD OF HYDROEXTRUSION USED IN INDUSTRY TO PRODUCE METALLURGICAL ITEMS FROM HIGH ALLOYS

V.I.Steepura[I], Yu.V.Manegin[I], Yu.F.Luzin[I], A.G.Batalov[2], A.D.Voloskov[2]

[I]I.P.Bardin Central Scientific and Research Institute of Ferrous Metallurgy, Moscow, USSR

[2]Omutninsk Steel Plant, Omutninsk, USSR

Studied was the effect of hydrostatic pressure on cold deformation of Nimonic-type alloys containing I2-20 % Cr, 70-75 % Ni, Ti, Al and other elements /I/. The alloy plasticity Ψ was found to increase more than 2-fold, with hydrostatic pressure going up from atmospheric level to I200-I400 N/mm^2 in the process of specimen stressing. Pre-breaking deformation λ_b increases more than 2-fold as well when the metal stressed state index $K=\frac{\sigma}{T}$ varies from +0.8 to -0.6, where σ is the mean hydrostatic pressure and T is the tangential stress intensity.

During hydroextrusion the metal being deformed is known to be affected by high hydrostatic pressures /2,3/; the stressed state index K of the metal in the deformation centre is K=-0.3 ÷ -0.7. From this it follows that the hydroextrusion process can be used to alter the shape of high steels and alloys.

Experimental data were used to develop the hydroextrusion process for rods of round and hexagonal cross-section with an circumscribed circle diameter of I0-20 mm from ЭИ437Б and ЭИ698 alloys. The Omutninsk steel plant started commercial production of such rods having a length of up to 5000 m.

Hydroextrusion was carried out with a force applied to the front end of the rod via a special device. Figure shows a nomogram for calculation of forces during hydroextrusion with front-end stressing. The nomogram is used to find the pressure of the liquid in the press depending on strength properties of alloys to to be deformed, extrusion (reduction) coefficient and stressing force.

As seen from Table, hydroextruded metal has higher long-term strength characteristics (time before failure) and better plastic properties. Investigations showed that cold deformation by hydroextrusion followed by heat treatment helps to minimize variations in grain size and provide for grinding and better distribution of

non-metallic inclusions, mostly titanium carbides and nitrides Ti (C,N), as compared with hot-rolled state.

Long-term strength of ЭИ698 alloy following hydroextrusion

Section	Reduction during hydroextrusion, ε,%	Heat treatment regime prior to testing	Testing regime: Stress, σ, N/mm^2	Testing regime: Temperature, °C	Properties: Long-term strength, τ, hr	Properties: Elongation, δ,%	Properties: Contraction of cross-section area, Ψ,%
ø I7 (bar)	-	Heating to II20 °C, holding for 4 hrs, air cooling + heating to I000 °C, holding for 4 hrs, air cooling + heating to 775 °C, holding for I5 hrs, air cooling	400	750	2I0	6.4	7.9
SI4 (hexagonal)	40.0		400	"	262	I8.2	23.8
			420	"	I35	I2.4	I3.4
Customer's requirements			420	"	50	8.0	I0.0

Geometric sizes of rod cross-sections meet the requirements to calibrated metal, namely, the surface roughness of rods conforms to class 6.

Thus, production of calibrated round and hexagonal rods from Nimonic-type alloys that are difficult to deform is one of the most advantageous applications of hydroextrusion method in industry. Use of such rods in place of hot-rolled ones helps to make irreversible losses of scarce metal two times as small and labour intensity required to fabricate parts used in engineering.

References

I. Khimushin F.F. Zharoprochnye stali i splavy (Heat resistant steels and alloys). In Russian. M., Metallurgiya, I969, 2nd edition, 752 p.

2. Uralsky V.I., Plakhotin V.S., Sheftel N.I. et al. Deformatsiya metallov zhidkostyu vysokogo davleniya (Defor-

mation of metals with high-pressure liquid). In Russian. M., Metallurgiya, 1976, 424 p.

3. Plastichnost i razrushenie (Plasticity and Failure). In Russian. Ed. by V.L.Kolmogorov, M., Metallurgiya, 1977, 336 p.

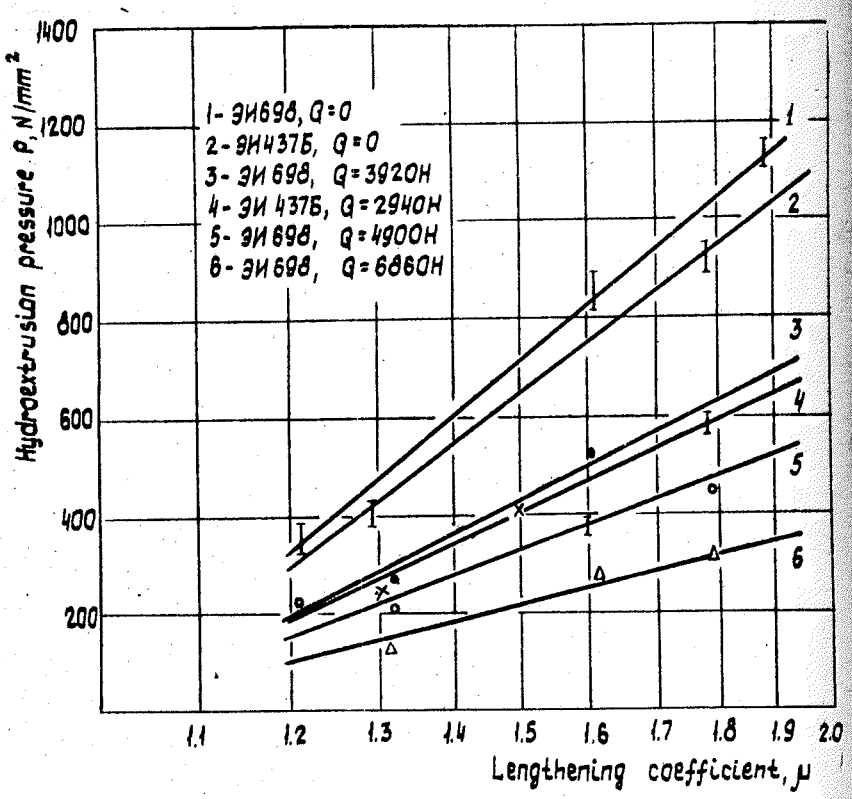

Hydroextrusion pressure versus lengthening coefficient μ and stressing force Q:
I, 2 - rods (I4 mm); 3 - hexagonal section SI2; 4 - hexagonal section SIO; 5 - hexagonal section SI4; 6 - hexagonal section SI7.

HYDROPRESSING METHODS AT HIGH PRESSURES AND DEFORMATION RATES

V.Z.Spuskanyuk, V.A.Bogdanov, I.M.Kovalenko, A.A.Lyadskaya, N.L.Sokolov, N.V.Shishkova

Donetsk Physico-Technical Institute;Ukrainian SSR Academy of Sciences, Donetsk, USSR

Development of hydropressing methods for solving of problems for increase in strength and plasticity of materials, formation of billets of products at high level of exploitation properties is a promising direction of scientific investigations. For providing of possibilities to realize effects of strenghening treatment development of practical hydropressing methods is necessary, and creation of reliable and high-productive plants.

Creation of favourable conditions of lubrication in the deformation zone and increase of equipment productivity is reached at realizing of the cold hydropressing process with high rates of deformation. Here, however, problems of process control increased, and also problems of product extraction at the final step of the process. As a result of developing and investigation of the hydropressing process model of billets at the direct action plant a range of optimal deformation rates was determined ca. 0,2...2.0 m/s, at which the minimum liquid pressure differential is provided at the process initial step. At low rates this pressure differential increases as it is known due to the long time period of stationary contact for a billet with the matrix under pressure, by extrusion of lubricant from the contact zone. At high rates the pressure differential dynamic component increases due to the fact that the working liquid continues to be compressed in the period of billet acceleration /1/.

Fundamentals for the cold hydropressing process of billets at mechanical presses with the initial deformation rate ca. 0.5 m/s are developed, its advantages in comparison with hydropressing at deformation rates ca. 10^{-3} m/s are revealed /2/. It is shown that due to elastic deformation of the system of a press at hydropressing of billets the additional high-frequency attenuated vibrations of the working liquid and rates of material extrusion from the matrix are developed. As consequence of said effects and the high deformation rate the hydropressing of billets is 30...40% lower in comparison to deformation at hydraulic

presses. At the mechanic presses the rate of plunger motion is smoothly decreased down to zero in the final lower position, this circumstance can be conveniently used to prevent extracting of a billet on accomplishing the treatment.

The methods of cold and warm hydrostatic and hydrodynamic pressing of billets are effectively used for realization of technological processes of thermomechanical treatment of steels and alloys. Thus, as a result of preliminary thermomechanical treatment (PTMT) it is provided increase of properties of tool steels and of operational characteristics of produced metal-cutting and die tools. As a result of thermomechanical and mechanicothermal treatment at rod hydropressing it is provided a limit of strength of construction steels ca. 2.4 GPa at relative lengthenening ca. δ =10%.

New possibilities to control structure and material properties are provided by methods of low-temperature hydropressing with preliminary cooling of a container, tools, working medium and a billet, to realize a series of practical results it is enough to cool in advance only billets. The low-temperature hydropressing method provides an additional effect at PTMT of high-speed steels, it is used for regulation of phase composition, structure and obtaining of advanced level of properties of stainless steels of austenite class, metastable two-phase ($\gamma + \varepsilon$) steels on Fe-Mn basis.

It is known that advantages of hydropressing in comparison to the traditional treatment one can apply more widely by controlling the level of hydrostatic pressure in the deformation zone, e.g., as a result of counterpressure generation. Hydropressing with counterpressure at present is not widely applied, because equipment needed is complicated and of low capacity. Plants are developed, in which counterpressure is produced as a result of liquid compression by shifting of an aggregate, including a work-container, a matrix and a counterpressure chamber (Fig.1,a). Cross-section areas of a work-container and a counterpressure chamber as well as aggregate shift range are chosen in order to reach the counterpressure level needed afore pressing is started, and the aggregate is at rest. By variation of the aggregate rest position the gear-free control of the initial counterpressure level is provided. The constant counterpressure level during pressing is maintained by liquid-leak from the counterpressure chamber by a special device (Fig.1,b).

It is stated that even at the counterpressure level ca. 0.5...1.0 GPa conditions for deformation of steels and alloys are considerably improved due to volume increase in the deformation zone, increase of pressure in this zone, decrease of external friction influence and increase of uniform deformation of a billet. As consequence of counterpressure application density and plasticity of deformed high-doped steels and composite alloys, as well as wear resistance of metal-cutting and die tools increased.

References

1. Spuskanyuk V.Z., Sokolov N.L., Beigelzimer Ya.E. Features and advantages of cold hydropressing at crank presses//Kuznechno-shtampovochnoye proizvodstvo. - 1987.- NI.- P.21-31 (in Russian).
2. Features of dynamics of cold hydropressing process at a crank press (in Russian)/N.L.Sokolov, V.Z.Spuskanyuk, A.P.Getmansky, Ya.E.Beigelzimer//Fizika i tekhnika vysokikh davleny. - 1986. - Vyp.23.- P.63-70.

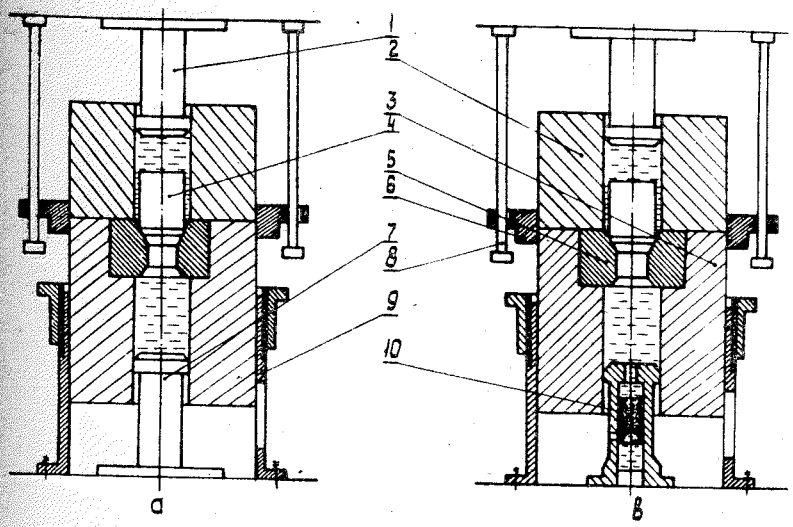

Devices for hydropressing with counterpressure:
I - mobile plunger; 2 - work-container; 3 - counterpressure container; 4 - billet; 5 - matrix; 6 - flange; 7 - stationary plunger; 8 - tension bars; 9 - rest; 10 - liquid-leak device.

THEORETICAL AND TECHNOLOGICAL ASPECTS OF HIGH STRAIN-RATE FORMING

Karol Polák
Slovak Technical University, Czechoslovakia

The structure and properties of metals depend on previous superposition mechanical and thermal effects. Therefore parameters of strain and heat treatment processes must be studied in relation to resultant properties of metals.

High-rate plastic strains with subsequent heat treatment relate in this paper to experiments with uniaxial stress state from centric direct impact of a rigging punch with flat face I on plastic body (specimen) 2 supported by a rigging target 3, Fig.I.

Main parameters of experiments: material (iron - carbon and alloyed steels), shape (cylinder) and geometry $d_o/h_o \in (I.0-0.I)$ of specimen; friction and character of contact surfaces; the specimen temperature $\vartheta \in$ (20-600°C); impact rate $v \in (0.00I-40\ ms^{-I})$ and strains $\dot{\varepsilon} \in (I0^{-4}-I0^{4}\ s^{-I})$ relative linear strains $\varepsilon \in (5-20\%)$; strain resistances $\sigma_\alpha (I-2)R_e$; resultant structures after quasi-static and dynamic plastic strains and after heat treatment. Within the range of the studied parameters we presumed isothermic plastic strains with hardening with minimum thermal effect /I/.

Parameters before, during and after loading of the specimens were measured: metal - by chemical analysis, friction - by ring test, temperature - by thermocouple, impact rate - by capacitance sensor, strain rate for small stages - by calculation $\dot{\varepsilon} = \frac{v\sigma}{h} =$ consts, relative linear strains - by strain networks, structures, slip bands and dislocation density, maximum strain resistances - by Cu crushers, structures and substructures - by optical, thermal and electron microscopies (thin foils and networks) /I,2/.

The study of the development of plastic strains, structures and properties after quasi-static and dynamic loadings was oriented to contact surfaces and/or surface layers of specimens. In these zones primary loss of stability connected with localization of plastic strains and hardening is presumed with regard to wave character of impact stress propagation.

It stems from wave differential equations for propagation of disturbances in elastoplastic bodies that they are the result of elastoplastic waves, each propagating by another rate. The rate of elastic wave c_e is higher than the rate of plastic wave c_p. Therefore the original linear faces of elastic wave are elongated in the direction of loading (Fig.I).

For post-critical impact rates $v<v_{cr}$ (for steels v_{cr} = 60-80 ms^{-I}) loss of stability on ultimate strength with low initial intensity of metal degradation is the significant high-rate forming processes. Loss of stability for uniaxial simple tension and pressure depends on the rate of plastic disturbance propagation for tension (c'_p) and pressure (c''_p), the following relation being valid

$$c'_p = \sqrt{\frac{I}{\rho}\frac{d\sigma}{d\varepsilon} - \frac{\sigma}{I+\varepsilon}} < \sqrt{\frac{I}{\rho}\frac{d\sigma}{d\varepsilon} + \frac{\sigma}{I-\varepsilon}} = c''_p$$

It means that limit state and simple tension is intensively destructive ($c_p = 0$) and therefore it is necessary also at high-rate forming to suppress to minimum the tensile stresses. On the contrary, for the study of limit states the simple tension is significant as a test, especially for processes at negligible thermal effect (Fig.I) /I/. From registration tensile diagrams these are the most significant conclusions: elastic dynamic strains are higher than static ones; plastic uniform (total) dynamic strains are lower than static ones; plastic dynamic strains cause strengthening with approximately the same density of dislocations like static strains, but with substantially different configuration /I, 3/.

Natural strain resistances σ'_p for low strains ε at simple tension on dull contact surfaces without lubrication confirmed validity of the equation:

$$\sigma'_p = \frac{a}{\varepsilon}$$

Relationships of specific strain work a (v) for different steels and 20°C, 600°C temperatures are shown in Fig.2 /I/. This knowledge represents the basis for technological applications of high-rate cold calibration and calibration at semi-heating. The total strain work is calculated from the product of specific strain work and displaced volume of metal /I,2,3/.

The study of structures after dynamic and static loadings on contact surfaces showed that twins (Fig.3*) as well as fragmentation of carbides and inclusions (Fig.4*) occur after dynamic loading. Dislocation substructures after dynamic loading have uniform configuration and after static loading they are in clusters from the very beginning (Figs.5,6*). There is no order diference in density of dislocations /I,3/.

* The Figures are given at the end of the book.

Dislocation substructures after dynamic loading had increased stability at higher temperatures. Studies on thermal microscope showed that phase transformations of $\alpha - \gamma$ steels have 2.5 times finer austenitic grain. This finding was confirmed by the studied of martensitic substructures, too. Fig.7* illustrates fine-grained twin substructure of martensite after dynamic plastic strain and Fig.8* shows coarse-grained substructure of martensite after static plastic strain /3/.

Significant effects of cumulation of dynamic hardening of surface layers on structure fineness also after heat treatment were utilized in fabrication and renovation of hollow pressing tools, especially tools for volume forming and forms for pressure casting and plastics (Figs.9,10*).The tools had higher wear resistance. Thus lifetime of tools increased 2-3 times /I,2/.

References

I. Polák, K., Dissertation work, Bratislava, I968.
2. Polák, K., Němec, J., Kovové materiály, No.4, I969, p. 299.
3. Polák, K., Bošanský, J., Kovové materiály, No.3, I97I, p.2II.
4. Veertman, J., Trans. of ACM 6I, I968, p. 68I.
5. Carrington, V., Halle, K.F., McLean, D., Proc. Proj. Soc. A 259, I960.

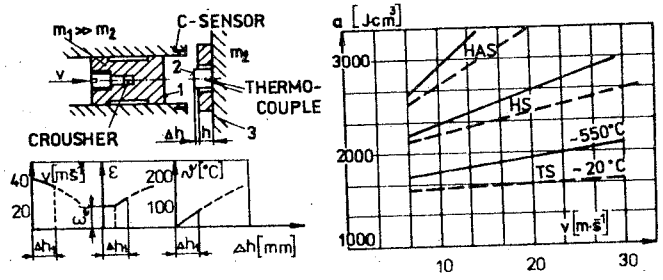

Fig.I. Centric direct impact.

Fig.2. Specific strain work.

* The Figures are given at the end of the book.

INDUSTRIAL APPLICATION OF IMPULSIVE HIGH PRESSURES IN SHEET FORMING WITH PARAMETERS OPTIMIZATION

V.K.Borisevitch, V.P.Sabelkin, V.T.Vovk

Kharkov Aviation Institute,Kharkov, USSR

Impulsive high pressures for the sheet forming are widely used in the modern industry. Applied aspects of the impulsive forming problem, including both control external stress and heat influence parameters are stated in the present research. The problem is reproduced in the vector representation in the multidimensional space of optimizing functions. In the case of limitation of measurements number the task leads to well known scalar representations with similar in physical sense, space of controlling parameters /1/.

In considered processes high pressures are generated by the impulsive energy sources on the base of the detonating gas mixtures and high explosives. Preheating of the deformed workpiece is performed from the autonomous heat power source or workpieces are heated during forming process.

Forming with high explosives

Pressing of the parts from low-ductility alloys and high strength materials with heating application from the blanks with wall thickness of 0.6-3.0 mm is very difficult using the conventional pressing equipment. It is simply impossible to form the parts of the closed shape. One of the alternative process may be forming in the heated dies. However it is practically impossible to generate the optimal temperature zones without its proof decreasing.

Equipment for high power explosive forming of the parts from the flat and cylindrical blanks was developed. Such installations are shown in Fig.1 (a,b*).

These installations structures are similar to that in the work /2/ and consist of horizontal and vertical guide units. The movable plate with mounting means arranged on it is installed on the horizontal guides. This movable plate is displaced from preparing zone to the technological zone by the hydraulic drive as in the first installation and by the electric drive in the second one. Forming blank heating is performed in the heat influence zone mainly with electrical-contact method in the first installation

*The Figure is given at the end of the book.

variant and with temperature radiation - in the second installation variant. Using the method of electrical-contact heating the installation is provided with compensating readjusting fixing device, arranged motionless in respect to the base. Temperature radiation heater is mounted in such a way that it can move vertically and during explosions it is protected by shutters.

Parts forming is carried out in special explosion chambers with the destructive of singular usage and elastic of multiply usage diaphragms. There are explosion chambers operating in the mode of the transmissing medium throw when the blast pressure, generated by the high explosives, has symmetrical characteristic in the vertical direction. The explosion chambers are installed on the vertically movable plate and the system for vertical displacement is arranged so that the loading of the drive during the explosions is excluded.

Technical data of the installations for explosion forming from the flat and cylindrical blanks (the latters are given in the brackets) are follows:

- Floor plan dimensions, m - 1.5x1.5x2.5 (2.0x2.0x3.2)
- Mounting means dimensions, m - 0.25x0.25x0.1 (1.2x1.2x1.0)
- Maximum charge weight, kg - 0.01 (0.1)
- Blank heating temperature, K - 1273 (1440).

Detonation gas forming.

The use of the detonatable gaseous mixtures as the source of high pressures and high temperatures is explained by their safety in operation as compared with high explosives. It is possible to mechanize and automatize the mixtures supply to the process zone and into the blanks cavities of the complex configurations, distributed into difficult-to-access places. High duration of the impulse, as compared with high explosives, is favourable for the forming parameters. At present such installations are used in the industry, that can operate in the open or closed scheme. They are shown in Fig.2(a,b*).

The construction of the installation is similar to that in the work /3/ and comprises supporting base in the form of the frame or bracket, with power supply unit arranged movable on it. The technological unit ensures the necessary displacement of the blank together with mounting means. Initial excess pressure of the gaseous mixture is held by pressurized destructive or multiply used

*The Figure is given at the end of the book.

elastic diaphragms. Forming may be performed by direct influence of the blast gaseous products or through the combined transmitting medium.

The developed equipment has the following technical data (in the brackets are given the data for the open scheme):

- Floor plan dimensions, m - 4.0x3.5x2.5 (3.0x4.0x2.5)
- Maximum part dimensions, m - 1.2x1.4 (3.2x1.4)
- Power supply, kJ - 1300 (320).

References

1. Borisevitch V.K., Sabelkin V.P., Potapenko A.N. Design of Optimal Technological Processes of Hydroexplosive Forming by Computer Simulation. - Proc.IX Int.Conf.HERF, Novosibirsk, Aug.18-22, 1986, p.209-213.
2. Sabelkin V.P., Solodyankin S.N. Equipment for Explosive Forming of Parts from Low-Ductility Alloys.-Proc.IX Int.Conf. HERF, Novosibirsk, Aug.18-22, 1986, p.375-379.
3. GB Pat.No.2 081 630, Int.Cl.^{3}, B 21d 26/08. Method, Apparatus and Gas Gun for Forming Articles by Impact Load. Sabelkin V.P., Borisevitch V.K., Solodyankin S.N. etc., Sept.19, 1984.

PULSE STAMPING OF INDIVIDUAL PROSTHETIC COMPONENTS

A.N.Sytenko, H.N.Bahzina
Ukrainian Research Institute of Prosthetics, Kharkov, USSR

Manufacture of individual prosthetic sockets for artificial limbs is a single-unit production requiring flexible technologies. A pulse stamping device (PSD) and its rigging were developed as a basic equipment for prosthetic plants /1,2/. The development applies the method of pulse energy stamping of blanks against a die reflecting individual relief of a residual limb. The gas detonating explosion of a stoichiometric mixture of oxygene with propane-butane (methane).serves as a source of pulse energy. Power--transmitting media is water. Simplified functional diagram of the PSD-03 is presented in Fig.1.

The key element of the device is the energy unit comprising the detonation energy tube (DET), the gas mixer, the mechanism sealing the open end of the DET and the gas mixture ignition system.

The DET is a thick wall tube with the diameter selected to fit for stamping requirements of small-size prosthetic sockets (below-knee prostheses for children, upper extremity prostheses).

The mixer placed in the upper part of the DET ensures proper mixing of the gases due to its shape, size and sites of holes, it has intake holes for gases as well as pressure release holes. Gases are delivered to the energy unit via special flexible hoses.

mechanism permits to shut tightly the open end
plug.
ment fuse lighter. The ener-
rough the electromechanic
ole for its vertical movement.
ded frame structure.
(filling of water into a
ergy unit, ignition of the gas
remote control panel. A sys-
designed for safety operation.
metal prosthetic sockets is

rication of the die is an impres-
al limb by means of plaster ban-

p
min
dustry
shown i
The
the work /3/
me or bracket,
technological un
together with moun
ous mixture is held

*The Figure is given a

dages. The stump is then encased in socks whose thickness should comply with the socket wall thickness including polymeric coating. The die is a solid-steel cone box into which the impression is placed, while the remaining space is filled with a rapidly solidifying material, for instance, liquid plaster. When the die is ready, the welded tapered blank is placed in the device so that the energy unit axis coincides with the blank axis. A special device is used to align the blank with respect to the energy unit. Inside the blank water is filled, the end of the DET being in the inner part of the blank is travelling upward in such a way that the blank's deformation starts from its lower part, permitting to pull blank's material to the zone of deformation. For the PSD-3 the zone of effective force application is 80-100 mm which determines the number of stamping cycles depending on the length of the blank. With respect to the blank's diameter, thickness and material the initial pressure of the gas mixture should be selected. For the PSD-03 its value may range from 0.1 to 0.6 MPa (for aluminium alloy).

Dimensions (mm) of the parts to be manufactured:

height, max.	- 450;
diameter, max.	- 200;
min.	- 60;
thickness, max.	- 2

A below-knee prosthetic socket is an elongated shaped part of complex asymmetry with inner cavity, closed cross-sections and open end faces. Socket surface cannot have a plane projection, it cannot be described analytically. It may be represented as a summary of consequent positions of a generating line rotating about a longitudinal axis.

Shape and size of cross-sections vary gradually along the length of the socket. The relation of the maximum cross-section perimeter to its minimum value can be 1.25, while the relation of the socket length to its minimum estimated diameter ranges from 1.2 to 6. Practical application proves that the socket wall thickness may range from 1.5 to 2 mm for aluminium alloys. To achieve full stamping result in socket blanks one should apply ductile enough metals. Ductility is not a characteristic but a state of material and it is dependent on a number of factors most significant of which are: time and temperature conditions of deformation and uniformity of its distribution.

Application of detonating energy of gas mixtures creates the

optimum deformation conditions in pulse stamping of blanks for prosthetic sockets. The rate of deformation is (10-20) m/s and the deformation force ranges from 5 to 10 MPa.

References

I. А.с. №878279, СССР, М.Кл[3] А 6I F I/02. Матрица для штамповки приемных гильз голени. В.А.Назаренко и др., БИ №4I, I98I.

2. А.с. №878277, СССР, М.Кл[3] А 6I F I/02. Способ изготовления приемных гильз протезов конечностей. А.Н.Ситенко и др. БИ № 4I, I98I г.

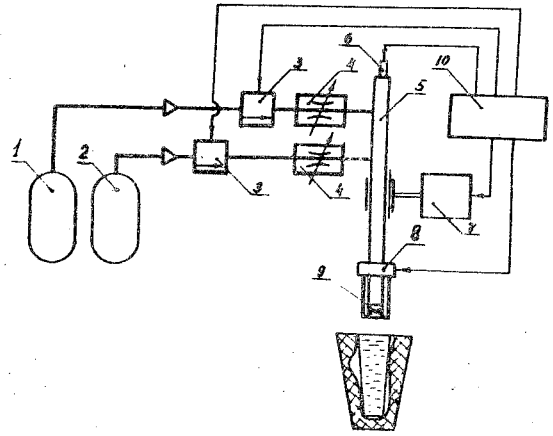

Fig.I. Schematic functional diagram of the pulse stamping device:
1,2 - gas tanks; 3 - valves; 4 - throttles; 5 - detonating gas source; 6 - spark plug; 7 -hoisting mechanism; 8,9 - sealing devices; 10 - control panel.

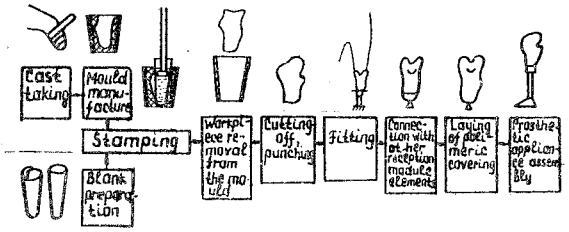

Fig.2. Technology for stamping of metal prosthetic sockets.

To the paper: Polák K. «Theoretical and technological aspects of high strain — rate forming».

Fig. 3. Twinning (250×).

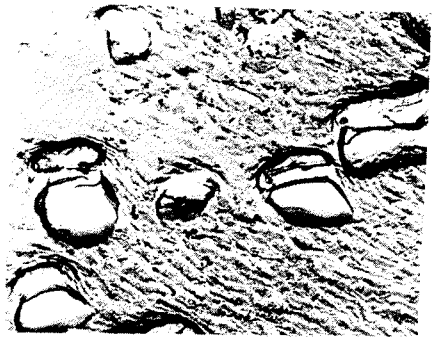

Fig. 4. Carbides fragmentation (9500×).

Fig. 5. Dislocation substructure after dynamic loading (30000×).

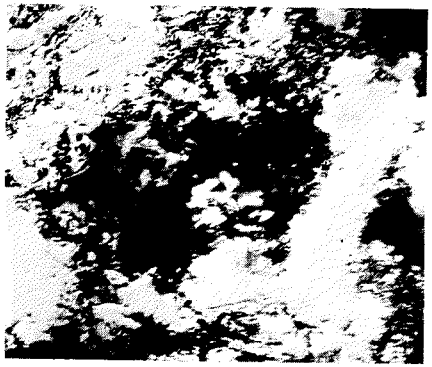

Fig. 6. Dislocation substructure after static loading (30000×).

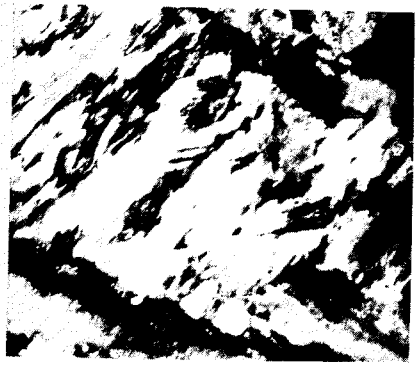

Fig. 7. Martensite substructure after dynamic distortion (30000×).

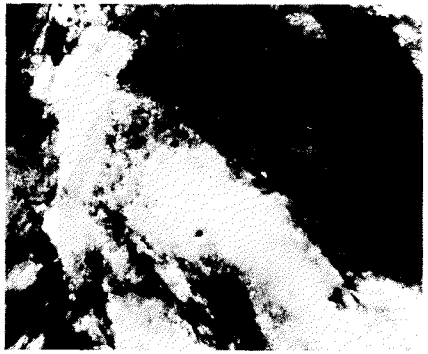

Fig. 8. Martensite substructure after static distortion (30000×).

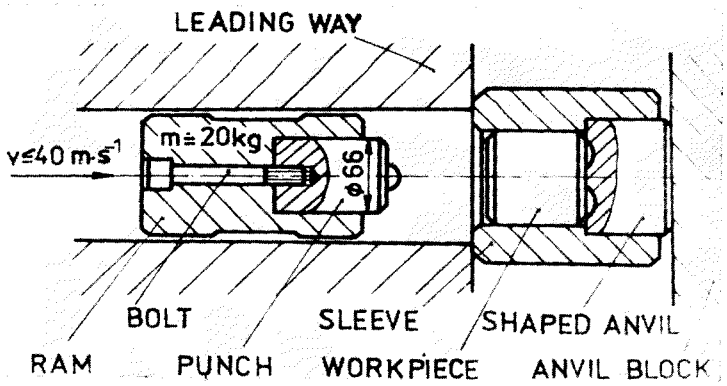

Fig. 9. Groove shat into material.

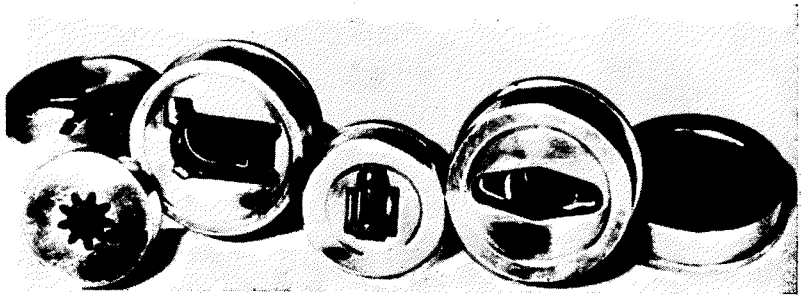
Fig. 10. Products made by shutting-in methods

To the paper: Borisevitch V. K., Sabelkin V. P., Vovk V. T. «Industrial application of impulsive high pressures in sheet forming with parameters optimization».

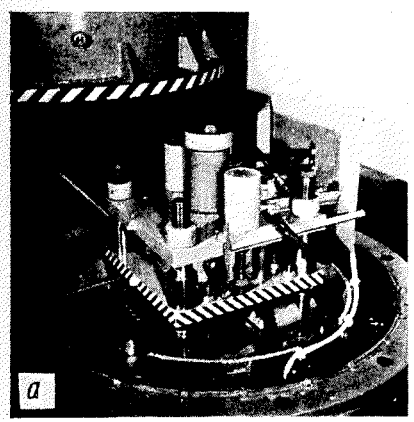

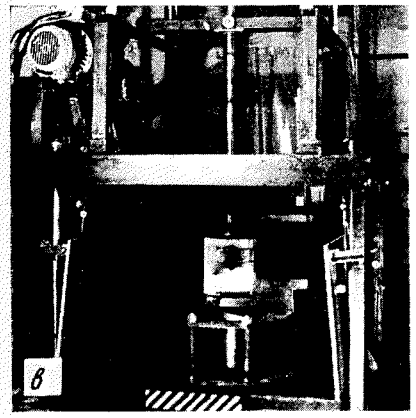

Fig. 1. Installation for heat forming: a — from the flat blanks; b — from the cylindrical blanks.

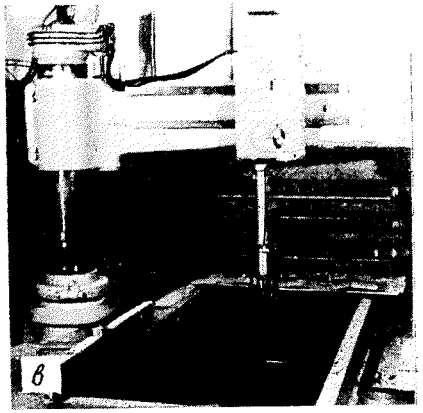

Fig. 2. Installation for parts forming by the detonable gaseous mixtures: a — closed scheme; b — open scheme

To the paper: Sharashenidze G. A., Kostava A. A. «Silicon carbide's treatment under the high pressure and temperature conditions».

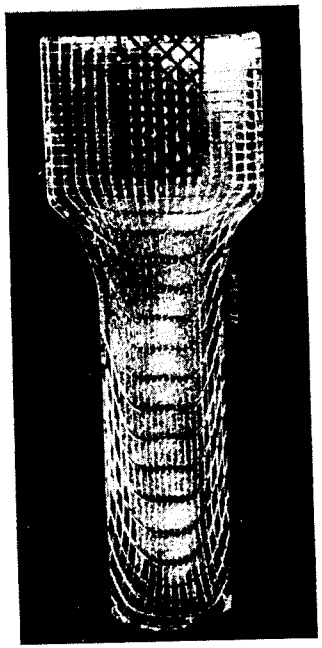

Fig. 2. Bar pressed through double channel matrix (dashed line shows the applicable zone for storage of SiC powder).

To the paper: Dyachenko S. S., Alexandrov N. G., Zolotko V. A., Miloslavskaya E. L., Gorelkova L. E. «Hydroextrusion used in the preliminary thermomechanical treatment cycle for improving the complex of mechanical properties of machine elements».

Fig. 1. Structure of 120Х3Г3 steel after hydroextrusion, ×40000.

Fig. 2. Structure of 120Х3Г3 ▶ steel after hydroextrusion and tempering (600 °C, 2h), ×40000.

Fig. 3. Substructure of austenite of 120Х3Г3 steel hydroextruded in α-state. Temperature of quenching 970 °C, ×40000.

To the paper: Marinov M., Vodenitcharov St. «Some sealing problems of the bayonet — type joints for big diameter pressure vessels».

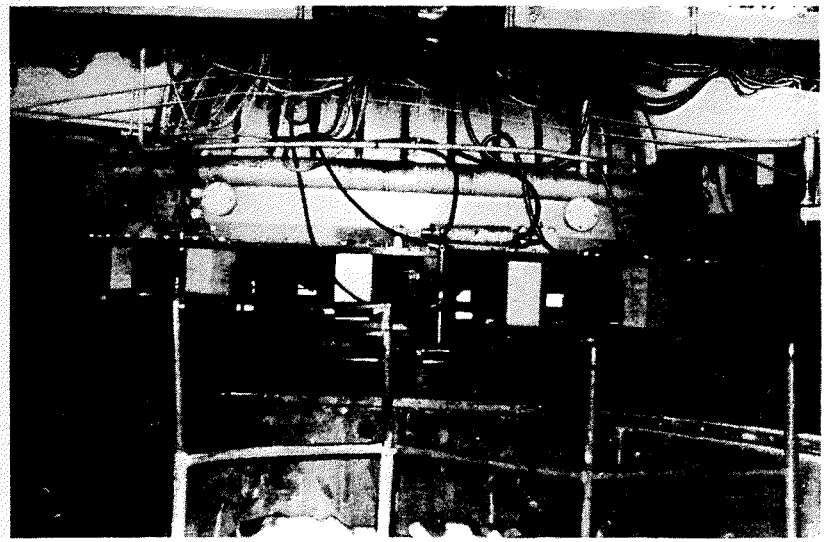

Fig. 6. Photograph of a pressing ring and a part of a bayonet — type joint for pressure vessel with 3600 mm diameter and $p_{op}=1.6$ MPa, having sealing assembly of the investigated type.

To the paper: Koviko V. S., Saakyants V. P. «Structure effect of hardening of carbon steels».

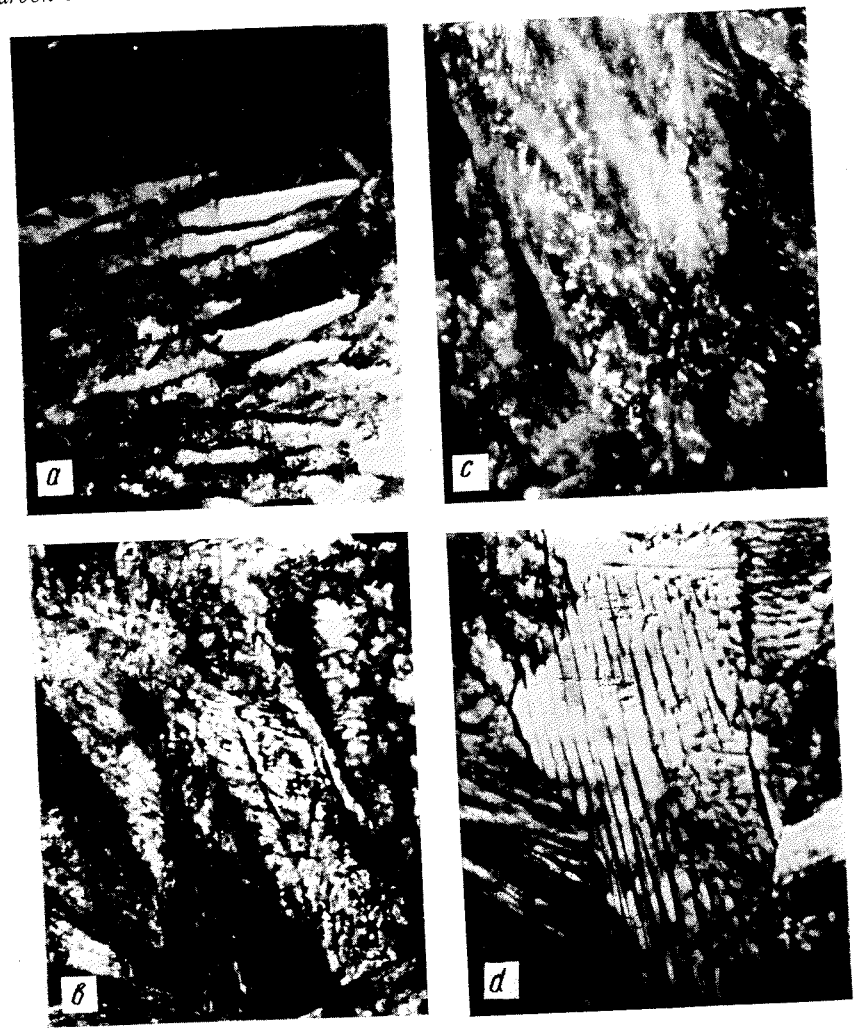

Fig. 2. Electron microphotographs of structures before (a — d) and after (e — g) hydrostatic pressing (×20000); a, f — higher bainite structure; b, e — lower bainite structure; c — dark — field image in cementite reflex; d — thin — plate pearlite of mixed structure; g — annealed plate pearlite.

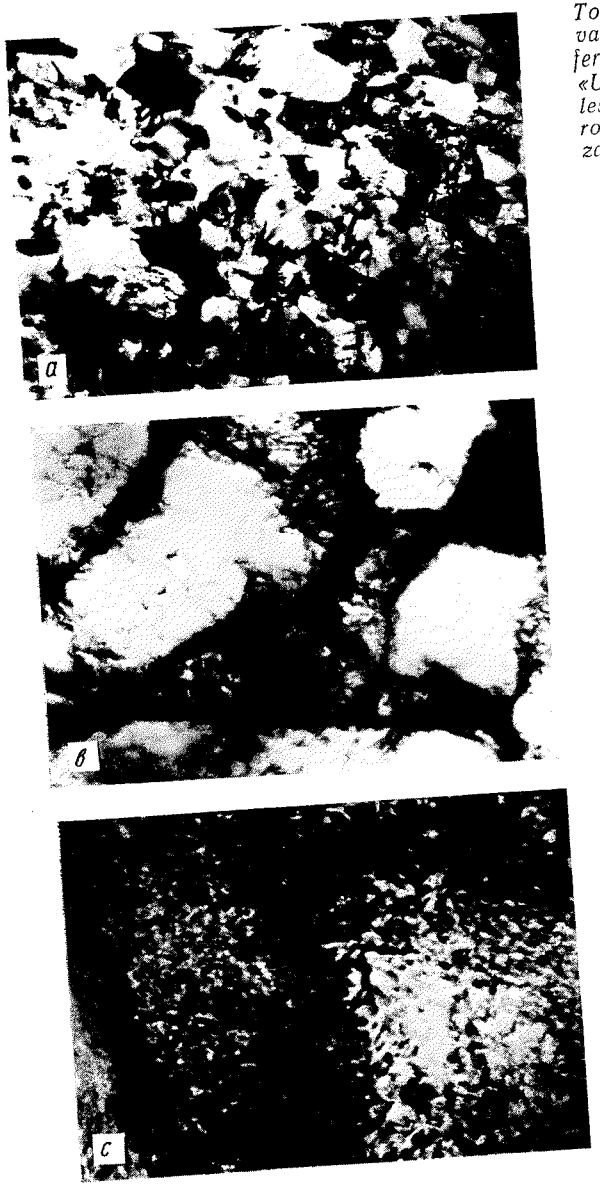

To the paper: Konstantinova T. E., Zaitsev V. I., Lyafer E. I., Dobrikov A. A. «Use of dislocation ensembles formed under high hydrostatic pressure for optimization of steel structure».

Fig. 2. A structure of steel: a — 30ХГСА steel tempered before deformation at 873 K and deformed by hydrostatic pressure on 50 %; b — cellular structure of X12M steel deformed after annealing; c — dislocational martensite in deformed and quenched X12M steel.

BAROFORMING OF COAL MATERIAL STRUCTURE. FUNDAMENTALS

N.K.Neronin

Donetsk Physico-Technical Institute, Ukrainian SSR Academy of Sciences, Donetsk, USSR

Rational energetic and technological application of coal materials, among them coals, peat and graphite, will become reality as we learn to effectively control its structure. In our laboratory we theoretically substantiated and experimentally demonstrated significance of such factor as high static pressure in control of molecular structure of these materials for obtaining products with desirable properties /1-3/. Traditional approach is heat treatment or chemical methods. In comparison to it pressure treatment offers considerable advantages as no admixtures are introduced in products and no undesirable transformation of product composition takes place. Structure of product is rebuilt in, so to say, pure manner. Also important is the well-known fact that at equal spendings to transform products pressure is more advantageous, than temperature.

Coal materials were treated by static pressure up to 2 GPa according to four mechanical deformation schemes by five methods (see Figure). The common factor for all of them is the stressed state of all-sided compression, uniform at hydrostatic pressing and nonuniform in other cases. At the same time the mentioned methods are different by certain factors, the main among them is the proportion of main deformations and main stresses.

For studies we used coal material of the whole metamorphic chain, of peat and natural graphite of different geological fields. Effect of pressure was observed using modern methods: optical microscopy, X-ray analysis, EPR and IR-spectroscopy. We studied also certain technological properties of materials and products.

As a result of studies we found the following:

1. Pressure treatment results in irreversible transformations of structure and properties of coal materials. Character and level of them are determined mainly by pressure level, mechanical scheme of deformation, metamorphism (degree) and physico-chemical state of substances.

2. Results of treatment are improved with rise of pressure and especially - if shift stresses are developed in specimens.

3. Direction of structure transformation of coal materials is determined by mechanical scheme of deformation.

4. Limiting pressures, at which irreversible changes in organic matter take place, depend on shift stresses. With increase in the latter limiting pressures are decreased.

We shall illustrate these conclusions by some examples.

As a result of one-sided pressure ca. $1.5 \cdot 10^2$ MPa molecular orientation of coal matter is observed due to rotation of carbon nets and destruction of side aliphatic chains, coupling the carbon framework of material. At hydrostatic compression anisotropy is not observed, but changes of mean dimensions of ordered regions of layers and inter-plane distance takes place at lower (1.2- - 1.3 times) pressures in comparison with one-sided pressing. In both situations destruction does not affect carbon layers.

More considerable changes of structure as a result of treatment according to schemes, which stimulate shift stresses in specimens, are observed. Thus, at hydropressing of coal destruction affects even aromatic layers, and the limiting pressures are 2-3 times lower in comparison with hydropressing treatment. Abruptly the reaction properties of coals are increased. For example, solubility in benzene of hydropressed gas coals are seven times higher in comparison with solubility of the same coal after hydropressing by the same pressure.

Baroforming application in economy, main branches

Fuel Production	Production Technologies	Food Production
Synthetic liquid fuel[1]	Brown coal wax[2]	Bioactive substances from peat, coal and lignites: poultry[3], cattle-breeding[1], plant farming[1], seed farming[3].
Coals with increased energy capacity[1]	Alkali coal reagent[2]	
Non-traditional methods of coal extraction[1]	Coal bitumen[4]	
Prediction of explosive regions of coal strata[2]	Thermocoals; coal-graphite materials[1]	
	Layer-like compositions of graphite[2]	

[1]prospect, [2]laboratory tests, [3]industrial pilot plants, [4]results of research and development are applied in economy

The role of shift stresses in structure transformation of materials can be demonstrated in experiments using plants of Bridgeman-anvil type. Increasing the shift by rotation of dies the li-

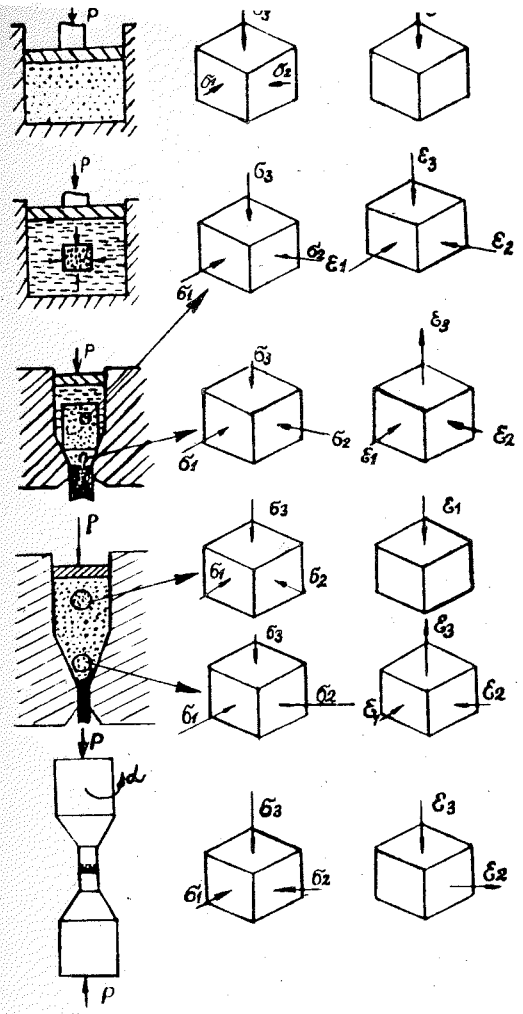

Schemes of mechanical deformed state ($\sigma_1, \sigma_2, \sigma_3$ - main stresses, $\varepsilon_1, \varepsilon_2, \varepsilon_3$ - main deformations): a - one-sided pressing in a rigid press-form, b - hydrostatic compression, c - hydropressing, d - extrusion, e - pressing with shifts developed.

miting pressures were decreased for anthracite down to 0.05 GPa (in absence of shifting it is equal to 0.4 GPa).

Dependence of structural transformation character on MSD can be illustrated using graphite, treated by three methods. X-ray study of specimens demostrated that after hydropressing and extrusion (here MSD can be compared) reflections became weaker (001), l -even. A row of reflections disappears, as follows: (101), (102), (202) and so forth. After hydropressing diffractional reflections do not disappear, in contrary they become more intensive. Thus, hexagonal framework of graphite at hydropressing and extrusion transforms and becomes rhombohedric, and at hydropressing a contrary transformation takes place /3/.

The obtained results permit to develop new methods and apply coal materials in new branches of economy. This is possible due to baroforming, a promising new technology for obtaining products with desirable properties (see Table) /2/.

References

1. Neronin N.K. Effect of high pressures on structure transforming of fossil coals of Donbas coalfields. Dissertation, Donetsk Physico-Technical Institute, Acad. Sci. Ukr.SSR, Donetsk, 1981, (in Russian).
2. Neronin N.K. Studies of effect of pressure treatment on fossil coals and prospects of applying research results in economy //Chemistry and coal treatment: Transactions of sci.soc.- Kiev: Izd. Naukova Dumka, 1987.- P.77-87, (in Russian).
3. Neronin N.K., Varankina O.P., Samoilenko Z.A. Structural changes in graphite at hydropressing//Fizika i tekhnika vysokikh davleny, 1983, vyp.14. - P.34-36, (in Russian).

HIGH PRESSURES IN MODERN TECHNOLOGY

G.A.Krivonos

VNIIMETMASH, Moscow, USSR

At all stages of science and technology development, material properties were one of the most important factors, determining the efficiency of social production and rate of its progress.

Today conventional methods of production and processing the main material for engineering - metals (i.e. casting, mechanical working, cutting, welding and heat treatment) have been brought to perfection. But nevertheless these methods can't meet modern engineering requirements.

As a result several new technological processes have been developed. They are based on the following: during material processing, a billet or an article is subjected to high all-round pressure. In some cases during processing high temperature is maintained (or changed according to the given law).

Up to the present several such technological processes have been developed, but the processes used most widely are hydrostatic and hydrodynamic compaction of powder and composite material, gas static treatment of powder and monolithic material and synthesis of synthetic materials.

Industrial hydrostatic compaction is usually carried out at pressures up to 400-600 MPa, and in some cases - up to I000 MPa. For this process hydrostats have been developed which ensure treatment of billets with diameters of I800 mm and length - of 3000mm.

Experimental analysis, carried out in VNIIMETMASH shows that for some materials during compaction processes billet holding at maximum pressure is not required, and speed of pressure increase and decrease does not affect article properties.

Accordingly in VNIIMETMASH quite new equipment - hydrodynamic machines have been designed which are manufactured only in the USSR. Principle of operation of hydrodynamic machines differs from that of hydrostats: high liquid pressure necessary for billet compaction is generated for a short period of time: $I0^{-4}$-$I0^{-3}$. The given pressure originates from liquid compression by a piston, preliminary accelerated up to high speeds (I00-200 m/s) as a result of gases expansion, which liberated during gunpowder charge combustion.

In hydrostats and hydrodynamic machines liquids are used as

working medium, providing all-round pressure on a billet. This fact significantly limits the permissible level of working temperature. As a rule billet is treated at room temperature, sometimes the temperature is increased up to 350-400°C and only in exceptional cases (when using special technological methods) the compaction can be done at higher temperatures.

When hydrostats and hydrostatic treatment are used, there are practically no limits to working temperatures. In this case gas is used as a working medium, which provides operation at temperatures up to 2000-2900°C, and operating pressures during production do not exceed 200 MPa. On VNIIMETMASH trial gas static equipment stable operation at pressures up to 800-100 MPa has been provided. However within the next 5-10 years pressures in industrial gas static equipment will not be likely to exceed 250 - 300 MPa.

Significantly higher pressures are used on presses for synthesis of synthetic materials in comparison with hydrodynamic machines.

Despite the difference in design of gas- and hydrostats, hydrodynamic machines and presses for synthesis of materials the whole range of equipment can be joint into one class of high-energetical units which follows from mutual character of their main phenomena inherent in the equipment operation.

The term "high-energetical" has double meaning in this context. As in case of conventional press-forging plant it meant that a unit per one cycle performs considerable work, i.e. consumes considerable energy. However unlike conventional equipment there is quite different relationship between energy consumed by a drive of gas- and hydrostat, hydrodynamic machines and press for synthesis and mechanical work of deformation. This is bound up with the fact that in gas- and hydrostats and hydrodynamic machines the billet is subjected to treatment through high pressed media (liquids and gases), hence they accumulate great store of potential energy. The same is characteristic of presses for synthesis as their working stroke is small, and the main cylinder holds a considerable liquid volume, and as a rule higher pressures are used in the drive.

Hence the second meaning of the term "high-energetical", when used in reference to gas- and hydrostats, hydrodynamic machines and presses for synthesis: it emphasizes that when operating, the unit systems accumulate great store of potential energy. This fact makes specific requirements on selection of equipment parameters,

its design, space where it is installed and safety operation conditions. Work consumed per one high-energetical unit working cycle at initial estimation can be considered as follows: $A_{пол} = A_{мех} + A_{рс} + A_{зеф}$, where $A_{пол}$ - total consumed work per one cycle, $A_{мех}$ - mechanical work of deformation, $A_{рс}$ - work consumed for elastic compression of working medium, $A_{зеф}$ - work consumed for elastic deformation of unit load-bearing elements.

Now we introduce the concept of high mechanical efficiency.

$$\eta = A_{мех}/A_{пол}$$

As working media (liquid and gases) are characterized by high compression, when estimating high-energetical unit mechanical efficiency one can neglect the value of the work of load-bearing elements deformation because

$$A_{рс} \gg A_{зеф}$$

Based on the assumption that

$$\eta = A_{мех}/(A_{мех} + A_{рс})$$

work of mechanical deformation of single volume billet can be considered as follows:

$$A_{мех} = \int_0^{\Delta V} p\,d(\Delta v),$$

where Δv - billet volume change while applying all-round uniform pressure p.

Work $A_{рс}$, consumed for working medium elastic compression can be presented as follows:

$$A_{рс} = \frac{b^2}{E_o}\left[\frac{p}{b} - \ln\left(1 + \frac{p}{b}\right)\right],$$

where E_o - volumetric modulus of liquid elasticity, b - equation constant.

For gasstats and presses for synthesis mechanical efficiency is practically equal to zero, and for hydrostats and hydrodynamic machines, it is much lower than that of conventional press-forging equipment. This is bound up with the fact that processes provided by these machines are based to the great extent on other physical phenomena than processes, carried out on conventional press-forging equipment and for them the concept of mechanical efficiency does not reflect the essence of the phenomena.

At the same time from engineering point of view low mechanical efficiency, connected with accumulation of great energy content in the unit systems requires detailed consideration of two groups of problems.

The first group includes analysis of mechanical system per-

formance (most loaded elements of hydrostats, hydrodynamic machines, gasstats and presses for synthesis) in which great store of potential energy is accumulated at simultaneous or quite high-speed change of load.

The other one deals with reasons of this or that process selection expedience (hence this or that kind of high-energetical equipment) for producing specific material or article.

As shown in works, carried out in VNIIMETMASH in space "pressure-temperature-time" there is a surface each point of which ensures production of an article with preset properties. This surface is invariant from the Customer's point of view. But it is not invariant from an engineer's or operator's point of view. Moreover, the interests of the latter are rather contradictive. We can, for example, decrease an operating pressure, which reduces the equipment weight, decreases its cost and improves operation conditions, but simultaneously decreases production owing to increasing working cycle.

In VNIIMETMASH on the basis of the analysis of these problems a modern complex of high efficient equipment for producing material with superior characteristics has been developed.

PLASTICITY AND FRACTURE OF METALS DUE TO DEFORMATION UNDER HIGH HYDROSTATIC PRESSURE

A.A.Bogatov, S.V.Smirnov, O.I.Miziridsky
The Urals Poly echnical Institute, Sverdlovsk, USSR

The study of plasticity was carried out on universal test installations incorporating chambers with controlled hydrostatic pressure of working liquid. The installations were developed in collaboration with the Institute of Physics of Metals of the Urals Branch of the Academy of Sciences of the USSR and allow to effect various mechanical investigations under the chamber pressures ranging from 0.1 to 1200 MPa.

Plasticity of metal was quantitatively evaluated as the degree of shear deformation $\lambda_p = \int_0^{t_p} H d\tau$, accumulated by the sample by the moment of macrofracture under predetermined thermomechanical parameters and ordinary stress (where H - speed intensity of the shear deformation, τ-deformation time). The effect of the type of strained condition was realized quite recently /1/. For this purpose we used different hydrostatic pressures in the working chamber in various types of tests. To interpret test results it is reasonable to use dimensionless invariant complexes as characteristics of strained condition: σ/T - strained condition index; $\sigma = \frac{1}{3}(\sigma_{11} + \sigma_{22} + \sigma_{33})$ - mean ordinary stress; T - tangent stress intensity) and Lode-Nadai index $\mu_\sigma = 2(\sigma_{22} - \sigma_{33})/(\sigma_{11} - \sigma_{33})$. The combination of indices σ/T and μ_σ makes it possible to evaluate the strained condition quantitatively and quite definitely, thus allowing to compare the results of various tests. Index σ/T shows the mean level of ordinary stresses; with $\sigma/T > 0$ torsional stresses prevail, while with $\sigma/T < 0$ - compressing ordinary stresses are predominant. Index μ_σ testifies to the type of strained condition; the value $\mu_\sigma = \pm 1$ corresponds to the axis-symmetrical strained condition of compression or stretching and $\mu_\sigma = 0$ to flat strained condition.

So far more than 80 steels and alloys of different grades have been studied. The plasticity of the majority of metals studied increases with the decrease of strained condition index, as shown in Fig.1a,b,d. A number of aluminium and copper alloys show unlimited plasticity under some critical values $(\sigma/T)_*$ (Fig.1b).

The effect of the type of strained condition is variable:

plasticity of alloy BT1-0 decreases with the increase of μ_σ; while that of alloy AD1 increases; with steel I2XIMΦ the effect of μ_σ on plasticity under various strained conditions is different. By now joint effect of structural and strained condition on plasticity is studied insufficiently though it can be essential and variable. Thus, Fig.1d gives plasticity curves of low-carbon structural steel after heating to 780 °C followed by cooling in air and in water. In the range of stretching strains plasticity of heat-treated steel with strained martensitic locations is 3-4 times low than after normalizing. The lowering of strained condition actively neutralizes the sources of inner superstrains which may sometimes cause microcracking, that is why plasticity of heat-treated steel quickly grows due to realization of potentially higher plasticity of finely dispersed structure. Substantial influence of the method of heat-treatment on the dependence of metal plasticity on strained condition may be shown by the steel 38X2MIOA (Fig.1d).

During deformation of unstable alloys plasticity is defined by the change of phase composition while straining and by the interrelation of plastic properties of main and depositing phases. Fig.1c gives plasticity curve of the alloy 05Г20С2. Visible plasticity gap is due to the formation of martensite ε which is more brittle than austenite.

The study of low-cycle fatigue under strain revealed the decrease of cyclic deformation effect on plasticity during the growing of compressive strains, and the value of Menson-Coffin index increases up to 1 upon reaching $(\sigma/T)_* \simeq -4.2$ (Fig.2).

Plasticity study results under hydrostatic pressure are widely used for prospecting metal fracture in technological processes of plastic deformation. This can be done by using the phenomenological theory of fracture /1,2/. The main conceptual parameter of the theory is the defectiveness of metal ω. Prior to deformation $\omega=0$, at the moment of initiation of cracking $\omega=1$. Intermediates values characterize the level of metal defectiveness due to deformation. To prospect the articles quality according to defectiveness one should plot the characteristics of strained-deformed condition (σ/T, μ_σ, λ) along the trajectory of material particles movement; get the diagram of plasticity λ_ρ and coefficient $1/\beta$ as a result of experiments (according to the manner and in the form described in /1,2/), plot metal defectiveness according to manner of /1/ and compare it with the admissible value for the given class of articles.

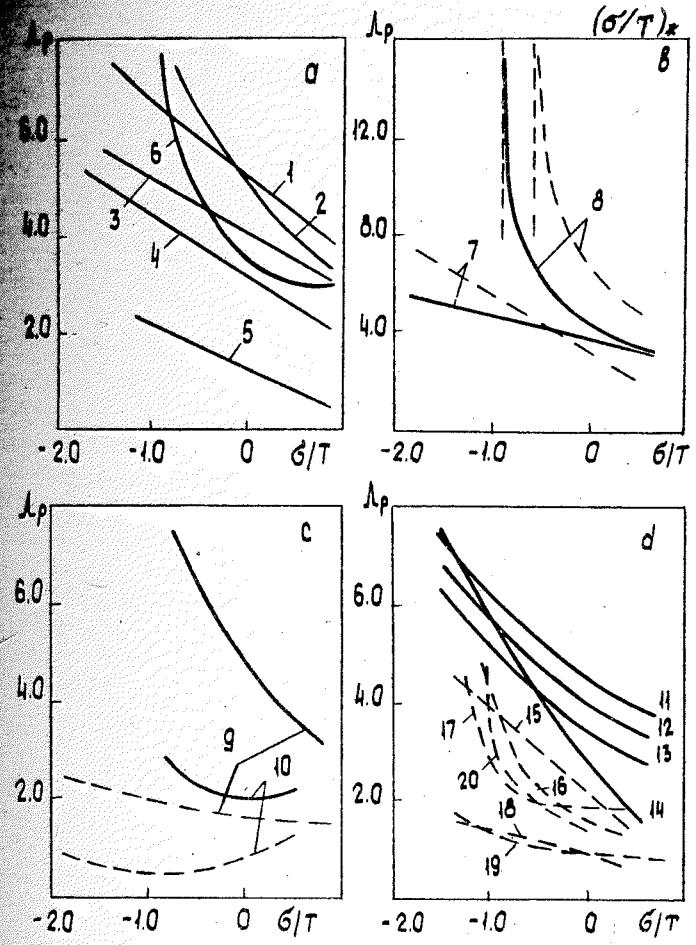

Fig.1. Metal plasticity curves: 1 - α-Fe; 2 - Ti; 3 - Nb; 4 - Mo; 5 - W (compositions); 6 - Al; 7 - I2XIMΦ; 8 - AD1; 9 - BT1-0; 10 - 05Г20С2; 11...14 - Ст 3сп (the size of ferrite grains 12 m.m.m., 20 m.m.m., 30 m.m.m.); 14 - Ст 3 сп (after thermal hardening); 15...20 - 38X2MIOA (tempering at 760 °C; annealing at 880 °C; normalizing at 960 °C - tempering at 760 °C; normalizing at 860 °C; normalizing at 960 °C; BTMO); $\mu_\sigma=0$; $\mu_\sigma=-1$.

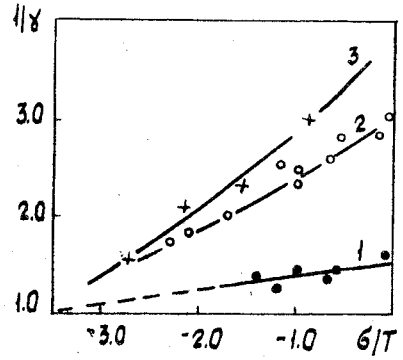

Fig.2. Interrelation of Menson-Coffin index γ and strained state index δ/T due to deformation by cyclic torsion under hydrostatic pressure of steel samples 45(3), ШХ-15(2) and I2XI8HIOT (I).

References

I. Богатов А.А., Мижирицкий О.И., Смирнов С.В. Ресурс пластичности металлов при обработке давлением. М.:Металлургия,1984 I44 с.

2. Колмогоров В.Л. Напряжения, деформации, разрушение.М. :Металлургия, 1970, 229 с.

SILICON CARBIDE'S TREATMENT UNDER THE HIGH PRESSURE AND TEMPERATURE CONDITIONS

G,A.Sharashenidze, A.A.Kostava

The Metallurgy Institute of the Academy of Sciences of Georgian SSR, Tbilisi, USSR

The present investigation has been aimed at the search of the methods providing the increase of mechanical characteristics and other qualities of silicon carbide. This task is supposed to be solved with the help of high pressure and high temperature*.

The object of the research was presented by both reaction-sintered silicon carbide and by powders for their successive treatment, based on the specific flow mechanism under the high temperature extrusion.

The device (Fig.1) admits pressure up to 1500 MPa under temperature up to 2600 °C.

The heating of bars is carried out on the apparatus of RF current.

Reaction-sintered silicon carbide or the powder silicon carbide has been placed into a glass made of sintered alloy 75% Mo + 25% W. The research of the peculiarities of high-temperature extrusion mechanism has been carried out with the use of various filling media (ferrochrome ~1400 °C, bentonite ~1700 °C, calcium oxide ~ 2500 °C and the powder SiC ~2550 °C) having different sintering temperatures. Depending on the temperature of the deformation the condition of the fillers changes from pouring to tough and that should be taken into account while estimating the process. By the change of the matrix geometry the reasonable zone of material location on the base of SiC and conditions for its uniform flow have been stated (Fig.2**).

Bars with pressed powder fillers inside the glass (p ~100 - 200 MPa) have been covered above and isolated to prevent the ingress of outer medium (oil, some medium transfering pressure). The volume of fillers has made up approximately 30%. The bars have been heated up to various temperatures and have been subjected to extrusion.

Fig.3 presents a plot of the change of the specific share as a function of the temperature under the extrusion of the composi-

* Гаршин А.П.,Карлин В.В.,Олейник Г.С.,Островерхов В.И. Конструкционные карбидокремниевые материалы.Л.Машиностроение,1972,152 с.

** The Figure is given at the end of the book.

te medium (75% Mo + 25% W)+SiC without back pressure ($\xi = F_0/F_1 \approx$ ≈1.3; 1.7).

The problem of optimization of thermo-mechanical conditions of the extrusion of filling media against deformation resistance which displays sensitivity to the temperature and changes in a wide range presents a complicated task.

Let's consider the kinematics of the flow of the two media (metal-filler) whose deformation resistance is presented as $k=k(\theta)$.

Equations of the physical state of such medium is as follows:

$$\sigma_r = \sigma + 2K(\theta)\frac{\dot{\varepsilon}_r}{H};$$
$$\sigma_\theta = \sigma + 2K(\theta)\frac{\dot{\varepsilon}_\theta}{H}; \qquad (1)$$
$$\tau_{r\theta} = K(\theta)\frac{\dot{\gamma}_{r\theta}}{H}$$

where $\sigma_r, \sigma_\theta, \tau_{r\theta}$ -stress tensor components;

$\sigma = \frac{\sigma_r + \sigma_\theta}{2}$ -hydrostatic pressure;

$\dot{\varepsilon}_r = \dot{\varepsilon}_\theta, \dot{\gamma}_{r\theta}$ -speed deformation tensor components;

$H = \sqrt{4\dot{\varepsilon}_r^2 + \dot{\gamma}_{r\theta}^2}$ -speed deformation shearing intensification;

θ -current angle

The kinematic speed field is accepted in the following form:

$$U = -U_0 \frac{r_0}{r} \exp\left(-\frac{\mu}{\alpha}\theta^2\right), \qquad (2)$$

where U_0 -speed extrusion;

α -solution angle;

μ -parameter proportional to friction factor;

r_0, r -parameters of matrix.

Finding $U(\theta)$ and $U'(\theta)$ we get

$$H = 2U_0 r_0 \exp\left(-\frac{\mu}{\alpha}\theta^2\right)\frac{1}{r^2}\sqrt{1+\left(\frac{\mu}{\alpha}\right)^2\theta^2} \qquad (3)$$

Under the condition of plastic non-uniformity of the kind

$$K(\theta) = K_0\sqrt{1+\left(\frac{\mu}{\alpha}\right)^2\theta^2},$$

for the physical state equation (1) we get

$$\sigma = -K_0\left[\left(2+\frac{\mu}{\alpha}\right)\ln r + \frac{\mu}{\alpha}\theta^2\right] + C, \qquad (4)$$

$$\sigma_r = -K_0\left[\left(2+\frac{\mu}{\alpha}\right)\ln r + \frac{\mu}{\alpha}\theta^2 - 1\right] + C, \qquad (5)$$

$$\sigma_\theta = -K_0\left[\left(2+\frac{\mu}{\alpha}\right)\ln r + \frac{\mu}{\alpha}\theta^2 + 1\right] + C, \qquad (6)$$

$$\tau_{r\theta} = \mu K_0 \frac{\theta}{\alpha} \qquad (7)$$

where k_0-is the flow limit to the shear of the material in the central tension zone.

While the filling medium and metal flow simultaneously it's necessary that normal and tangent of the tension for the metal and the medium when $\theta=\alpha_r$ should coinside.

While pressing when back pressure of $\sigma_{r(bac)}$ is applied for resistance to the outlet of the metal from the deformation site we have:

$$\sigma_r = -K_0\left[\left(2+\frac{\mu}{\alpha}\right)\ln\frac{r}{r_0} + \frac{\mu}{\alpha}\theta^2 - 1\right] + \sigma_{r(bac)}.$$

For practical purposes $\sigma_{r(bac)} \approx 2\ k_0$, then

$$\sigma_r = -2K_0\left\{\left[\left(1+\frac{\mu}{2\alpha}\right)\ln\frac{r}{r_0} + \frac{\mu}{2\alpha}\theta^2 - \frac{1}{2}\right] + 1\right\}. \qquad (8)$$

Equations (7) and (8) show that the central location of the medium can ensure sufficiently uniform all-sided reduction of the body (filling medium). This has been confirmed experimentally.

Reaction-sintered silicon carbide has been treated under the pressure of 700-750 MPa and T up to 1800 °C.

The powder medium SiC up to T of 2500-2600 °C and pressure up to 500-750 MPa.

The central location of the medium (α=0-15°) ensures uniform flow and medium packing.

The experimental investigations have shown that the effects of pressure upon the reaction-sintered silicon carbide may increase the bending strength limit up to 25% (from 180 MPa up to 220-240 MPa) the compression changes by 0.1-0.3%.

The tests of the above mentioned materials in the range of high temperatures (800-1700 °C) have shown the tendency to a considerable increase of stability of mechanical properties.

C o n c l u s i o n s:

1. The use of extrusion processes makes it possible to get composite materials with the content of the medium on the base of SiC.

2. The effect of high pressure and high temperature brings forth a certain improvement of mechanical properties of carbide silicon production.

Authors thank I.G.Savchinsky for his cooperation in this work.

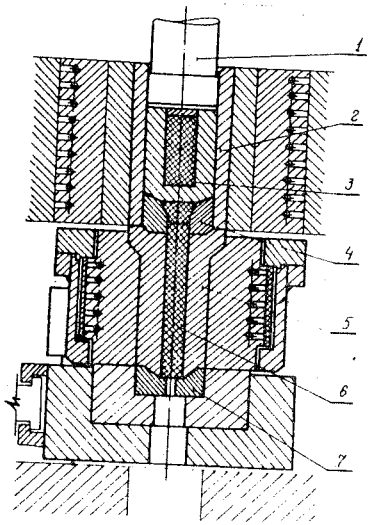

Fig.1. Device for extrusion of compositional bar with back pressure: 1 - punch; 2 - high pressure container; 3 - compositional bar; 4 -double angle matrix; 5 - low pressure container; 6 - back pressure medium; 7 - pressure control matrix.

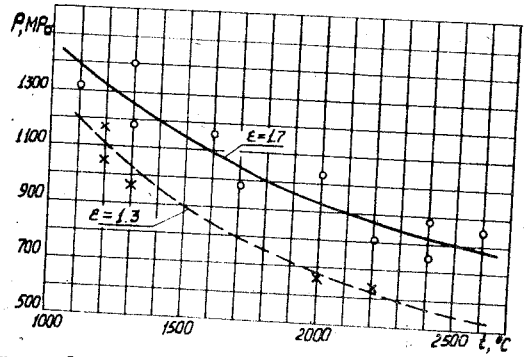

Fig.3. Change of specific force in extrusion of compositional medium (75% Mo+25% W)+SiC without back pressure.

HEALING OF DEFECTS UNDER HIGH HYDROSTATIC PRESSURES AND INDUSTRIAL USE OF HEALING PROCESSES

L.Yu.Maksimov, G.A.Krivonos, R.S.Vasiljeva
VNIIMETMASH, Moscow, USSR

For the last few years hydrostatic and high-temperature gas static treatment have been widely used for healing billets defects caused by conventional methods of production and also for elimination of nuclei fatigue damages in parts which guaranteed life is partially used.

Theoretical analysis* shows that if there are isolated spherical pores in the material and they are such that relative density is $\bar{\gamma}_0$ and all-round pressure P is exerted on it, then in time t the relative density will increase up to the value of $\bar{\gamma}$. Time t can be determined from the following equation:

$$t = \frac{\eta}{\sigma_s} \ell_n \frac{1+\sqrt{2}\cdot\sigma_s/p\cdot(1-\bar{\gamma}_0)}{1+\sqrt{2}\cdot\sigma_s/p\cdot(1-\bar{\gamma})},$$

where η and σ_s are plastic viscosity and yield strength of the material under treatment.

Therefore complete healing of defects requires time:

$$t_n \geq \sqrt{2}\,\frac{\eta}{p}\,(1-\bar{\gamma}_0) \qquad (1)$$

Experimental studies confirm the theoretical results of the analysis. In experiments billets of 40X steel were used in which defects have been caused artificially in the form of cylindrical cavities 2 and 3 mm in diameters and 80 mm in length. After gas static treatment for 4 hours at pressure of 140 MPa and temperature 1473 K defects vanished completely (were not visually found at 200x magnification). According to the equation (1) healing time under conditions should be not less than 10^4 s ($\sim$ 3 hours).

For mechanical properties study in the affected zone, standard samples were cut from a billet in such a way that the sample axis crossed the axis of the vanished defect at right angle. The experimental results given in Table 1 show high efficiency of the healing process.

VNIIMETMASH together with other institutes and plants successfully employs hydrostatic and gas static treatment for producing high-density articles from wide range of materials: from ductile metals to hard alloys.

*Mackensi S., Snutte Worth R.Proc.Phys.Soc. 62, 833 (1949).

Data shown in Tables 2 and 3 characterise the efficiency of such treatment for brass ЛС 59-I and zinc alloy ЦАМ4-I.

22 modes of operation have been studied for the optimal selection of high temperature gas static treatment parameters for hard alloys.

Table I. Mechanical properties of 40X steel after gas static treatment

Zone of sample cut	σ_B, MPa	$\sigma_{0.2}$, MPa	ψ, %	δ, %
Defectless material	516	308	71	22.9
Zone of defect	533	291	67.4	24.0

Table 2. Relative density value of brass

Material condition	T=20 °C p=1500 MPa τ=30s	Modes of treatment		
		T=20 °C; p=1500 MPa; τ=30s+T=400 °C; P=1500 MPa; τ=120 s	T=400 °C p=500 MPa; τ=120 s	T=700 °C P= 70 MPa τ= 60 s
Initial	8.21	8.21	8.15	8.21
After treatment	8.3	8.33	8.37	8.37

Table 3. Relative density value of zink alloy

Material condition	Modes of treatment		
	T=100 °C p=600 MPa τ=120 s	T=100 °C; p=1300 MPa; τ=120 s	T=150 °C p=1100 MPa; τ=120 s
Initial	6.28	6.4	6.35
After treatment	6.67	6.7	6.71

Treatment temperature T varies within the limits of 1200 °C - 1400 °C, maximum pressure p - from 80 to 100 MPa, holding time at constant pressure and temperature: 0-50 min., heating speed: 5-20 deg/min. Taking into consideration the versatility of the experiment, its results have been summarized by means of correlation-regression analysis (T.A.Emeljanova, Yu.F.Rudakov, V.F.Ochkesova, G.V.Alekseev, A.I.Belinicher et al took part in the work).

Changing of physical-mechanical properties and material structural characteristics after gas static treatment have been presented as functions of response ϕ depended on mode parameters. On the basis of studies (22 modes) functions ϕ were as follows:

$$\phi = A_o + A_1 T + A_2 \tau + A_3 V + A_4 \rho + A_5 T\tau + A_6 T_V + A_7 T\rho + A_8 \tau_V + A_9 \tau\rho + A_{10} V\rho \ .$$

The experimental results show that stable correlation exists between changes of density (degree of defects healing), strength, failure viscosity and properties uniformity depending on modes of operation in gas static apparatus.

Taking into consideration the obtained results, processing modes have been selected for gas static treatment of hard-alloyed block-dies inserts for synthesis processes. The above-mentioned treatment increases the block-dies durability by 1.4...2.3 times depending on alloy grade synthesis regimes.

APPLICATION OF HIGH HYDROSTATIC PRESSURES FOR PRODUCTION OF HARD-CARBIDE TOOLS

L.I.Alistratov, G.P.Mikhailenko, N.G.Kasatka, N.S.Gontarevskaya

Physico-Technical Institute, Ukr.SSR Academy of Sciences, Donetsk, USSR

Increase of durability of hard-carbide tools, broadening of range of products, reduction of specific consumption of materials and manufacturing cost are provided by the improvement of manufacturing technology. Hard-carbide products are manufactured by means of powder metallurgy: billets are pressed from powder mixtures, subjected, if necessary, to mechanical treatment and then sintered.

Operation of billet forming out of powder is an essential stage in the technological cycle and it greatly determines the quality of the obtained products. Hard-carbide mixtures are characterized by low plasticity due to presence of hard-carbide particles in them as the main mass, therefore to improve mouldability and to obtain high-strength pressing (at sufficiently low pressures) mixtures are plasticized. Introduction of plasticizer (rubber, paraffin) is a forced measure. The more plasticizer (sometimes 10% by mass) is introduced, the more plastic mixture becomes. And this makes it possible to use nozzle pressing for manufacturing profile billets of drills, reamers and so on. Plasticizer, however, unfavourably affects the quality of sintered products: porosity increases, mechanical and performance characteristics becomes worse, distortions and cracks may appear and so on.

There is one more aspect of the problem. The matter is that conventional forming methods (in moulds, nozzle pressing) do not allow to increase the density of a pressing at the expense of high pressures due to possible appearance of laminating cracks. At conventional pressures (50...150 MPa) used for pressing plasticized hard-carbide mixtures a pressing with relative density of 48... 52% is obtained. When the pressing is then subjected to sintering considerable shrinkage occurs and though this is accompanied by the formation of liquid phase its effect, in view of complete elimination of residual porosity, is not always efficient.

Therefore, quite natural is the desire to increase the pressing density before sintering which can be realized by using high hydrostatic pressures (HHP) directly at hydrostatic pressing (HSP) of powder mixture in elastic shell or by the following

final pressing (hydrostatic treatment HST) of a preformed billet.

The latter version is more preferable since it makes possible to use high-productive methods of powder materials forming and, which is very important, permits to perform final pressing after removal of plasticizer from a pressing (by means of preliminary sintering at 600...1050°C). It should be noted that at the same pressure pressing density obtained at hydrostatic pressing is higher than that obtained at hydrostatic treatment (Fig.1) which is due to non-uniform density of the initial product (powder in the former case and pressing in the latter one) and, consequently, to non-uniform compacting under pressure.

From the technological point of view factor of considerable strengthening of a pressing with hydrostatic pressure increase (Fig.2) is of great importance since it allows to subject the pressing to mechanical treatment thus minimizing its treatment after sintering.

At sintering of billets subjected to hydrostatic pressure of 1.0 GPa their porosity to the moment of the liquid phase appearance (1280...1300°C) is about twice as small as that of usual billets (without final pressing) therefore the liquid phase more efficiently wets carbide particles in narrower capillaries and since carbide motion under the liquid surface tension forces is considerably less sintering efficiency also increases: number of pores, especially large ones, decreases, stresses caused by the gradient of shrinkage magnitude and rate also become smaller, and all this increases the product strength. Thus for 8.4 mm drills made of BK10 alloy with the HST pressure of 1.0 GPa bending breaking load is 1.3...1.8 times as big as for drills manufactured by conventional technology (nozzle pressing, sintering).

High hydrostatic pressure treatment also produces such favourable effect as deformation action on hard-carbide mixture components /1/.

Compacting pressure considerably affects particles of bonding metal powder which is manifested in their wear hardening, destruction of surface oxide films. However some grinding of carbide fraction is observed. At pressures higher than 0.9...1.0 GPa indentation of carbide particles occurs, i.e. vertices of one carbides indent into faces of others. This may lead to chipping of vertices (rounding) of carbides and appearance of local plastic deformation in contact points of tungsten carbide particles /2/.

This results in increase of dislocation density in tungsten carbide crystals and growth of the potential energy of the system.

Though at the following sintering recrystallization processes take place hereditary effect of deformation treatment remains, i.e. carbide fraction of the alloy is distinguished by the increased density of dislocations /3/.

Application of HST high pressure makes bending strength 10-25% higher, ultimate deformation and deformation work 10-20% higher.

Optimum pressure providing obtaining hard-carbide tools with the most favourable set of properties is HST pressure of 800... 1000 MPa.

The technology was realized with the help of industrial hydraulic presses completed with high pressure sets.

References

1. Mikhailenko G.P., Cherny Yu.F. Investigations of compactability of briquettes of hard-carbide mixture powders at hydrostatic treatment// Powder Metallurgy.-1977.-N9.-p.21-27.
2. Mikhailenko G.P. Effect of high hydrostatic pressure compression of billets on structure and properties of sintered hard alloys.-Fiz.techn.vysokikh davlenii.- 1982.-iss.9.-p.44-49.
3. Cherny Yu.F., Mikhailenko G.P., Labiskaya N.G. et al. Effect of recompacting of briquettes at high hydrostatic pressures on fine structure of carbide fraction of pressings of sintered alloy BK10// Powder Metallurgy.-1977.-NII.-p.76-80.

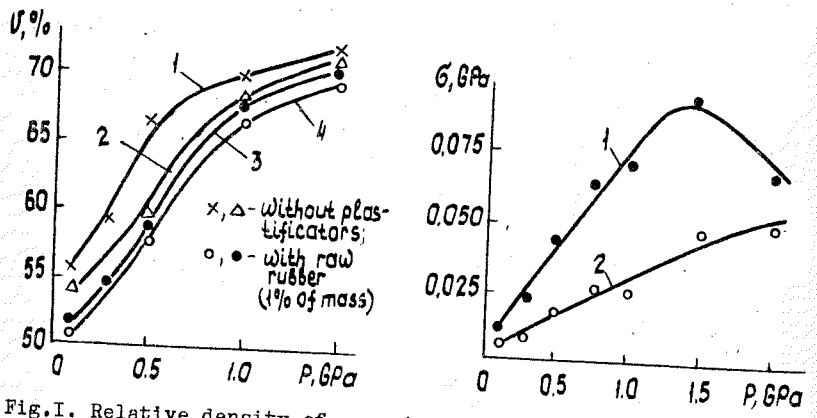

Fig.I. Relative density of pressings of mixture BK15-C as a function of pressure at hydrostatic pressing (1,3) and hydrostatic treatment (2,4).

Fig.2. Dependence of ultimate strength at compression of pressings of mixture BK6 on hydrostatic treatment pressure: 1 - mixture with rubber (1% by mass), 2 - without plasticizer.

LOW-TEMPERATURE DEFORMING OF MATERIALS AT HIGH PRESSURE

N.V.Shishkova

Donetsk Physico-Technical Institute, Academy of Sciences of the Ukrainian SSR, Donetsk, USSR

The questions of hydrostatic pressing at temperatures up to 77K were considered. The designed apparatus were efficient at deforming many structural materials. Influence of the above-mentioned processing on variation of structure and properties of copper, armco-iron and a number of carbon and tool steels has been established. These variations are defined by the cold-work hardening characteristics as well as by the phase transition during low-temperature deforming under pressure.

Metals possessing high-strength properties may be produced through forming of optimal defective structures which are high-resistant to plastic deformation. The different methods of strain-and-heat treatment hardening are used to create them. Usually the deformation at room temperature is accompanied by an essential loss of strength for a number of materials due to dynamic recovery. The deformational temperature decrease results in the decrease of thermal activity and in the increase of a number of residual defects /1,2/. So the low-temperature deforming of a number of materials at high pressure helps to retard a process of dynamic recovery. This is the way to get high-defective and, probably, high-strength structures. The utilization of subzero temperatures during the deformation of materials undergoing phase transitions under pressure may essentially increase a number of ways to get the structural states of solids possessing scientifically and practically important properties.

From the analysis of the obtained results it was established that the low-temperature deforming at high pressures acted effectively on structure and properties of a number of structural materials.

The extrusion of materials through the influence of a medium being under hydrostatic pressure was employed to effect the low-temperature deforming. The test specimen is placed in the high pressure apparatus operating space. The extrusion fluid is contained in this operating space. The high pressure apparatus is placed in the cryostat for cooling the tested material to a temperature of 77K. The high pressure apparatus and the cryostat are positioned on the hydraulic press table. The press generates desired

extrusion pressure. In some cases the precooling of specimens /3/ was sufficient to obtain results which are on approximation to the results obtained during the operation of the shown apparatus.

It is known /4/ that the most important condition of successful hydrostatic extrusion process is the appropriate choice of an operating medium and the machining tool shape. It was revealed that many of the known dependences were possible to employ in the case of low-temperature deforming. Investigations show the possibility to smooth the character of specimen outflow at subzero temperatures using a mixture of glycerol and ethylene glycol as an operating medium and the operating media including isoamyl and some other alcohols. The addition of substances (MoS_2) removing the frictional force in a site of deformation may have an effect on the pressure level at which outflow of a metal occurs. The conducted experiments showed possibility to get specimens deformed uniformly practically under isothermal conditions along the crosssection as well as along their length during the low-temperature extrusion.

Using described methods we deformed the billets of copper, armco-iron, low-alloyed molybdenum, Y8 and P6M5 tool steels at room temperature and at a temperature of liquid nitrogen to the different degrees of deformation λ = I.I7-3 ($\lambda = D_o^2/D_I^2$, where D_o- the billet diameter, D_I is the specimen diameter).

The structure and the properties of specimens received under these conditions have been studied. The properties variation being the result of the low-temperature deforming at high pressure /2,3/ has been also evaluated.

Fig.I shows the cold-work hardening characteristic features under low-temperature deforming. All the metals showed an increasing tendency to cold-work hardening with the increase of a degree of deformation as well as with the increase of forming temperature. This type of hardening may be preserved for some materials after the subsequent heat treatment. It is known /3/ that the employment of hydrostatic extrusion during the thermo-mechanical pretreatment results in the improvement of the tool steel cutting properties. This effect is attributed to the variation of austenitic grain size and the variation of carbide reduction ratio under this process of plastic deformation.

Influence of the hydrostatic pressing at subzero temperatures on the phase transitions was studied using I2XI8HIOT austenitic stainless steel. Fig.2 shows the different character of hardening

the steel deformed at room and cryogenic temperatures. The level of steel hardening under hydrostatic extrusion at room temperature is determined by the process of cold-work hardening of austenite as in this case the phase transition $\gamma \rightarrow \alpha$ is suppressed (at λ = 2.5 the quantity of α -phase constitutes 4-5%, Fig.2 curve 2). Under low-temperature extrusion this level is defined by the intense martensitic transformation (the quantity of α -phase constitutes 65-70%, Fig.2 curve I).

References

I. Gindin I.A., Starodubov Ya.D., Aksenov V.K. Structure and strength properties of metals with ultimetely deformed crystal lattice.- Metallofizika, I980, vol.2, N 2, p. 49-67.

2. Beresnev B.I., Spuskanyuk V.Z., Efros B.M., Shishkova N.V., Dolgikh G.V. Effect of plastic deformation conditions under pressure on structure and properties of molybdenum.- Docl. Akad. nauk Ukr. SSR, I983, N 7, p. 8I-83.

3. Certificate of invention N 757600 (USSR). Method of high-speed steel processing/ Spuskanyuk V.Z., Mandrovskaya V.I., Shishkova N.V. - Published in Bull. Izobr., I980, N 3I.

4. Beresnev B.I., Trushin E.V. The process of hydrostatic extrusion. - Moscow: Nauka, I976, 200 p.

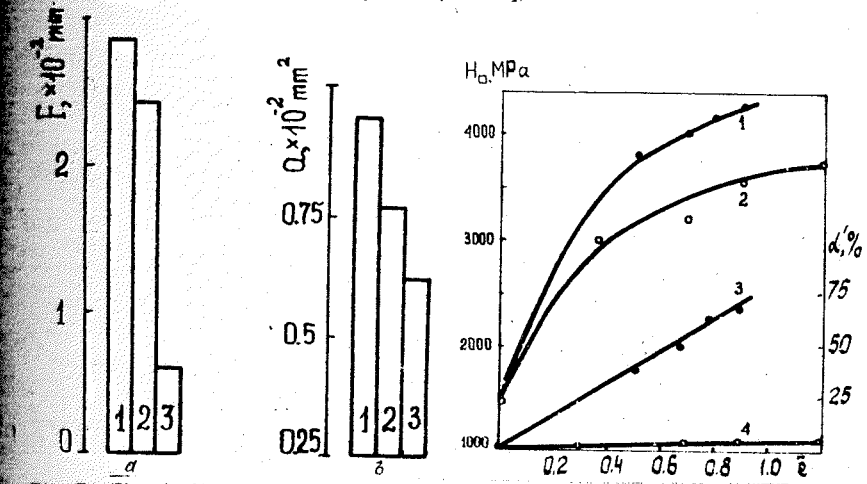

Fig.I. The influence of the hydrostatic extrusion temperature on the P6M5 steel structure: a - carbide grain size (F): I - initial state; 2 - T_{HE} = 20°C; 3 - T_{HE} = -I96°C; b - austenite grain size (a): initial state; 2 - T_{HE} = 20°C: 3 - T_{HE} = -I96°C.

Fig.2. The influence of temperature and degree of deformation on the hardening and variation of the phase content of I2XI8HIOT steel: I,2 - microhardness (H_o); 3,4 - α' -phase content; ● - T_{HE} = -I96°C; o - T_{HE} = 20°C.

HYDROEXTRUSION USED IN THE PRELIMINARY THERMOMECHANICAL TREATMENT CYCLE FOR IMPROVING THE COMPLEX OF MECHANICAL PROPERTIES OF MACHINE ELEMENTS

S.S.Dyachenko, N.G.Alexandrov, V.A.Zolotko,
E.L.Miloslavskaya, L.E.Gorelkova
Automobile Highway Institute, Kharkov, USSR

The use of high hydrostatic pressures considerably contributes to the effective production of pieces by cold plastic deformation since it permits to obtain them from low-plastic materials at a single pass and achieve high surface quality and high uniformity of deformation in the section. As hydroextrusion is applicable for producing pieces of high-strength steels, it is advisable to include this method of cold plastic deformation into the preliminary thermomechanical treatment cycle (PTMT). The efficiency of the TMT with the use of hereditary strengthening is primarily dependent upon the thermal stability of the dislocational structure formed and upon the possibility of its conservation during the following heating up to the beginning of the $\alpha \rightarrow \gamma$ transformation. In its turn, the substructure stability is a function of several factors, the most important of which are: composition and initial structure of steel, method and degree of deformation, post-deformation heating conditions and temperature-time conditions of the final heat-treatment.

This work considers the role these factors play in the inheritance of strengthening in 45ХН2МФА, 50Н6МФА, 12ОХ3Г3 steels. The deforming was performed by hydroextrusion and upsetting (ε = 30 - 35%). Prior to the deformation the steels were subjected to the spheroidizing heat treatment that permitted to obtain dispersed spherical carbides as well as to fix the boundaries of austenitic grains, the size of which did not exceed 5 μm. The analysis of the thin foils of the deformed steels has shown that unlike the upsetting which brings about a chaotically distributed dislocation structure, the hydroextrusion leads to the forming of a fragmented substructure homogeneous throughout the volume with discrete misorientation of fragments and with a number of dislocations preserved within them (Fig.1*). This structure has a high stability in subcritical temperature range, which is manifested in a slower decrease of physical broadening of X-ray diffraction lines of the hydroextruded steels as compared to those subjected to the upset-

* The Figure is given at the end of the book.

during the increase of the post-deformation tempering temperature. The temperature of the beginning of α-phase recrystallization (t_r^s) of the hydroextruded steel is considerably higher (by 100°C) than that of one upsetted. The recrystallization in the hydroextruded steel follows the mechanism "in situ" (Fig.2*) with the boundaries of initial fragments preserved.

The peculiarities of the substructure formed in the course of hydroextrusion permit to combine efficiently the processes of polygonization and strain aging during the tempering in the range of 350-400°C, since the atmospheres and segregations are chiefly formed on the walls of fragments, and the dislocations within them rearrange themselves forming the sub-boundaries of the second order. Besides, the presence in steel of strong carbide-forming elements, which strengthen the bonds of carbon in carbide, impedes strain-aging and ensures greater mobility of dislocations and the perfection of boundaries. The carbides left undissolved in the process of heating contribute, in their turn, to preserve the substructure at high temperatures. The stabilizing tempering temperature for steels with a strain-aging tendency should be above the temperature interval of strain-aging but lower than t_r^s. This temperature range for hydroextruded steels is widened due to the elevation of t_r^s.

The most important factor in securing the thermal stability of substructure is the increase of its homogeneity, i.e. the uniformity of deformation in macro- and microvolumes which depends to a great extent on the steel initial structure. In the given work the structures were obtained for a 12ОХ3Г3 steel with carbides uniformly distributed in ferrite and with carbides located mainly along the grain boundaries. It has been established that in the first case the strengthening effect after PTMT is greater by 15 - 20% than that achieved under the same conditions in the second initial structure.

The substructure created by the deformation followed by optimal tempering is inherited to some extent during the $\alpha \rightarrow \gamma$ transformation. This manifested in the changed kinetic parameters of austenite decomposition in pearlitic and bainitic regions similar to those obtained during the deformation of austenite itself. As a result of the direct observation of the austenite dislocational structure of a 12ОХ3Г3 steel hydroextruded in α-state it has been

* The Figure is given at the end of the book.

found that the substructure of ferrite is inherited during the $\alpha \rightarrow \gamma$ transformation (Fig.3*).

Mechanical properties of 45XH2MΦA and 50H6MΦA steels

Steel	Treatment	Properties						KCV, MJ/m^2
		σ_t, MPa	$\sigma_{0.2}$, MPa	σ_{ny}, MPa	δ, %	δ_p, %	ψ, %	
45XH2MΦA	usual	2070	I740	I635	3.0	9.0	43.5	0.45
	PTMT	2I40	I830	I750	3.3	I0.0	45.5	0.57
50H6MΦA	usual	2I55	I720	I600	-	I0.8	4I.0	0.56
	PTMT	2230	I840	I720	-	II.6	45.2	0.60

Mechanical tests of the hydroextruded high-strength 45XH2MΦA and 50H6MΦA steels after the final heat treatment show that the PTMT with hydroextrusion results in the simultaneous improvement of strength, plasticity and toughness (see Table).

* The Figure is given at the end of the book.

EFFECT OF HOT HYDRAULIC EXTRUSION ON IRON PROPERTIES AND STRUCTURE

M. I. Kalachev, Yu. T. Antonishin, N. I. Yuriev
The Physical Technical Institute of the Byelorussian Academy of Sciences,
Minsk, USSR

The mechanical properties of cast iron subjected to induction heating and hot hydraulic extrusion with subsequent oil quenching have been investigated. The range of extrusion ratio values was from 30% to 95%. The tests were carried out at room temperature. The investigation results are presented in Fig. 1 and Fig. 2.

The curves in Fig. 1 show that with increasing the extrusion ratio in the process of hot hydraulic extrusion the ultimate strength of iron billets increases from 420 MPa to 900 MPa at 75%-extrusion ratio. The ultimate strength of some billets was above 1000 MPa.

Thus, the deformation of iron under the conditions of high-temperature mechanical processing makes it possible to double the ultimate tensile strength.

With increasing an extrusion ratio bending strength values of iron billets monotonously increase from 920 MPa to 2180 MPa at extrusion ratio of 83%, id. by a factor of 2.3.

The shear strength values of iron billets also monotonously increase from 480 MPa to 750 MPa at the deformation ratio of 70%, id. by a factor of 1.6.

The monotonous increase of plastic characteristics depending on the extrusion ratio at hot hydraulic extrusion was observed. Thus, a sag on bending tests at increase of the extrusion ratio increased from 2 mm to 8.9 mm at the extrusion ratio of 83%,

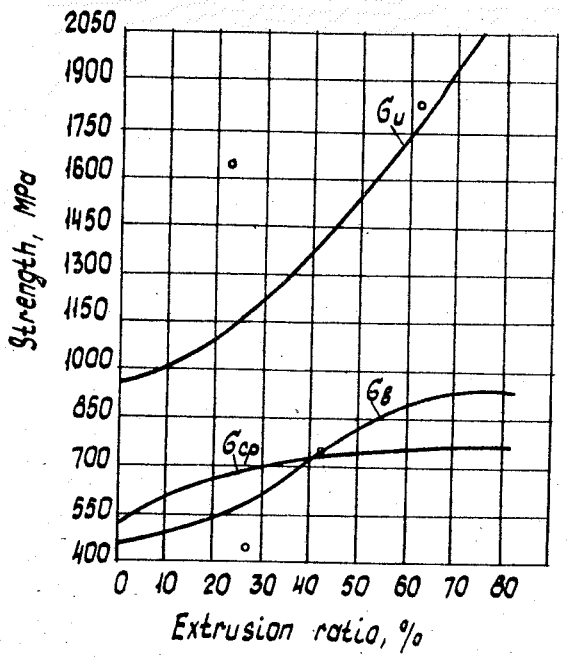

Fig. 1. Dependence of strength properties of cast iron on extrusion ratio.

an elongation increased from 0.6% to 3.3%, id. by a factor of 4.5 to 5.5.

In upsetting test carried out till the formation of a first visible crack a still greater increase of iron plasticity was obtained. The deformation ratio of nondeformed billets was 3% and that of 79%-extruded billets became 28%, id. it increased by a factor of 9.3.

The hot hydraulic extrusion improves an iron fatigue resistance. The extrusion at 960°C with the extrusion ratio of 64% ensures a two-fold increase of cyclic strength (at symmetric pure bending with rotation) defined from 10^7 cycles and in the range of limited fatigue it increases the number of cycles before failure by a factor of 3 to 4.

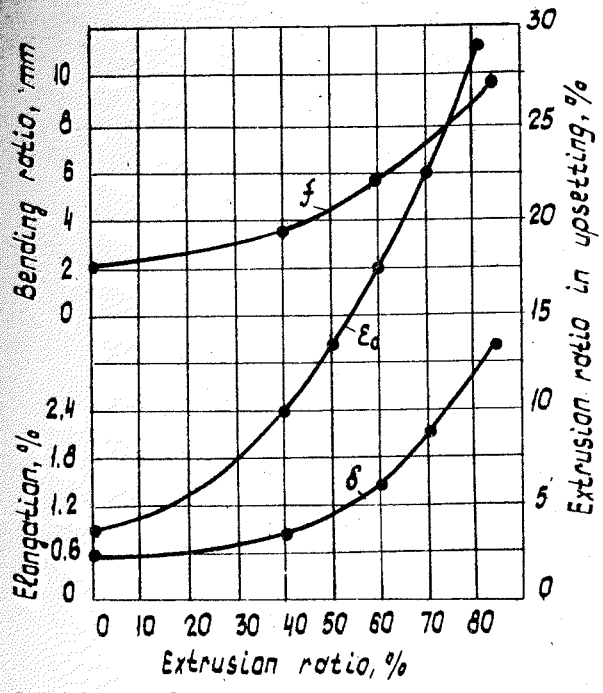

Fig. 2. Dependence of cast iron plasticity on extrusion ratio.

The electron fractographic investigation of iron sample fracturing (the examination of the whole fractured surface being statistically even) indicate that brittle intergranular failure caused by spalling on the grain boundaries would result in appearing quite smooth surfaces in fractograms. In this case the grain boundaries are distinct and microrelief is mainly presented by brittle elements.

The electron-fractographic investigation of fracturing iron billets shows that in some areas transcrystalline fracture is observed which is indicative of viscous failure. In a fracture of extruded iron billet transition areas of brittle-viscous failure are observed. With increasing the extrusion ratio the number of these areas increases.

INFLUENCING FERROUS ALLOYS STRUCTURE AND PROPERTIES THROUGH THE THERMODEFORMATIONAL TREATMENT DURING HIGH TEMPERATURE GAS-PRESSURE EXTRUSION

A.P.Bashchenko, A.V.Omel'chenko, V.I.Soshnikov, V.N.Filimonov, G.S.Belousov, A.G.Koslova, V.I.Kiriyenko, Yu.S.Konyayev, V.D.Berbentsev, V.V.Solovyev

I.P.Bardin Central Research Institute for Iron and Steel, Moscow, USSR

The thermodeformation effects of the high temperature gas-pressure extrusion (HTGE) should be revealed and investigated. The present work was conducted in order to study influence of the HTGE performed as part of a high temperature TMT cycle on structure and properties of a hard-to-deform high-speed steel.

In HTGE experiments, round rods were forced through on extruding die 2 mm in diameter. The deformation ratio was determined by the initial rods size, extrusion temperatures of 900°C and 1050°C were used. For each steel, the operating hydrostatic pressure which was sufficient to force a given steel rod through a die, depended on a steel's resistance to deformation, i.e. on the temperature and the deformation rate, and amounted to 100 MPa at maximum. The deformation rate was 1-2 s^{-1}. The forced section cooling rate was 15-20°C/s. Cooling conditions were sufficient to provide for a deformed austenite to undergo martensite transformation immediately at the outlet of a die.

In steel subjected to quenching as well as after HTGE metallographically observed intergranular network is, evidently, the premartensitic austenite grain boundaries inherited by the martensite. The grains are mostly equiaxed, recrystallized ones. Their mean dimension after HTGE is considerably smaller than after a common heat treatment (number 14 and 9, respectively).

After HTGE, the steel structure is martensite with retained austenite and carbide inclusions. Unlike the common as-quenched martensite structure, the HTGE martensite is mostly composed of curved crystals and a minor amount of laths in pockets. There are small retained austenite interlayers or islands between the martensite crystals, their amount being considerably less than in a commonly quenched steel.

In steel subjected to tempering after HTGE, in addition to relatively coarse carbide particles observed by usual light microscopy, finely dispersed carbide particles can be detected using electron and field ion microscopy. They can be identified as (W,

...C type carbides with the lattice parameter of 0.417 nm. These particles are coarser and their percentage in steel is higher after HTGE at 1050°C than at 950°C, their average dimension being ...4 and 3.7 nm and their volume fraction 13 and 9% respectively.

Characteristic of steel after HTGE is a pronounced subgrain structure in the martensite crystals. Subgrains are not coarser than 10 nm. High dislocation density is observed in both types of crystals (curved-and-lath-shaped). Axial texture of <100> with the <110> traces has been detected in steel rods after HTGE.

These characteristic features of the grain and fine steel structure after HTGE are due to the dynamic recrystallization processes that develop in austenite under extrusion conditions and terminate as soon as the rod cools on leaving the die.

Both after usual heat treatment and after HTGE steel strength parameters, such as hardness and red-hardness, are the higher the higher the treatment temperature is. A possibility should be noted of using a 1050°C - HTGE for obtaining strength properties equal to those after a usual heat treatment with the heating temperature of 1250°C. In bending tests, maximum bending strength was attained in HTGE-produced rods deformed at the increased temperature of 1050°C.

Bend angle for HTGE rods, as compared to usual heat treatment, is so much greater (up to 30 to 50 times), that HTGE should be considered as a plasticity-inducing treatment.

Field testing of products manufactured of HTGE rods confirms their increased mechanical properties. Small diameter (Ø 2 mm) long drills made of HTGE steel are 1.8 times more resistant to fracture and wear than similar drills made of commonly produced steel rods.

In our experiments, the fact of the <100> crystallographic texture parallel to the extrusion direction has been established. Predominant axial texture as well as the lengthwise orientation of a certain part of the carbide particles bring about an increase in plasticity observed in bending thin rods and also an increased resistance to breakage of small-sectional long products.

Another reason for the increased mechanical properties of the HTGE steel is a profoundly new combination of conditions which govern mechanism of the solution-and-precipitation reactions in the carbide phase at different stages of the HTGE process, that is, during heating for austenitization; during extrusion per se, in the austenite state; at cooling of the extruded austenite; at tempering of the extruded rods.

As a result of HTGE, without any special tempering treatment, the carbide phase contents in steel are at least 2 times greater than after a usual quenching. This increase is accompanied by a corresponding decrease in carbon and the carbide-forming elements contents in the solid solution. It is prooved by the decrease in the austenite stability and the lessened amount of retained austenite in structure. The carbide particles in HTGE-steel are fine-dispersed and evenly distributed.

Thus, an increase in mechanical properties as a result of gas extrusion within the high-temperature thermomechanical treatment cycle can be attributed to the following factors: the grain structure refinement; changes in martensite morphology and substructure; higher dispersion and more uniform distribution of carbide particles; axial texture development and carbide precipitates orientation along the extrusion direction; reduced retained austenite contents.

INDUSTRIAL EQUIPMENT FOR HOT ISOSTATIC PRESSING OF POWDER AND SOLID MATERIALS

A.Kurovich, I.Fieldblum, A.Zverev, V.Snop, V.Trishkin
VNIIMETMASH, Moscow, USSR

In world practice, hot isostatic presses are now widely used for manufacturing of compacted powder billets and treatment of solid materials to improve their service characteristics due to healing of macro and microdefects and also nucleuses of fatigue damages, appeared during the process of operation, for the production of high-quality parts from hard alloys and materials of "carbon--carbon" type.

The main design element of hot isostatic press is a vessel having plugs, inside which a thermo-insulating mantle and a cylindrical heater assembly are placed, thus restricting a working zone with a billet. The argon gas pressure, temperature and dimensions of the working zone are considered as the main parameters of the press. A derived parameter of the hot isostatic press is an axial force acting on the plugs.

The design scheme of the hot isostatic press depends on the arrangement of the device taking up axial forces, on loading and unloading billets (upper or down), on mechanization degree of loading operation and the operation of removing the billet, and also on the ratio of the diameter of the billet to its height.

From the safety point of view hot isostatic presses of VNIIMETMASH design are provided with multi-element frame, prestressed with the help of a high-tensile strip or produced of some separate plates. The vessels are also of multi-element design, prestressed by means of a large number of separate rings or a high--tensile strip. Such designs exclude the possibility of crack propagation and instant release of energy, accumulated in compressed gas. The number of design elements must be selected so that failure of one of them should not involve the failure of the others.

When using prestressed design, the most loaded elements of the press are under compressive stresses. As a result the probability of arising and spreading the cracks in them is diminished. An absence of preliminary compressive stresses in multi-element frame made of plates should be taken into account while calculating a strength of the design. In addition, it is necessary to take into consideration that the high-tensile strip makes it possible to provide a desirable scheme of stresses in elements of prestressed design.

Hot isostatic press consists of the following main systems: gas-supply, heating and cooling systems, hydraulic and electric drives, and a control system. Gas system includes a balloon station, compressors, pipelines, gas apparatus and fitting. Gas system is intended for creation of set pressure in a working chamber of the press. Gas is fed with membrane compressors, thus excluding the contamination of the gas by the fumes of oil. The main element of the heating system is the heater assembly - a heater and a thermo-insulating mantle. Durability of the heater and the mantle depends on materials and design made of these materials, and also on the quality of maintenance. Cooling system of industrial hot isostatic presses includes open and closed pipelines for circulation of cooling liquids. In closed part of cooling system the distilled water, inhibited with anticorrosive additions, is used.

Technical characteristics of some of hot isostatic presses in our country

Type of press	Axial force, MN	Working pressure, MPa	Working temperature, K	Inner diam. of a vessel, mm	Billet dimensions, mm		Working media
					diam.	height	
ITC-330	3.3	200	2273	140	40	100	nitrogen
Г-450	4.5	100	1773	230	50	250	argon
ITC-2000	20	200	2273	350	100	250	nitrogen
Г-5000	50	200	1493	560	320	550	argon
ЯО60I3	50	200	1773	560	340	550	argon
ЯО60I5	50	200	1523	560	320	1000	argon
КП-379	125	200	1523	900	630	1700	argon
ЯО60I6	125	200	1773	900	465	1800	argon
ЯО6022	400	200	1525	1600	1100	2000	argon
ГУ-40	400	150	1473	1800	1300	1500	argon

VNIIMETMASH in cooperation with other institutes and plants of the country has developed hot isostatic presses with axial forces from 3.3 up to 400 MN.

Technical characteristics of some of them are given in Table

...ivonos, L.Maximov, Rosanov and others took an active part ...heir development).

In connection with a rapid improvement and utilization of ... isostatic processes of treatment it may be possible to exp... ...t that in the nearest future hot isostatic presses with a dia... ...ter of the working zone up to 2.5-3 m and a height up to 6 m ...ll be developed. Working pressures from 250... to 300 MPa and ... temperature of 2573 K can be obtained.

MODERN DESIGNS AND TECHNOLOGICAL POTENTIALS OF COLD HYDROSTATIC PRESSES

A.N.Kurovich, I.E.Feldblum, N.I.Zarankin, G.A.Iljin, R.S.Vasiljeva, L.I.Gurjeva, V.S.Solodukhin
VNIIMETMASH, Moscow, USSR

At a present time, both in the Soviet Union and in foreign countries two technological methods of operation are mainly used for hydrostatic compaction of powdered materials: "dry bag" and "wet bag" compaction. The first of these methods is used in the batch production of identical products of relatively simple shapes. It is used, in particular, in refractory, electronic, electrical and optical industries. The method of "wet bag" is considered to be the most universal one. It is employed for the manufacture of products of complicated shapes from metallic powders at a pressure up to 600 MPa.

At present, work is being conducted in VNIIMETMASH for designing cold hydrostatic presses intended for operation with both methods.

The method of "dry bag" is used in cold hydrostatic presses having, as a rule, "frameless-type" design. The cold hydrostatic press is a thick-walled cylinder (container) with a bottom and a threaded bayonet plug at the top side (in some cases bayonet plugs are installed on both sides of container). The working pressure is generated by high pressure pumps or multiplicator.

According to this design scheme VNIIMETMASH has developed cold hydrostatic presses with an axial force from 6 to 20 MN. The main characteristics of some of them are given in Table 1.

VNIIMETMASH cold hydrostatic presses whose operation is based on the method of "dry bag" are mainly of frame-type design. The working container of such presses is a smooth thick-walled cylinder, in the bore of which near the sides, the plugs with packings are placed. Plugs must not be firmly fixed to the container. For this reason only radial pressure are taken up by container's walls. Axial force, resulted in the action of the pressure upon the plugs, is transmitted to a special power frame.

The major advantage of cold hydrostatic presses of such a type is a great safety of operation due to the absence of concentrators of stresses in container and the possibility of application of multielement power frame and container. The multielement power frame is made of separate plates or prestressed with the help of high-tensile strip, and the container is prestressed by means of

same high-tensile strip or with a large number of separate ...gs.

...ble 1. The main characteristics of cold hydrostatic presses ... "frameless-type" intended for operation on the method of ...ry bag"

...ial ...rce, MN	Working pressure, MPa	Working chamber dimensions (products), mm		Pressing schedule	Scope of application
		diameter	height		
6.3	100	180-190	-	outwardly on core	electronic industry
12.5	100	275	500	outwardly on core	optical industry
20	100	440	305	inwardly on container	electronic industry
17	100	250-290	-	outwardly on core	electronic industry

When using the prestressed design, the most loaded elements of the press are under compressive stresses. As a result the possibility of arising fatigue damages is diminished. In addition, it is necessary to take into account that the high-tensile strip, especially the strip of container makes it possible to provide a desirable scheme of stresses in elements of prestressed design. The choice between the high-tensile strip or another multi-element design depends on the mass and cost of design assemblies, adopted technology, possibilities of production at the manufacturer plant and conditions of transportation.

In cold hydrostatic presses of frame-type design of the first generation, the working pressure was generated by high-pressure pumps or multiplicators placed outside the power frame.

VNIIMETMASH together with the Izhorsk Works named after Zanov and KSPO has developed a great number of machines, including one of the largest cold hydrostatic presses in the world having axial force of 630 MN. The main characteristics of some of cold hydrostatic presses of such a type are given in Table 2.

In the last few years, VNIIMETMASH has developed the original design scheme for the frame-type cold hydrostatic presses equipped with built-in multiplicators. The multiplicator placed within the power frame allows to restrict the pressure exerted by external sources to 150-180 MPa, and to create much higher pres-

sure, necessary on technological considerations, by direct compression of working liquid in container. This design provides a considerable improvement in reliability and safety of operation.

Table 2. Technical characteristics of the frame-type cold hydrostatic presses of the first generation

Type of press	Axial force, MN	Working pressure, MPa	Working chamber dimensions, mm		Working liquid
			diameter	height	
УГС 150/1000	20	400	150	1000	oil
УГС 350/1000	130	400	450	1000	oil
		300	700	1600	
Я06023	160	200	1000	1500	water emulsion
	630	350	1500	2500	oil

According to a new design scheme, many types of cold hydrostatic presses of Г-3000 standard series with an axial force of 30 MH have been developed. The inner diameter of containers of such presses ranges from 250 to 415 mm and the working length ranges from 750 to 2200 mm. The working pressure is within the limits of 100-600 MPa. Design of cold hydrostatic presses equipped with built-in multiplicators has received a further development in the course of engineering cold hydrostatic presses with an axial force of 31.5 MN. It consists of container with a diameter of 190 mm and a working height of 750 mm. Pressure of the external drive may reach up to 200 MPa. This pressure can be improved up to 600 MPa due to the built-in multiplicator.

Engineering developments of VNIIMETMASH and experience gained during the period of designing of these presses make it possible to work out the equipment the parameters of which will correspond to the high world's demand.

SOME SEALING PROBLEMS OF THE BAYONET-TYPE JOINTS FOR BIG DIAMETER PRESSURE VESSELS

M.Marinov, St.Vodenitcharov

Bulgarian Academy of Sciences, Institute of Metal Science and Technology, Sofia, Bulgaria

Introduction

The invention of bayonet-type joints for big diameter pressure vessels without any helical teeth of the flanges introduced some complications in the main sealing assembly. First of all, the sealed gap here is relatively wider. On the other hand, the same operational quality of the joint must be guaranteed for all sealed gap varying widths and at any level of a given pressure in the vessel. The so called convex-concave profile of the sealing ring dominates in the practice nowadays because of its low height (Fig.I).

Function problems of the sealing assembly

It was established by the authors, that to prevent leakages at the very beginning of the vessel filling up, by using the examined profile, it was expedient to feed in advance the space under the sealing ring with a sealing fluid at a pressure $p_2 \geq$ I.0 MPa. It was further established that the sealing assembly completely retained its functioning up to $\Delta p = p_2 - p_I$ = 0.I MPa, where p_I was the pressure in the operating space. Under that level of pressure difference there occurred fluid leakages. Up to Δp =-0.I MPa the leakage level remained low and then it started rapidly to increase. In order to increase the function reliability of the system, one of the authors suggested a scheme /I/ - in case of interrupting the sealing fluid flow from the external source to the bayonet-type joint, a connection is automatically established between the space under the sealing ring and the vessel space.

Mobility of the sealing ring

The elimination of forced tightening of the two front sealing surfaces of the bayonet-type joint introduced an axial mobility in the assembly, dependent on the pressure in the vessel. The sealing ring was subjected to wear along the side sealing surfaces S. To evaluate the role of this wear, the authors carried out stand tests of the examined profile sealing rings at a continued cyclic loading with a value of the specific surface pressure up to 4 MPa.

The sealing axial displacement was varied within the range of 0 to 6 mm. It was established that up to approximately 400 cycles wearing of the ring material (chloroprene rubber; $H_{Shore} = 74$; $\gamma = 1.2$; $\sigma_{ten.\ frac.} > 8.0$ MPa) remained within the limits, which did not cause any disturbances in the normal operation of the sealing assembly. From 400 to 2000 cycles a gradually increasing wear of those surfaces S occurred, expressed by the appearance of macroscopic notches across the direction of the displacement. However, noticeable effect of the notches on the assembly solidity was not observed untill 1500–2000 cycles.

Sealing application limits

The authors assume that the elastomer behaviour in the sealed gap area may serve for a general estimation of the above top application limit of the considered profile as regards to the fluid operating pressure in the vessel, having in mind that only here in the body of the element tensile stresses may arise, as the appearance and propagation of the fatigue cracks is due to such stresses /2/. This advantage was taken to build a simulation model for formulating a correlation between the fluid static pressure and the deformation of the sealing ring in the sealed gap. Fig.2 shows the scheme of the model. The letter A indicates the tested element - segment (symmetrical I/2 part) of the sealing ring, the letter B - a seat, simulating a part of the sealing ring groove, and the letter C - the sealed surface of the bayonet joint pressing flange. The sensors D_I and D_2 measure the value of the surface pressing on the seat B side surface or on the surface C respectively, which is exercised by the element A under the influence of the force F of the pressing piston K. Another sensor D_3 controls the change of deformation δ of the element A in the sealed gap area, considered from a point which is accepted for a conditional onset. By varying the form of the front surfaces $\mathcal{J}$ and φ of piston K and the distance m of the surface φ from the tested element front, an artificial equalizing is achieved of the sensors' D_I and D_2 indications about the tested fluid static pressure simulations. According to the expectation, above a certain degree of the element loading, the change of the indicated by sensors D_I and D_2 (Fig. 3) forces follows a dependence of the piston K drive, analogous to that of the force F.

Some of the obtained test results are shown in Fig.4. The pressure values in the diagram are given as a function of the sealed

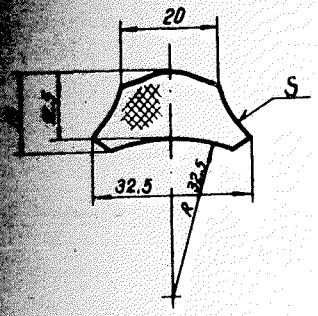

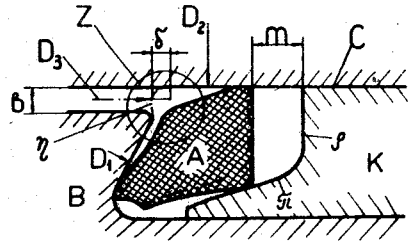

Fig.1. Profile of sealing ring for bayonet-type joint of big diameter pressure vessels.

Fig.2. Scheme of the simulation model for mechanical exercising of fluid static load on the profile.

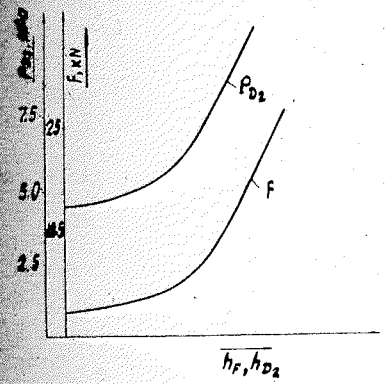

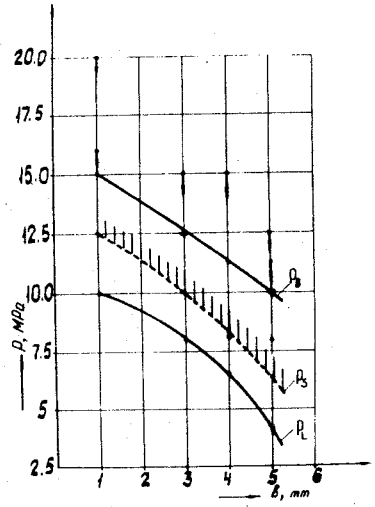

Fig.3. Variation curves of the tested detail pressing force F and the surface pressing on the sealed surface C, indicated by sensor D_2, as a function of the pressing piston K drive.

Fig.4. Dependence of the conditional pressures, sustained by the elastomer ring with the investigated profile, on the sealed gap width b. p_B – pressure at which cracks appear on the element surface η after a time $\tau \leq 240$ min and such cracks are detected with the help of a penetrating liquid only; p_s – pressure at which $d\delta/d\tau$ remains less than $1.5 \cdot 10^{-6}$ m/min; p_L – pressure at which no residual deformation arises in the elastomer body in the sealed gap area.

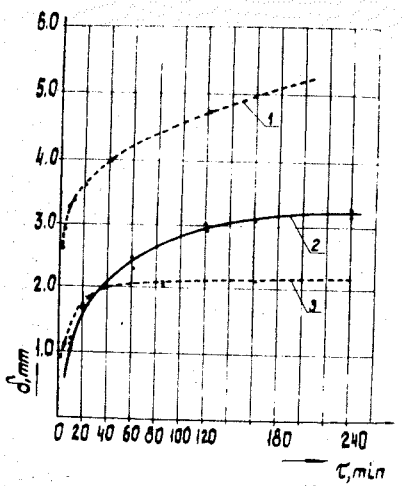

Fig.5. Curves of the variations in the time of the element body deformation δ in the sealed gap. Curve I - at p_t = I2.5 MPa, b = 5 mm; curve 2 - at p_t = I2.5 MPa, b = 3 mm; curve 3 - at p_t = 5 MPa, b = 5 mm.

gap width. The value of δ, measured from the conditional onset, continues to grow in the time along different dependences of b and at different levels of the test pressure p_t (Fig.5). For lower loadings $d\delta/d\tau$ rapidly reaches acceptable for the practice values. As an example of the results' application Fig.6* shows a part of a bayonet-type joint of a pressure vessel with a 3600 mm inner diameter.

References

I. Устройство за уплътняване на бързодействуващо съединение. Авт. св. № 37634 България F16D15/46 М. Ив. Маринов, Р. Радков, I5.05.I986.

2. Бартенев Г.М., Зуев Ю.С. Прочность и разрушение высокоэластических материалов, Химия, Москва, I964, Ленинград, 388.

* The Figure is given at the end of the book.

THE TREATMENT OF Ti-ALLOYS UNDER THE CONDITIONS OF HIGH HYDROSTATIC PRESSURE

A.A.Popov, W.A.Beloglasov, S.G.Ushinskaya
The Urals Polytechnical Institute, Sverdlovsk, USSR

Parallel with presently wide used rolling, pressing, forging and other deformation modes the regime of hydropressing is recognized to be applicable to treatment of Ti-alloys.

The aim of the present work is to compare the influence of two different modes of deformation (rolling and hydroextrusion) on changes in structure and mechanical properties of commercial Ti-alloy WT22. The forging-rods with section I6xI6 mm were examined. Rolling was carried out on the laboratory rolling-mill with roller diameter 250 mm. The regime of hydroextrusion was realized on the way of hot (cold) hydrodynamic squeezing. The bar-heating up to the necessary temperature was conducted with the help of high-frequency current, then the specimens together with graphite inset were placed into container of high pressure. During punch movement the graphite inset destorted and filled space between the bar and the deforming instrument, being medium transfering pressure. The scheme used allows to deform the bar in the conditions of all-round pressing.

Three principal different variants of combination of thermal treatment and deformation are realized:

Variant I: The alloy deformation being in one-phase β-condition when the stability of BCC-phase is high enough; hot rolling (hydroextrusion) at 950°C and above or deformation at room temperature after preliminary treatment on β-solution.

Variant 2: The alloy deformation with two-phase ($\alpha+\beta$) structure which stability at rolling (hydroextrusion) temperature is high: deformation at 750°C and 20°C after preliminary annealing at 800°C.

Variant 3: The alloy deformation in which simultaneously with rolling (hydroextrusion) phase transformations proceed, connected with either β - or α-phases unstability: warm alloy deformation, preliminary treated on β-solution which at deformation temperature is decomposed with α-phase formation; hot alloy deformation in which two-phase ($\alpha+\beta$) structure is created preliminary. It was undergone polymorphic $\alpha+\beta \rightleftarrows \beta$ transformation at the heating up to the temperature of hydroextrusion.

The hot deformation at temperature above 950°C (variant I)

doesn't lead to considerable changes in structure and mechanical properties of WT22 alloy. The elevation of deformation temperature up to 1100°C is accompanied by considerable brittleness of alloy and by lowering of plasticity values (Ψ decreases from 30 to 4%) which is caused by grain-size growth of β -phase. At some degree it is possible to prevent the plasticity-losses at the cost of increasing of deformation degree.

Rolling or hydroextrusion at room temperature (variant I) on the contrary promotes the considerable deformation strengthening. However the formation of many twinnings and ununiformly distributed on the alloy structure dislocation zones doesn't allow to guarantee high plastic properties after aging hardening.

In this aspect more favorable is the scheme which is foreseen by variant 2. The creation of stable two-phase ($\alpha + \beta$) structure before hydroextrusion guarantees in the deformed material considerable strengthening by preservation of high level of plasticity. After annealing at 800°C and following deformation at 750°C the tensile strength reaches $\simeq$ 1100 MPa and $\Psi \simeq$ 25-30%. The comparison of mechanical properties after deformation at various temperatures and following aging hardening demonsrates that optimal complex of properties may be received as the result of rolling (hydroextrusion) at 750°C and aging at 500°C. In this case one succeeded not only to increase the strengthening values (σ_B may easily reach the level 1500 MPa) but also to preserve sufficient supply of plasticity ($\Psi \simeq$ 20-25%) and fracture toughness (0.4-0.3 MJ/m^2). The so high complex of properties may be created owing to the presence in the structure of alloy the massive precipitates of primary α-phase which were formed during preliminary annealing at 800°C and the dispersive-strengthened particles of the secondary phase. The dislocations formed during deformation are sites of precipitations of these particles at aging. The chosen temperature of rolling (hydroextrusion) guarantees the uniform distribution of dislocations along the solution structure and therefore the uniform precipitation of the second phase.

Important results are received by the alloy investigation treated in the accordance with variant 3. The deformation in the conditions of primary stages of decomposition of metastable β -phase (alloy rolling at 600-650°C preliminary treated on β -solution) leads to considerable decrease of volume of α-phase particles formed before rolling. The dissolution of the second phase is observed which is connected with the influence of plastic deformation. The structure of deformed alloy is described by high density

dislocations and it may be seen intensive diffuse dispersion at ...lar sites of α-phase reflections at micrographs. α-particle ...solution is accompanied by anomalous high alloy strength not ...cterized for cases when in deformed material only β-solution ...present. The decrease of volume part of the second phase after ...ling is possible only on the primary stages of decomposition, ... means that chemical composition of forming particles is not ...uilibrious. A long predeformation treatment at 600-650°C stabi...ises the precipitate and rolling doesn't lead to decrease of vo...me part of α-phase. The deformation effect in this case consists ...n bending and particle cutting which influences well plasticity ...parameters simultaniously strengthening the alloy.

Anomalous influence of plastic deformation was revealed in ...e more case. The alloy having stable ($\alpha + \beta$) structure was hydroextruded at temperature above polymorphic $\beta \rightleftarrows \alpha + \beta$ transformation (950°C), i.e. in the conditions of thermal unstability of the second-phase precipitate. Mechanical tests of deformed specimens showed that in the result of hydroextrusion the strength values had increased. The phase composition was near 100% of β-solution by x-ray analysis. Thus the both described schemes although the deformation was realized at various temperatures lead to similar results in change of strength properties. We mind that this fact may be accounted for unstability of phase composition in the conditions of plastic deformation. The mechanism of anomalous strengthening consists perhaps in formation of considerable tetragonal distortions in microvolume of structure in the result of mechanical effect where the phase transformation has begun connected with reconstruction of one crystal lattice into another.

Conclusions

1. The more optimal complex of mechanical properties of pseudo-β-Ti-alloys may be received using warm hydroextrusion (rolling) at 750°C with obligatory preliminary annealing in two-phase ($\alpha + \beta$) region.

2. The plastic deformation carried out in the conditions of unstable phase equilibrium causes anomalous changes in alloy structure and mechanical properties connected with structure volume formation with heavy tetragonal distortions.

STRUCTURE EFFECT OF HARDENING OF CARBON STEELS

V.S.Koviko, V.P.Saakyants
Physico-Technical Institute, Donetsk, USSR

Cold plastic deformation combined with thermal treatment or without it provides changes in material properties.

Combination of plastic deformation with thermal treatment in different sequences allows to increase the strength characteristics of steel with conservation and even increase in some cases of its plasticity and viscosity /1/.

In the present paper peculiarities of structure formation were studied of 45 and 60 carbon steels in the intermediate region as well as influence of this structure on hardening effect and increase of plasticity of these steels under cold hydropressing.

The intermediate-type structures were prepared for hydropressing using diagrams of austenite isothermal transformation by the following regimes: for 45 and 60 steels the austenitization temperatures were 880 and 950 °C, respectively, the isothermal hardening was done from 310 and 340 °C with subsequent treatment in salt bath (55% $NaNO_2$ and 45% KNO_3) during 15 min with final cooling in water. As variants, structures obtained in the intermediate region with subsequent tempering at 650...670 °C during 1 hour with air cooling were studied. For comparison, as-delivered steels were used having structure of plate pearlite.

Structure studies were done by optic and electron microscopy. The Glagolev method was used to estimate quantitatively structure components. Strength and plasticity of steels were found under tensile testing standard samples (type III according to GOST 1497-84). Billets were deformed by the method of cold hydropressing with deformation degrees of 10, 20, 30, 40%.

The investigation results of structure obtained in the intermediate region have shown the presence of bainite and thin-plate pearlite, the so called mixed structure. The amount of bainite in 45 steel was 70...80% and in 60 steel it amounted to 26...40%. During heat treatment of the carbon-steel massive samples in the intermediate region it was hard to obtain the bainite structure only in the result of austenite transformation because the region of intermediate transformation of these steels is not clearly found and there is a common maximum of the transformation rate for the intermediate and the pearlite regions. As a result,

formation of the intermediate type precedes the pearlite formation /2/. Structure obtained in the intermediate region subsequent tempering is a ferrite-pearlite mixture with coated carbides. In the as-delivered state coarse grains of plapearlite surrounded by ferrite are observed.

Microhardness change at different deformation degrees was studied to define the efficiency of hardening steel with different structure modifications. Fig.I shows curves for microhardness change. The largest cold-work hardening was observed in plastic structure having the least hardness in the case of small deformation degrees (up to 20%). At further increase of deformation degree there was practically no hardening, plastic ferrite matrix with disperse carbides was hardened intensively at negligible deformation degrees only. Hardening of materials having pearlite structure (grains of plate pearlite surrounded with ferrite) is weak under all deformation degrees studied. The curve for hardening change of the mixed structure shows that at different deformation degrees a kind of mild slip is observed characterized by linear dependence, and in the 20-30% deformation interval the hardening threshold is observed where formation of cellular dislocation structure is possible.

To judge the influence of structure state of the material on change of its properties under cold hydropressing we have studied peculiarities of structure formation in the intermediate region for the case of 60 steel thin foils (Fig.2*). In this case, the presence of structure of the "feather" type with a different dispersivity degree was found. The α-phase crystals alternate with cementite precipitations stretched along these crystals. At some α-phase crystals the homogeneously oriented carbide particles are observed (Fig.2,a*), this is the specific structure of upper bainite. Besides, crystals of needle-like ferrite are observed having carbide precipitations whose orientation doesn't coinside with the long axis of the α-phase crystal which is typical of lower bainite (Fig.2, b*). Dark-field image in cementite reflex is indicative of the presence of disperse carbides of one orientation inside the α-phase crystals of lower bainite (Fig.2, c*). This is the main peculiarity of crystallogeometry of cementite precipitations in lower bainite which differs it from tempered martensite characterized by the presence of several orientations of cementite precipitations in each martensite crystal /3/. Alongside with bai-

*The Figure is given at the end of the book.

nite a thin-plate pearlite is also observed with thickness of cementite plates equal to 0.01 m and distance between them of 0.2 m (Fig.2, d*).

After hydropressing 60 steel with deformation degree of 40% in the needle-like ferrite of lower bainite a cellular structure forms. Small number of cells is observed which have clear configuration and are free from dislocations, but, in general, the cell boundaries are smeared (Fig.2, e*) because of the presence of disperse carbides in needle-like ferrite, conditioning increase of the dislocation density, delays the formation of cells having clear outline /4/. In crystals of higher bainite the dislocation structure forms and cementite precipitations prevent motion of dislocations (Fig.2, f*) restraining formation of clear cellular structure and to some extent limiting development of plastic deformation. However, cementite plates of both higher bainite and thin-plate pearlite are not so large obstacles in the development of plastic deformation as, for example, cementite colonies of annealed plate pearlite are, whose dimension is several times larger as compared to cementite precipitations in mixed structures (Fig.2, g*).

The presence of disperse structures obtained in the intermediate region, peculiarities of formation of these structures influenced by plastic deformation at hydrostatic pressure stand for possibility of obtaining necessary strength, plasticity and viscocity of steel which allows to deform it to a high degree with no risk of failure /5/.

The results of tensile tests are also indicative of high plasticity of mixed structures. Thus, ultimate strength of 60 steel containing up to 40% of bainite in its structure is 1.3 ... and reduction of area is 1.7 (for a mixed structure) and 2 times (for a mixed structure after tempering) higher than for the same steel in the as-delivered state. For 45 steel containing up to 80% bainite in its structure the ultimate strength is 2 times higher and plasticity remains at the level of the as-delivered state (Fig.3). Steel of mixed structure after tempering at 650... 670 °C is of higher plasticity. Varying the quantitative ratio of the mixed structure components, it is possible to obtain necessary combination of plastic and strength properties of carbon steels.

*The Figure is given at the and of the book.

References

Bernstein M.L. Thermomechanical Treatment of Alloys. -M.: Metallurgiya, 1968, v.1, -594 pp.

Goodremon E. Special Steels. -M.: Metallurgiya, 1966, v.I.- 736 pp.

Klshevskii Yu.A., Usikov M.P. Crystallogeometry of cementite precipitation in lower bainite. - Fiz. Metallov.i Metallovedeniye, 1982, 53, N3, p.615-618.

Gordienko L.K. Substructural Hardening of Metals and Alloys.- -M.: Nauka, 1973. -223 pp.

Kurdyumov G.V., Utevskii L.M., Entin R.I. Transformations in Iron and Steel. -M: Nauka, 1977.- 238 pp.

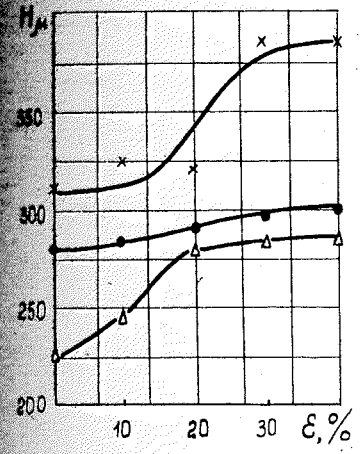

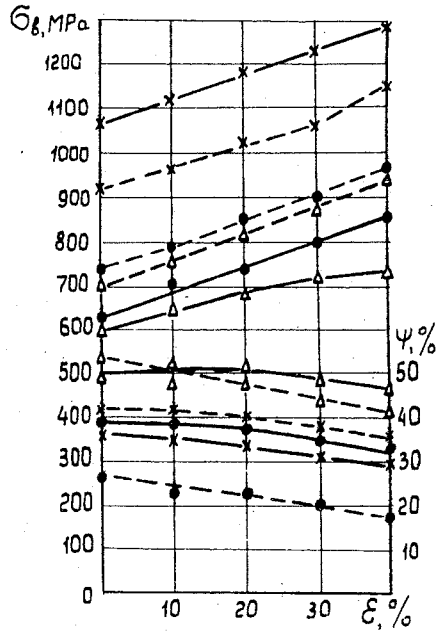

Fig.1. Change of 60 steel microhardness with deformation degree: ● - as-delivered state structure; × - mixed structure; Δ - mixed structure after tempering.

Fig.2. Change of strength and plasticity of 45 (solid lines) and 60 (dotted lines) steels in different structure states depending on deformation degree:
-●- as-delivered state structure; -×- mixed structures; Δ- mixed structures after tempering.

CREEP AND DISLOCATION STRUCTURE OF METALS AFTER PRELIMINARY ACTION OF HIGH PRESSURE

O.V.Presnyakova, V.I.Zaitsev, V.A.Fomchenko
Physico-Technical Institute, Ukrainian Academy of Sciences, Donetsk, USSR

It is known /I/ that preliminary action of high hydrostatic pressure (HHP) can considerably influence concentration of crystal-lattice defects as well as mechanical properties of metals and alloys containing inclusions or cavities.

The aim of the present paper is to study the influence of dislocation structure formed during HHP action on creep regularities of anisotropic (Zn) and two-phase (Al-Si alloy) materials.

Material and experimental procedure. The investigation was carried out on Al-I.3% Si model alloy with incoherent inclusions of Si of mean size d = 0.I4 μm. Under creep tests the Zn single crystals were so oriented that the basal plane (000I) was parallel to the axis of tension and basal slip was disabled there. HHP preliminary treatment was done at pressures up to I500 MPa during t = 20 min at T = 293 K. Creep tests under uniaxial tension were carried out at T = 293-3I3 K and P = 0.I MPa. The dislocation structure was studied by such methods as electron microscopy (in Al-Si alloy) and the etch pits in Zn crystals.

Experimental results and their discussion. Zinc single crystals having twins. It has been established that HHP preliminary action on zinc single crystals having twins essentially influences the characteristics of creep curves $\varepsilon(t)$ at P = 0.I MPa (Fig.I). After HHP action one can observe the increase of instantaneous deformation ε_o and maximum deformation before fracture ε_{max}, the rate of unsteady creep. The mentioned effects of HHP preliminary action are maximum in the pressure range $600 \leq P \leq I000$ MPa (Fig.2,a).

Structure studies have shown that HHP action results in dislocation multiplication in zinc single crystals containing twins. At $P \geqslant I00$ MPa a sharp increase in the pyramidal dislocation mean density was observed (Fig.3). Comparison of results of structure studied and of obtained dependences $\varepsilon(t)$ and $\varepsilon_{max}(P)$ (Fig.I, 2,a) shows that the increase of plasticity and creep rate of zinc after HHP action is connected with intensification of pyramidal slip.

According to /I,2/ HHP effect on crystals with compressibility anisotropy containing interfaces between the misoriented regions results in initiation of shear stresses τ_a:

$$\tau_a = P \cdot f(C_{\alpha,\beta}; \varphi), \qquad (I)$$

where $C_{\alpha,\beta}$ are the elastic constants of a crystal, $\alpha, \beta = I,2...6$, φ is the angle of boundary misorientation. In the case studied (Zn single crystals having twin boundaries) at $P \geqslant I00$ MPa there appear stresses $\tau_a(I)$ sufficient for the pyramidal dislocation multiplication (Fig.3). It was found that HHP action ($P \geqslant I000$ MPa) favours the development of multiple twinning and degradation of the crystal plasticity under deformation at P = 0.I MPa (Fig.2).

Al-Si alloy. It has been established that HHP preliminary action results in changing all typical values of creep curves $\varepsilon(t)$ of Al-Si alloy. After HHP action the increase is observed in the instantaneous and the maximum deformation before fracture, the creep rate and the duration of all types of creep and durability. Dependence of the secondary-creep rate on pressure value is of the extreme character with the maximum at P = I000 MPa (Fig.2,b).

The electron-microscopic study of the Al-Si alloy structure has shown the increase in mean dislocation density after HHP action, $P \geqslant 500$ MPa (Fig.3). The characteristic property of the alloy dislocation structure after HHP treatment is high local dislocation density near inclusions and at interfaces. Under subsequent creep the dislocation tangles formed near inclusions at HHP action become disentangled.

According to /I/, action of HHP on crystals containing elastic inclusions results in initiating of shear stresses at interfaces:

$$\tau_p(P) = P \cdot \frac{3G(K - K_i)}{K(3K_i + 4G)}, \qquad (2)$$

where G is the modulus of matrix shift, K and K_i are moduli of volumetric compression of matrix and inclusion. The results obtained show that at $P \geqslant 500$ MPa in the studied Al-Si alloy the stresses τ_p (2) appear which are sufficient for dislocation multiplication in the aluminium matrix.

Comparison of structure analysis results and dependences $\varepsilon_o(P)$ and $\varepsilon_{max}(P)$ obtained (Fig.2,3) shows that increase of the movable dislocation density results in increase of plasticity and deformation at all stages of the Al-Si alloy creep.

It is known that at moderate temperatures stationary creep velocity $\dot{\varepsilon}_2$ is connected with density of movable dislocations by the relation

$$\dot{\varepsilon}_2 = A\rho \left(\frac{\sigma - \sigma_i}{E}\right)^n \exp\left(-\frac{U}{kT}\right), \qquad (3)$$

where A and n are alloy constants, σ and σ_i are external (applied)

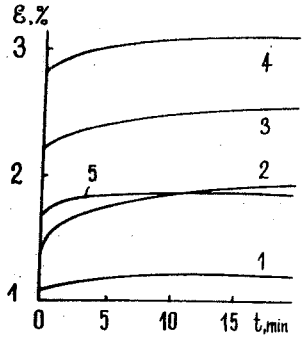

Fig.I. Creep curves of zinc single crystals having twins at T = 293 K, σ = I5 MPa and P = 0.I MPa: I - initial state after HHP action; 2 - P = 200 MPa; 3 - 600 MPa; 4 - I000 MPa; 5 - I500 MPa.

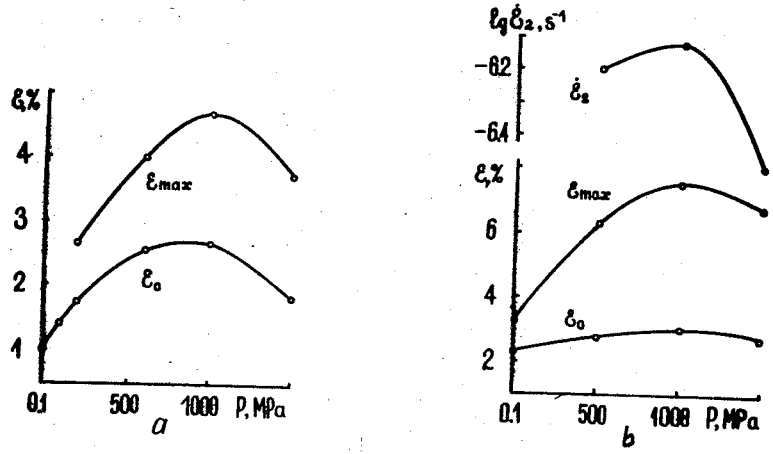

Fig.2. Influence of HHP preliminary action on characteristics of creep curves of zinc single crystals having twins at T = 293 K and σ = I5 MPa (a) and Al-Si alloy at T = 3I3 K and σ = 60 MPa (b): ε_0 - instantaneous deformation, ε_{max} - deformation before fracture, $\dot{\varepsilon}_2$ - stationary creep velocity.

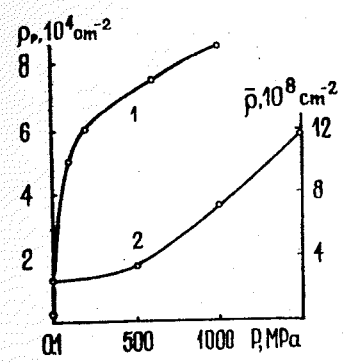

Fig.3. Dependence of mean dislocation density $\bar{\rho}$ on HHP value in zinc single crystals having twins (I, left scale) and Al-Si alloy (2, right scale).

and internal stresses, respectively, U is the activation energy, B is the Young's modulus. The extreme character of $\dot{\varepsilon}_2(P)$ dependences (Fig.2) is probably connected with the fact that HHP action results in the dislocation density increase and thus the increase of internal stresses σ_i at $\Delta\sigma_i(P) = \alpha Gb\sqrt{\rho(P)}$ (where b is the Burgers vector modulus, α is a constant).

References

I. Radcliffe S.V. Influence of hydrostatic pressure on structure defects and properties. In: Mechanical Properties of Materials under High Pressure.-M.:Mir, I973, v.I, p.254-295.

2. Zaitsev V.I., Presnyakova O.V., Fomchenko V.A. Creep and dislocation structure of zinc single crystals having twins after high pressure action.-Metallophysics, I986, v.8, N 2, p.70-74.

REVEALING AND INVESTIGATION OF A BAROPLASTIC PHENOMENON UNDER SUPERPLASTICITY

I.I.Papirov, E.S.Karpov, K.V.Kovtun, G.F.Tikhinsky, P.I.Stoev, V.S.Shokurov, A.I.Pikalov

Kharkov Institute of Physics and Technology, the Ukrainian Academy of Sciences, Kharkov, USSR

Tests under conditions of high hydrostatic pressures (HHP) show an improvement of plastic characteristics of solids (Bridgman effect). The plastification of materials under pressure is explained by reasons of two kinds: mechanical (increase of a spherical compression tensor) and physical (pressure effect on the dislocation multiplication and motion). Until recently, the Bridgman effect has been considered to be of universal character and common for all materials. However, when testing the validity of this effect for superplastic materials, it was found that the plasticity of an ultrafine-grained ($d \sim 1$ μm) superplastic Zn-0.4% Al alloy appreciably decreased rather than enhanced under the HHP conditions /1,2/. Thus, the phenomenon was found, which was opposite to the Bridgman effect and was called a baroplastic effect under superplasticity or the superplasticity suppression under the HHP conditions.

When studying the origin of this effect, the problem arose if the observed phenomenon was associated with a direct application of pressure during the tests or with the results of the material stay under pressure. The problem was put to investigate the properties of superplastic materials after their pressure treatment.

Ultrafine-grained ($d \sim 1 - 3$ μm) superplastic Zn-0.4% Al and Sn-38% Pb alloys were used as test materials. The samples of the alloys mentioned were pretreated in a hydrostat under different pressures ranging from 0.25 to 2 GPa with exposure under pressure for 2 hours. After the treatment under the HHP conditions the samples were removed from the hydrostat and were subjected to tensile and creep tests at room temperature.

The main result of this work is the detection of an appreciable deterioration of superplastic characteristics of the investigated materials after the pressure treatment. Figs. 1 and 2 show the variation of relative elongations of samples of the alloys (Zn-0.4% Al and Sn-38% Pb, respectively) with the pretreatment pressures. As under the baroplastic effect /1,2/, the plasticity at strain rates $\dot{\varepsilon} < 2 \cdot 10^{-3}$ s^{-1} decreases with the HHP in-

...se, but is weakly dependent on the pressure treatment at a ...ain rate $\dot{\varepsilon} \sim 2 \cdot 10^{-2}$ s^{-1}, when materials lose their superplasti... Under the conditions of a superplastic flow the plasticity ...reases smoothly in the whole pressure range from 0.25 up to ...Pa in the Zn-0.4% Al alloy, whereas in the Sn-38% Pb alloy the ...sticity after the HHP treatment decreases rapidly as the pres... ...e grows up to 0.5 GPa and then depends slightly on pressure. ...ter the HHP treatment of the Zn-0.4% Al and Sn-38% Pb alloys, ...e absolute value of the plasticity decrease $\Delta\delta$ is about 100-130% and 400%, respectively. The comparison of $\Delta\delta$ values for ...e Zn-0.4% Al alloy with those obtained previously /1,2/ in tests ...f the samples under pressure shows that the deplastification ef... ...ects are comparable.

The pressure treatment somewhat enhances the yield strength, ...though the absolute value of the effect is insignificant. At the ...same time, the parameter of the strain rate sensitivity of the ...flow $m = \partial \ln \sigma / \partial \ln \dot{\varepsilon}$ after the pressure treatment of the Sn-38% ...Pb alloy remains practically constant. In the Zn-0.4% Al alloy ...case, m can decrease by 20-30%.

In a creep test of the Sn-38% Pb alloy it was found that the ...relationship between the steady-state creep rate ($\dot{\varepsilon}_{ii}$) and the ...stress σ has a sigmoidal character, typical of superplastic ma... ...terials, for both initial and pressure-treated samples. The steady ...-state creep rates for the samples treated under the HHP condi... ...tions and for the initial ones were also found to be comparable. ...The main difference in the behaviour of the samples before and ...after pressure treatment consists in a shortening of the second ...stage duration of the creep for the pressure-treated samples, and ...the transition to accelerated creep and fracture at lower defor... ...mations.

The investigations of the characteristics of a superplastic ...flow before and after the treatment of materials under the HHP ...conditions, of the creep parameters, as well as preliminary struc... ...tural studies during deformation show that the mechanism of a flow ...before and after the treatment remains, in principle, the same: ...the parameter m remains at the same level and the main (leading) ...process is still grain boundary sliding. At the same time, the ...difference in the flow between pressure-treated and nontreated ma... ...terials at an initial stage of the deformation is much smaller ...than in the process of the flow itself. Thus, we have to deal with ...a phenomenon, in which the structural changes, due to the pressu...

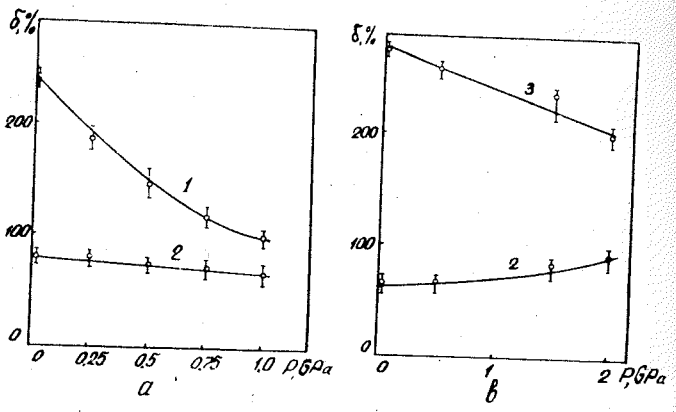

Fig. 1. Relative elongation of samples of the Zn-0.4% Al alloy versus the pretreatment pressure for the samples of two different series A(a) and B(b):
1 - $\dot{\varepsilon} = 2 \cdot 10^{-3}$ s^{-1}; 2 - $\dot{\varepsilon} = 2 \cdot 10^{-2}$ s^{-1}; 3 - $\dot{\varepsilon} = 6 \cdot 10^{-4}$ s^{-1}.

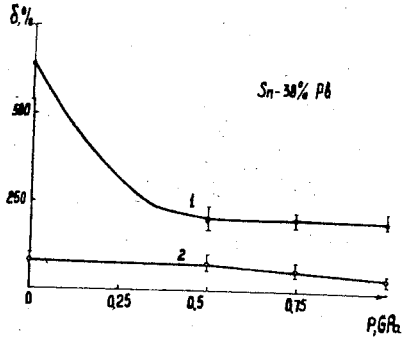

Fig. 2. Relative elongation of samples of the Sn-38% Pb alloy versus the pretreatment pressure:
1 - $\dot{\varepsilon} = 2 \cdot 10^{-3}$ s^{-1}; 2 - $\dot{\varepsilon} = 2 \cdot 10^{-2}$ s^{-1}.

...tment, show up weakly at the initial stage of the deforma-
...though they initiate some processes having a marked effect
...rheological behaviour of the material , its tendency to
...ng. In view of the above, further studies of the baroplas-
...effect should be aimed at clarifying, on the one hand, phy-
...l aspects of the phenomenon, structural changes due to the
...treatment and their influence on the mechanism of a superpla-
...o flow, and, on the other hand, on the mechanics of a plastic
...formation, mainly the process of necking before and after the
...atment of superplastic materials under the HHP conditions.

References

1. Papirov I.I., Zajtsev V.I., Akimov G.Ya. et al. Baroplasticheskij effekt pri sverkhplastichnosti. Dokl.Akad.Nauk SSSR, 1982, v.262, N2, p.370-372.
2. Papirov I.I., Zajtsev V.I., Akimov G.Ya, et al. Baroplasticheskij effekt pri sverkhplastichnosti. Tezisy dokl. 10 Vsesoyuznoj konf. po fizike prochnosti i plastichnosti. Kujbyshev, 1983.

THE EFFECT OF HYDROSTATIC PRESSURE ON THE DISLOCATION STRUCTURE OF α-Fe

V.F.Shishmintsev, V.P.Ketova, N.L.Pecherkina, V.A.Pavlov
The Urals Branch of the USSR Academy of Sciences, Sverdlovsk, USSR

The dependence of the position of internal friction dislocation peaks of α-Fe on the hydrostatic pressure has been measured for the first time.

The features of formation of the dislocation structure of α-Fe during hydroextrusion were reported in /1/. It was shown that under such conditions of deformation screw dislocations, having a high Peierls barrier and lower mobility than edge dislocations, predominate in the structure of iron. As a result of this, iron deformed by 25, 50 and 75% at a hydrostatic pressure of 400 and 1000 MPa after annealing at 680 °C had a high brittleness threshold and a low impact strength.

However, hydroextrusion is characterized by a complex stress state and, consequently, the obtained results are difficult to interpret. It is natural that a need has arisen to carry out such investigations with a less complex stress state.

In this investigation specimens of armco iron were subjected to a uniaxial tension on a high-pressure set-up intended for testing materials under conditions of complex stress /2/. Castor oil was used as a medium for transmitting pressure which was varied from atmospheric to 800 MPa and was maintained at a constant level during a test. The deformation rate was 50 mm/min. All the tests took place at room temperature. The working parts of specimens measured 100 mm (length) x 6 mm (diameter). Prior to deformation the specimens were annealed in vacuum 10^{-5} tor at 1200 K for three hours. After deformation no additional heat or mechanical treatment was given.

The specimens were stretched on a tensile test arrangement, Fig.1. The tension was applied to produce a 5% length increase of the specimen, the tensile strain remaining uniform along the entire length. Such an arrangement made it possible to investigate the effect of hydrostatic pressure on the character of the dislocation structure being formed with axial tension.

The dislocation structure was studied by the internal friction technique using an "Elastomat" unit, the natural frequency of the specimen oscillations being 3000-3500 Hz and the amplitude 10^{-6}

internal friction spectrum was registered in the temperature range of 120-350 K to provide data on the dislocation structure.

Fig.2 shows temperature dependence curves of internal friction Q^{-1} for specimens of armco iron deformed at various hydrostatic pressures. Curve 1 plotted for atmospheric pressure features two internal friction peaks at approximately 150 and 270 K. The first peak is due to edge dislocations, the second to screw dislocations /1/. With hydrostatic pressure raised to 400 MPa the character of the internal friction spectrum remains unchanged, but both peaks are noticeably displaced into the region of higher temperatures, the first one more than the second. The elevation of hydrostatic pressure to 800 MPa leads to the further displacement of the internal friction peaks in the direction of higher temperatures.

Fig.3 depicts the temperature positions of peaks versus hydrostatic pressure. It is readily seen that the peak shift is approximately linear. The internal friction peak pertaining to edge dislocations has a more pronounced dependence than that responsible for screw dislocations.

Such a variation in the arrangement of internal friction peaks of edge and screw dislocations leads to their gradual drawing together. The internal friction peak due to edge dislocations moves toward the peak of the screw dislocations, the position of the latter changing little. This can be interpreted as follows: the edge dislocations change into dislocations of mixed type, their screw component continuously growing with the rise of hydrostatic pressure.

If we admit that with further rise of hydrostatic pressure the behaviour of the peaks remains unchanged, then at a pressure of about 1400-1600 MPa both peaks may merge. This will correspond to a structure having mobile dislocations of the screw orientation type only.

The obtained results do not contradict the available data on the effect of hydrostatic pressure on the movement and formation of dislocations /3/ and agree with those of /1/.

The authors wish to thank Yu.A.Axenov and I.L.Chernogorov for aid in carrying out the tests.

References

1. Pavlov V.A., Filippov Yu.I., Ketova V.P., Pecherkina N.L. Fiz. met. i metalloved., 1982, 53, 575-580.

2. Shishmintsev V.F., Rodaikin A.A., Bogatov A.A., Mizhirit
sky O.I. Zav. lab., 1978, 44, No.10, 1044-1045.
3. Zaitsev V.I., Presniakov O.V., Fomchenko V.A., DAN AN SS
1983, 272(2), 362-365.

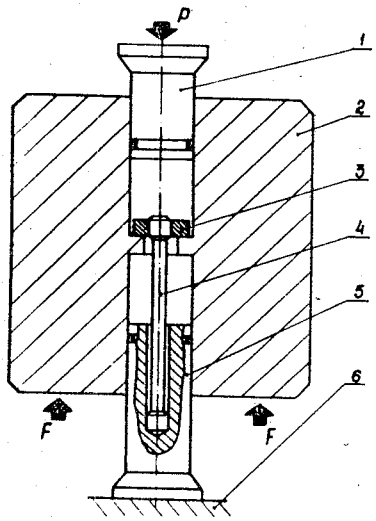

Fig.1. Tensile test arrangement, 1 - upper plunger, 2 - container, 3 - thrust washer, 4 - specimen, 5 - lower plunger, 6 - fixed support. P - hydrostatic pressure force, F - container displacement force.

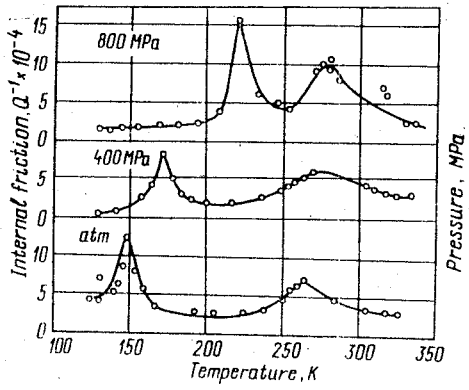

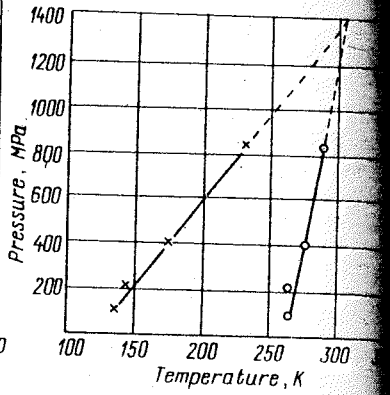

Fig.2. Dependence of internal friction dislocation peaks on hydrostatic pressure.

Fig.3. Dependence of internal friction dislocation peaks on hydrostatic pressure and temperature:
+-edge dislocation internal friction peak, o - screw dislocation internal friction peak.

IGH PRESSURES IN PROCESSES OF METALWORKING BY COLD PLASTIC EFORMATION

O.A.Rozenberg
Institute for Superhard Materials, Academy of Sciences of the UkrSSR, Kiev, USSR

The Institute for Superhard Materials of the Ukrainian Academy of Sciences has been conducting comprehensive investigations into the physics and mechanics of the tool-workpiece interaction in the process of the stepwise cold plastic deformation. This permitted to develop power- and materials-saving high technology processes for machining engineering industry components resulting in improved performance properties.

One of the most important factors in the proposed technological processes for axially symmetric deforming sleeve- and tube-type components (expansion, deforming broaching, reduction, etc.) is represented by the contact pressure present in the tool-workpiece interaction zone which defines the surface quality of components machined. Stresses developed within the tool-workpiece interaction zone in the process of the deforming broaching are of a great interest as they reach high levels, define friction processes during the relative sliding and the wear rate of a tool, they define the development of heat in the contact zone, the roughness of the surface machined, the efficiency of lubricants used and the stressed-state of the body deformed. It has been shown that all the components of sleeve- and tube-type can be subdivided into two groups, that of finite and infinite wall thickness and that of varied stress-strain state in the tool-workpiece contact zone. In components belonging to the first group the contact pressure in the tool-workpiece interaction zone can vary and reach 6 to 9 yield points in metal machined depending on deformation conditions and component dimensions. In components belonging to the second group the contact pressure can reach a limit equal to 2.6 q_{cr} where q_{cr} is the critical contact pressure and does not grow with further occurences of contact with deforming elements, the pressure being defined by the bearing capacity of metal in component within the contact zone and is independent on the deforming conditions and the component dimensions.

The contact pressure values and their interrelations with the deforming conditions are brought about by the tool (deforming elements)-workpiece interactions. The pattern of the interactions in

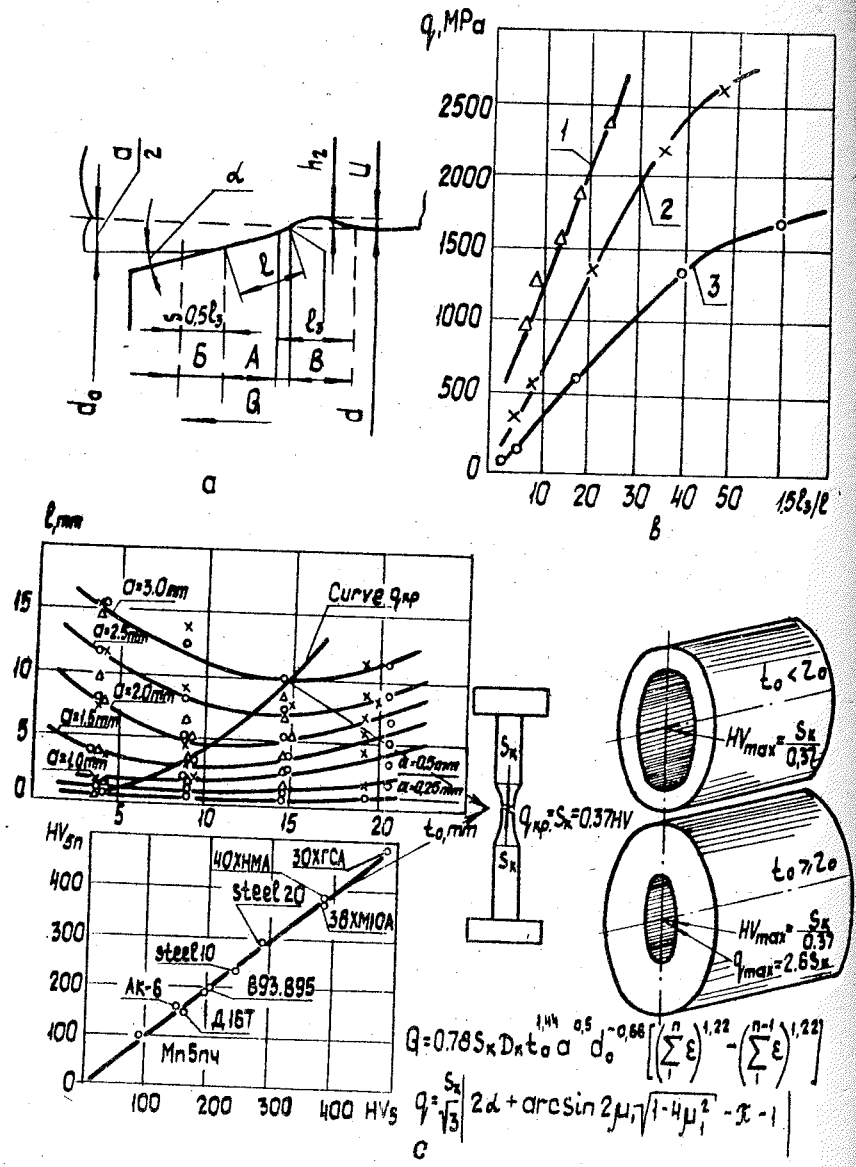

Interaction between the tool and the workpiece during the deforming broaching.

process when the working surface of the element is conical comprises three regions; the contact region A, the out-of-contact region Б, located in front of the element defining the width of contact, l, and the out-of-contact region B located behind the deforming element which sizes the diameter of the machined (Fig.1,a). The interrelations between all the phenomena taking place in the tool-workpiece interactions zone are so complicated that cannot be fully calculated theoretically as yet and have therefore been studied experimentally. Fig.I shows the influence of the out-of-contact zone relative to the contact one, I.5 l_3/l (line I), the wall thickness, t_o, (line 2) and the tightness, a, (line 3) on the contact pressure in the process of the deforming broaching of a 45-steel tube with the initial hole diameter of 50 mm. It can be seen from Fig.I that high contact pressures developed during the deforming broaching confirm in an indirect way the existende of the out-of-contact deformation zones in the process. Naturally, the contact pressures rise with the wall thickness. It was also disclosed in the process of the cold stepped plastic deformation of components the existence of a critical contact pressure causing an intensive local plastic flow in the tool-workpiece contact zone and shown that the value of the critical contact pressure for a given metal is invariant in relation to the tool geometry, the deformation level, the dimensions of the component deformed, the lubricant used and is equal to the true rupture stress for a given metal.

It was found in our studies that in the process of broaching holes in sleeves of both finite and non-finite wall thickness the maximum surface hardness of a sleeve would be of the same level for a given metal and equal to the hardness measured at the neck of the specimen ruptured under tension and prepared of the same metal. This finding allows to define limit contact pressures when machining holes in components of non-finite wall thickness if the maximal hardness which can be obtained when hardening the metal of interest is known. Fig.I depicts the interrelation between the phenomena in the tool-workpiece contact zone in the process of broaching holes in components of any wall thickness based on the physical constant of the metal machined, i.e. the true stress at the neck of the ruptured specimen S_k.

USE OF HIGH PRESSURES OF THE LUBRICANT IN INDUSTRIAL PLASTIC DEFORMATION PROCESSES

G.L.Kolmogorov, V.Yu.Shevlyakov, Yu.A.Barkov, V.L.Karlinsky
Perm Polytechnical Institute, Perm, USSR

The outer friction plays an important role in plastic deformation processes. A great amount of energy, necessary for the plastic deformation, wastes on overcoming the friction. The friction gives rise of wear of tool, leads to the appearance of thermal stresses, frequently limits working velocities and lowers the quality of a product.

The realization of fluid friction regime is the most effective way of friction forces decreasing. This regime is provided either by the pressure feed of the lubricant (hydrostatic feed) or by the discharging of lubricant under force from the workpiece itself (hydrodynamic feed). At present time the hydrodynamic feed of the lubricant has a vast using in such plastic deformation processes as wire-drawing, rolling, die forging, sheet forming and hydroextrusion. There have been developed the constructions of lubricating pump units and a body of mathematics for their calculation.

The technological parameters, providing a hydrodynamic lubricant regime, are calculated by means of continuum mechanics equations. A set of differential equations of motion, incompressibility and energy balance, characterizing a lubricant flow is written as follows /I/:

$$\left.\begin{aligned} &[\sigma_{ij}(p,t,v_i)]_{,j} = \rho w_i;\\ &v_{i,i} = 0;\\ &(\lambda t,i),i + T(p,t,H)\cdot H = \rho \frac{d(ct)}{d\tau}, \end{aligned}\right\}$$

where σ_{ij} is the stress tensor; p and t are pressure and temperature of lubricant; v_i is the component of velocity vector; w_i is the total derivative of velocity with respect to time; ρ, λ and c are density, heat conduction and mass heat capacity per degree respectively; T and H are intensities of tangential stresses and velocities of shear. At the time of investigation of the lubricant flow behavior initial equations are simplified and main technological tasks have been solved in terms of approximate equations of viscous liquid motion.

The hydrodynamic lubricant regime is realized with the help of nozzles, providing the discharging of lubricant to the site of deformation. The pressure in the nozzle in the case of wire-drawing

Newtonian fluid is

$$p_H = -\frac{I}{\alpha}\ln\left[I - 6\alpha\mu_o v_o(I - 2\bar{q})l/h^2\right],$$

l is the length of nozzle; h is the gap; α is the piezocoefficient of viscosity; μ_o is the dynamic viscosity of lubricant under atmospheric pressure; v_o is the speed of wire-drawing; $\bar{q}$ is the relative lubricant throughput.

The rheological properties of lubricants depend to a considerable extent on a temperature, so the dissipative heating of lubricant layer is taken into account in hydrodynamic calculations. The heat, given off in lubricant volume, is evaluated; the middle temperature of lubricant and the pumping ability of nozzle are calculated in terms of equation of a heat balance. The pressure produced by nozzle increases with increasing in the velocity and the nozzle length (Fig.I). The decreasing of nozzle length is achieved by using of optimal gap sizes $h_{opt} = I.5h_o$ (h_o is the thickness of lubricant layer in the site of deformation). The optimal nozzle length is equal /2/

$$l_o = h_{opt}^2(I - 1^{-\alpha p_H})/2\alpha\mu_o v_o$$

The hydrodynamic effect of Newtonian fluid in rolling (Fig.2) is estimated by pressure, developed in the lubricant layer between roll and strip

$$p = -\frac{I}{\alpha}\ln(I - 6\alpha\mu_o v_o \cdot J_I/R),$$

where J_I is the parameter, taking into account the geometry of the lubricant layer; R is the roll radius.

Produced pressures increase and friction coefficient decreases with the increasing of rolling velocity and roll radius, with the decreasing of reductions.

Using the hydrodynamic lubricant theory, one can make studied selection of the working liquid parameters in hydroextrusion. The working liquid viscosity, necessary for the provision of hydrodynamic lubricant regime, equals /2/

$$\mu_o = h_o tg\alpha_M(I - e^{-\alpha\sigma_s})/3\alpha v_o e^{\alpha p_K},$$

where p_K is the pressure in container; α_M is the slope of the die's generating line; σ_s is the resistance to deformation of extruded material.

There is known in wire-drawing industry the scheme, overlapping hydroextrusion and hydrodynamically-aided drawing /3/. Fig.2 shows the scheme of this process. Moving within the ring packing

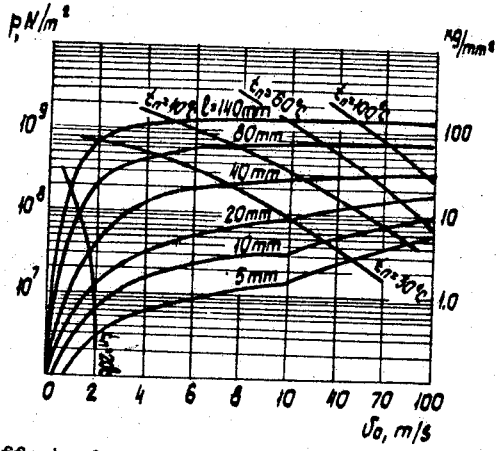

Fig.I. The effect of wire-drawing velocity on nozzle's pumping ability.

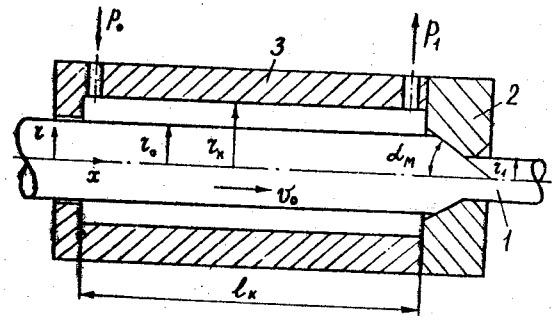

Fig.2. The scheme of hydrodynamically-aided wire drawing: I - the billet; 2 - the die; 3 - the high pressure chamber.

chamber under the pressure differential $p_o - p_I$ the working liquid provides the hydrodynamic reinforcement. The hydrodynamic thrust is calculated as

$$T_o = 2\pi\mu v_o l_k F(\bar{r}_k, \bar{q}),$$

where $\bar{q} = q/\pi v_o(r_k^2 - r_o^2)$ is the relative throughput of pumping working liquid; $r_k = r_k/r_o$.

References

Kolmogorov G.L. Hydrodynamic Lubrication in Metal-Working. Metallurgiya, Moscow, I986, I68 p.

Kolmogorov G.L., Melnikova T.E. Problems of hydrodynamics forced-fluid lubrication at extrusion of materials. -Fizika i tekhnika vysokikh davleny, I98I, iss.3, p.9I-96.

Kolmogorov G.L. et al. Hydrodynamically-aided drawing of wire. -Fizika i tekhnika vysokikh davleny, I983, iss.II, p. 45-49.

USE OF DISLOCATION ENSEMBLES FORMED UNDER HIGH HYDROSTATIC PRESSURE FOR OPTIMIZATION OF STEEL STRUCTURE

T.E.Konstantinova, V.I.Zaitsev, E.I.Lyafer, A.A.Dobrikov

Physico-Technical Institute of the Ukrainian SSR Academy of Sciences, Donetsk, USSR

It is well-known /1-3/ that plastic deformation under high hydrostatic pressure (HHP) in combination with heat treatment - barothermomechanical treatment - can be successfully used for increase of strength without essential decrease of plasticity. A possibility of plasticity increase without strength decrease has been deficiently investigated.

The investigations have been carried out on commercial 30ХГСА and Х12М steels.

Steel 30ХГСА is well-known because of high susceptibility to reversible temper brittleness. Steel treatment consisted in hardening, high tempering in the temperature range 773-973 K with water-cooling, hydrostatic extrusion with the reduction ratio 50% and final high tempering. The brittle state was achieved by tempering at 773 K or 923 K, the cooling rate was 30-50 K/hour.

The main characteristics of the mechanical properties were controlled. The microstructure was studied by using the method of transmission electron microscopy. The temperature of the start of recrystallization was estimated according to the data of structural investigations and hardness variations.

The barothermomechanical treatment causes increase of fracture energy at any variants of initial tempering used in the given paper. This effect is the more pronounced, the higher the temperature of tempering. However, with due account of strength obtained and thermal stability of steel, the regime with initial tempering at 873 K is the better one. It eliminates practically the dip on curve of fracture energy dependence on tempering temperature (Fig.I).

The different levels of properties and thermal stability are due to changes in dislocational structure of steel. The steel prior to deformation tempered at 773 K, shows high density of random distributed dislocations ($\rho > 10^{11}$ cm^{-2}). Such structural state turned out to be stable enough and subsequent hydrostatic pressure does not cause the forming of ordered structure. Preliminary tempering at 973 K provides the resonably low density of dislocations ($\rho \sim 10^{8}$ cm^{-2}) and the high degree of carbide phase coagula-

...llowing deformation of steel with such a structure the ... dislocation is increased up to 10^{11} cm^{-2} and more. ...tribution is inhomogeneous, but the clearly pronounced ... structure is not revealed. In both cases recrystalliza... initiated at comparatively low temperatures (923 and 873 K, ...tively), goes on at a high rate, irregularly, with sharp ...se of strength.

The third variant including the tempering at 873 K before ...static pressure, is of a particular interest. Deformation in ...conditions causes the all-round-forming of the cells of 0.I - ...μm in size, and misorientation 10-15° (Fig.2,a*). At following heating the uniform structure with grain size 0.5-I μm is ...med in steel, resulting in two-fold increase of fracture energy in temper brittleness state and 40% increase of yield strength. In this case, the temperature of the start of recrystallization is 973 K.

Therefore, predominant influence of preliminary tempering reduces to forming of a structure, in a process of hydrostatic pressure of which, the forming of cells is promoted.

Steel Х12М is tool steel having high strength, but very small reserve of plasticity. This is due to the fact, that martensite of high-carbon steels is mainly twinned one.

The steel investigated after annealing was hydrostatically pressed with the reduction ratio 50%. Further, a part of samples was subjected to heating up to 673 K, austenitization, quenching and low-temperature tempering. The second part of the samples deformed was quenched without inter-heating. The samples after quenching and low tempering were the controls.

It was established, that using of hydrostatic pressure in combination with thermal treatment makes possible the 1.5-fold increase of fracture energy without hardness decreasing. The absence of heating at 673 K of the samples deformed has a negative effect on steel properties, which appeared to be lower, then those of the controls.

Structural investigation shows, that deformation in the HHP-conditions causes forming of cellular structure (Fig.2,b*). The following heating favours the polygonized processes. It was found that after quenching in the samples subjected to hydrostatic pressure with inter-heating at 673 K, the twinned martensite content is decreased compared to the controls and its substitution

* The Figure is given at the end of the book.

with dislocational martensite takes place (Fig.2,c*). In our opinion, this fact determines increase of steel plasticity. Inter-heating plays a part of stabilizing treatment favouring inheriting of the defect structure at $\alpha \rightarrow \gamma \rightarrow \alpha$ recrystallization.

References

1. Piu H.L. Mechanical property of materials under high pressure. -M: Mir, 1973, iss.I, 296 p.
2. Beresnev B.I., Martinov E.D., Rodionov K.L. et al. Plasticity and strength of solids under high pressures. M: Nauka, 1970, 162 p.
3. Zaitsev V.I. Physics of plasticity of hydrostatically compressed crystals. - Kiev: Naukova dumka, 1983, 188 p.

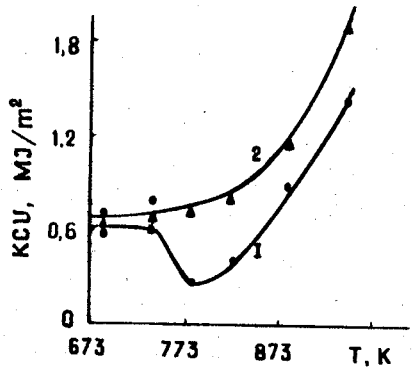

Fracture energy dependence of 30ХГСА steel on tempering temperature.
I - without deformation; 2 - treatment including deformation in HHP-conditions.

* The Figure is given at the end of the book.

PRODUCTION OF SHAPED HOLLOW ITEMS BY METHOD OF HYDROSTATIC REDUCING

M.I.Kalachev, N.I.Jurijev, Ju.T.Antonishin

The Physical-Technical Institute of the Byelorussian Academy of Sciences, Minsk, USSR

In various technical fields there is a big class of items having shaped internal relief (e.g. dies and some parts) which production involves substantial technological difficulties and a high labour consumption. In some cases it is most advantageous to fabricate these items using shaping hollow billet by a high-pressure liquid.

The machine for hydrostatic reducing (Fig.I) comprises a multilayer container I, a lower seal 2 and a mandrel 3. The pressure generator is a hydraulic press of 20 MN press force. The shaping of a billet 4 is performed in the following way. A working chamber of the container is filled by a liquid 5 and then the billet is placed. During a working press pass the billet is lowered down, the liquid is compressed, its pressure increases and the billet is reduced.

In this way a number of dies has been produced from the XI3 (ICXI3 to 4CXI3) stainless tool steels with a wall thickness up to 30 mm (Fig.2). The maximum liquid pressure in the working chamber was 2000 MPa. The labour consumption for shaping a die working surface decreased by a factor of I00 as compared with prior-art operations such as machining on metal-cutting machine tools with subsequent hand polishing or electroerosion machining. The dimensional accuracy of dies increased. This is the result of replacing the operations which cannot ensure a multiple reproduction of sizes. A high similarity of dies is especially important when operating on multiposition automatic lines designed for production of glass items. In the case of great variation of sizes and surface finish classes glass items fail on their subsequent quenching due to high thermal stresses. This machine can be used for production of various items which overall dimensions fit those of a working chamber with the aid of replacing a shaping tool (a mandrel).

This makes the process of hydrostatic reducing efficient from the economic viewpoint even for a small-scale production.

The specific feature of the method is the possibility of producing shaped hollow items with a bottom which have side relief elements inclined towards the axis of a shaping tool. A favourable

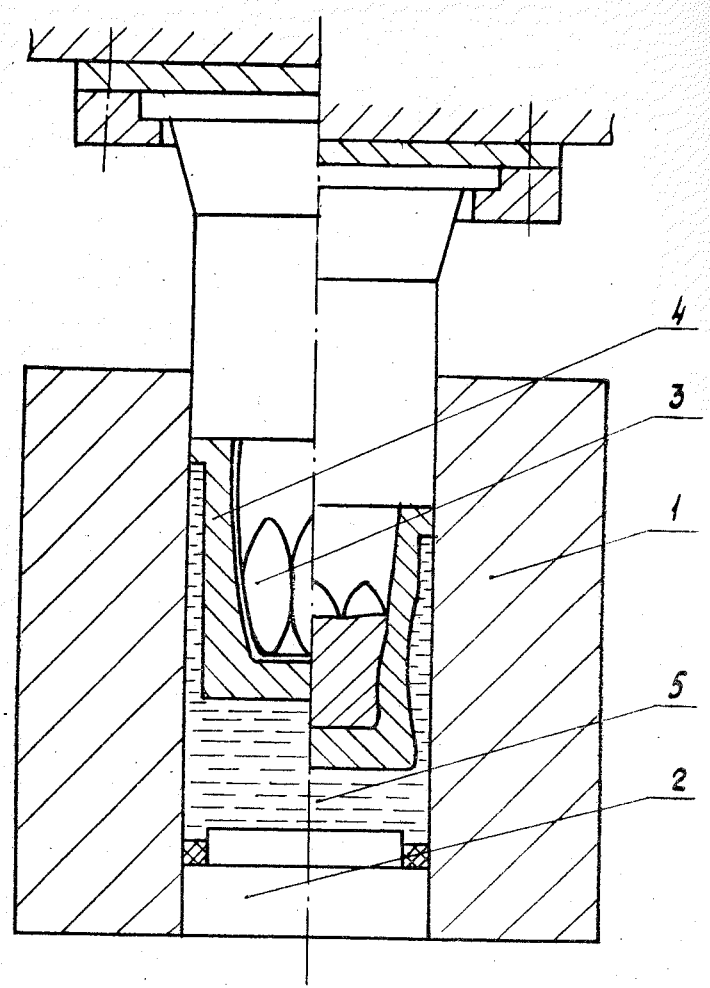

Fig.I. Diagram of machine for hydrostatic reducing: I - container, 2 - lower seal, 3 - mandrel, 4 - billet, 5 - liquid.

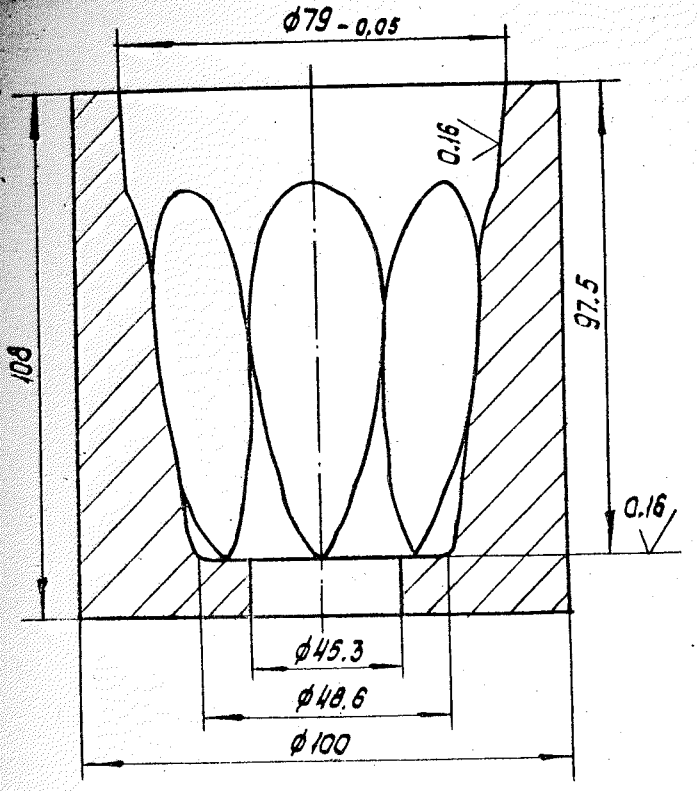

Fig.2. Die.

diagram of a stressed state makes it possible to strain low-plasticity materials with a great amount of deformation. The absence of axial motion of shaping tool relative to a billet favoures its prolonged life.

МЕЖДУНАРОДНАЯ АССОЦИАЦИЯ ПО РАЗВИТИЮ ИССЛЕДОВАНИЙ
В ОБЛАСТИ ВЫСОКИХ ДАВЛЕНИЙ

ВЫСОКИЕ ДАВЛЕНИЯ В НАУКЕ И ТЕХНИКЕ

ТРУДЫ
XI МЕЖДУНАРОДНОЙ КОНФЕРЕНЦИИ МАРИВД

В 4 томах

Том 3

Ответственный редактор Н.В.Новиков

На английском языке

Киев, издательство "Наукова думка"

Художник обложки В.С.Мельничук
Художественный редактор И.Е.Писарева
Технические редакторы Т.М.Зубрицкая, Л.Н.Муравцева

Н/К

Подп. в печ. 13.06.88. Формат 60x84/16. Бум. офс. № 2. Офс. печ. Усл. печ. л. 22,55. Усл. кр.-отт. 22,78. Уч.-изд.л. 20,83+вкл.0,43= = 21,26. Тираж 720 экз. Заказ 9-2. Цена 1 р. 10 к.

Издательство "Наукова думка". 252601 Киев 4, ул. Репина, 3.
Киевская книжно-журнальная типография научной книги. 252004
Киев 4, ул. Репина, 4.